Studies of Earthquake Ground Motions and Soil-Structure Interaction for Diablo Canyon Nuclear Power Plant

by

A. S. Veletsos, Y. Tang and A. M. Prasad

Submitted to

Brookhaven National Laboratory
Department of Nuclear Energy
Upton, Long Island, New York 11973

Department of Civil Engineering
Rice University
Houston, Texas 77251

December 10, 1988

8901250058 XA

214 pp.

INTRODUCTION

This report summarizes the results of the studies on the Diablo Canyon Plant conducted at Rice University under sponsorship of the Brookhaven National Laboratory in the period between July 1, 1988 and October 31, 1988.

The objectives of these studies were to:

1. Make an independent evaluation of reasonably large subsets of the ground motions and of the associated response spectra employed in the Long Term Seismic Program for the Plant; and
2. With the aid of simplified modeling and analysis techniques, to assess the sensitivity of critical responses for the containment structure to possible variations in the characteristics of the ground motion and the structure itself.

The response quantities examined include the peak values of the base shear, base moment, and of the displacements and accelerations at selected points of the structure, as well as the floor response spectra for these points. The containment structure is analyzed considering it to be either rigidly or elastically supported at the base. Due provision is made in the latter case for both the kinematic and inertial interaction effects.

ANALYSIS OF GROUND MOTIONS

Motions Considered

Two sets of earthquake ground motions are examined: an empirical set, composed of the 24 horizontal components of 12 near-source recordings; and a set of 28 horizontal components of 14 numerically generated ground motions. Digitized versions of these records were supplied by the Pacific Gas & Electric Company (PG&E).

The empirical set of motions, along with the maximum values of their acceleration, velocity and displacement histories, and the mean and mean plus one standard deviation values of these maxima, are listed in Table 1. The individual histories, normalized with respect to their absolute maximum

values, are shown in Figs. A.1 through A.24 in the Appendix. Some of the velocity and displacement values in these figures are somewhat smaller than those listed in Table 1, as a finer time interval was used for the computation of the latter values.

The corresponding information for the numerically generated set of records is given in Table 2 and in Figs. A.25 through A.52 of the Appendix. Only the first 25 seconds of each record are shown in these figures, and the peak values of ground motion listed therein are for this duration. By contrast, the values given in Table 2 are for the 'actual' longer durations. The responses presented in the following sections were computed for the longer durations.

The values marked with an asterisk in Table 2 are believed to be incorrect, as the relevant ground motion records were not properly balanced. As an illustration, the complete histories for Record Nos. 31 through 34 are presented in Figs. A.31b through A.34b in the Appendix. The resulting discrepancies, however, are of no consequence within the range of natural frequencies which is of interest to the project, and these records were used with no further adjustments.

Examination of the data presented in Tables 1 and 2 lead to the following conclusions:

1. The peak ground accelerations for the empirical set of records are substantially higher than for the numerically generated set. In particular, whereas the mean value of peak accelerations for the empirical set is 0.834 g, the corresponding value for the numerical set is 0.584 g. Similarly, the mean plus one standard deviation values of these quantities are 1.11 g and 0.748 g, respectively. Inasmuch as high-frequency systems are acceleration sensitive, the maximum responses of such systems would be expected to be materially higher for the empirical set of records than the numerical set.

2. The relative values of maximum ground displacement and maximum ground acceleration for the empirical set of records are substantially different from those for the numerical set. In fact, when properly balanced,

the maximum displacements for the empirical set will be unrealistically low, and so will be the maximum responses of very-low-frequency systems. Such systems, however, are of no interest in this project.

Response Spectra

For the aforementioned ground motions, pseudo-acceleration response spectra were computed for systems with four different percentages of critical damping, ζ, in the range between 0.02 and 0.07. The responses were evaluated for 59 frequency values equally spaced on a logarithmic scale between 0.3 cps and 30 cps. The resulting spectra have been plotted on logarithmic scales, with the abscissa representing the natural frequency of the system, f, in cps, and the ordinate representing either the pseudo-acceleration of the system, A, or the associated pseudo-velocity, $V = A/p$, in which $p = 2\pi f$ = the undamped circular natural frequency of the system.

The resulting spectra for systems with $\zeta = 0.02$, 0.04 and 0.07 are shown in Figs. B.1 through B.52 of the Appendix in the first format, and in Figs. C.1 through C.52 in the second format. In addition, the pseudo-acceleration response spectra for the mean, median, mean plus one standard deviation, and the 84th percentile levels of non-exceedance for systems with 5 percent of critical damping subjected to the entire ensemble of empirical ground motion records are presented in Fig. 1, and the corresponding spectra for the ensemble of numerical records are displayed in Fig. 2. Finally, the response spectra for the mean and mean plus one standard deviation levels of non-exceedance for both ensembles are compared in Figs. 3, and those for the individual ensembles are compared in Figs. 4 and 5. It can be seen that the spectra for the numerically generated set of records differ from those for the empirical set in two respects:

1. Their shapes are different, particularly within the lower frequency range; and
2. Their magnitudes are significantly lower.

It follows that enriching the empirical set of records with numerical records would tend to decrease the magnitudes of the resulting spectra, and that the resulting changes would be particularly significant for low-frequency systems.

Average and Maximum Spectral Values

For each of the response spectra examined herein, an effort was made to identify the frequency range within which the pseudo-acceleration values could be considered to be nearly constant. For the entire set of records, this range was judged to extend from 3 cps through 7.8 cps. The average or mean values of pseudo-acceleration within this frequency range for each of the records and damping values considered are listed in Table 3, along with the corresponding values for the complete sets of empirical and numerical records. The mean pseudo-accelerations for systems with 5 percent of critical damping presented in Table 3 are compared in Table 4 with those obtained for the 4.8 cps to 14.7 cps frequency range used in PG&E's fragility studies. Also listed in this table are the maximum values of the accelerations for the individual ground motion records as well as the complete sets of records considered.

Critical elements of the response spectra presented in Figs. 3 and 4 are summarized in the following tabulation. They include the mean and mean plus one standard deviation values of the absolute maximum pseudo-accelerations, their average values within the 3 cps to 7.8 cps and 4.8 cps to 14.7 cps frequency ranges, and their high-frequency limits which are, of course, equal to those of the ground accelerations.

Level of Non-Exceedance	Pseudo-acceleration, in g's			
	Absolute Maximum	Average within Frequency Range		High-Frequency Limit
		3 - 7.8 cps	4.8 - 14.7 cps	
		Empirical Records		
Mean	1.91	1.79	1.61	0.834
Mean + Sigma	2.57	2.39	2.14	1.108
		Numerical Records		
Mean	1.67	1.51	1.31	0.584
Mean + Sigma	2.30	2.03	1.76	0.748

The relationship of the spectra presented herein to those employed in PG&E's deterministic studies has been examined in Ref. 3 and is not considered further here.

Shapes of Spectra. Normalized versions of the pseudo-acceleration response spectra for the mean and mean plus one standard deviation levels of non-exceedance are presented in Fig. 6 for the empirical set of records and in Fig. 7 for the numerical set. The ordinates in each case are normalized with respect to their high-frequency limit, A_∞. It is observed that the shapes of the spectra for each set of records is quite similar, indicating that responses computed for one level of non-exceedance may, to a reasonable degree of approximation, be transformed readily to a different level.

Effect of Weighting Factors. Several of the ground motion records used in the development of the response spectra presented herein are for earthquake magnitudes of about 6.5, and these records have not been upgraded to the 7.2 magnitude event stipulated for the Hosgri fault. Had these records been upgraded to the 7.2 event, the peak ground accelerations and the associated response spectra would in all likelihood have been higher. On the other hand, no weighting factors have been used to adjust the influence of those records for which the tectonic setting, local topography and source to site geometry are different from those deemed to be appropriate for the plant site.

In an effort to assess the sensitivity of the response spectra to the use of such weighting factors, the pseudo-acceleration spectra for the mean plus one standard deviation level of non-exceedance presented in Fig. 3 were recomputed with the following changes:

1. Using weighting factors of 0.3 for the Nahanni records (Nos. 17 & 18) and 0.5 for the Gazli records (Nos. 19 & 20).
2. Deleting both the Pacoima Dam records from the San Fernando earthquake (Record Nos. 3 & 4) and the records from the Morgan Hill earthquake (Record Nos. 13 & 14).

The effect of the first change is displayed in Fig. 8, whereas that of the second change is shown in Fig. 9. Note that both the absolute maximum

spectral values and the average values within the 3 cps to 7.8 cps frequency range are quite insensitive to these changes, although some of the responses are reduced substantially. The peak values are compared in the following tabulation:

Solution	Pseudo-acceleration, in g's	
	Absolute Maximum	Average Within 3 - 7.8 cps Range
Without Adjustment	2.57 g	2.39 g
With Change 1	2.53 g	2.40 g
With Change 2	2.63 g	2.36 g

ANALYSIS OF CONTAINMENT STRUCTURE

This section deals with the response to representative earthquake ground motions of the containment structure and its internals. The properties of these structures are given in Table 5 and Fig. 10, and the properties of the supporting medium are presented in Table 6. Note that the internal structure has different characteristics in two orthogonal horizontal directions. The responses evaluated herein are for the N-S or x-direction.

Referred to also as the external structure, the containment shell is modeled as a stick-like system with 9 dynamic degrees of freedom, and the internal structure is modeled as a two-degree-of-freedom system (see Fig. 10).

The first few fixed-base natural frequencies of these structures are listed in Table 7, along with the associated modes of vibration. The corresponding modal masses, expressed as weights, W_j^*, and the modal heights, h_j^*, are given in Table 8.

Response of Rigidly Supported System

The fixed-base responses of these structures were computed for each of the empirical and numerically generated ground motion records referred to previously using a damping factor of $\zeta = 0.05$ for each natural mode of vibra-

tion. The response quantities evaluated include the base shears and base moments above and below the foundation mat; the displacements relative to the moving base at the springline of the containment structure and the top of the internal structure; and the absolute accelerations at the foundation mat, springline, and top of the internal structure.

The mean, median, mean plus one standard deviation, and 84 percentile values of the peak critical responses obtained for the empirical set of records are listed in Table 9, and the corresponding values obtained for the numerically generated set are listed in Table 10. In addition to the exact solutions obtained by considering all modes of vibration, the approximate solutions obtained from the first and the first two natural modes also are presented. It is clear that the principal contribution to the response comes from the fundamental mode of vibration, and that the solutions based on the first two modes are excellent approximations of the more nearly exact solutions.

The maximum critical responses for the empirical and numerical set of ground motion records are compared in Table 11. It is observed that the responses for the numerically generated records are consistently lower than those for the empirical records. This result could, of course, have been predicted from the response spectra for single-degree-of-freedom systems already presented in Fig. 3.

The coefficients of variations for the maximum responses presented in Table 11 are listed in Table 12. Also listed at the bottom of the latter table are the values obtained from the mean and mean plus one standard deviation response spectra presented in Fig. 3, using as natural frequencies the fundamental natural frequencies of the systems involved, i.e., 4.68 cps for the containment shell structure, and 13.9 cps for the internal structure. Note that the two sets of results are in excellent agreement. This finding should not be surprising, since the responses of these systems are dominated by the contributions of their fundamental modes of vibration.

It is important to note that the coefficient of variation for the maximum responses due to the empirical set of ground motion records is approximate-

ly 30 percent for the containment structure and 49 percent for the internal structure. At the May 12, 1988 meeting of PG&E and NRC representatives in Rockville, Maryland, the maximum "peak-to-peak variability" of the spectral ordinates was reported to be 19 percent, in response to which the following was noted in Ref. 3:

> "Provided I am not misinterpreting the meaning of this term, the reported value appears to be too low, and recommend that it be checked independently."

Although the results for the rigidly supported structures considered so far may not be totally representative of those for the actual, elastically supported systems, it should be clear from the information presented that the variability in spectral ordinates referred to in the May 12, 1988 meeting is materially smaller than that indicated by the coefficients of variation presented herein.

The sections of the PG&E's Final Report on the Long Term Seismic Studies dealing with the deterministic assessment of plant safety does not address the magnitude of the responses experienced by the containment and internal structures. As a result, the information presented in the preceding sections cannot be compared with corresponding data obtained by PG&E.

Response of Elastically Supported System

For the solutions presented in this section, the foundation of the structure is presumed to rest at the surface of a homogeneous, viscoelastic halfspace for which the velocity of shear wave propagation $v_s = 3{,}300$ ft/sec. Both the containment structure and its internal are presumed to deform in their fixed-base fundamental natural modes. Thus, the structure-foundation system is analyzed as a four-degree-of-freedom system, of which two degrees refer to the lateral and rocking motions of the foundation. Poisson's ratio for the supporting medium is taken as $\nu_s = 0.45$; and the unit weight and material damping factor for the medium are taken as $\gamma_s = 140$ lb/ft^3 and as $\tan\delta = 0.10$, respectively (The quantity $\tan\delta$ is twice as large as the damping factor, D_s, used by some authors.). The structural damping for each fixed-base natural mode of vibration is taken, as before, as 5 percent of the critical value.

The free-field ground motion beneath the foundation mat is considered to be non-uniform, and its spatial variation is defined by a coherence function, Γ, of the form

$$\Gamma = \exp\left\{-\left(\frac{\gamma\omega|\vec{r}_1 - \vec{r}_2|}{v_s}\right)^2\right\}$$

in which ω = the circular frequency of the relevant Fourier component of the ground motion; $\vec{r}_1$ and $\vec{r}_2$ are the position vectors for two arbitrary points; $|\vec{r}_1 - \vec{r}_2|$ is the distance between the two points; and γ = a dimensionless incoherence parameter which, for the solutions presented herein, is taken as 0.3.

The responses of the structure were evaluated in the frequency domain for Records No. 7, 9 and 12 of the empirical set identified in Table 1. The foundation impedances were determined from the empirical relations of Veletsos and Verbic (Ref. 5), and the effect of spatial variation of the ground motion was provided for by use of an approximate, semi-deterministic method of analysis which will be described elsewhere.

The maximum values of the critical responses for both the external and internal structures are presented in Table 13 for the following three conditions:

- Without any soil-structure interaction (SSI), i.e., considering the structures to be rigidly supported at the base;
- With inertial interaction (II) only, i.e., providing for the dynamic coupling between the structure, foundation and supporting medium, but disregarding the spatial variation of the free-field ground motion; and
- With total soil-structure interaction, i.e., considering both the II effects and the so-called kinematic interaction (KI) effects, which are associated with the spatial variation of the free-field ground motion.

The response accelerations in these solutions were evaluated for points located along the center line of the structure; accordingly, they are not influenced by the torsional response induced by the spatial variation of ground motion.

It is well known (e.g., Ref. 2) that soil-structure interaction may increase or decrease the maximum response of a structure depending on the characteristics of the free-field ground motion and the characteristics of the structure itself. For the conditions examined herein, inertial interaction increases all peak responses of the internal structure but decreases some of the maximum responses of the containment structure. The changes range from a maximum reduction of 18 percent to a maximum increase of about 40 percent. These results are obtained for the containment shell subjected to Records 7 and 9, respectively.

Floor Response Spectra

In Figs. 11a through 11c are presented pseudo-acceleration response spectra for light equipment items attached along the centerline of the structure at the following locations: (a) the foundation mat; (b) the top of the internal structure; and (c) the springline of the containment structure. The damping for the equipment items in these solutions is taken as 5 percent of the critical value. The corresponding spectra for 2 percent of critical damping are presented in Figs. 12a through 12c. Note that the peak-to-peak variability of the individual spectra and the spread between spectra are substantial. Note further that the spectra for 2 percent of critical damping are substantially higher than those for 5 percent damping.

The mean floor response spectra for the set of three records and each of the two damping values considered are displayed in Figs. 13a through 13c. It is observed that the spectral ordinates are generally sensitive both to the natural frequency of the system and the amount of damping involved, the sensitivity to natural frequency being particularly prominent for equipment items located at or near the springline of the containment structure.

Although a direct comparison of the spectra presented herein with those presented in Chapter 7 of the PG&E Final Report (Ref. 1) is strictly not possible, the results presented here appear to be generally higher than those presented in the PG&E report. In making this comparison, it is important to keep in mind that whereas the data in Figs. 13 refer to the mean

values of peak response, those in the PG&E report presumably correspond to the 84 percentile level of non-exceedance.

As an indication of the relative importance of the inertial and kinematic interaction effects, the floor response spectra obtained for ground motion Record 7 are compared in Figs. 14a through 14c with the corresponding spectra computed for no soil-structure interaction and for inertial interaction only. These particular spectra are for equipment items with 5 percent of critical damping. It is observed that inertial interaction leads to a leftward shift in the floor response spectra and to either an increase or reduction in the absolute maximum response, whereas kinematic interaction leads to a reduction in response, the reduction being generally small and most pronounced for high-frequency systems. For the conditions examined herein, the effects of inertial interaction are substantially greater than those of kinematic interaction. The relative magnitudes of the two effects on the mean values of floor response spectra for the three ground motion records considered are shown in Figs. 15a through 15c. Soil-structure interaction has a relatively minor influence on the absolute maximum spectral values in this case.

SUMMARY AND CONCLUSIONS

The principal findings of the studies reported herein may be summarized as follows:

Ground Motion Studies

1. The analyses of ground motion records and of the associated response spectra presented provide the basis for an independent assessment of the adequacy of the ground motions employed in PG&E's deterministic studies. The results of such an assessment have been described in Ref. 3.

2. Both the mean and mean plus one standard deviation levels of non-exceedance of the response spectra for the numerically generated ground motion records are materially lower than those for the empirical records. Accordingly, enriching the empirical records with numerical records would tend to decrease the magnitudes of the resulting response spectra.

3. The shapes of the response spectra for the mean and mean plus one standard deviation levels of non-exceedance are quite similar. Accordingly, responses evaluated for one level of non-exceedance may be converted readily and with reasonable accuracy to a different level. This is true both of the empirical records and of the numerical records.

4. For the particular set of empirical records examined, both the absolute maximum spectral acceleration and the average value within the 3 cps to 7.8 cps frequency range were found to be insensitive to the weighting factors used to account for differences in tectonic setting, topographic conditions, and source to site geometry.

Analyses of Containment Structure

1. The fixed-base responses of the containment and internal structures may be evaluated with good accuracy by considering only the contributions of their fundamental modes of vibration.

2. For the ensembles of ground motions examined, the coefficients of variation for the maximum values of critical responses for these structures were found to be in good agreement with those obtained from the response spectra for single-degree-of-freedom systems using the fundamental natural frequencies of the systems involved. For the set of empirical records considered, the values of this coefficient were approximately 0.30 for the external structure and 0.49 for the internal structure. The corresponding values for the numerical set of records were 0.40 and 0.32, respectively. These values are substantially higher than the "peak-to-peak variability" of spectral ordinates referred to in the May 12, 1988 meeting of PG&E and NRC representatives in Rockville, Maryland.

3. The maximum values of such global forces as the base shear and base moment for these structures cannot be compared with those computed by PG&E, as the latter values are not included in PG&E's Final Report.

4. For the conditions examined herein, soil-structure interaction increases the maximum responses of the internal structure and may increase or decrease the corresponding responses of the containment structure. These changes, which range from a maximum increase of 40 percent to a

maximum reduction of 18 percent, are due mainly to inertial interaction effects. The kinematic interaction effects are normally associated with a reduction in response, and they are generally small, particularly for the containment structure.

5. The floor response spectra for the different ground motions examined exhibit considerable spread, and their magnitudes appear to be higher than those used in PG&E's deterministic studies.

6. The variability in the floor response spectra due to the effects of soil-structure interaction are generally small compared to that due to the uncertainties involved in the definition of the free-field ground motion.

REFERENCES

1. Pacific Gas & Electric Company, "Final Report of the Diablo Canyon Long Term Seismic Program," July, 1988.

2. Veletsos, A. S., "Some Perspectives on Dynamics of Soil-Structure Interaction," Proceedings of Workshop on Soil-Structure Interaction, H. L. Graves and A. J. Philippacopoulos, Editors, NUREG/CP-0054, BNL-NUREG-52011, Superintendent of Documents, U. S. Printing Office, P.O. Box 37082, Washington, D. C., 1986, pp. 213-232.

3. Veletsos, A. S., "Comments on PG&E's Final Report on Long Term Seismic Program for Diablo Canyon Plant," Letter Report to Dr. M. Reich of Brookhaven National Laboratory, Long Island, New York, November 4, 1988.

4. Veletsos, A. S. and Tang, Y., "SSI Studies for Containment Structure of Diablo Canyon Power Plant," Summary Report, Brookhaven National Laboratory, Long Island, New York, November 3, 1987.

5. Veletsos, A. S. and Verbic, "Vibration of Viscoelastic Foundations," Journal of Earthquake engineering and Structural Dynamics, Vol. 2, 1973, pp. 87-102.

TABLE 1 Maximum Values of Acceleration, Velocity and Displacement for Empirical Ground Motions Considered

Earthquake; Record Name; Date	Record No.	Component	$\ddot{x}_g$ (in g's)	$\dot{x}_g$ (in/sec)	x_g (in)
Tabas, Iran; Tabas	1	Long.	0.812	36.40	18.44
16 September 1978	2	Trans.	0.705	40.92	35.57
San Fernando; Pacoima Dam	3	S16E	1.170	44.98	13.96
9 Feb. 1971	4	S74W	1.075	22.97	7.82
San Fernando; Lake Hughes No. 12	5	N21E	0.902	15.39	2.04
9 Feb. 1971	6	N69W	0.711	12.02	3.27
San Fernando; Castaic	7	N69W	0.853	41.40	11.84
9 Feb. 1971	8	N21E	1.025	22.91	6.56
Imperial Valley; Differential Array	9	N00E	0.567	12.50	2.90
15 Oct. 1979	10	N90W	0.514	15.84	5.19
Imperial Valley; El Centro No. 4	11	S50W	0.483	17.84	11.14
15 Oct. 1979	12	S40E	0.693	15.90	3.05
Morgan Hill; Coyote Lake Dam	13	N75W	1.663	48.73	11.44
24 April 1984	14	S15W	0.886	33.77	14.26
Coalinga; Pleasant Valley Pump Plant	15	045	0.854	40.74	8.24
2 May 1983	16	135	0.738	21.79	3.33
Nahanni; Site 1	17	N10W	1.101	18.98	16.56
23 Dec. 1985	18	280	1.345	18.64	19.67
Gazli; Karakyr Point	19	East	0.699	18.97	3.96
17 May 1976	20	North	0.655	17.84	3.24
Parkfield; Temblor	21	N65N	0.550	18.89	8.65
27 June 1966	22	S25W	0.703	23.11	10.88
Tabas, Iran; Dayhook	23	Trans.	0.683	17.83	11.00
(Scaled by 1.7)	24	Long.	0.635	20.12	46.04
Mean Values			0.834	24.94	11.63
Mean plus Sigma Values			1.108	35.88	21.87

TABLE 2 Maximum Values of Acceleration, Velocity and Displacement Histories for Numerically Generated Ground Motion

Record No.	Name and Direction	$\ddot{x}_g$ (in g's)	$\dot{x}_g$ (in/sec)	x_g (in)
25	FILE1-C2E	0.584	7.64	17.19*
26	FILE1-C2N	0.474	8.93	13.44*
27	FILE1-I3N	0.521	12.74	6.11*
28	FILE1-I3E	0.503	13.26	13.06*
29	FILE2-I9N	0.429	12.40	39.63*
30	FILE2-I9E	0.584	7.64	17.19*
31	FILE3-C6N	0.514	9.66*	126.48*
32	FILE3-C6E	0.524	21.64*	290.93*
33	FILE3-I6N	0.516	13.67*	178.69*
34	FILE3-I6E	0.411	31.54*	384.71*
35	FILE4-C4N	1.052	14.92	0.96
36	FILE4-C4E	0.844	18.74	1.82
37	FILE4-C5N	0.728	11.79	0.97
38	FILE4-C5E	0.585	9.55	0.95
39	FILE4-I7N	0.312	7.86	0.76
40	FILE4-I7E	0.363	7.57	0.95
41	FILE5-C5N	0.604	10.89	0.82
42	FILE5-C5E	0.750	15.17	1.00
43	FILE5-I6E	0.441	9.08	1.09
44	FILE5-I6E	0.330	8.08	1.21
45	FILE6-C4N	0.800	13.52	18.69*
46	FILE6-C4E	0.772	14.64	1.26
47	FILE6-I1N	0.591	14.56	1.61
48	FILE6-I1E	0.486	11.32	1.17
49	FILE7-C1N	0.611	8.98	0.65
50	FILE7-C1E	0.641	8.94	0.82
51	FILE8-C2N	0.690	10.25	2.18*
52	FILE8-C2E	0.703	10.24	2.08*
	Mean Values	0.584		
	Mean Plus Sigma Values	0.748		

*Records not properly balanced

TABLE 3 Effect of Damping on Mean Spectral Values of Pseudoacceleration within Frequency Range f = 3 - 7.8 Hz

Record No.	Mean Value of A, in g's				Record No.	Mean Value of A, in g's			
	$\zeta = 0.02$	$\zeta = 0.04$	$\zeta = 0.05$	$\zeta = 0.07$		$\zeta = 0.02$	$\zeta = 0.04$	$\zeta = 0.05$	$\zeta = 0.07$
	Empirical Records					Numerical Records			
1	3.22	2.49	2.28	1.98	25	2.43	1.85	1.70	1.50
2	3.34	2.73	2.53	2.20	26	2.15	1.63	1.48	1.27
3	2.68	2.14	1.98	1.77	27	1.46	1.20	1.12	1.02
4	2.47	2.01	1.88	1.69	28	1.36	1.12	1.04	0.92
5	3.19	2.63	2.45	2.21	29	1.25	1.03	0.97	0.88
6	3.12	2.53	2.33	2.06	30	2.43	1.85	1.70	1.50
7	2.17	1.79	1.67	1.50	31	2.00	1.53	1.40	1.25
8	2.76	2.32	2.19	1.98	32	2.30	1.82	1.67	1.45
9	1.96	1.52	1.38	1.20	33	1.49	1.20	1.12	1.00
10	2.27	1.74	1.58	1.35	34	1.48	1.15	1.05	0.92
11	1.28	1.05	1.00	0.92	35	3.12	2.55	2.37	3.08
12	1.88	1.61	1.53	1.40	36	2.70	2.12	1.96	1.76
13	2.58	2.33	2.28	2.23	37	2.69	2.16	1.99	1.73
14	2.28	1.99	1.88	1.71	38	2.10	1.62	1.47	1.27
15	2.19	1.76	1.63	1.45	39	1.16	0.90	0.82	0.71
16	3.25	2.59	2.38	2.06	40	1.13	0.92	0.86	0.77
17	2.67	2.30	2.17	1.95	41	2.47	1.87	1.71	1.48
18	2.12	1.87	1.78	1.62	42	2.34	1.90	1.76	1.57
19	1.69	1.41	1.33	1.21	43	1.52	1.20	1.10	0.96
20	1.74	1.39	1.29	1.16	44	1.17	0.92	0.84	0.72
21	1.48	1.33	1.28	1.20	45	3.36	2.60	2.36	2.01
22	1.45	1.32	1.28	1.22	46	2.53	2.02	1.90	1.74
23	1.48	1.16	1.08	0.97	47	1.84	1.49	1.38	1.20
24	2.01	1.77	1.67	1.51	48	1.25	1.04	0.99	0.90
All Records	2.30	1.95	1.79	1.61	49	2.74	2.12	1.91	1.63
					50	2.16	1.70	1.55	1.36
					51	3.04	2.32	2.11	1.81
					52	2.76	2.08	1.90	1.65
					All Records	2.09	1.64	1.51	1.32

TABLE 4 Mean Values of Pseudoacceleration, A, within Indicated Frequency Ranges; Systems with $\zeta = 0.05$

Record No.	Mean Value of A, in g's, within Frequency Range		$\ddot{x}_g$ in g's	Record No.	Mean Value of A, in g's, within Frequency Range		$\ddot{x}_g$ in g's
	3 - 7.8 Hz	4.8 - 14.7 Hz			3 - 7.8 Hz	4.8 - 14.7 Hz	
	Empirical Records				Numerical Records		
1	2.28	1.98	0.812	25	1.70	1.54	0.584
2	2.53	2.10	0.705	26	1.48	1.36	0.474
3	1.98	1.81	1.170	27	1.12	0.98	0.521
4	1.88	1.77	1.075	28	1.04	0.94	0.503
5	2.45	2.03	0.902	29	0.97	0.77	0.429
6	2.33	1.70	0.711	30	1.70	1.54	0.584
7	1.67	1.48	0.853	31	1.40	1.14	0.514
8	2.19	1.71	1.025	32	1.67	1.21	0.524
9	1.38	1.21	0.567	33	1.12	0.85	0.516
10	1.58	1.51	0.514	34	1.05	0.87	0.411
11	1.00	0.85	0.483	35	2.37	2.04	1.052
12	1.53	1.36	0.693	36	1.96	1.59	0.844
13	2.28	2.06	1.663	37	1.99	1.78	0.728
14	1.88	1.25	0.886	38	1.47	1.22	0.585
15	1.63	1.51	0.854	39	0.82	0.83	0.312
16	2.38	1.53	0.738	40	0.86	0.70	0.363
17	2.17	2.46	1.101	41	1.71	1.44	0.604
18	1.78	2.32	1.345	42	1.76	1.42	0.750
19	1.33	1.55	0.699	43	1.10	1.00	0.441
20	1.29	1.71	0.655	44	0.84	0.78	0.330
21	1.28	0.85	0.550	45	2.36	2.11	0.800
22	1.28	1.02	0.703	46	1.90	1.46	0.772
23	1.08	1.10	0.683	47	1.38	1.15	0.591
24	1.67	1.66	0.635	48	0.99	0.88	0.486
All Records	1.79	1.61	0.834	49	1.91	1.72	0.611
				50	1.55	1.51	0.641
				51	2.11	1.93	0.690
				52	1.90	1.89	0.703
				All Records	1.51	1.31	0.584

TABLE 5 PROPERTIES OF THE STRUCTURAL MODELS OF THE CONTAINMENT BUILDING AND INTERNALS

Joint Properties			Member Properties			
Mass No.	Weight (kips)		Location between Joint No.	Area (ft^2)	Shear Area (ft^2)	Moment of Inertia x 10^{-6} (ft^4)
1	2421.44					
			1 to 2	1119	560	0.494
2	3815.70					
			2 to 3	1119	560	1.604
3	4169.90					
		C	3 to 4	1412	706	3.260
4	6417.46	O				
		N	4 to 5	1656	828	4.280
5	6407.80	T				
		A	5 to 6			
6	6388.48	I				
		N	6 to 7			
7	6481.86	M				
		E	7 to 8			
8	5924.80	N				
		T	8 to 9			
9	5393.50					
			9 to 10			
10	-			(BASE)		
		I			1172 For motion in x-direction	1.720 (E-W)
	13,470	N	10 to 11	2013		
		T			1192 For motion in y-Direction	1.913 (N-S)
11	~~13647.0~~	E				
		R			816 For motion in x-Direction	1.785 (E-W)
		N	11 to 12	1991		
		A			1372 For motion in y-Direction	2.036 (N-S)
12	16903.0	L				

Note:

Modulus of Elasticity: Containment $E_c = 5.1 \times 10^5$ ksf, $G_c = 2.04 \times 10^5$ ksf
Internal $E_i = 6.5 \times 10^5$ ksf, $G_i = 2.61 \times 10^5$ ksf

TABLE 6 SOIL FOUNDATION SYSTEM PROPERTIES

A. Soil Layer Profile

Layer No.	Elev. (ft)	Layer Thickness (ft)	Shear Wave Velocity (ft/sec)	Poisson's Ratio	Mass Density (k-sec2/ft)4	Damping (%)
	85'-0"					
1		10	2600	0.45	.00435	2.0
	75'-0"					
2		20	3300	0.43	.00435	2.0
	55'-0"					
3		125	4000	0.37	.00444	2.0
	-70'-0"					
4		∞	4800	0.36	.00436	2.0

B. Basemat Lumped Masses

	Radius (ft)	Mass (k-sec^2/ft)			Mass Moment of Inertia X10^5 (k-ft-sec^2)		
		X	Y	Z	X	Y	Z
Foundation	76.5	1544	1544	1544	55.6	53.6	39.7

TABLE 7 Fixed-Base Natural Frequencies and Modes of Containment Structure and its Internal Structures in N-S Direction

Quantity	Node	First	Second	Third
			External Structure	
Natural Frequency, in cps		4.68	13.96	24.86
Natural Mode	1	1.000	1.000	1.000
	2	0.897	0.639	0.346
	3	0.826	0.362	-0.312
	4	0.699	-0.101	-0.674
	5	0.572	-0.443	-0.571
	6	0.442	-0.644	-0.0335
	7	0.306	-0.669	0.559
	8	0.175	-0.505	0.732
	9	0.0767	-0.262	0.456
	10	0.000	0.000	0.000
			Internal Structure	
Natural Frequency, in cps		13.92	38.53	
Natural Mode	12	1.000	1.000	
	11	0.390	-3.215	
	10	0	0	

TABLE 8 Modal Weights and Heights of Containment Structure in its Fixed-Base Condition

Quantity	Mode 1	Mode 2	Mode 3	Mode 4
		External Structure		
Modal Weight, W_j^*, in 10^4 kips	3.592	0.749	0.205	0.089
Modal Height, h_j^*, in ft	134.82	0.12	13.05	-0.96
		Internal Structure		
Modal Weight, W_j^*, in 10^4 kips	2.590	0.447		
Modal Height, h_j^*, in ft	41.13	3.47		

TABLE 9 Mean and Mean Plus Sigma Values of Response for Containment Structure When Rigidly Supported at Base; for 24 Empirical Records, $\zeta_i = 0.05$

No. of Modes Considered	External Structure				Internal Structure			
	Mean Value	Median Value	Mean + Sigma	84% Value	Mean Value	Median Value	Mean + Sigma	84% Value
			Base Shear Above Mat, in 10^5 kips					
1	0.676	0.650	0.881	0.886	0.330	0.289	0.490	0.433
2	0.705	0.682	0.909	0.920	0.357	0.318	0.517	0.474
All	0.717	0.697	0.920	0.945				
			Base Shear Below Mat, in 10^5 kips					
1	1.083	1.059	1.391	1.330	Same as for			
All	1.179	1.181	1.519	1.435	External Structure			
			Base Moment Above Mat, in 10^7 kip-ft					
1	0.911	0.875	1.186	1.193	0.136	0.119	0.202	0.178
2	0.911	0.875	1.186	1.193	0.137	0.120	0.203	0.179
All	0.911	0.878	1.186	1.194				
			Base Moment Below Mat, in 10^7 kip-ft					
1	1.157	1.126	1.481	1.549	Same as for			
All	1.170	1.139	1.496	1.569	External Structure			
			Displacement of Springline Relative to Moving Base, in inches					
1	0.892	0.857	1.162	1.168				
2	0.893	0.858	1.162	1.171				
All	0.892	0.855	1.162	1.169				
			Displacement of Top of Internal Relative to Moving Base, in inches					
1					0.075	0.066	0.112	0.098
All					0.075	0.065	0.111	0.098
			Acceleration of Base, in g's					
	0.834	0.725	1.108	1.080	Same as for External			
			Absolute Acceleration at Springline, in g's					
1	1.999	1.921	2.602	2.616				
2	2.020	1.949	2.623	2.614				
All	2.003	1.904	2.618	2.614				
			Absolute Acceleration at Top of Internal, in g's					
1					1.495	1.318	2.223	1.973
All					1.394	1.191	2.123	1.810

TABLE 10 Mean and Mean Plus Sigma Values of Response for Containment Structure When Rigidly Supported at Base; for 28 Numerically Generated Records, $\zeta_i = 0.05$

No. of Modes Considered	External Structure				Internal Structure			
	Mean Value	Median Value	Mean + Sigma	84% Value	Mean Value	Median Value	Mean + Sigma	84% Value
			Base Shear Above Mat, in 10^5 kips					
1	0.604	0.587	0.846	0.843	0.250	0.237	0.331	0.324
2	0.622	0.632	0.861	0.877	0.271	0.259	0.359	0.354
All	0.633	0.647	0.874	0.892				
			Base Shear Below Mat, in 10^5 kips					
1	0.894	0.869	1.200	1.255	Same as for			
All	0.967	0.928	1.293	1.356	External Structure			
			Base Moment Above Mat, in 10^7 kip-ft					
1	0.808	0.791	1.127	1.038	0.103	0.097	0.136	0.133
2	0.814	0.791	1.140	1.136	0.104	0.098	0.137	0.134
All	0.815	0.791	1.140	1.137				
			Base Moment Below Mat, in 10^7 kip-ft					
1	1.015	1.043	1.395	1.427	Same as for			
All	1.025	1.056	1.406	1.439	External Structure			
			Displacement of Springline Relative to Moving Base, in inches					
1	0.797	0.774	1.116	1.112				
2	0.798	0.775	1.117	1.114				
All	0.797	0.775	1.116	1.112				
			Displacement of Top of Internal Relative to Moving Base, in inches					
1					0.057	0.054	0.075	0.074
All					0.057	0.053	0.075	0.073
			Acceleration of Base, in g's					
	0.584	0.584	0.748	0.740	Same as for External			
			Absolute Acceleration at Springline, in g's					
1	1.788	1.738	2.501	2.505				
2	1.798	1.779	2.516	2.539				
All	1.780	1.726	2.485	2.481				
			Absolute Acceleration at Top of Internal, in g's					
1					1.134	1.076	1.497	1.462
All					1.058	0.977	1.398	1.358

TABLE 11 Comparison of Mean and Mean Plus Sigma Values of Maximum Response for Containment Structure When Rigidly Supported at Base; Empirical and Numerically Generated Ensembles of Records, $\zeta_i = 0.05$

Record	External Structure		Internal Structure	
	Mean Value	Mean + Sigma	Mean Value	Mean + Sigma
	Base Shear Above Mat, in 10^5 kips			
Empirical	0.717	0.920	0.357	0.517
Numerical	0.633	0.874	0.271	0.359
	Base Shear Below Mat, in 10^5 kips			
Empirical	1.179	1.519	Same as for External	
Numerical	0.967	1.293		
	Base Moment Above Mat, in 10^7 kip-ft			
Empirical	0.911	1.186	0.137	0.203
Numerical	0.815	1.140	0.104	0.137
	Base Moment Below Mat, in 10^7 kip-ft			
Empirical	1.170	1.496	Same as for	
Numerical	1.025	1.406	External Structure	
	Displacement of Springline Relative to Moving Base, in inches			
Empirical	0.892	1.162		
Numerical	0.797	1.116		
	Displacement of Top of Internal Relative to Moving Base, in inches			
Empirical			0.075	0.111
Numerical			0.057	0.075
	Acceleration of Base, in g's			
Empirical	0.834	1.108	Same as for	
Numerical	0.584	0.748	External Structure	
	Absolute Acceleration at Springline, in g's			
Empirical	2.003	2.618		
Numerical	1.780	2.485		
	Absolute Acceleration at Top of Internal, in g's			
Empirical			1.394	2.123
Numerical			1.058	1.398

TABLE 12 Coefficients of Variation for Maximum Responses of Rigidly Supported Containment Structure Subjected to Empirical and Numerically Generated Ensembles of Records; $\zeta_i = 0.05$

Response Quantity	External Structure		Internal Structure		Entire Structure	
	Empirical	Numerical	Empirical	Numerical	Empirical	Numerical
Base Shear:						
Above Mat	0.283	0.381	0.448	0.325		
Below Mat					0.288	0.337
Base Moment:						
Above Mat	0.302	0.399	0.482	0.317		
Below Mat					0.279	0.372
Relative Displacement:						
Springline	0.303	0.400				
Top of Internal			0.480	0.316		
Acceleration:						
Base					0.329	0.281
Springline	0.307	0.396				
Top of Internal			0.523	0.321		
Estimates Based on SDF Approximation	0.30	0.40	0.49	0.32		

TABLE 13 Effects of Soil-Structure Interaction on Maximum N-S Responses of Containment Structure; for 3 Empirical Records, $\zeta = 0.05$, $\gamma = 0.3$, $\tan\delta = 0.1$

Record	External Structure			Internal Structure		
	No SSI	Only II	Total SSI	No SSI	Only II	Total SSI
	Base Shear Above Foundation Mat, in 10^5 kips					
7	1.110	0.932	0.906	0.342	0.399	0.377
9	0.688	0.972	0.946	0.281	0.364	0.346
12	0.975	0.960	0.938	0.321	0.391	0.365
	Base Shear Below Foundation Mat, in 10^5 kips					
7	1.391	1.634	1.589	Same as for External Structure		
9	1.204	1.639	1.594			
12	1.514	1.567	1.525			
	Base Moment Above Foundation Mat, in 10^7 k-ft					
7	1.492	1.252	1.217	0.141	0.164	0.155
9	0.925	1.306	1.271	0.115	0.150	0.142
12	1.310	1.290	1.261	0.132	0.161	0.150
	Base Moment Below Foundation Mat, in 10^7 k-ft					
7	1.771	1.562	1.523	Same as for External Structure		
9	1.217	1.740	1.698			
12	1.664	1.718	1.687			
	Displacement of Springline Relative to Moving Base, in inches					
7	1.461	1.226	1.192			
9	0.906	1.279	1.245			
12	1.282	1.263	1.235			
	Displacement of Top of Internal Relative to Moving Base, in inches					
7				0.0779	0.0909	0.0859
9				0.0639	0.0828	0.0788
12				0.0732	0.0890	0.0832
	Acceleration of Base, in g's					
7	1.206	1.225	1.177			
9	0.983	1.069	1.028			
12	1.083	1.165	1.133			
	Absolute Acceleration at Springline, in g's					
7	3.262	2.738	2.662			
9	2.023	2.856	2.780			
12	2.864	2.821	2.758			
	Absolute Acceleration at Top of Internal, in g's					
7				1.543	1.800	1.701
9				1.266	1.641	1.562
12				1.450	1.764	1.648

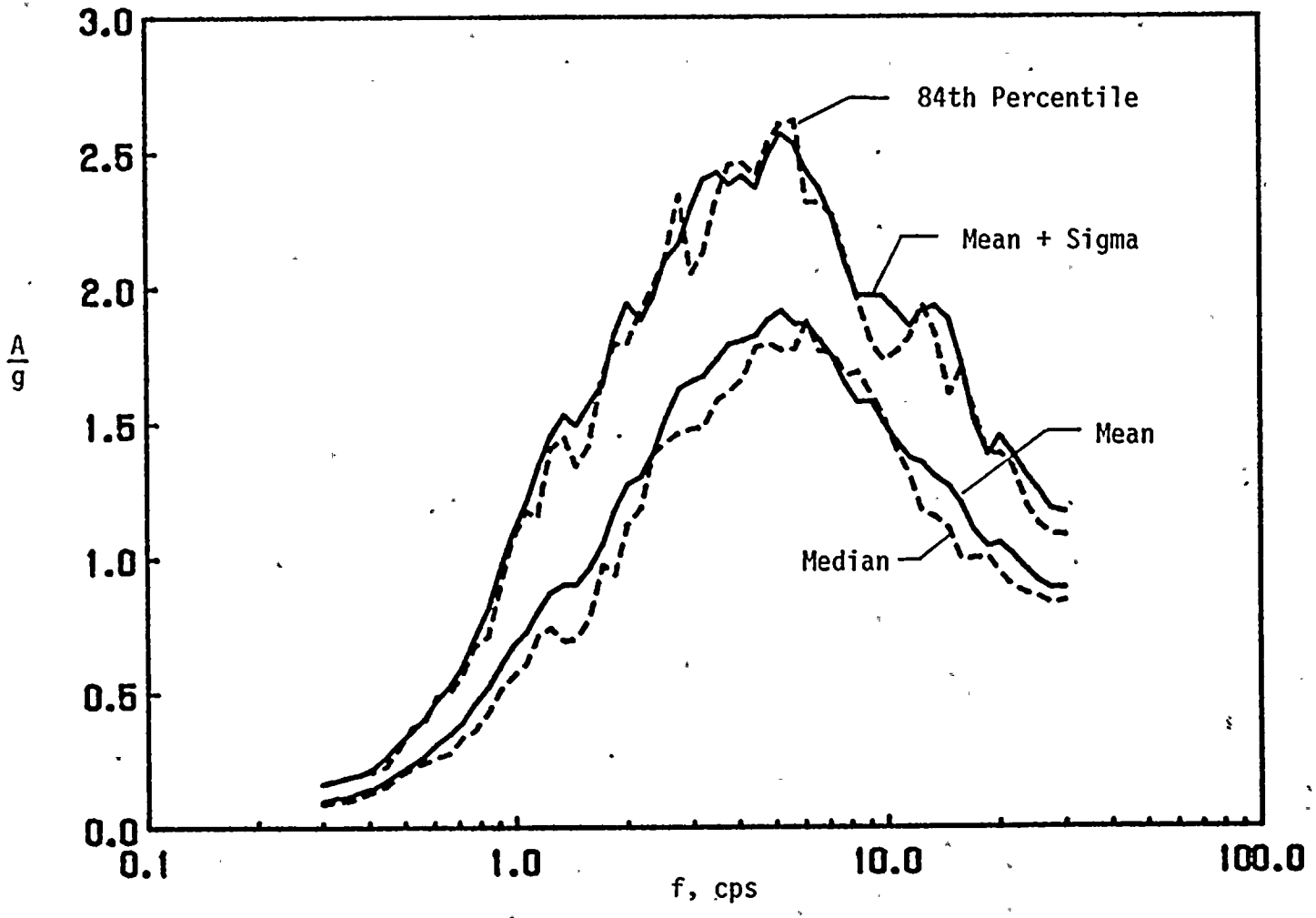

FIG. 1 Pseudo-acceleration Response Spectra for Ensemble of Empirical Ground Motion Records; Systems with $\zeta = 0.05$

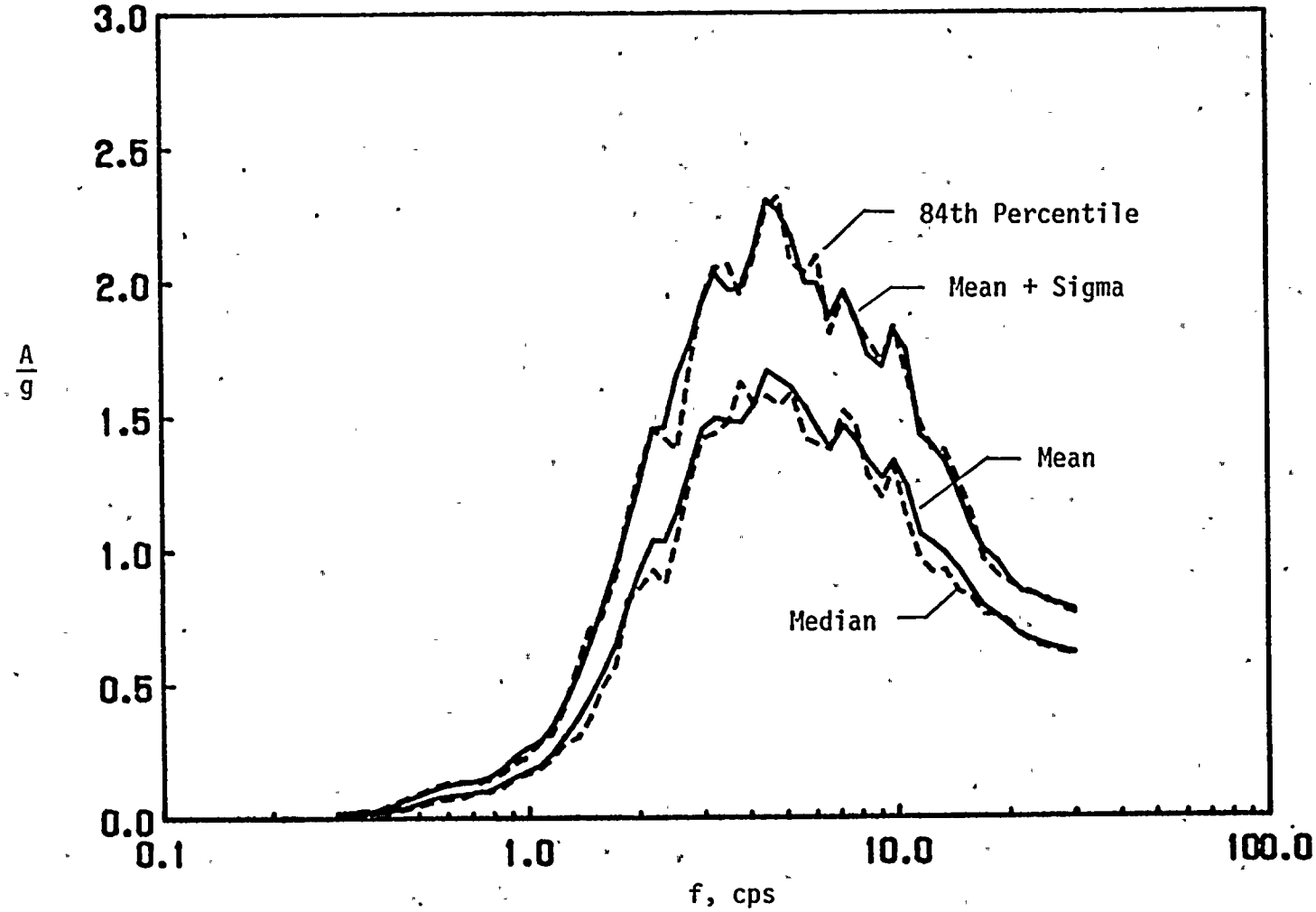

FIG. 2 Pseudo-acceleration Response Spectra for Ensemble of Numerically Generated Ground Motion Records; Systems with $\zeta = 0.05$

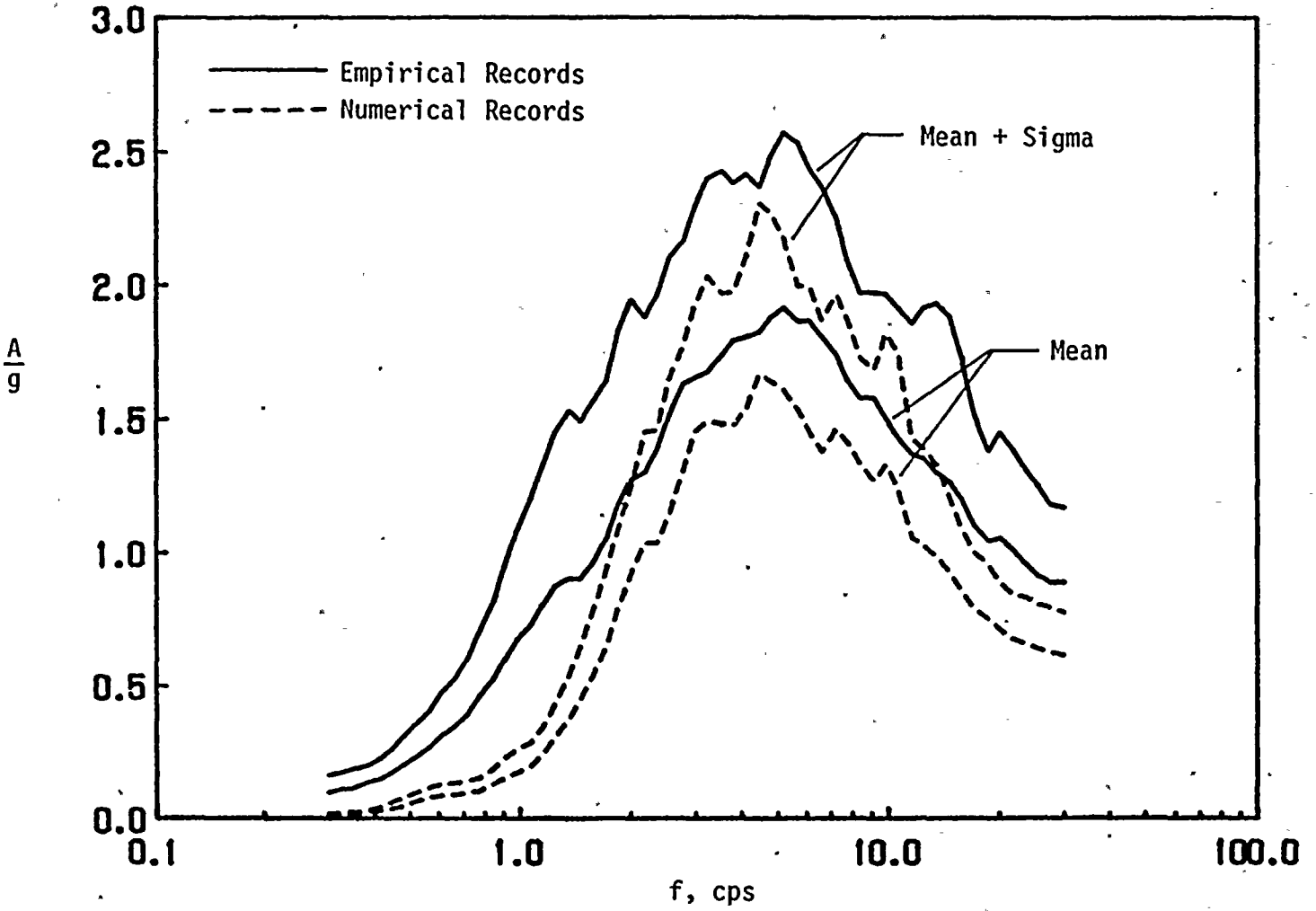

FIG. 3 Comparison of Mean and Mean Plus One Standard Deviation Response Spectra for Ensembles of Empirical and Numerical Records; Systems with $\zeta = 0.05$

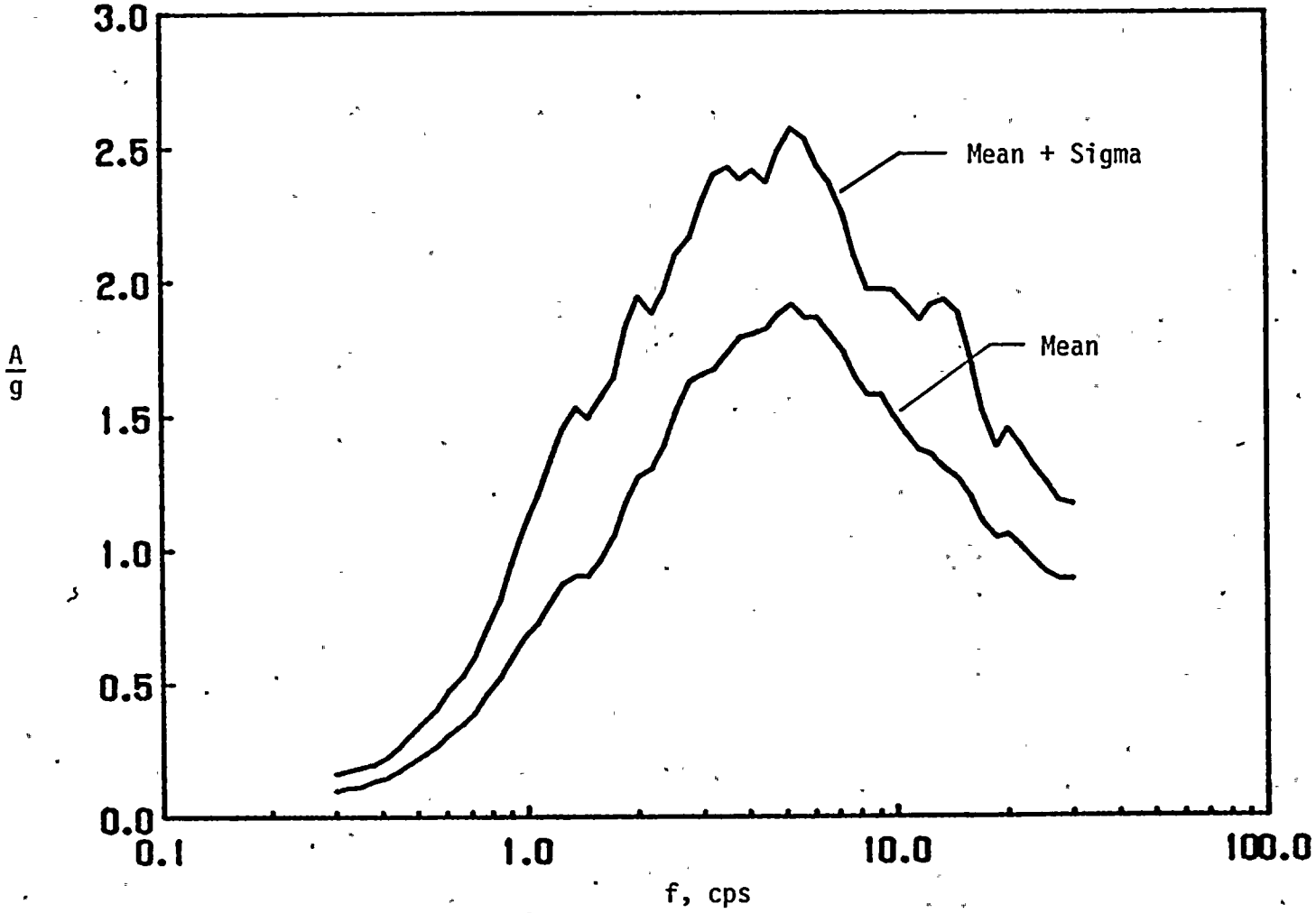

FIG. 4 Comparison of Pseudo-acceleration Response Spectra for Mean and Mean Plus One Standard Deviation Levels of Non-Exceedance for Ensemble of Empirical Records; Systems with $\zeta = 0.05$

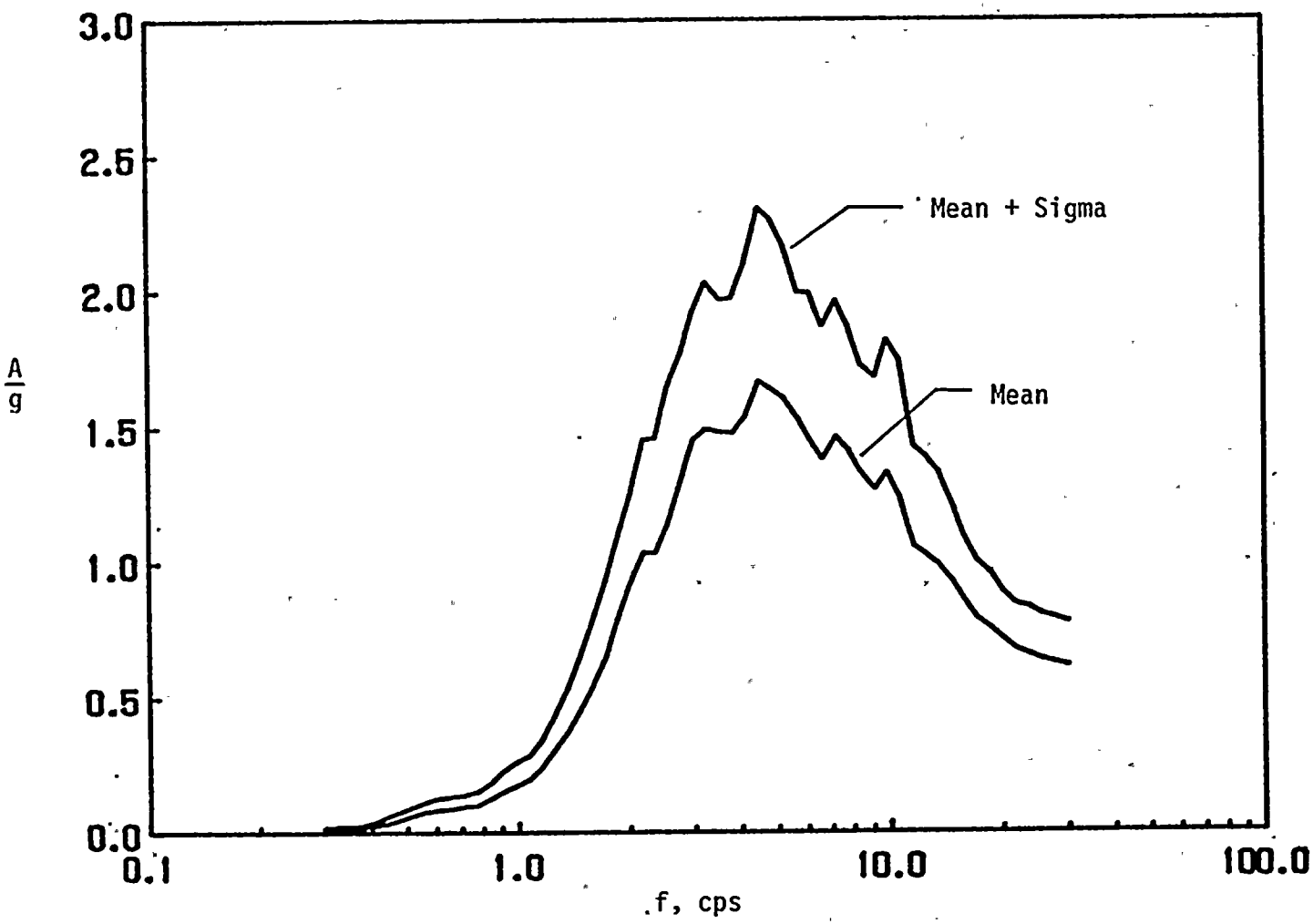

FIG. 5 Comparison of Pseudo-acceleration Response Spectra for Mean and Mean Plus One Standard Deviation Levels of Non-Exceedance for Ensemble of Numerically Generated Records; Systems with $\zeta = 0.05$

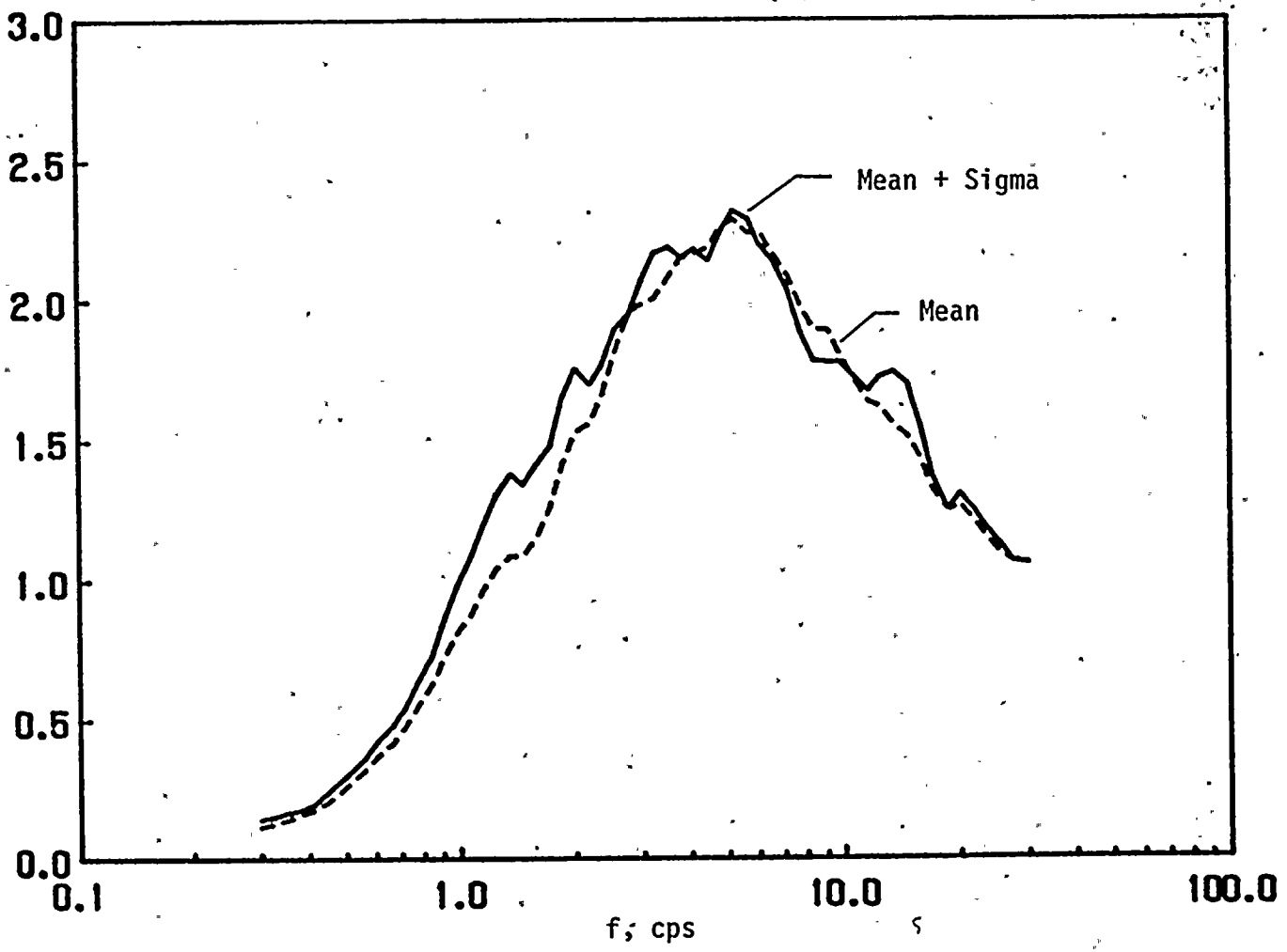

FIG. 6 Normalized Pseudo-acceleration Response Spectra for Mean and Mean Plus One Standard Deviation Levels of Non-Exceedance for Ensemble of Empirical Records; Systems with $\zeta = 0.05$

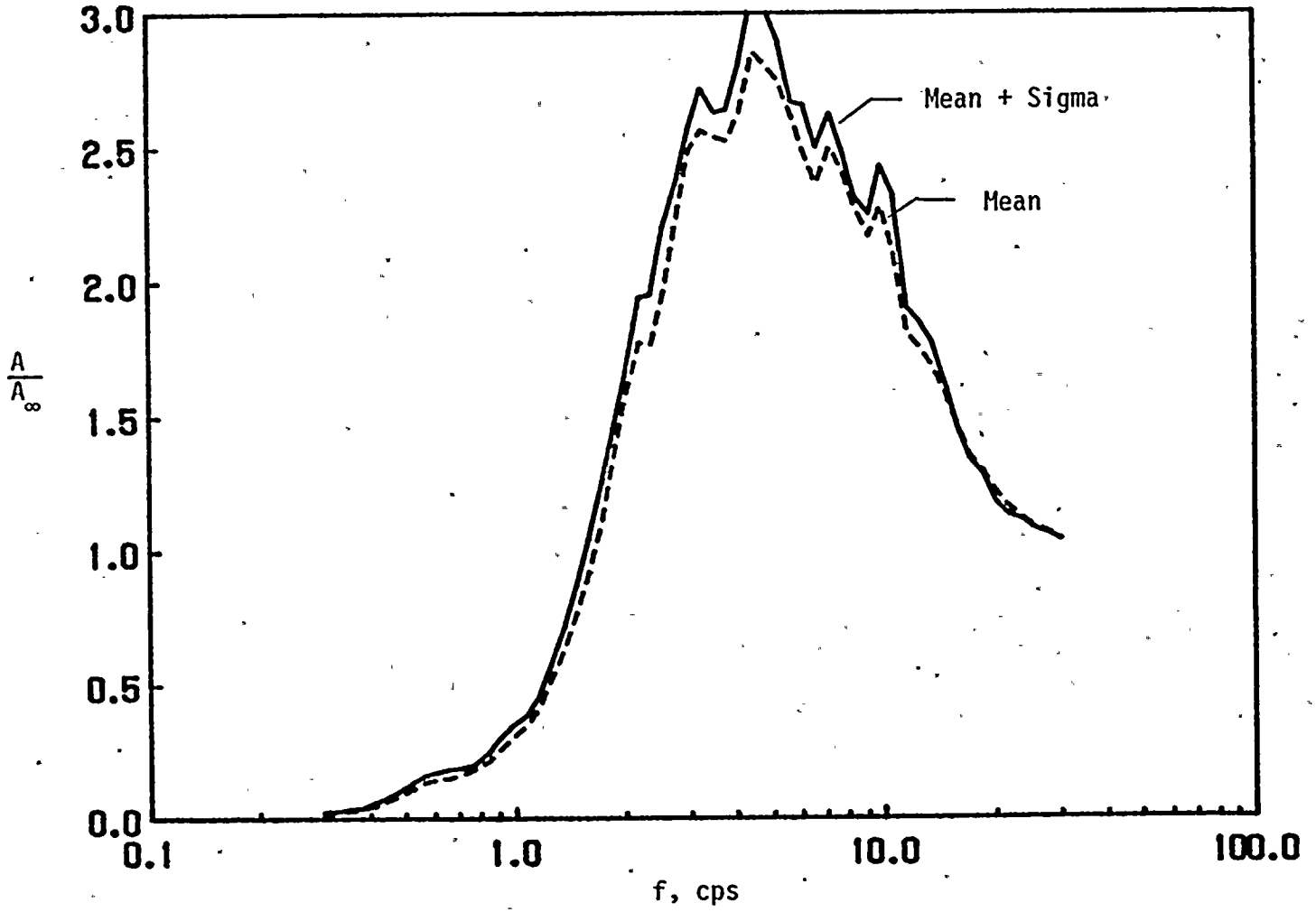

FIG. 7 Normalized Pseudo-acceleration Response Spectra for Mean and Mean Plus One Standard Deviation Levels of Non-Exceedance for Ensemble of Numerically Generated Records; Systems with $\zeta = 0.05$

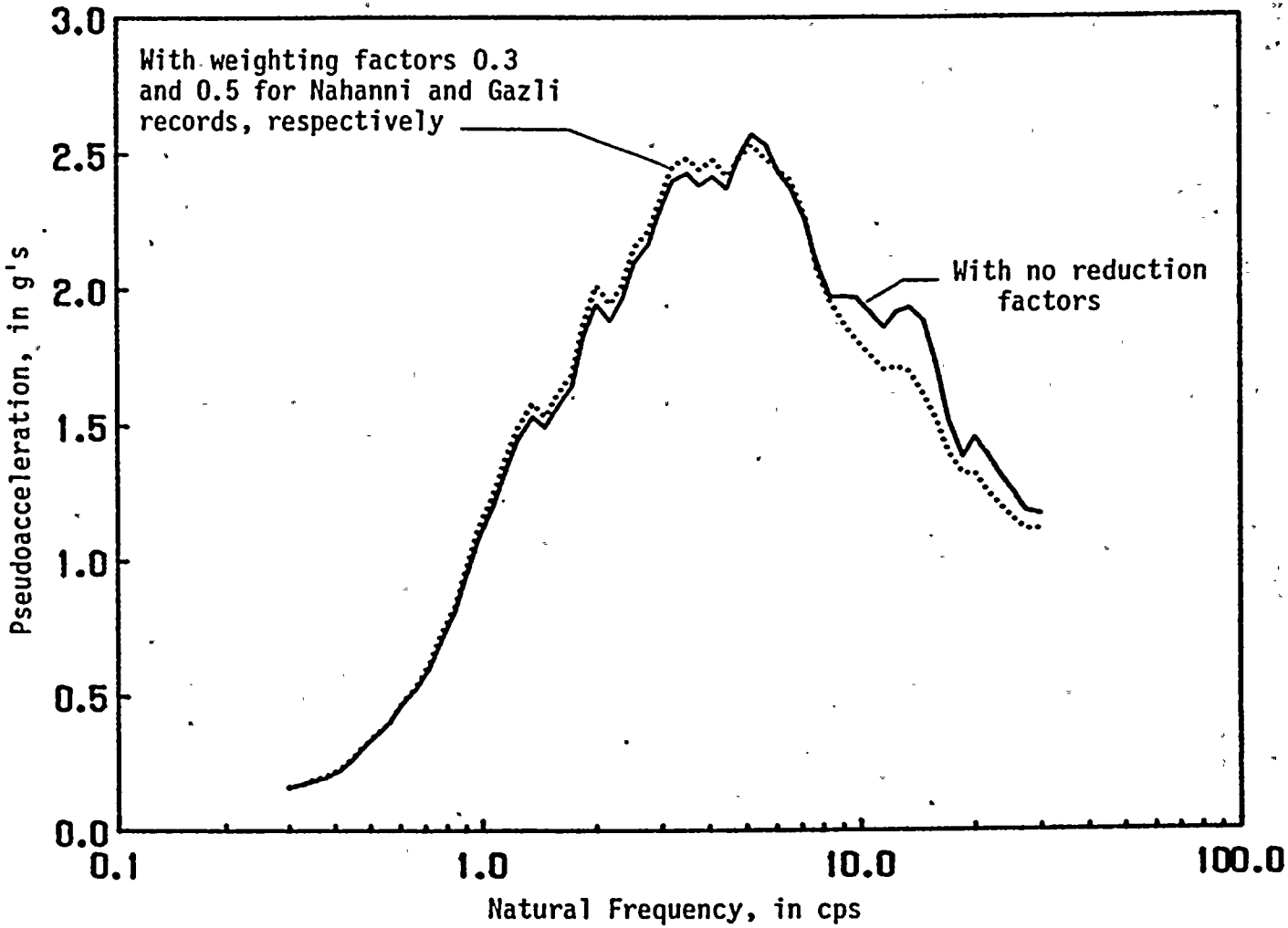

FIG. 8 Comparison of Mean Plus One Standard Deviation Pseudoacceleration Spectra Obtained Without and With Reduction Factors; Systems with 5 percent of Critical Damping

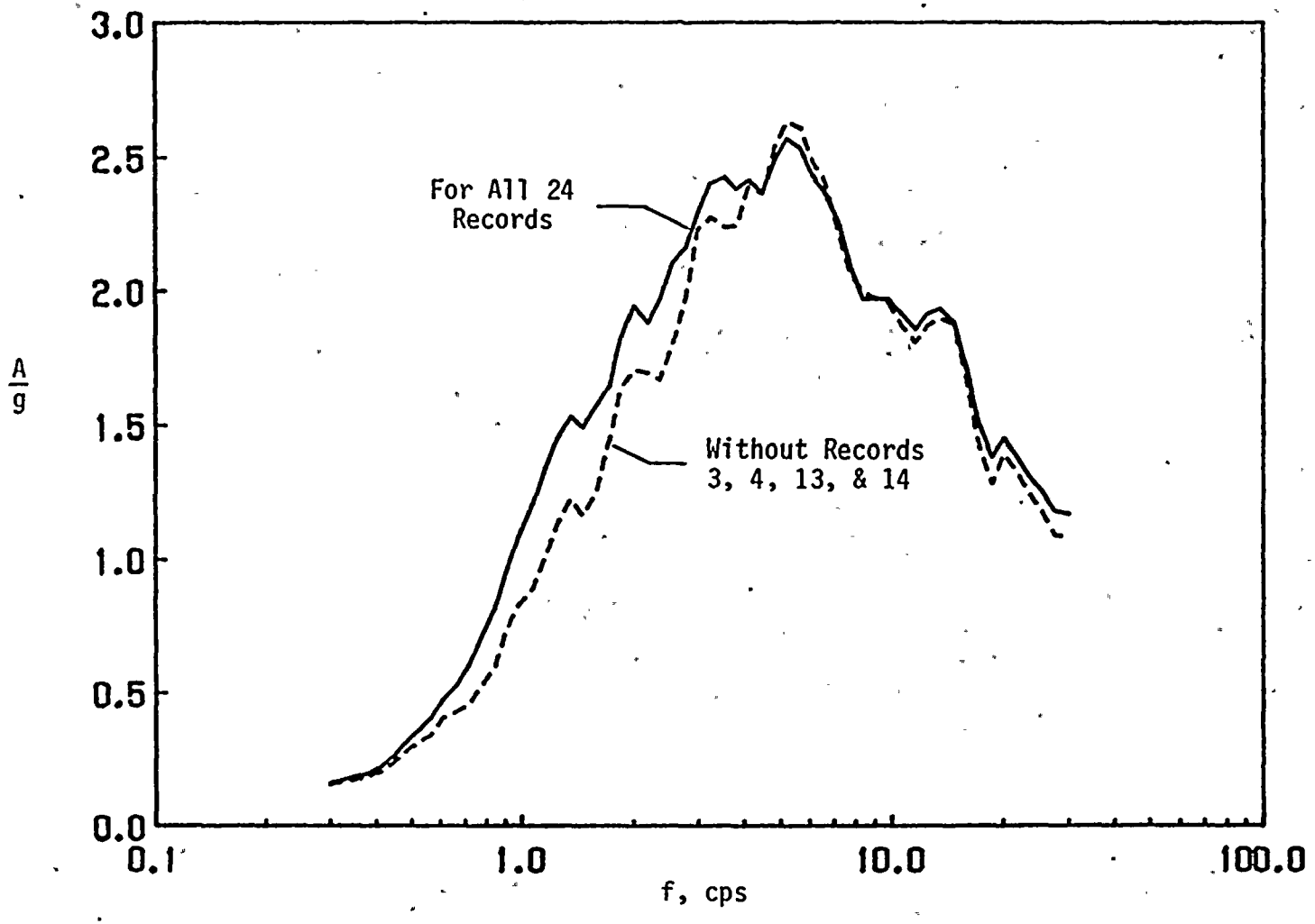

FIG. 9 Comparison of Mean Plus One Standard Deviation Pseudo-acceleration Spectra Obtained for All 24 and Only 20 Empirical Records; Systems with 5 Percent of Critical Damping

FIXED-BASE STRUCTURE MODEL

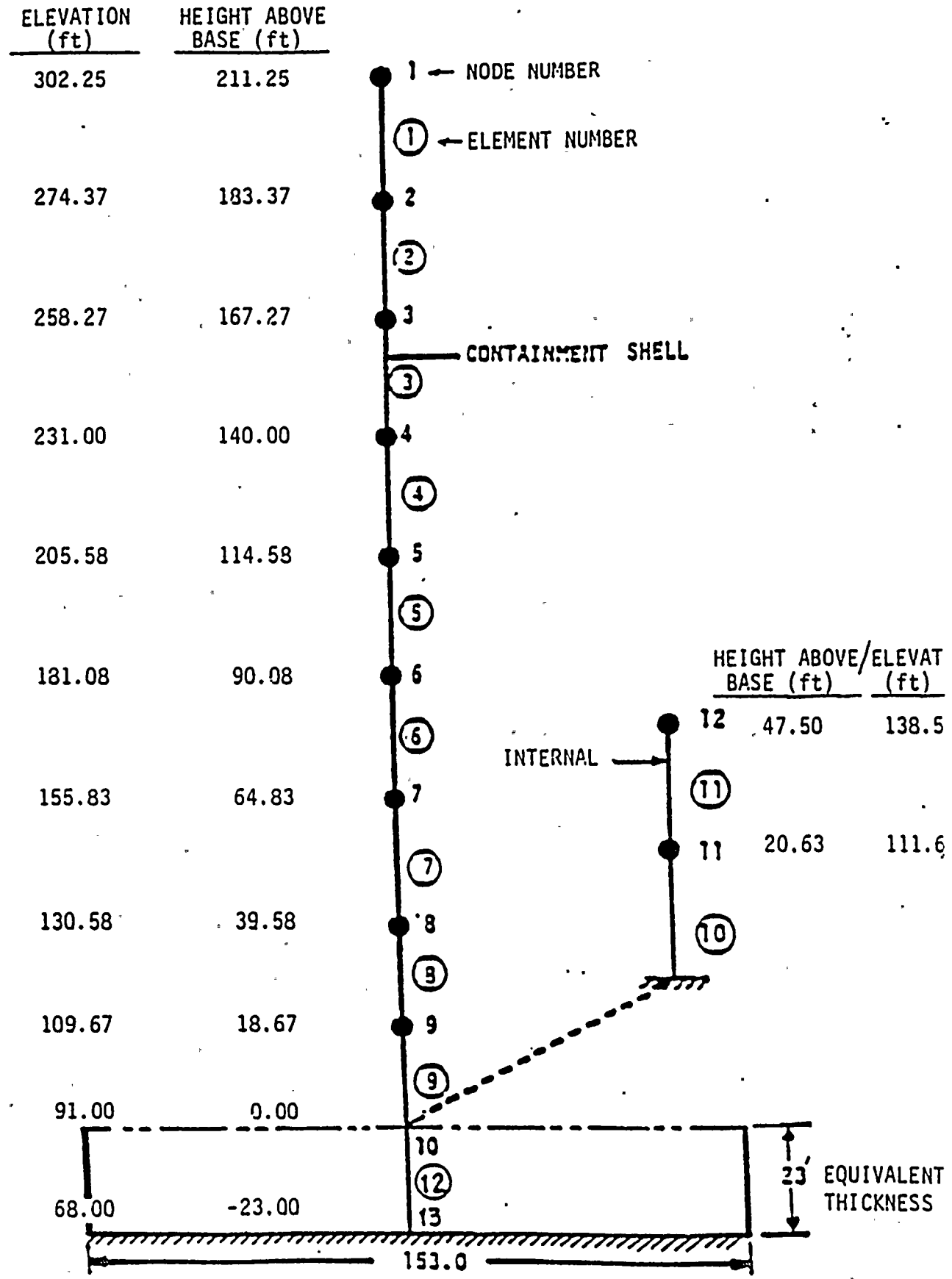

FIG. 10 CONTAINMENT AND INTERNAL STRUCTURES COUPLED SYSTEM

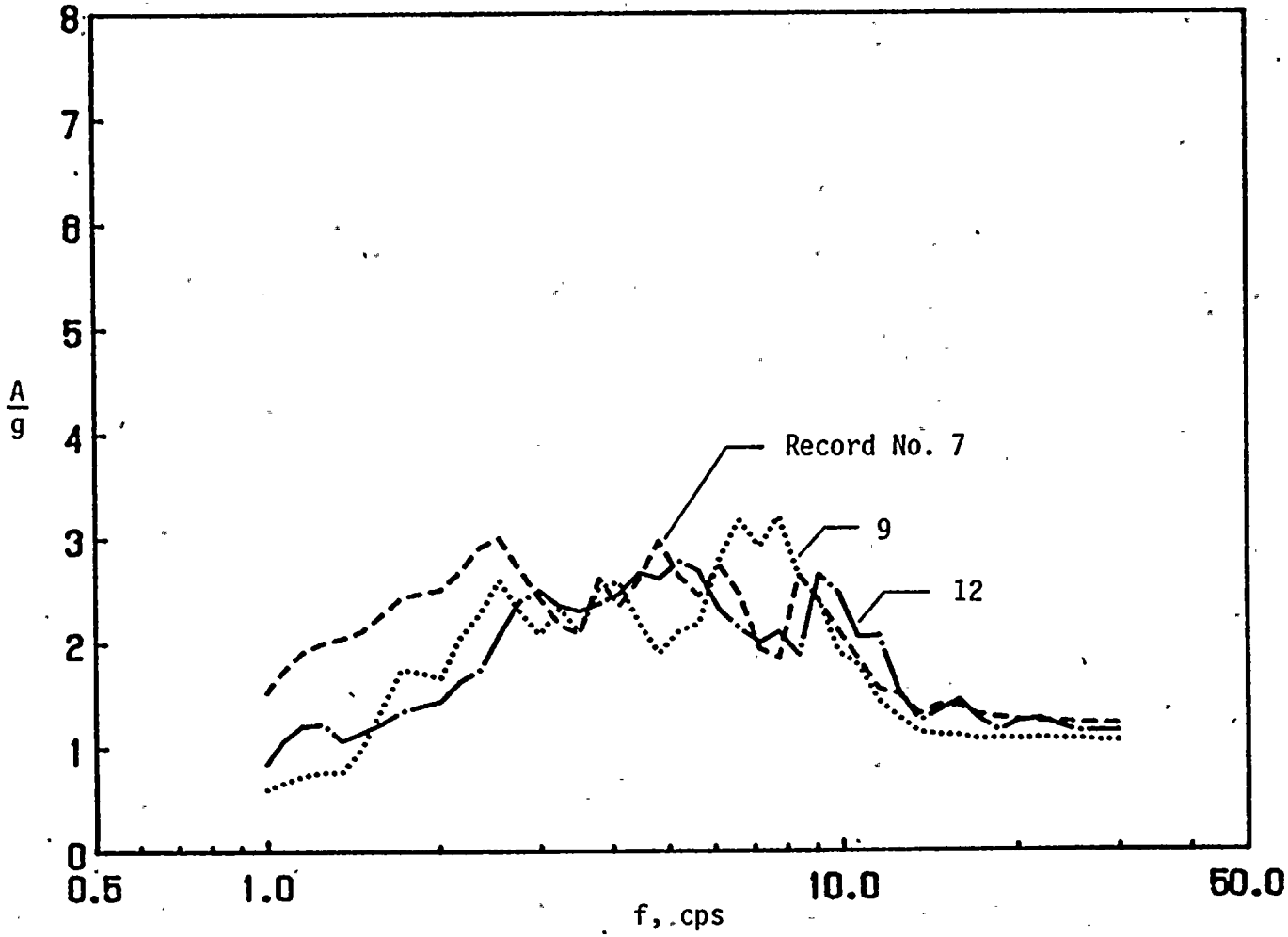

FIG. 11a Pseudo-acceleration Floor Response Spectra for Systems with 5 Percent of Critical Damping Mounted on Foundation Mat

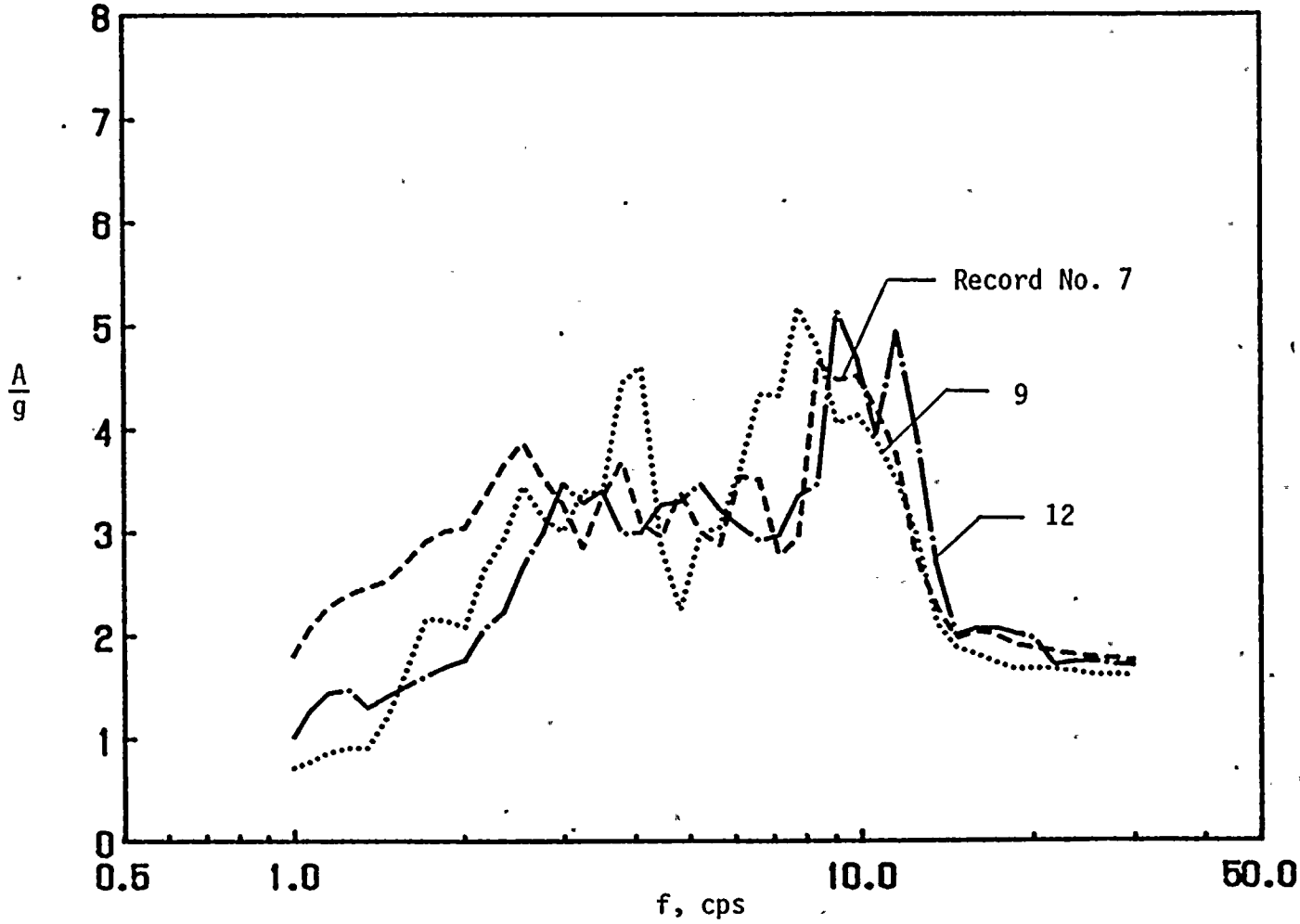

FIG. 11b Pseudo-acceleration Floor Response Spectra for System with 5 Percent of Critical Damping Mounted at Top of Internal Structure

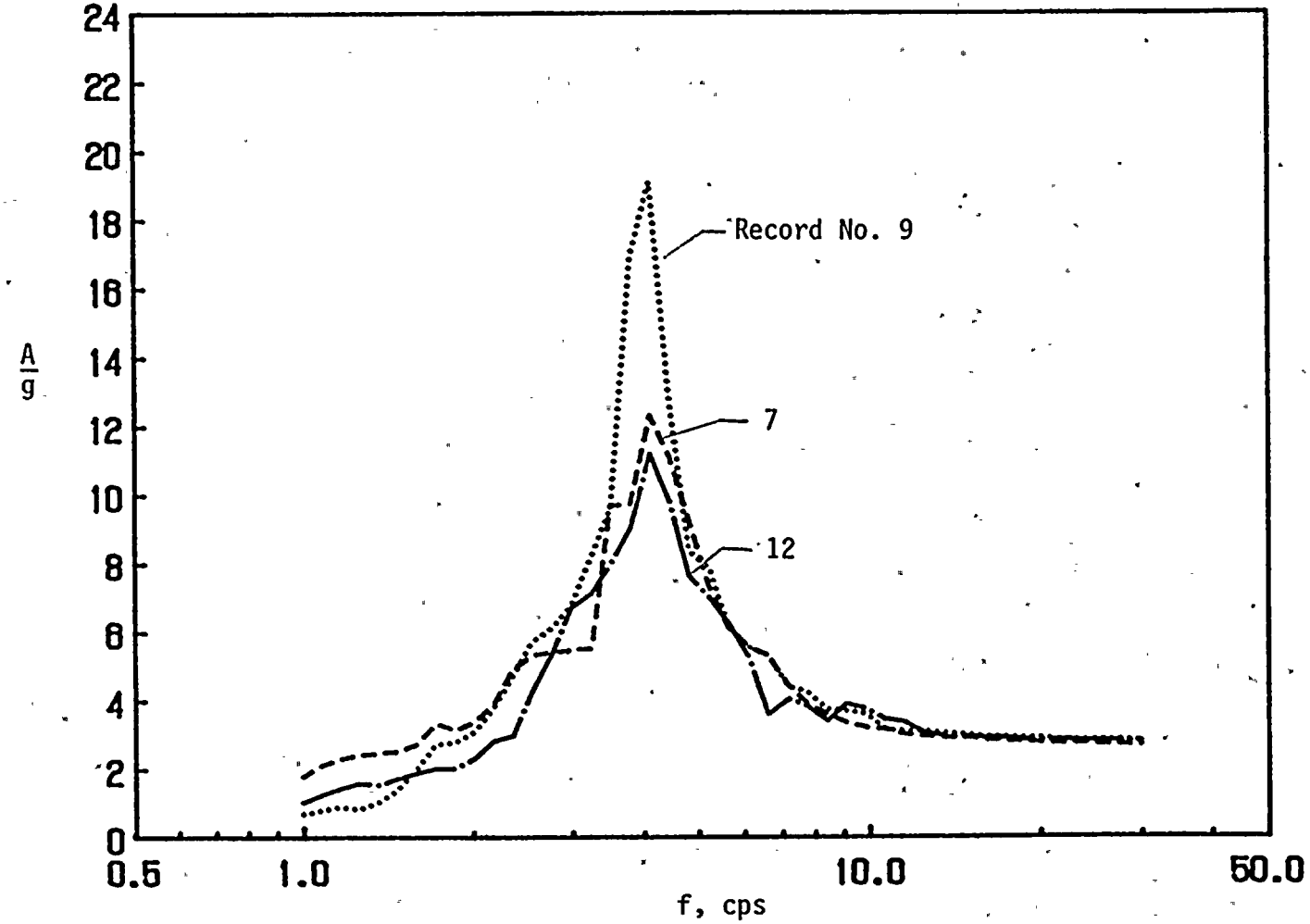

FIG. 11c Pseudo-acceleration Floor Response Spectra for System with 5 Percent of Critical Damping Mounted at Springline of Containment Structure

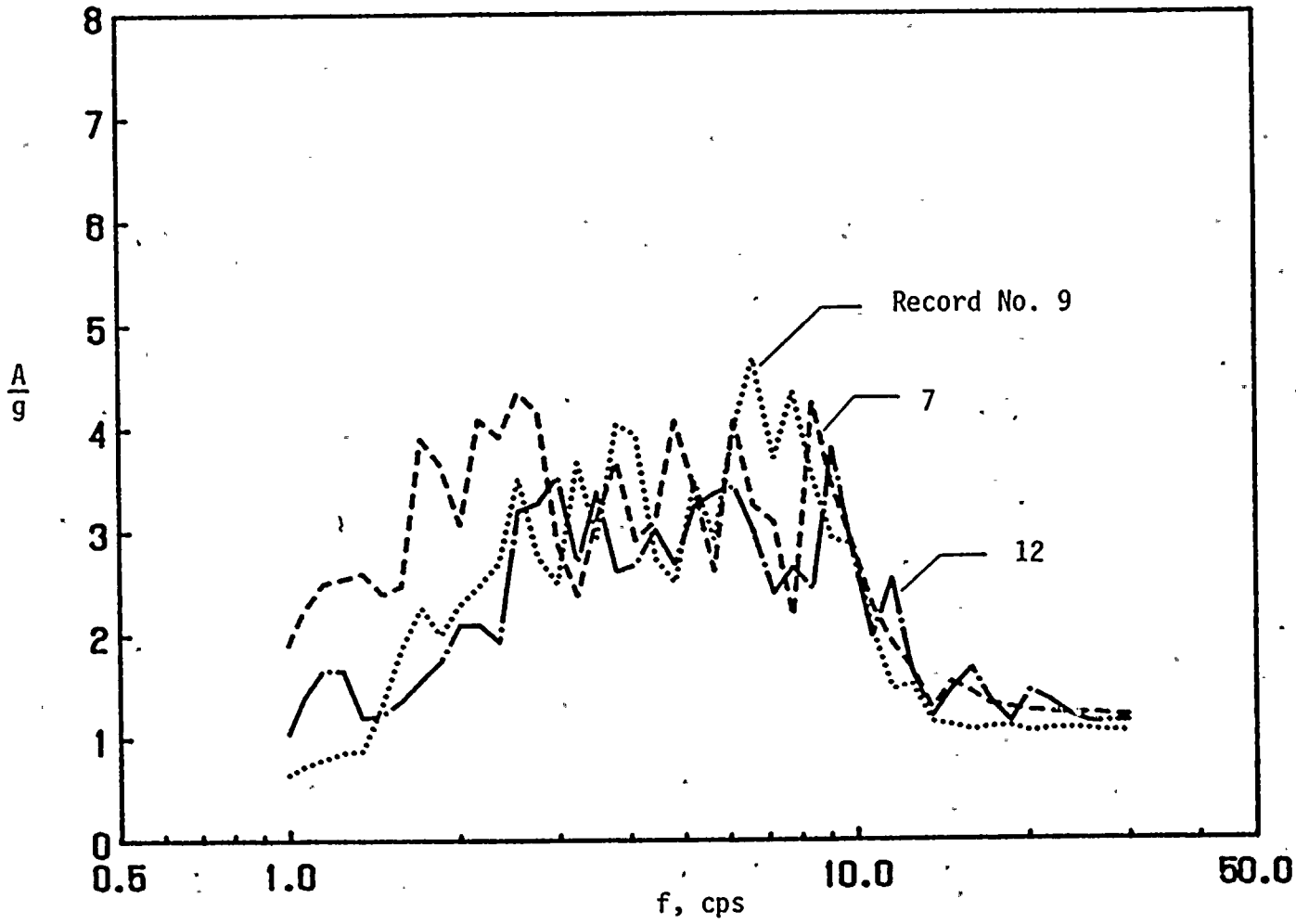

FIG. 12a Pseudo-acceleration Floor Response Spectra for System with 2 Percent of Critical Damping Mounted on Foundation Mat

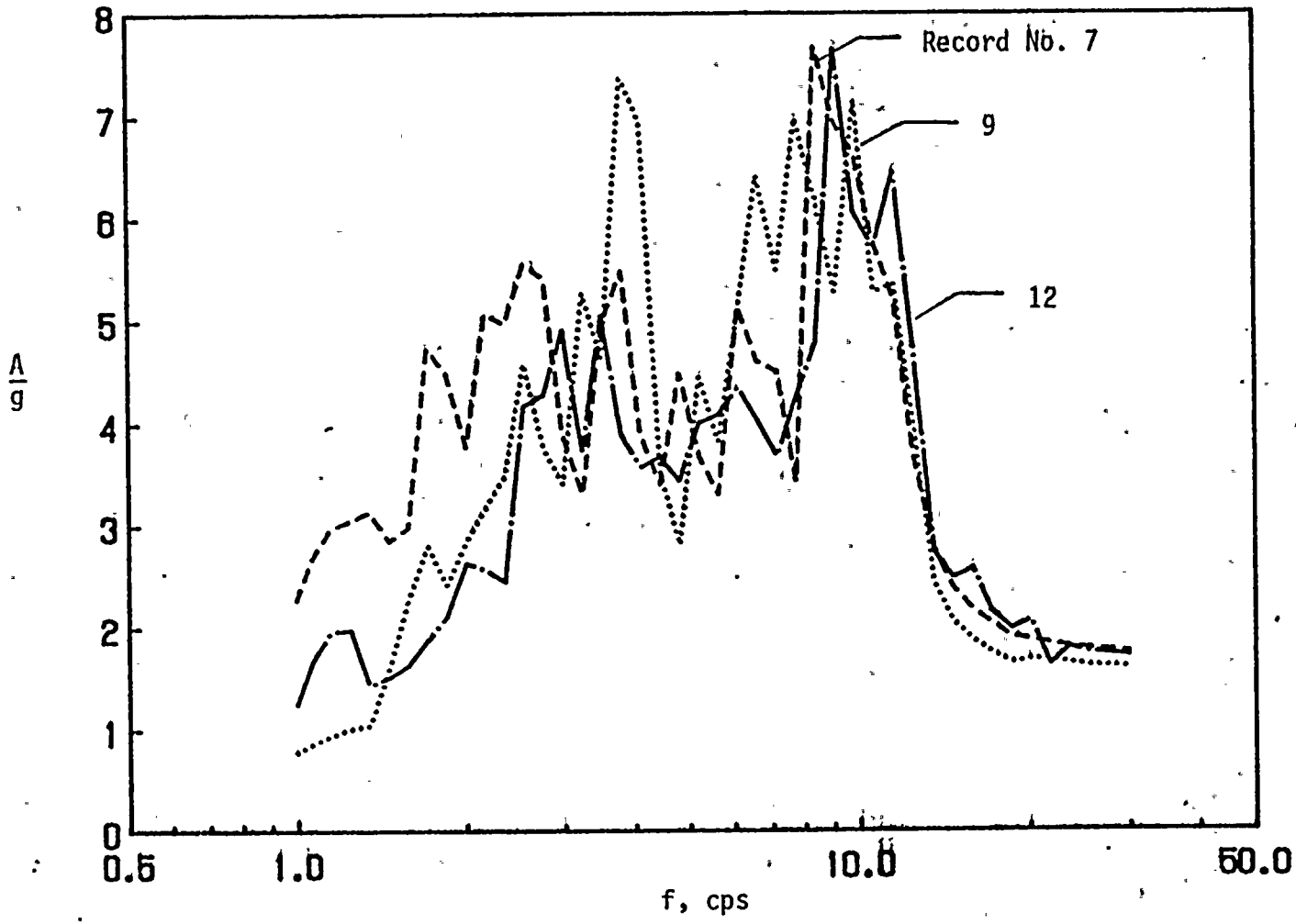

FIG. 12b Pseudo-acceleration Floor Response Spectra for System with 2 Percent of Critical Damping Mounted at Top of Internal Structure

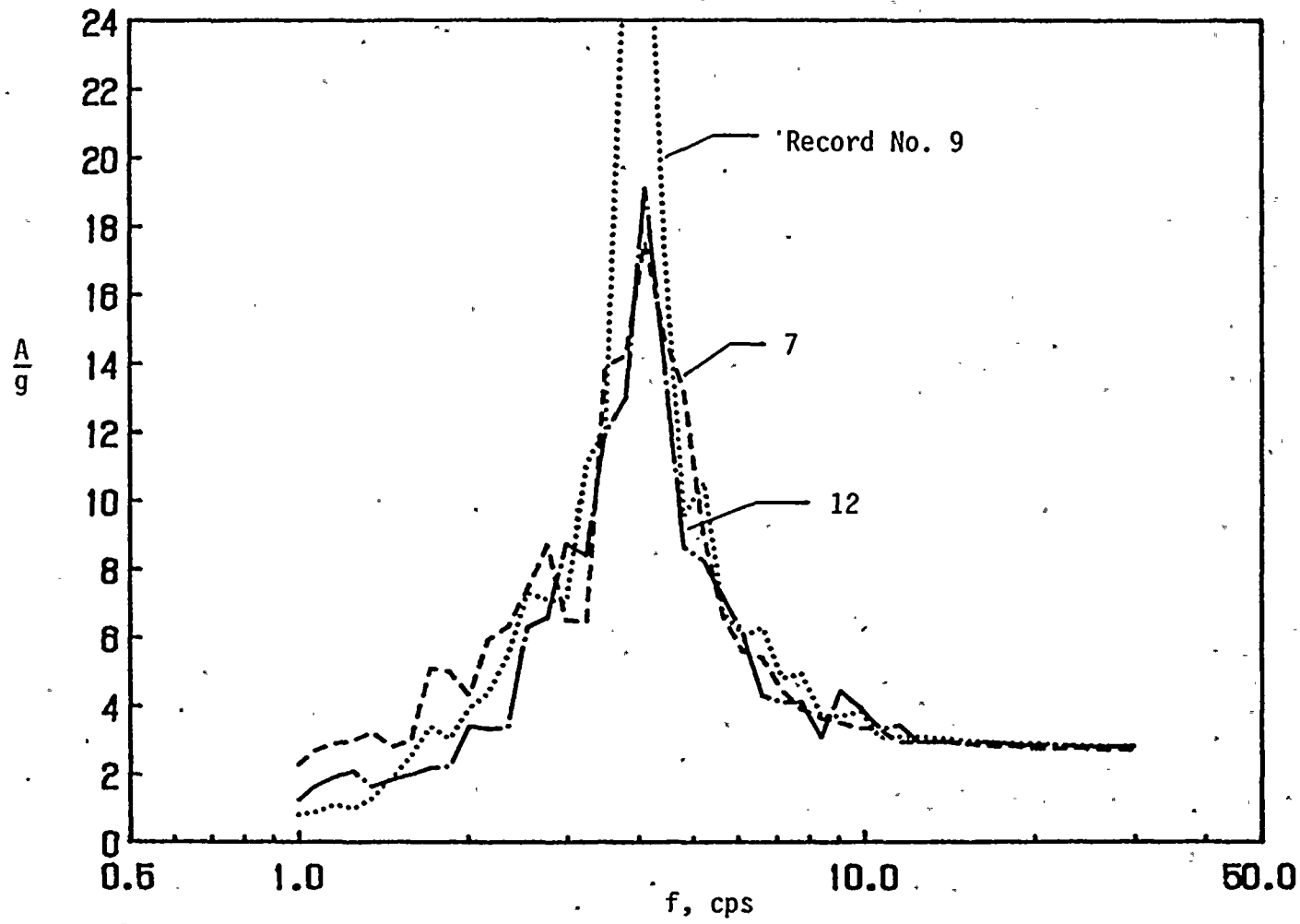

FIG. 12c Pseudo-acceleration Floor Response Spectra for System with 2 Percent of Critical Damping Mounted at Springline of Containment Structure

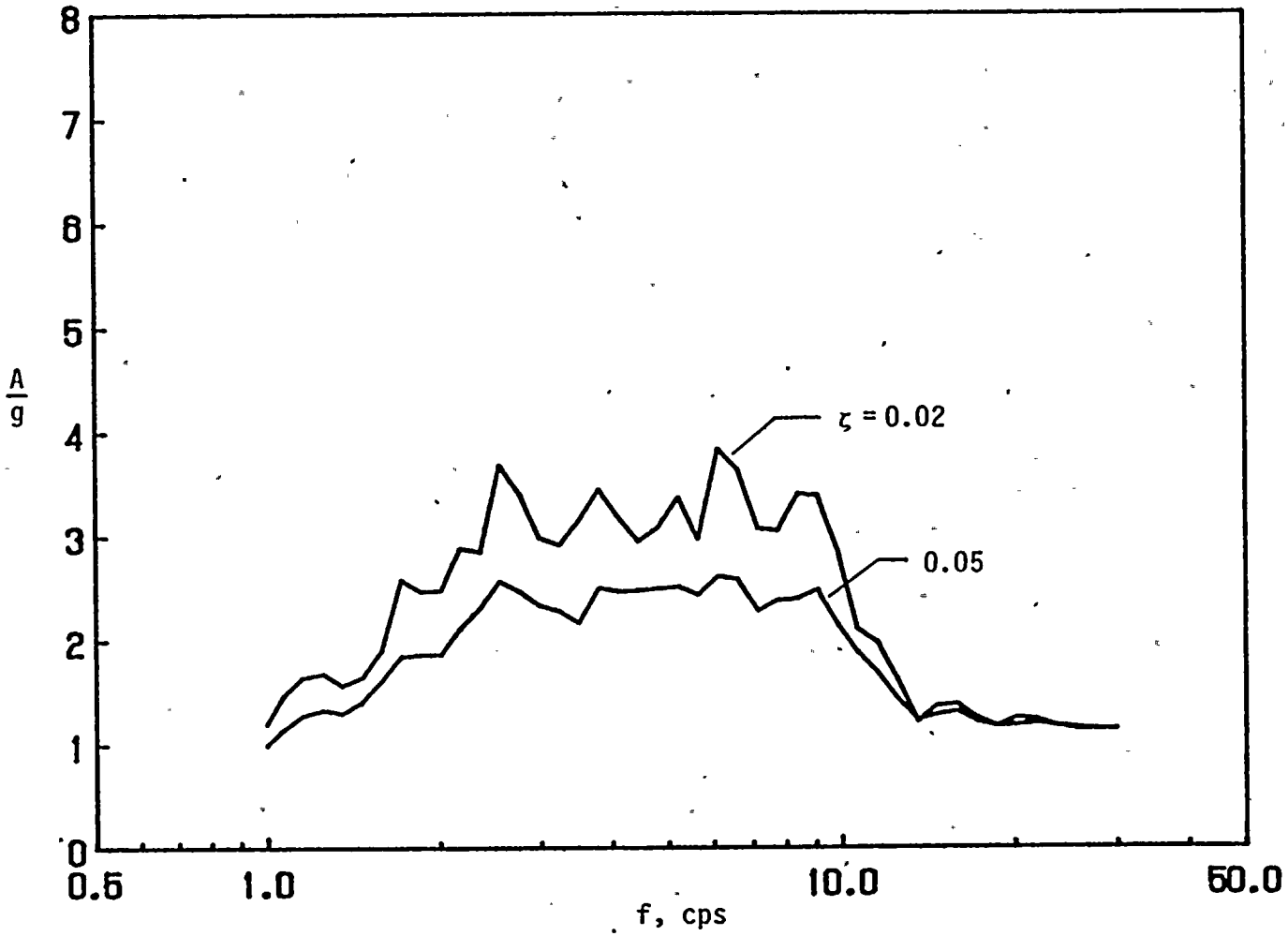

FIG. 13a Mean Floor Response Spectra for Ground Motion Records 7, 9 & 12; Systems with Damping Factor ζ on Foundation Mat

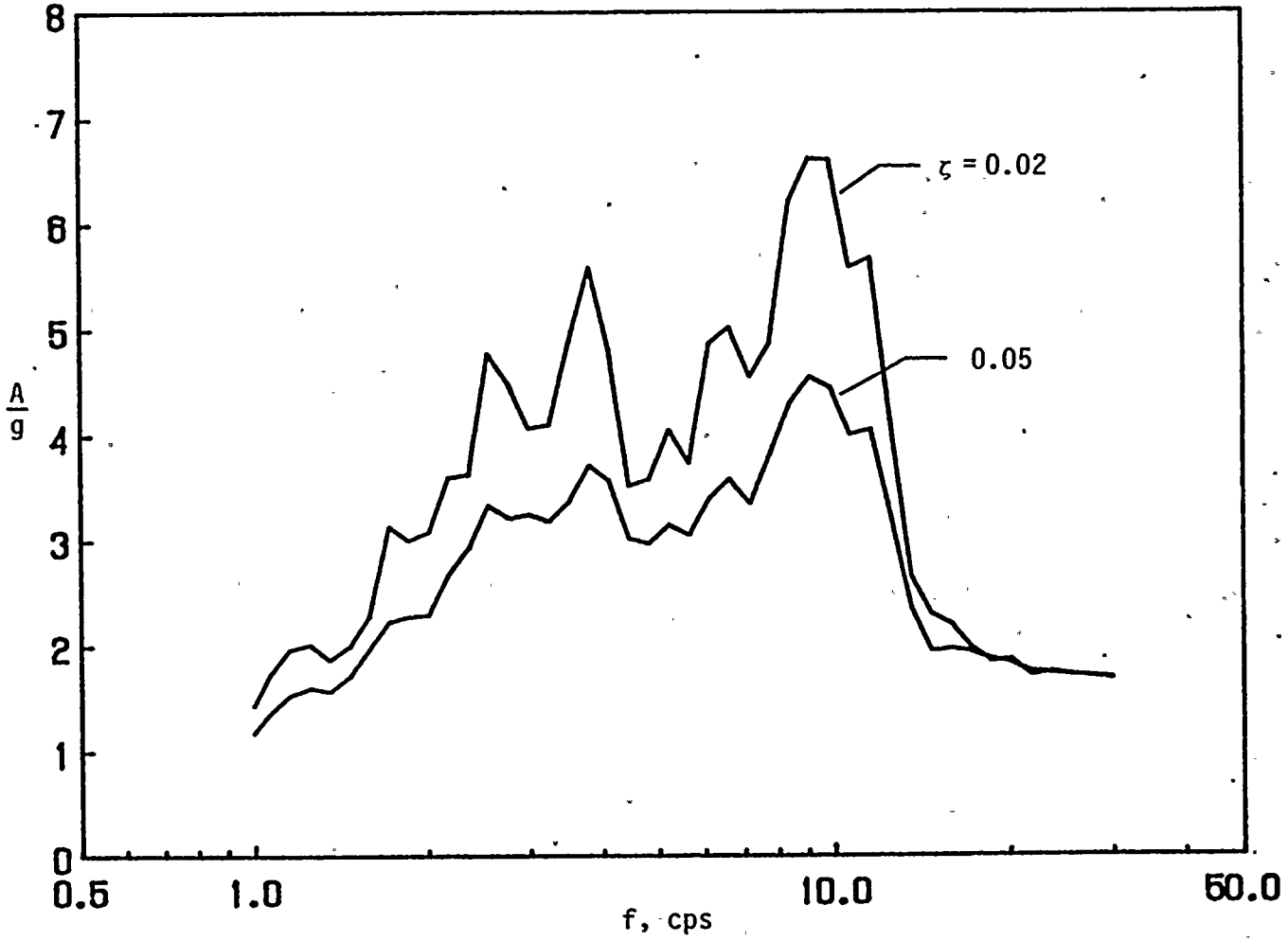

FIG. 13b Mean Floor Response Spectra for Ground Motion Records 7, 9 & 12; Systems with Damping Factor ζ at Top of Internal Structure

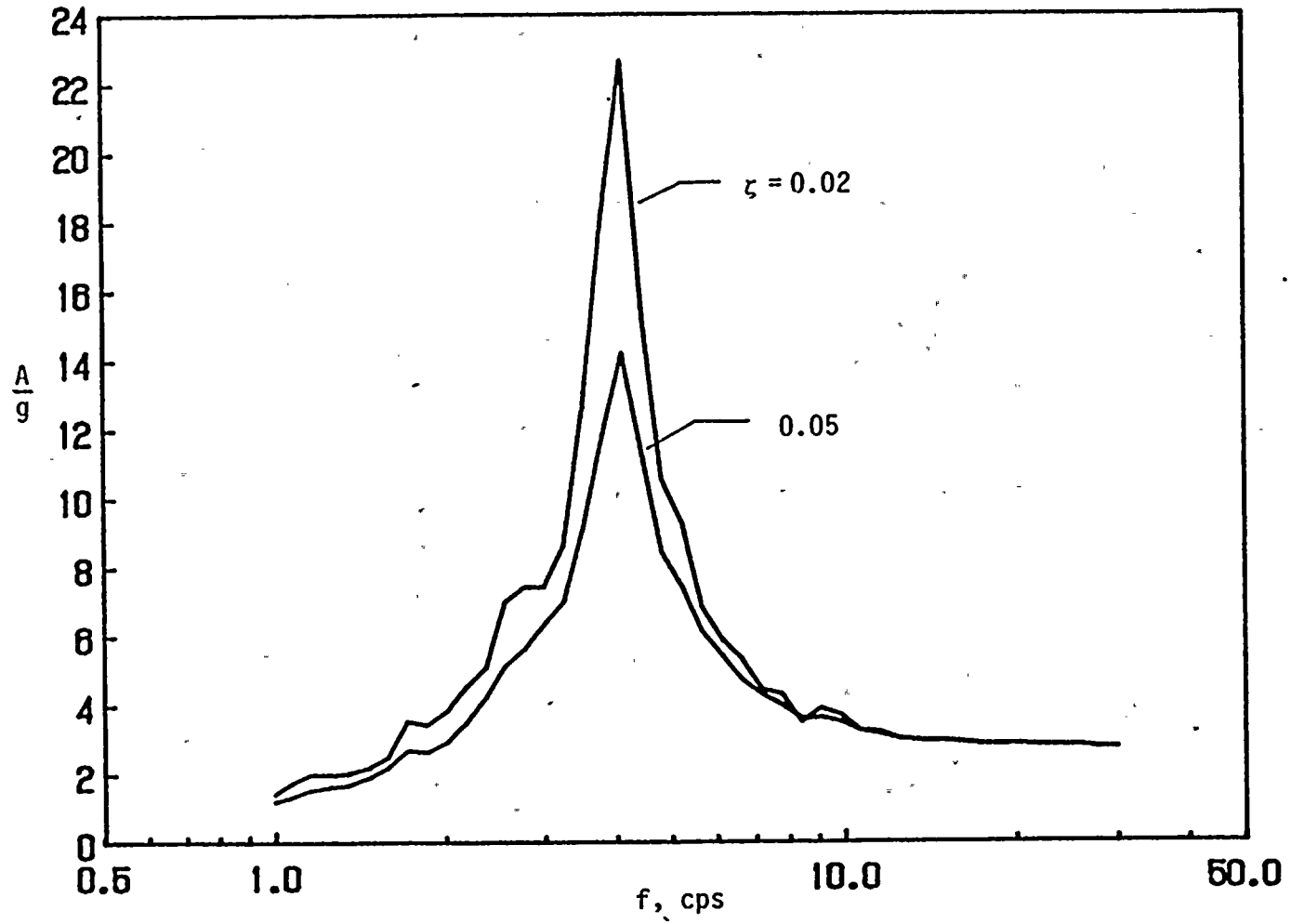

FIG. 13c Mean Floor Response Spectra for Ground Motion Records 7, 9 & 12; Systems with Damping Factor ζ at Springline of Containment Structure

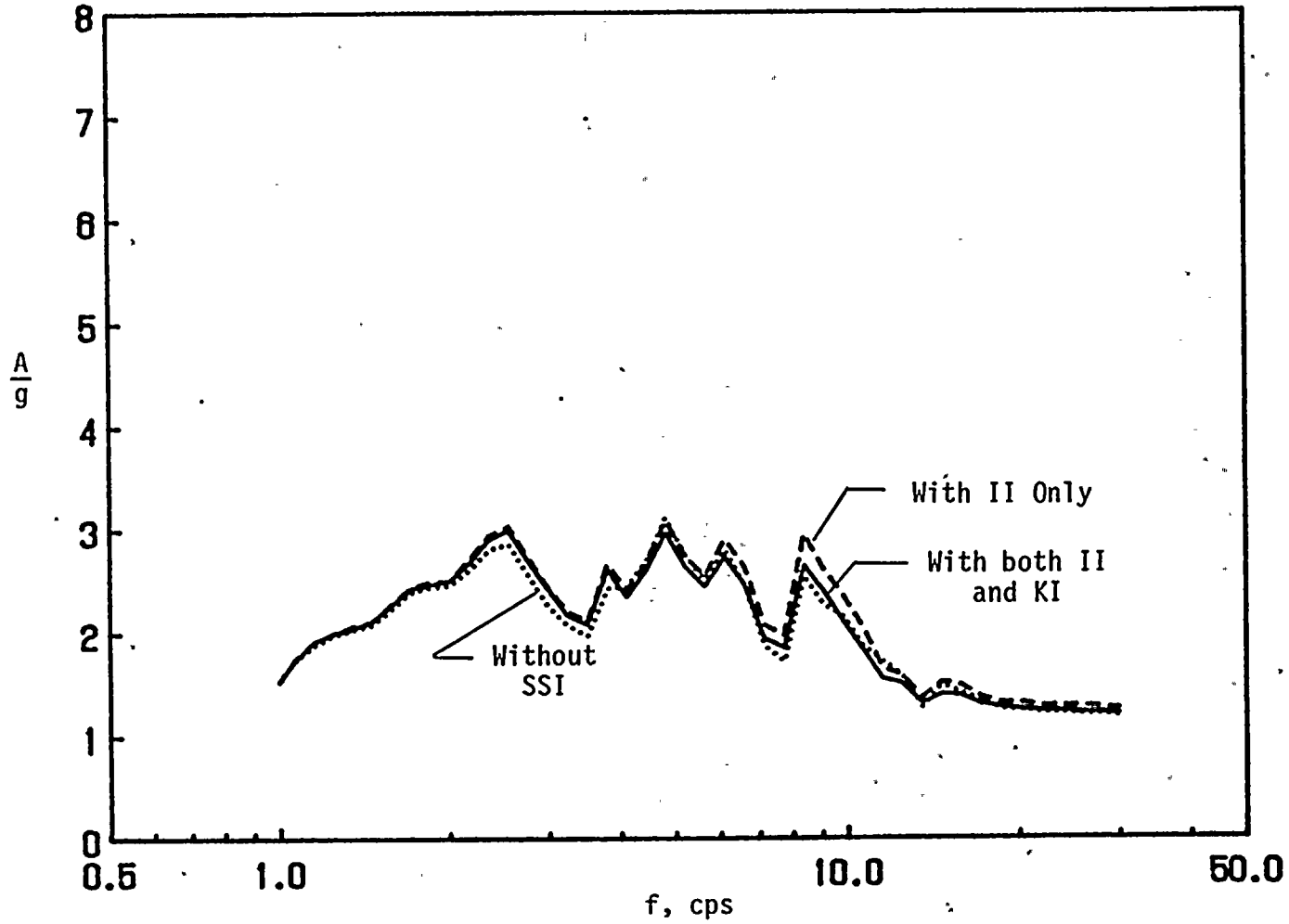

FIG. 14a Effects of Inertial and Kinematic Interaction on Floor Response Spectra of Systems with $\zeta = 0.05$ Mounted on Foundation Mat; Ground Motion Record No. 7

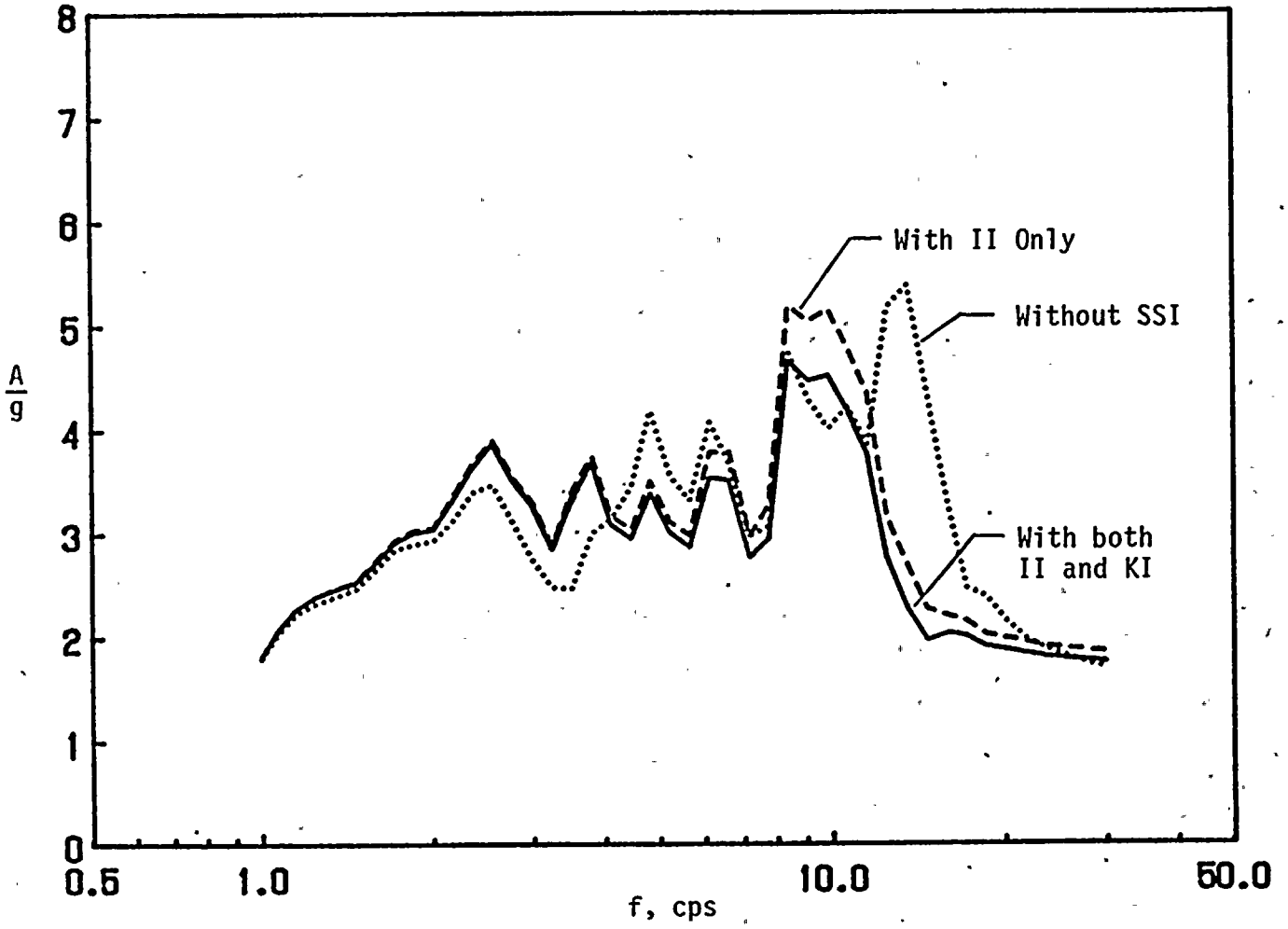

FIG. 14b Effects of Inertial and Kinematic Interaction on Floor Response Spectra of Systems with $\zeta = 0.05$ Mounted at Top of Internal Structure; Ground Motion Record No. 7

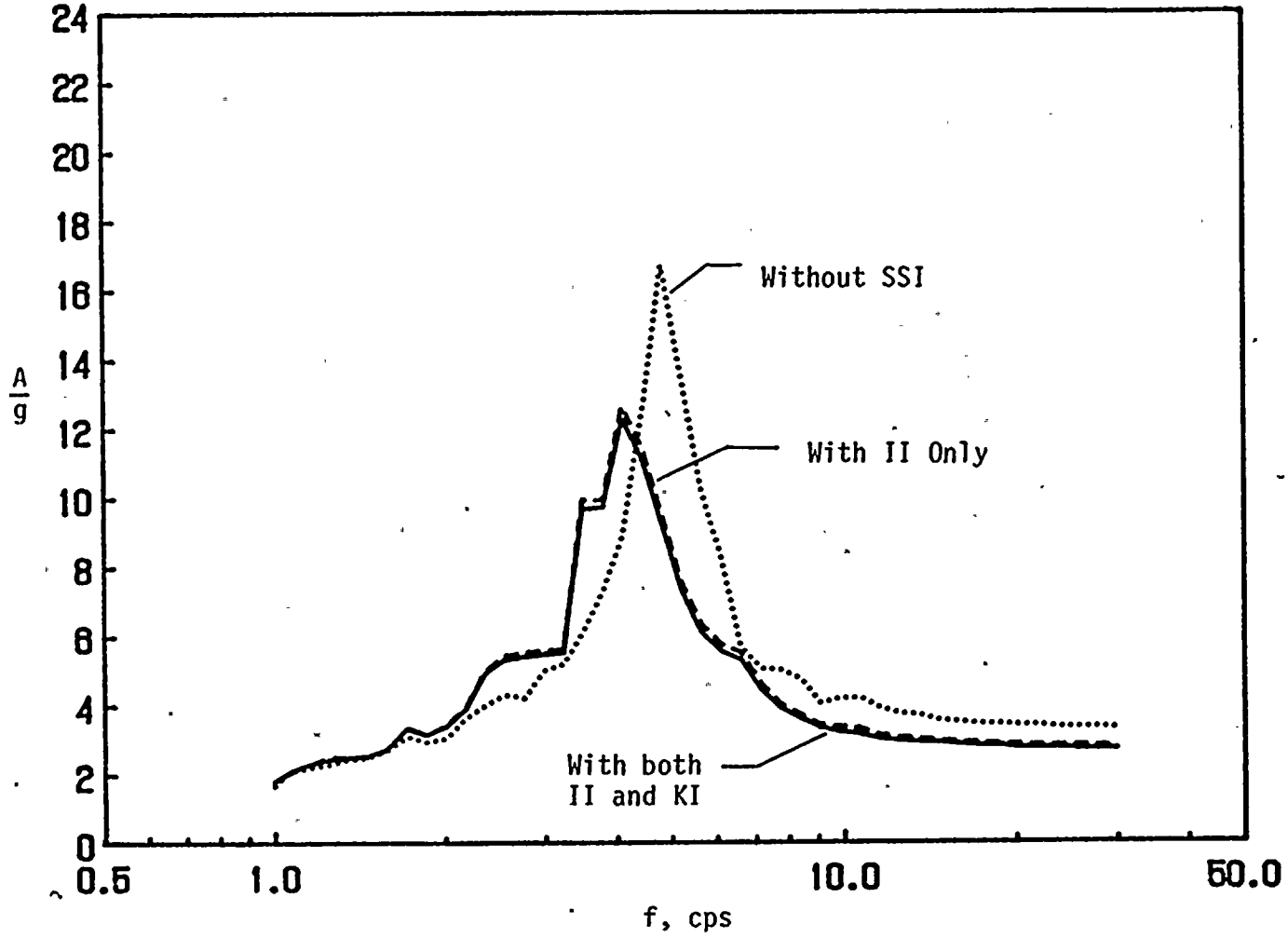

FIG. 14c Effects of Inertial and Kinematic Interaction on Floor Response Spectra of Systems with $\zeta = 0.05$ Mounted at Springline of Containment Structure; Ground Motion Record No. 7

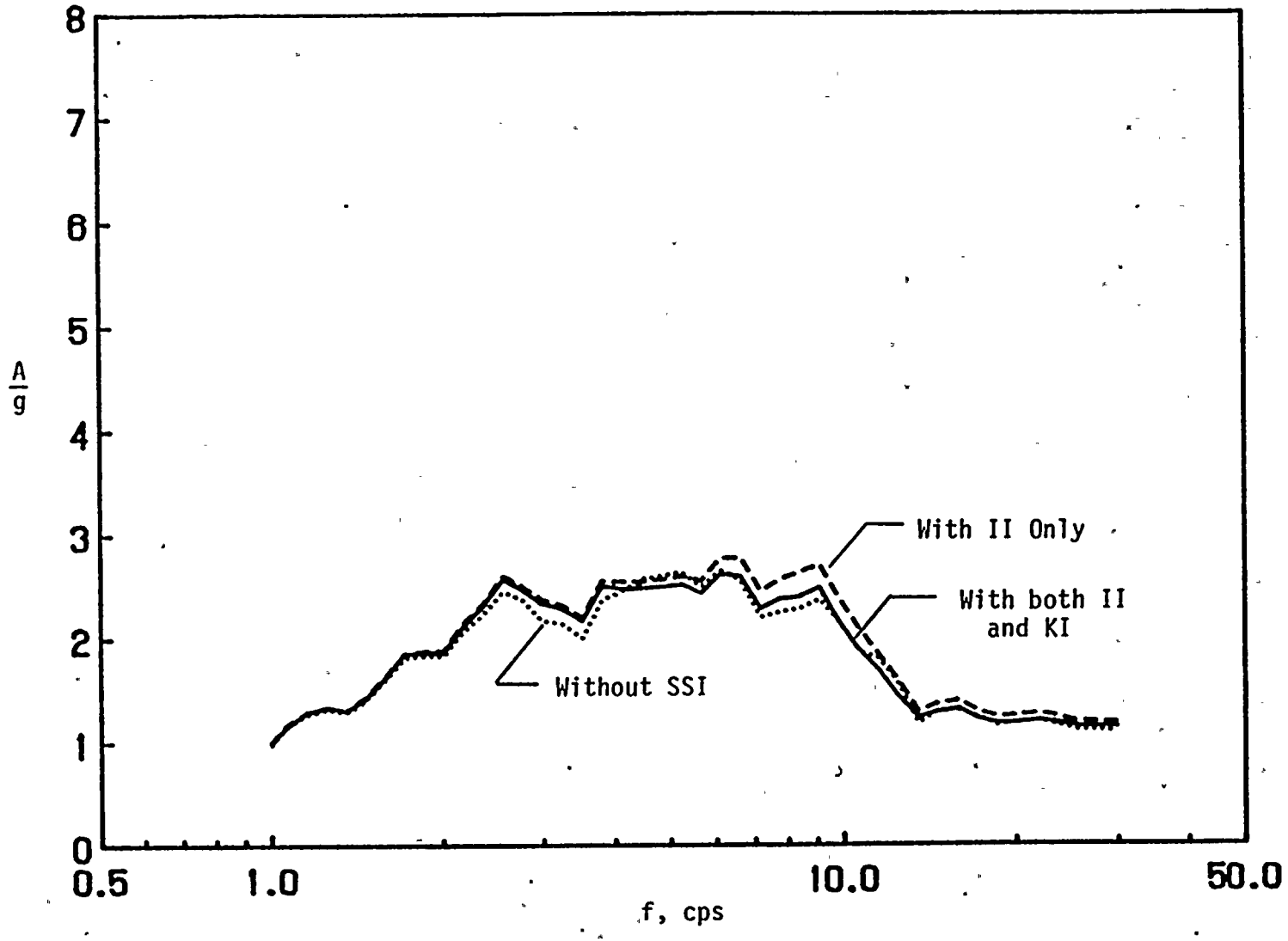

FIG. 15a Effects of Inertial and Kinematic Interaction on Mean Floor Response Spectra for Ground Motion Records 7, 9 & 12; Systems with $\zeta = 0.05$ at Foundation Mat

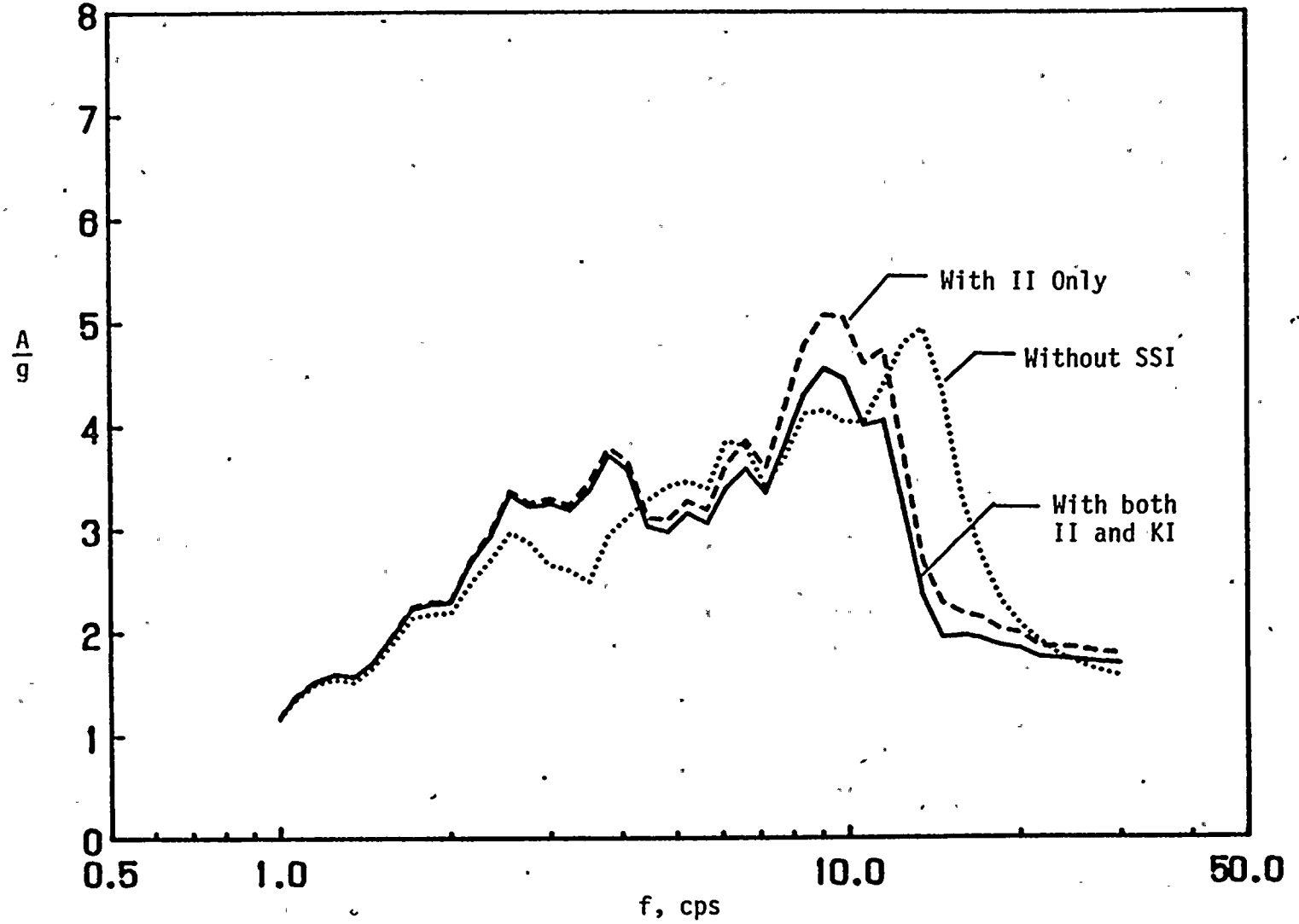

FIG. 15b Effects of Inertial and Kinematic Interaction on Mean Floor Response Spectra for Ground Motion Records 7, 9 & 12; Systems with $\zeta = 0.05$ at Top of Internal Structure

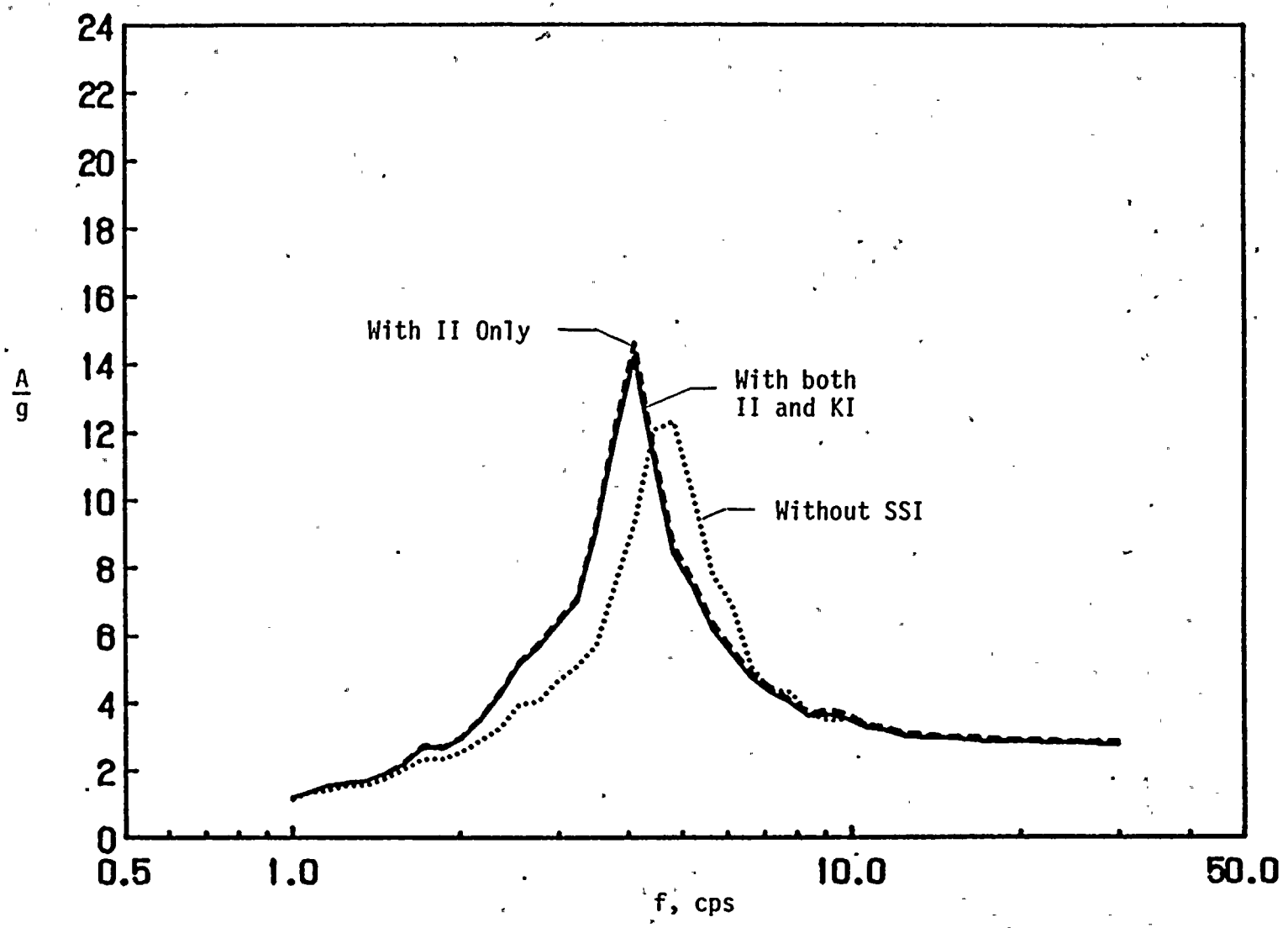

FIG. 15c Effects of Inertial and Kinematic Interaction on Mean Floor Response Spectra for Ground Motion Records 7, 9 & 12; Systems with $\zeta = 0.05$ at Springline of Containment Structure

APPENDIX

to

Studies of Earthquake Ground Motions and Soil-Structure Interaction for Diablo Canyon Nuclear Power Plant

by

A. S. Veletsos, Y. Tang and A. M. Prasad

Submitted to

Brookhaven National Laboratory
Department of Nuclear Energy
Upton, Long Island, New York 11973

Department of Civil Engineering
Rice University
Houston, Texas 77251

December 10, 1988

CONTENTS

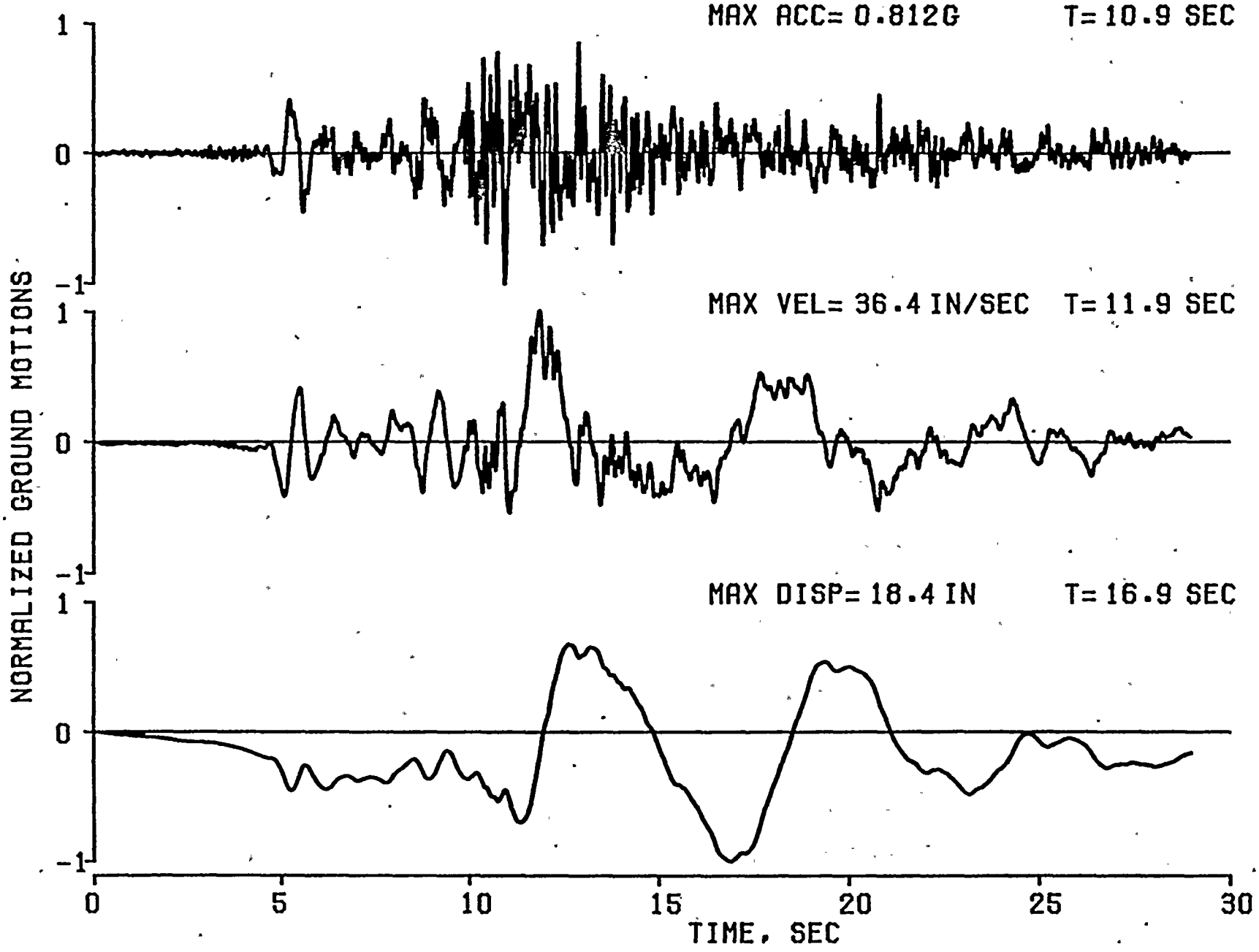

FIG. A.1 ACCELERATION VELOCITY AND DISPLACEMENT HISTORIES FOR RECORD NO. 1

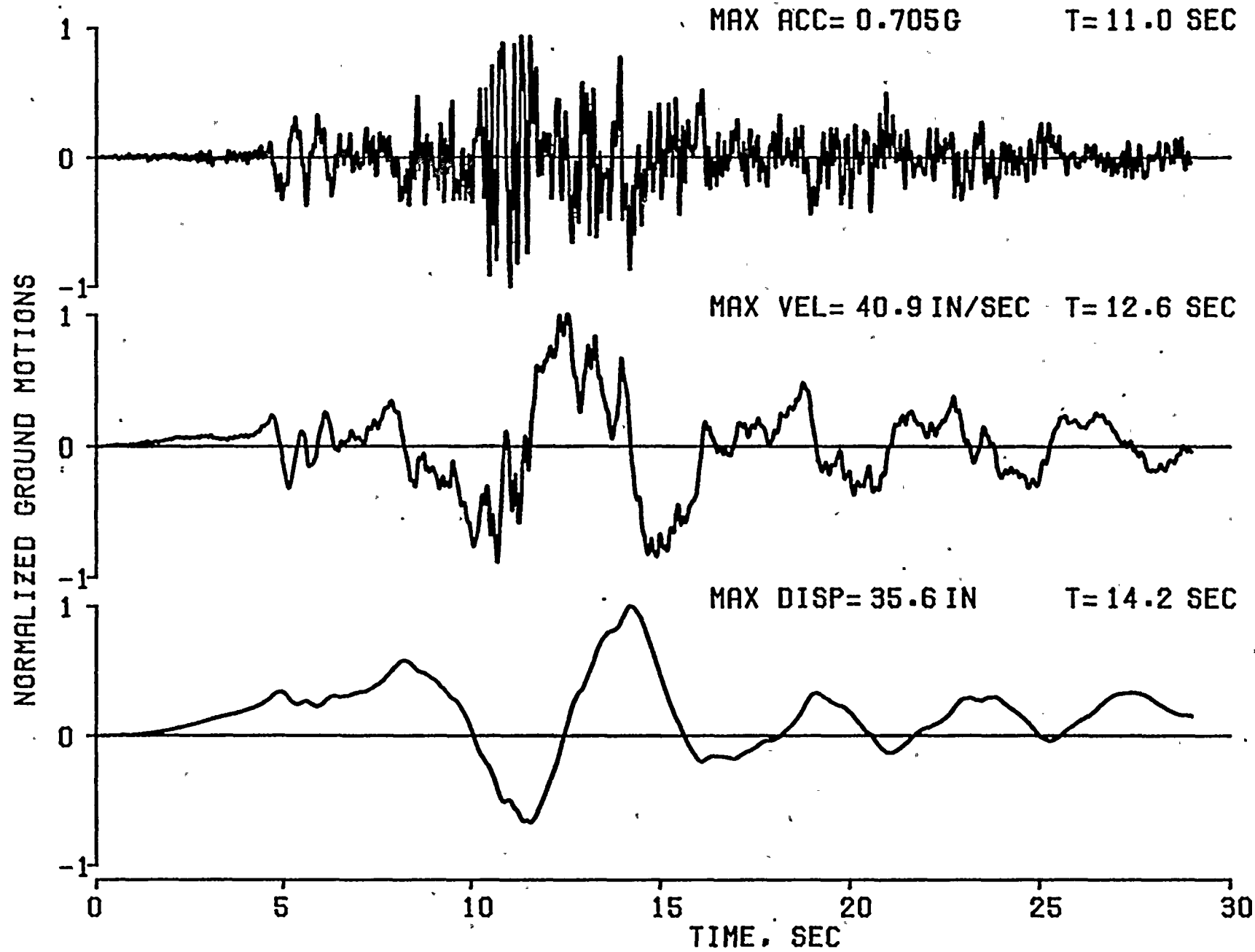

FIG. A.2 ACCELERATION VELOCITY AND DISPLACEMENT HISTORIES FOR RECORD NO. 2

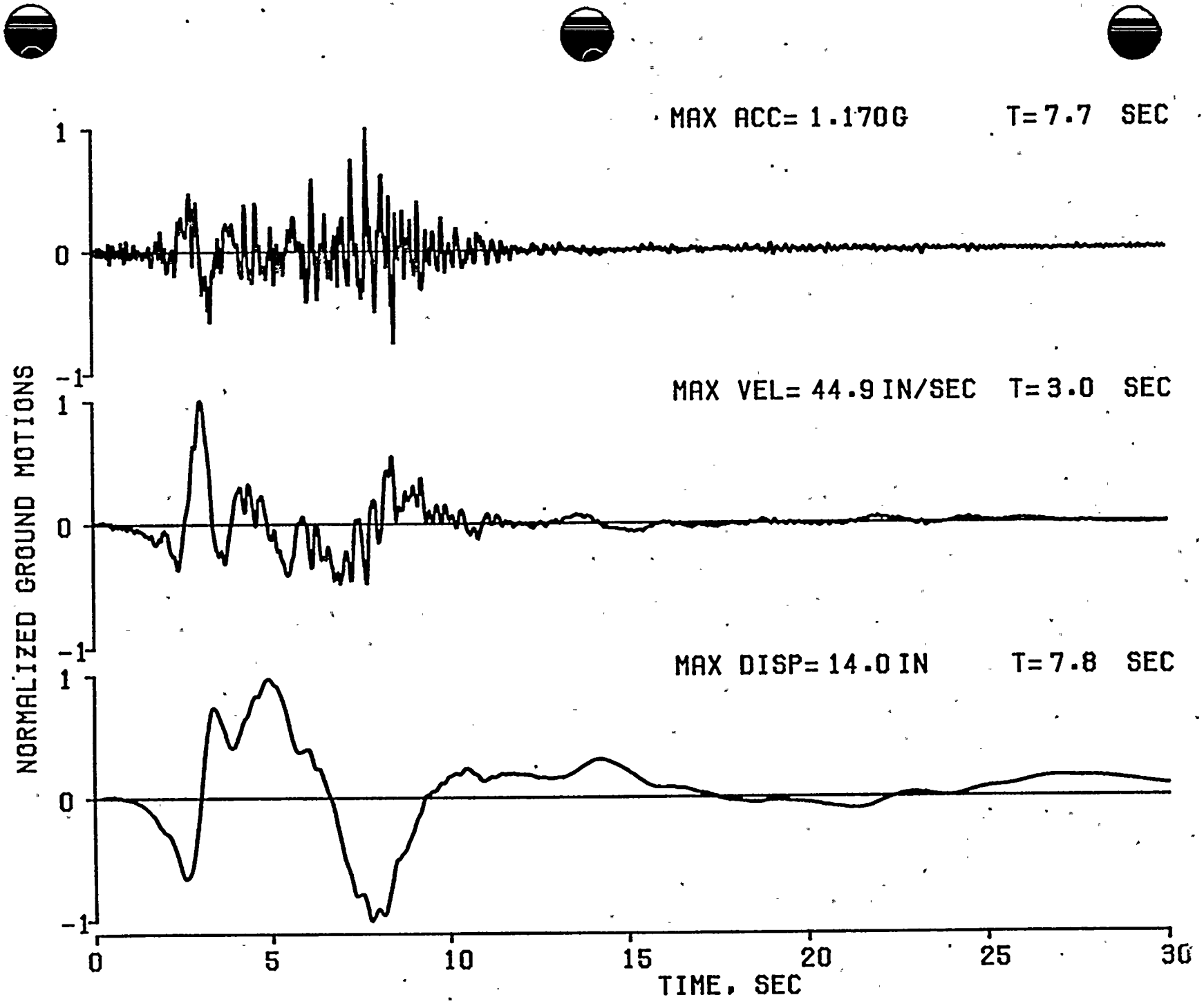

FIG. A.3 ACCELERATION VELOCITY AND DISPLACEMENT HISTORIES FOR RECORD NO. 3

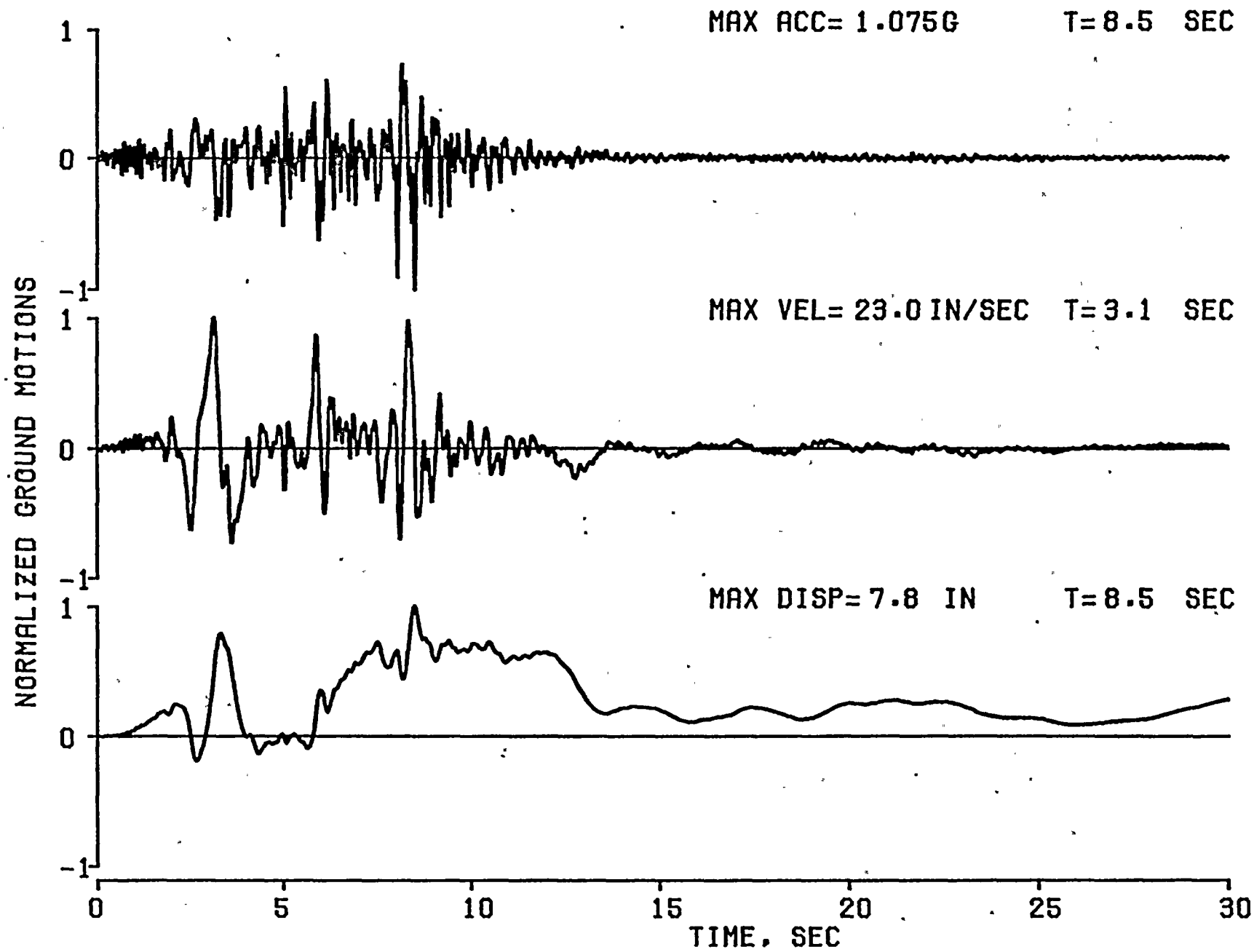

FIG. A.4 ACCELERATION VELOCITY AND DISPLACEMENT HISTORIES FOR RECORD NO. 4

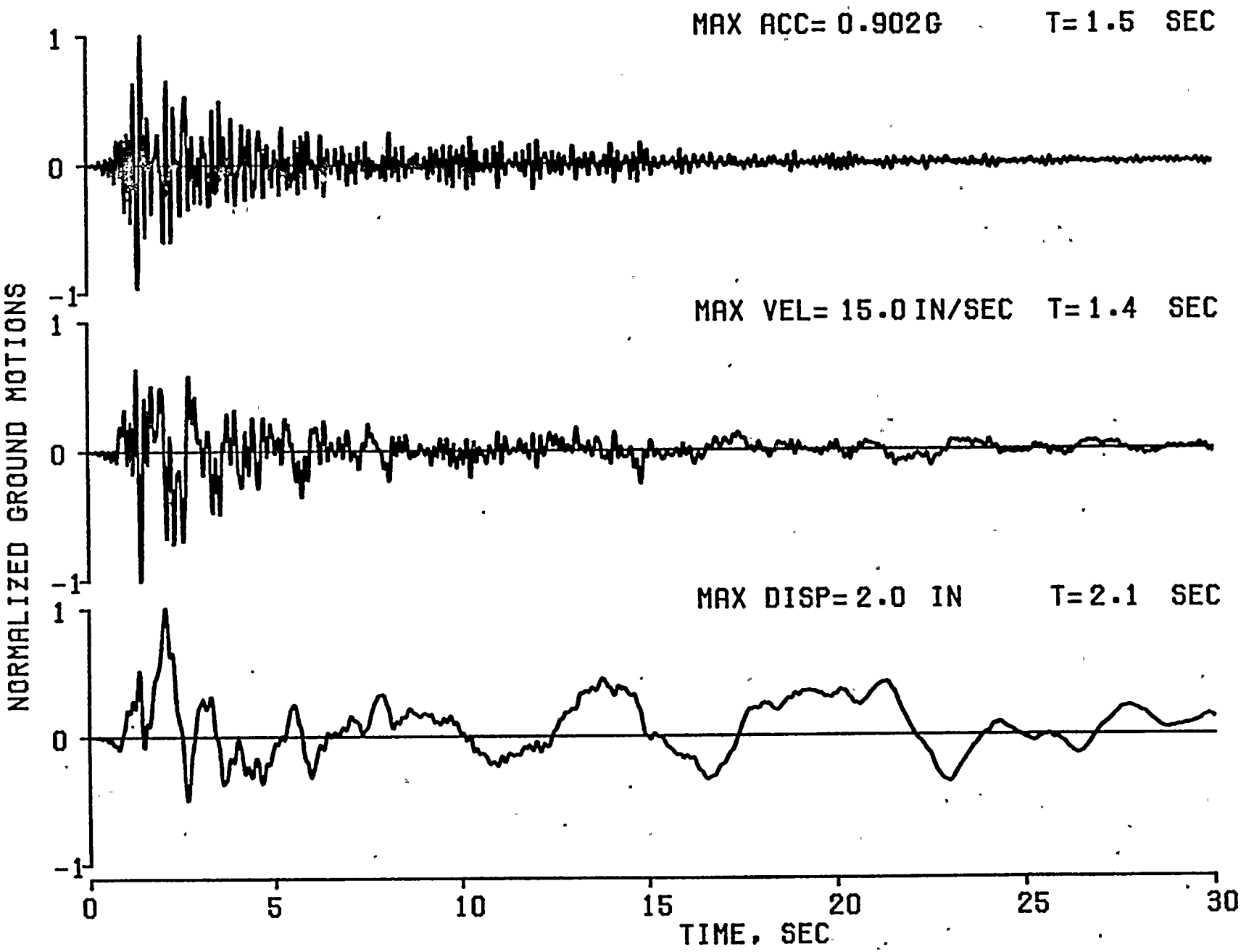

FIG. A.5 ACCELERATION VELOCITY AND DISPLACEMENT HISTORIES FOR RECORD NO. 5

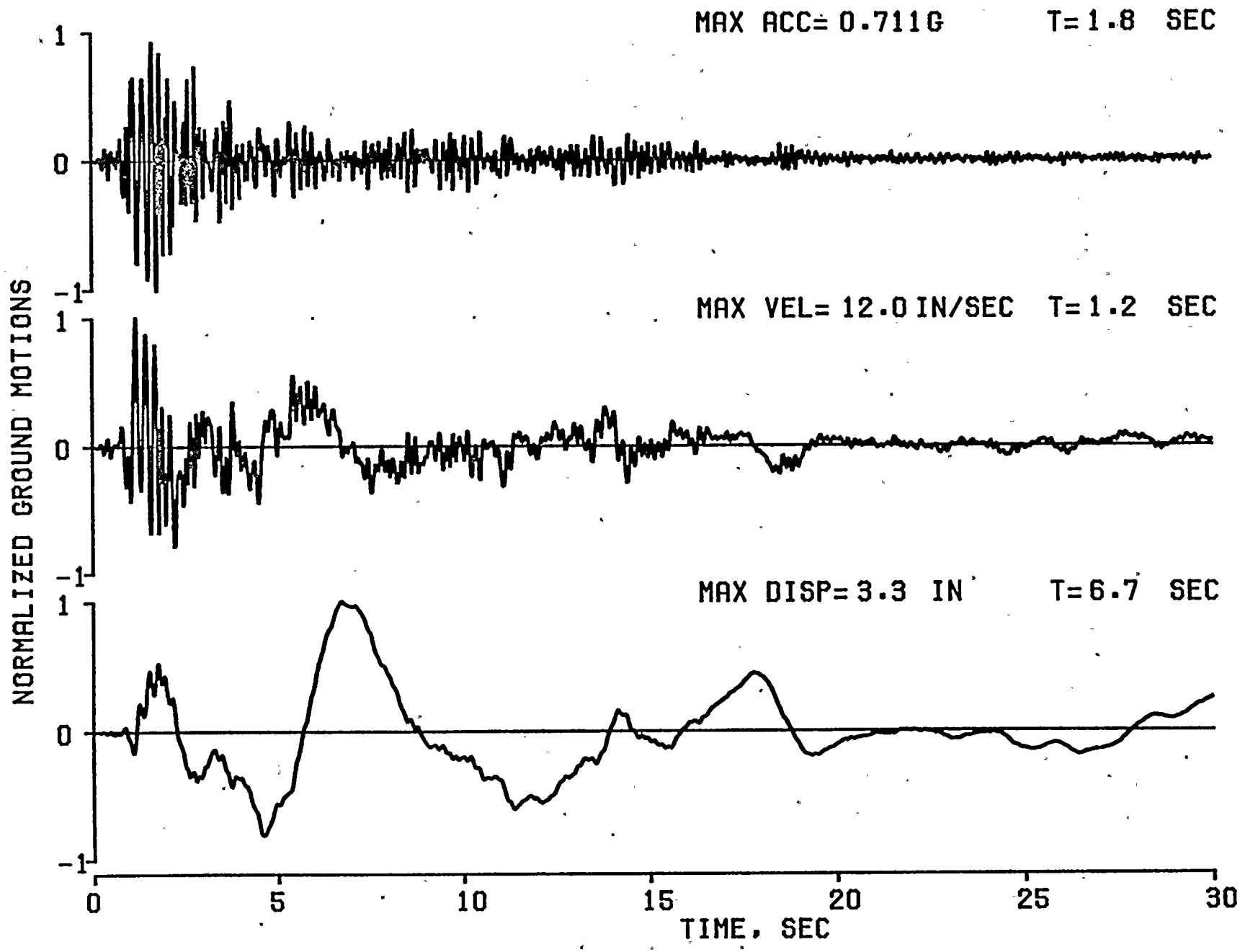

FIG. A.6 ACCELERATION VELOCITY AND DISPLACEMENT HISTORIES FOR RECORD NO. 6

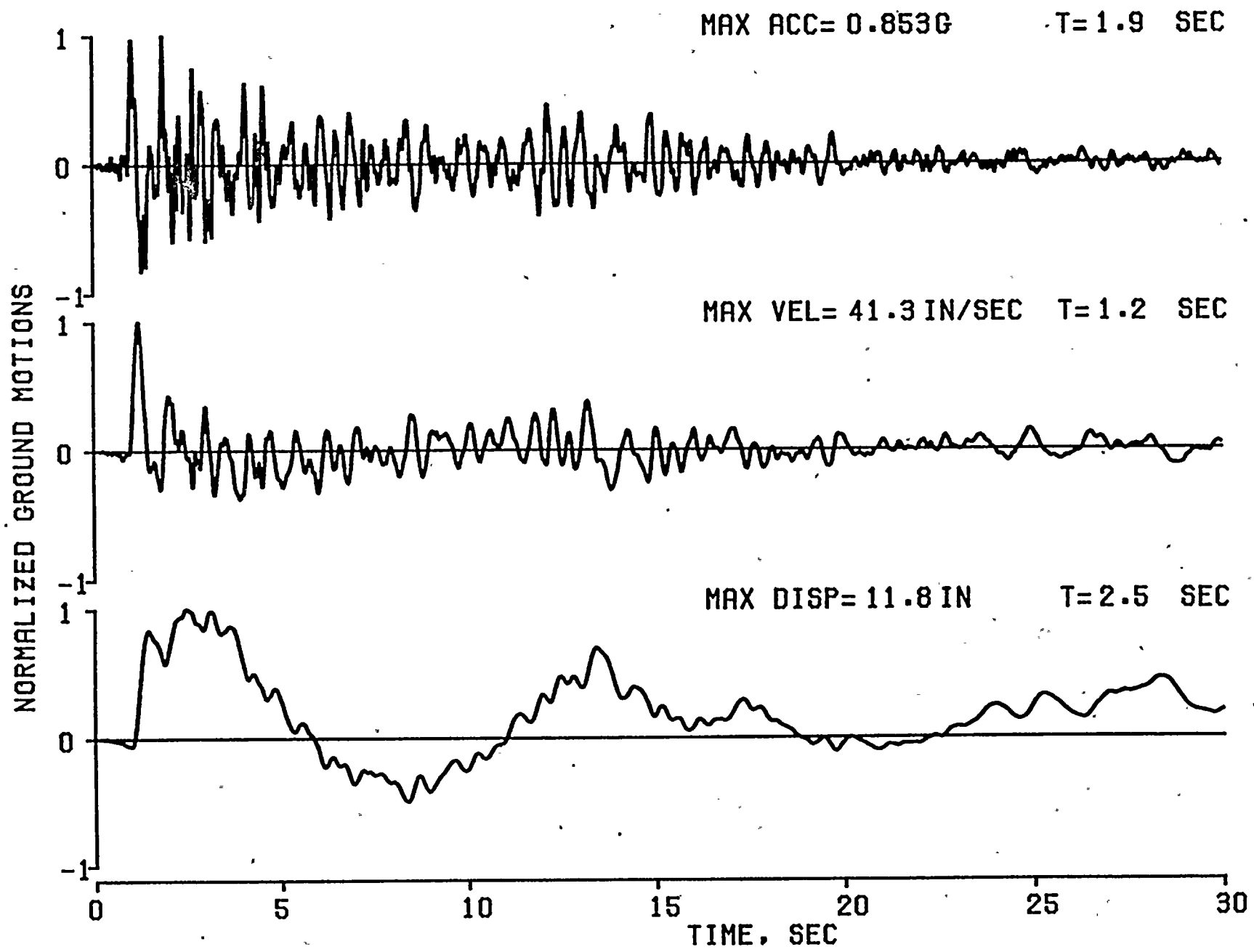

FIG. A.7 ACCELERATION VELOCITY AND DISPLACEMENT HISTORIES FOR RECORD NO. 7

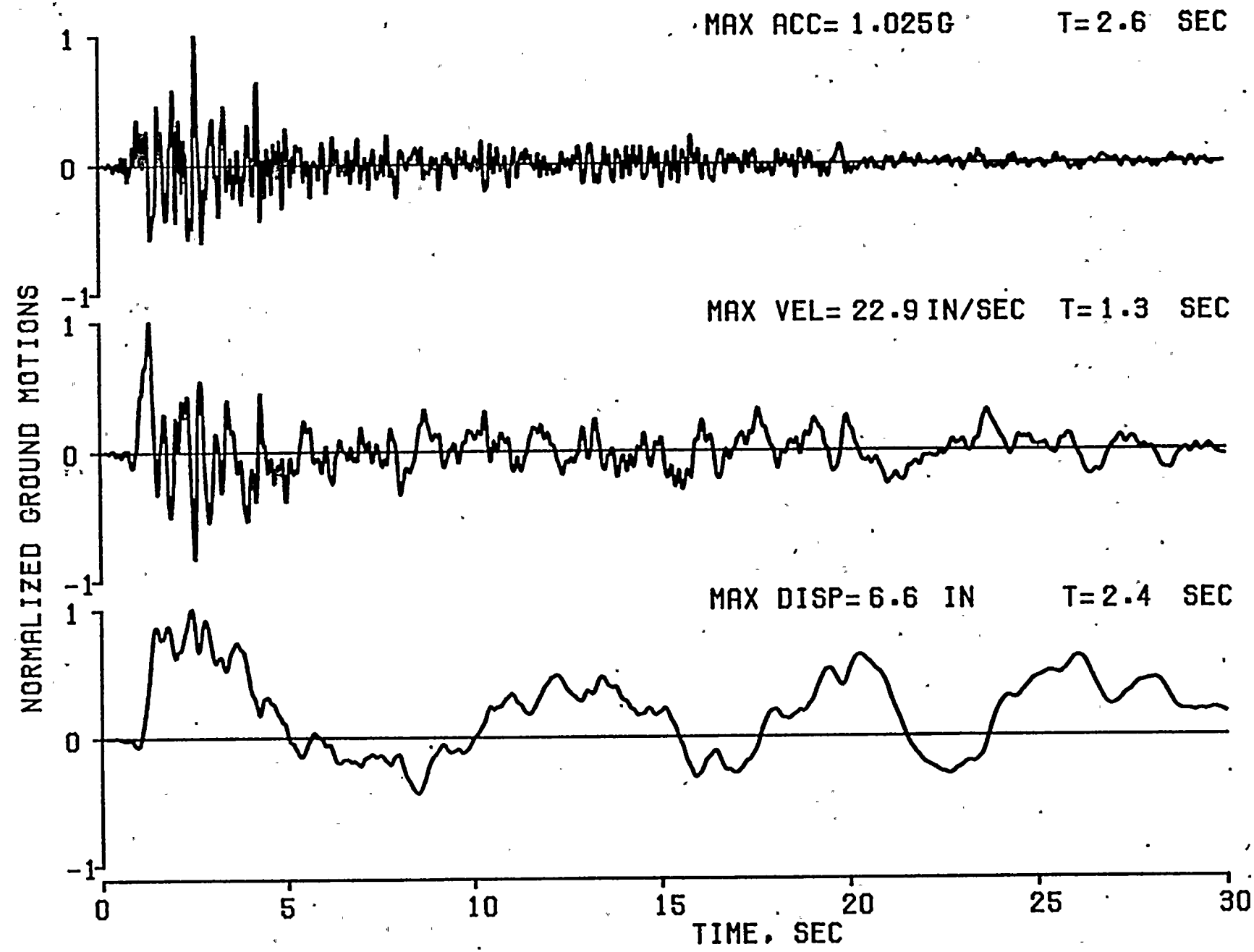

FIG. A.8 ACCELERATION VELOCITY AND DISPLACEMENT HISTORIES FOR RECORD NO. 8

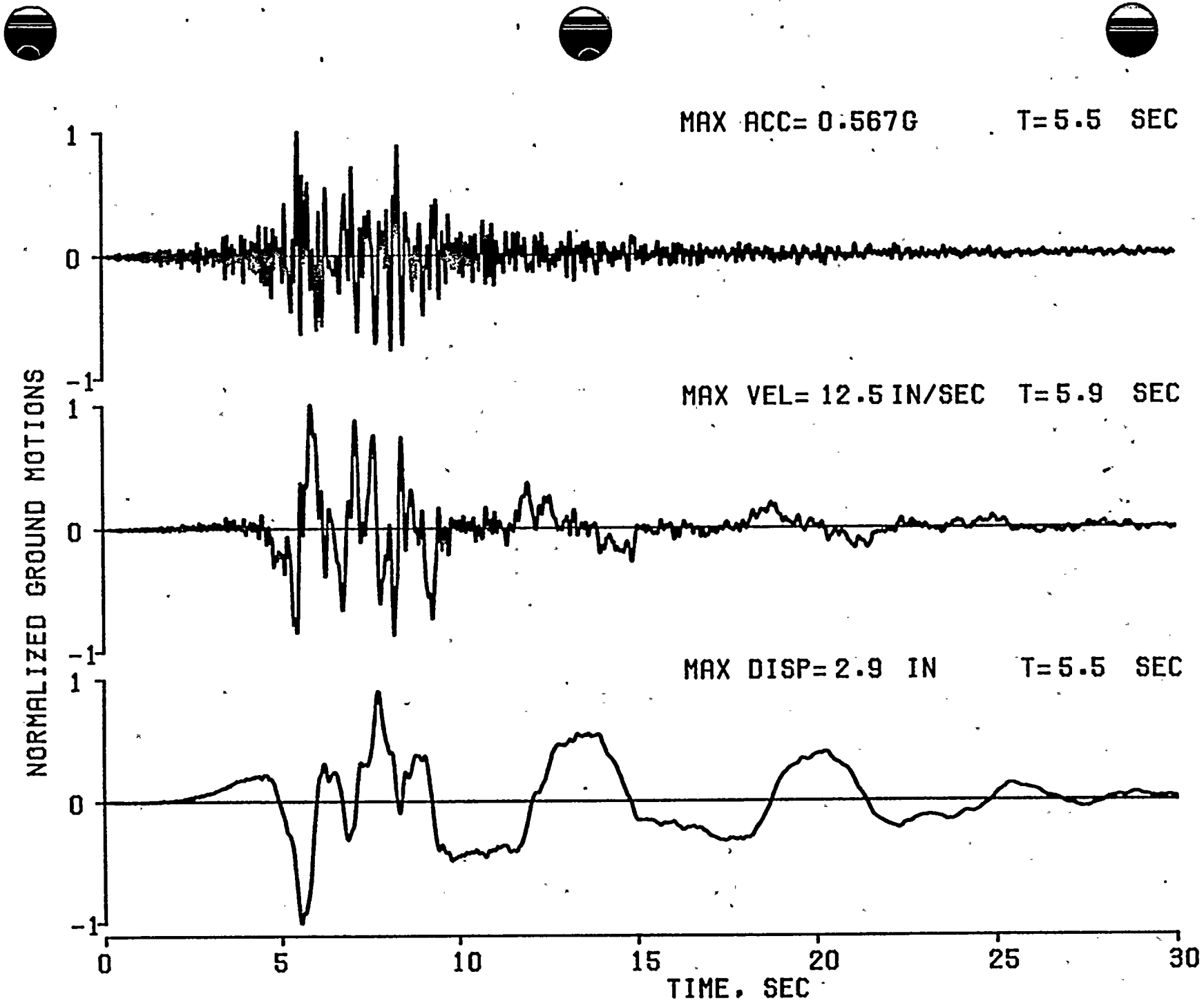

FIG. A.9 ACCELERATION VELOCITY AND DISPLACEMENT HISTORIES FOR RECORD NO. 9

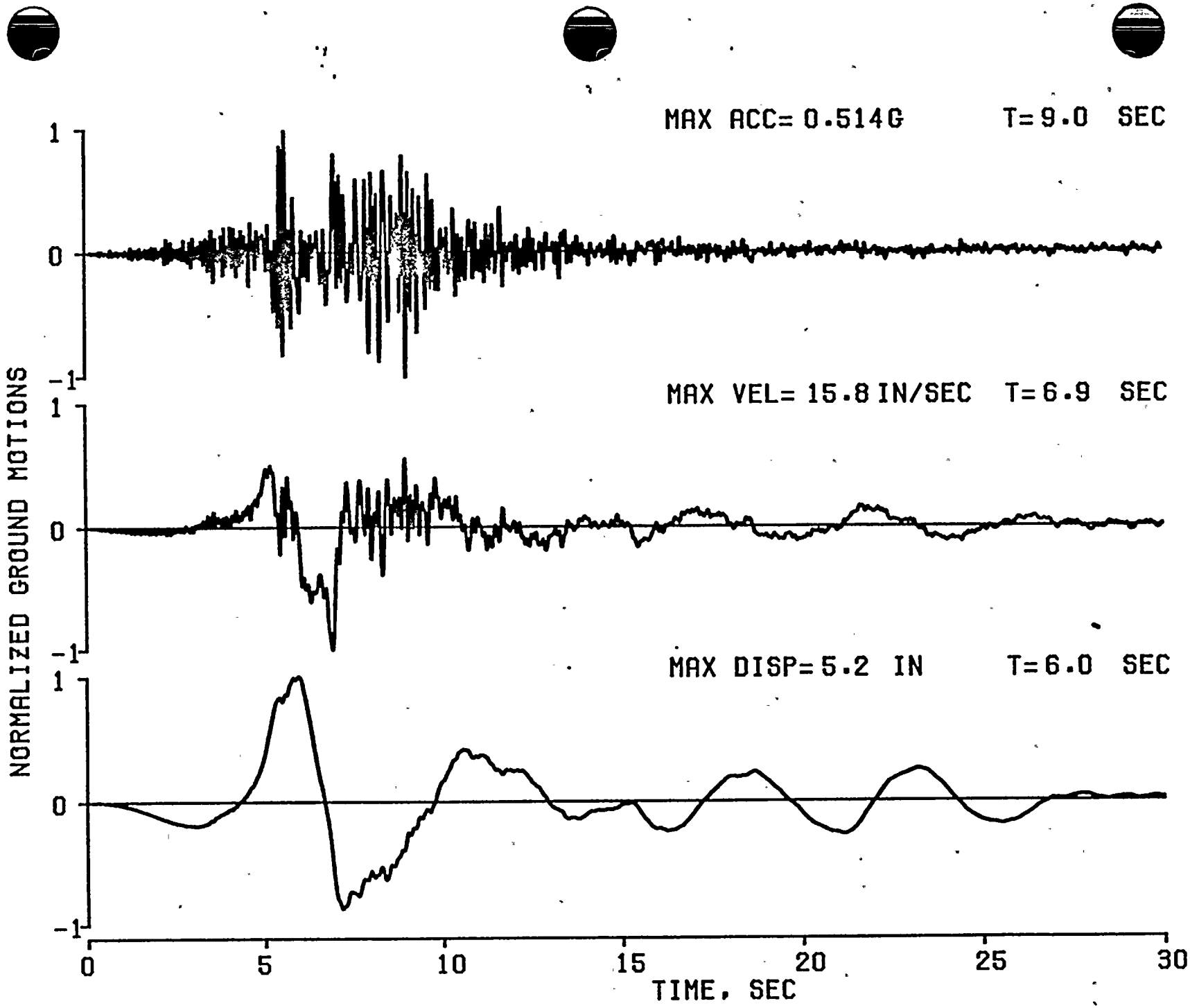

FIG. A.10 ACCELERATION VELOCITY AND DISPLACEMENT HISTORIES FOR RECORD NO. 10

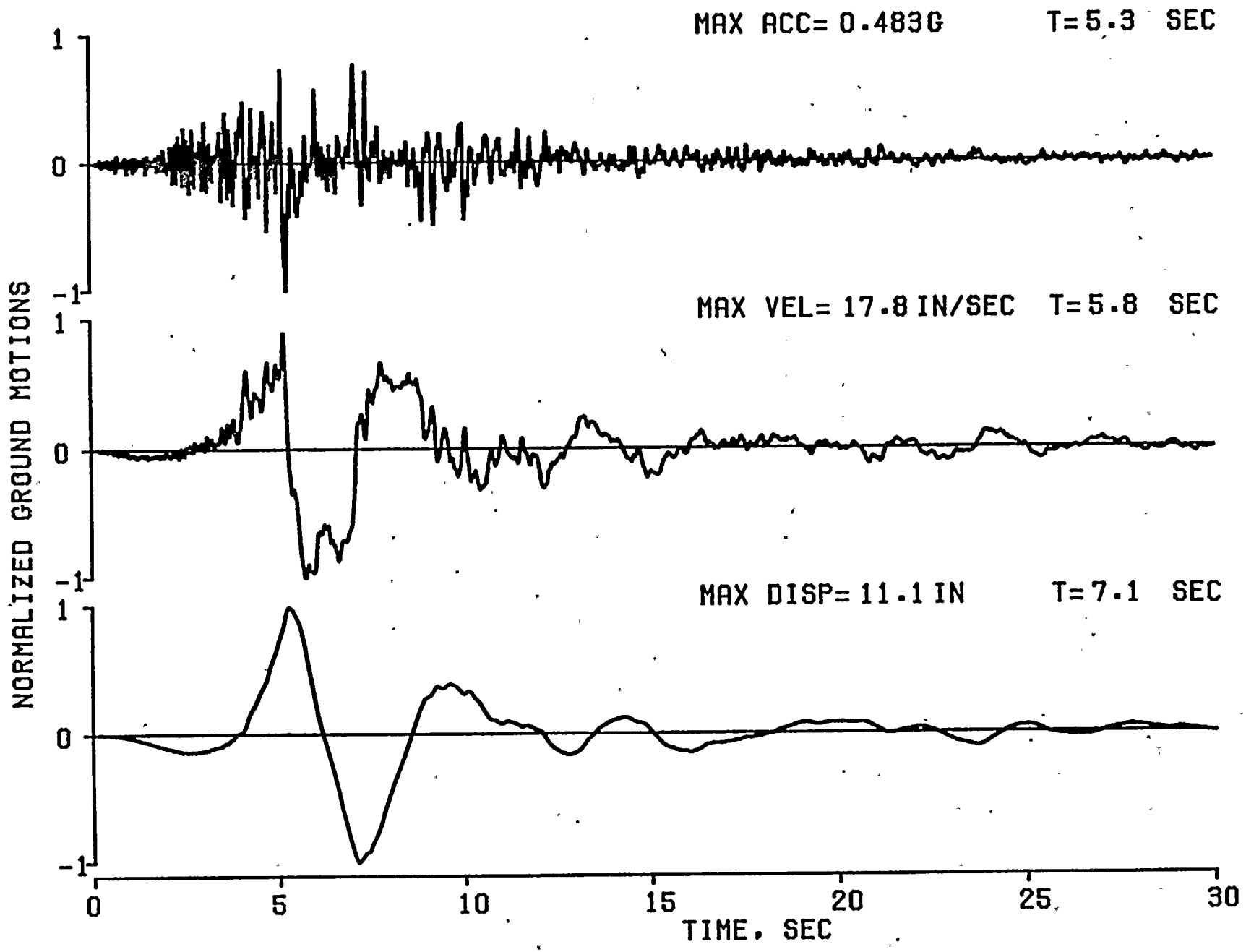

FIG. A.11 ACCELERATION VELOCITY AND DISPLACEMENT HISTORIES FOR RECORD NO. 11

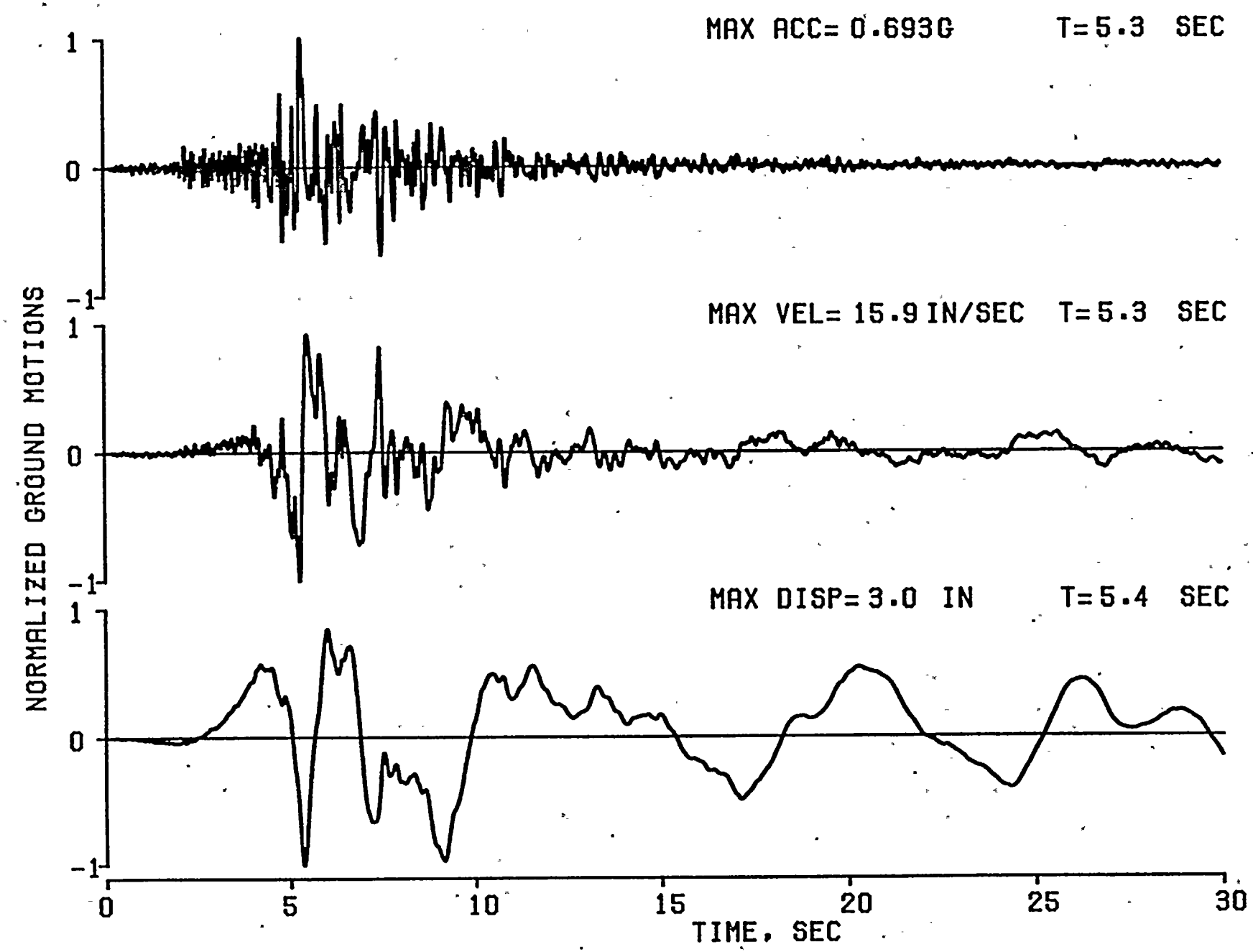

FIG. A.12 ACCELERATION VELOCITY AND DISPLACEMENT HISTORIES FOR RECORD NO. 12

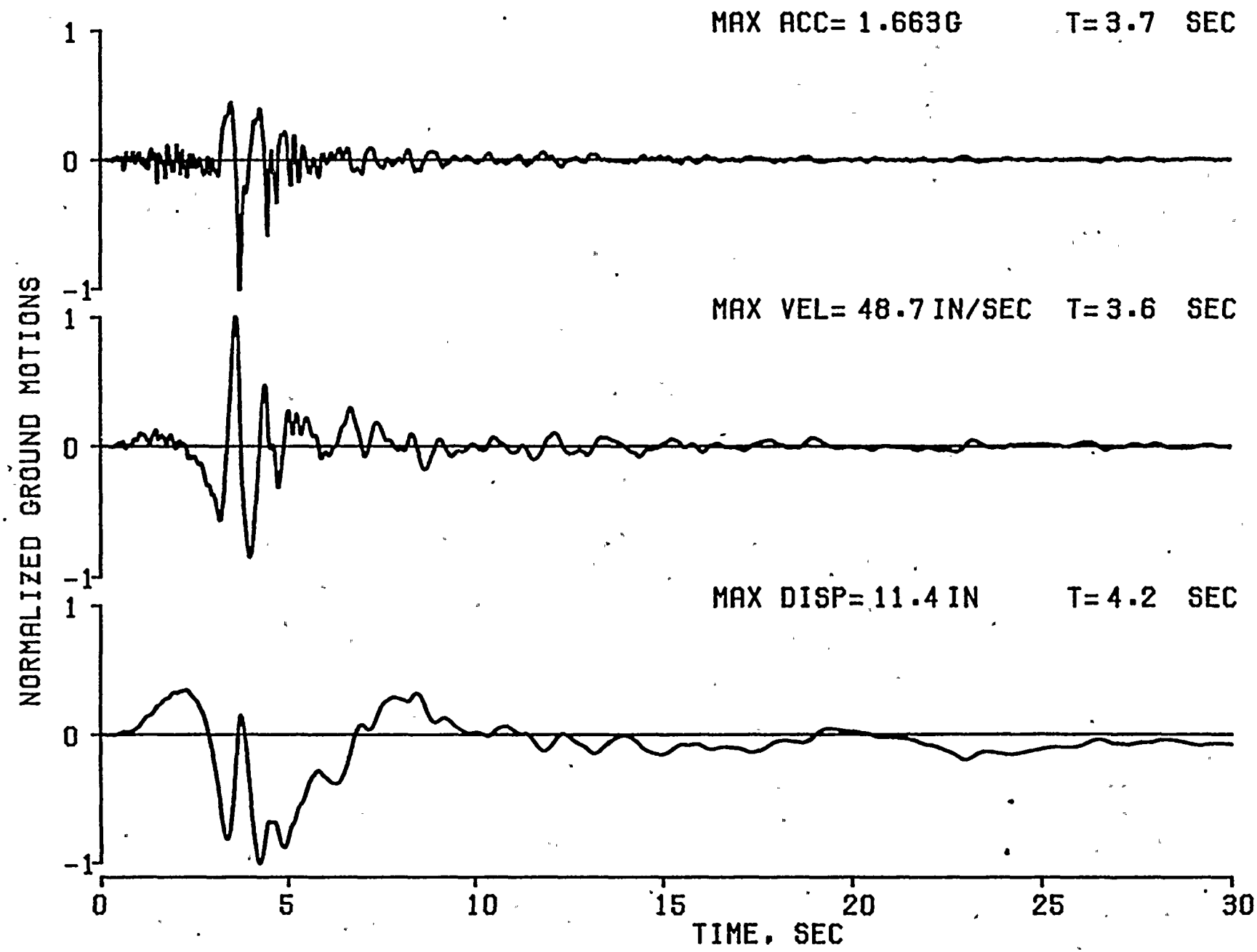

FIG. A.13 ACCELERATION VELOCITY AND DISPLACEMENT HISTORIES FOR RECORD NO. 13

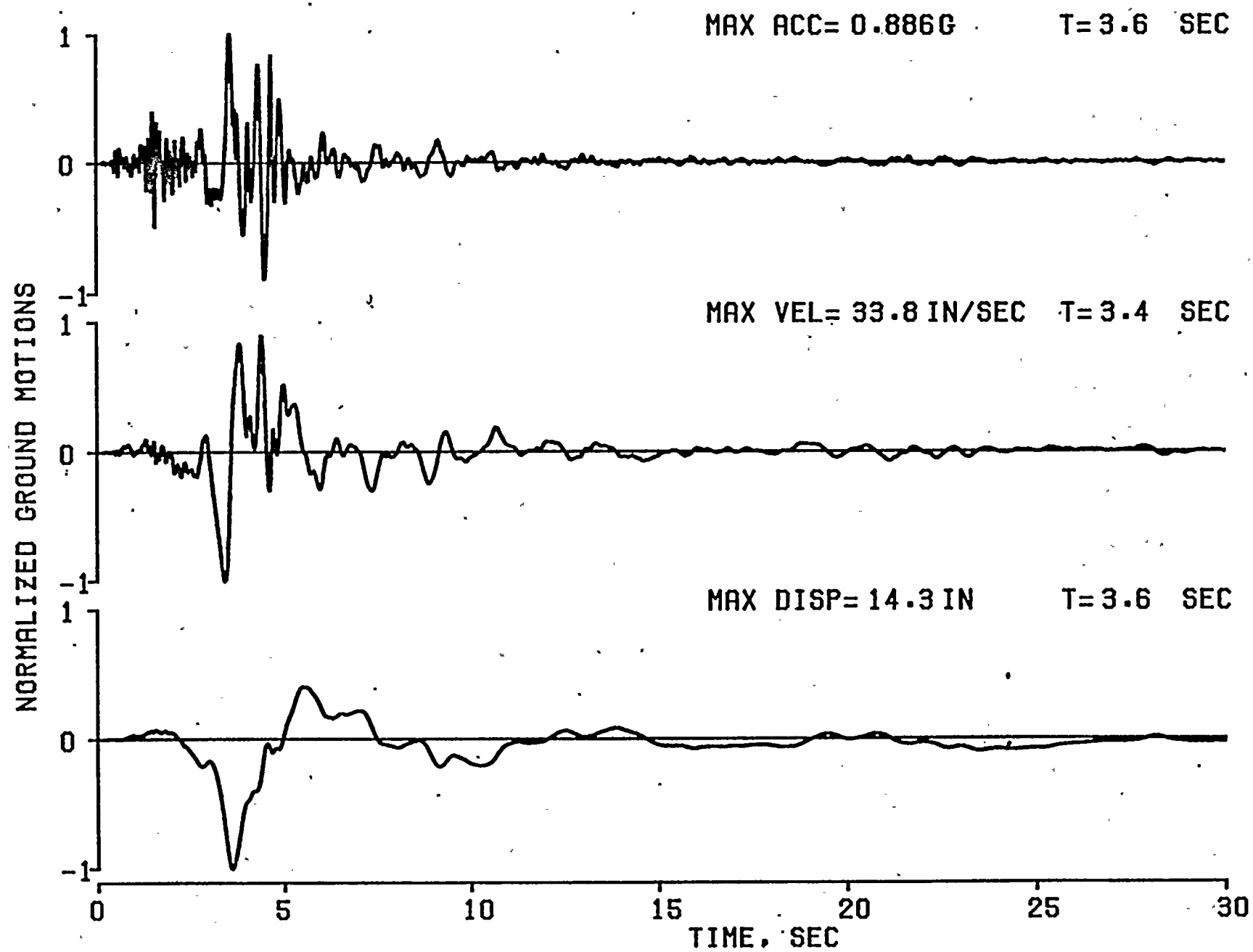

FIG. A.14 ACCELERATION VELOCITY AND DISPLACEMENT HISTORIES FOR RECORD NO. 14

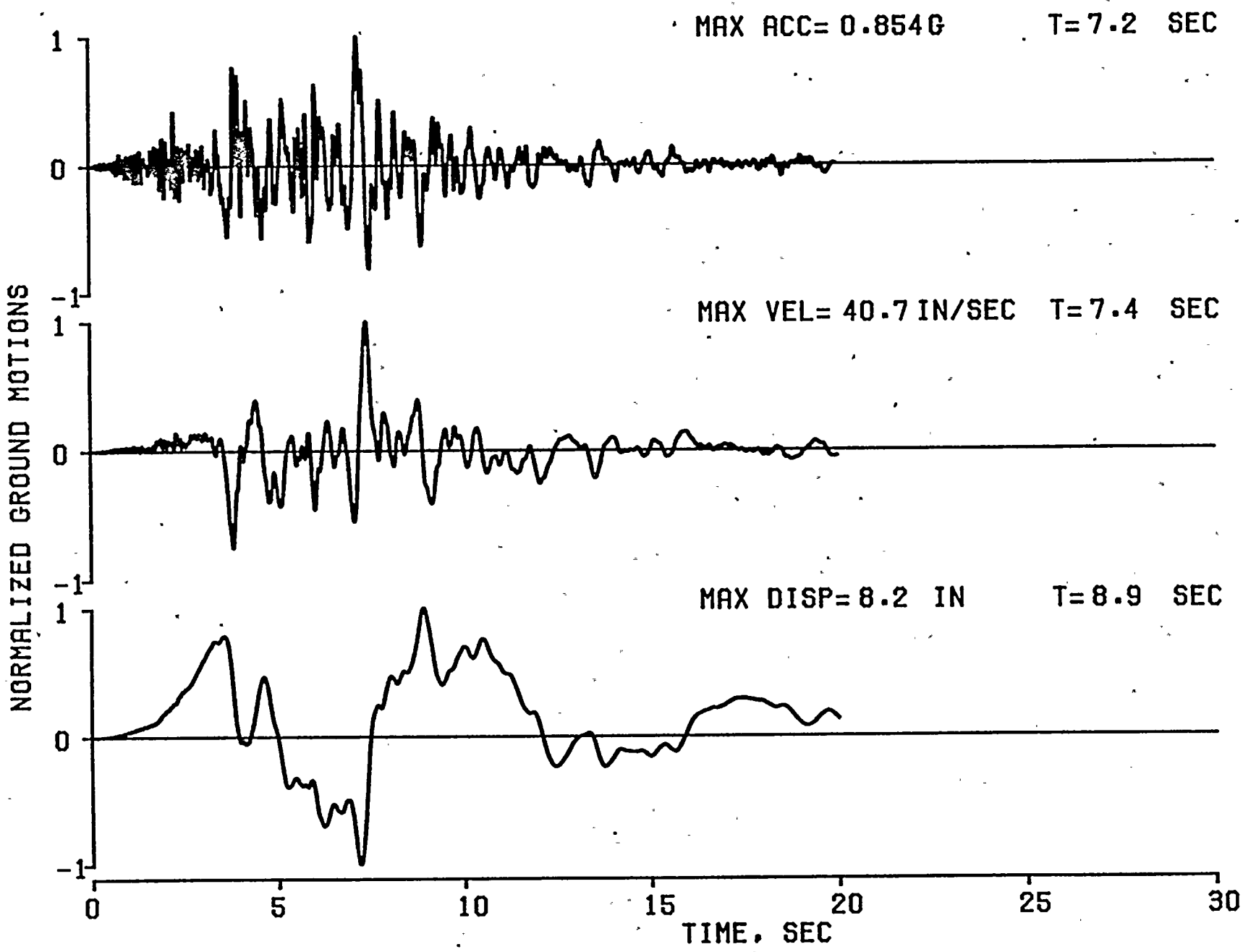

FIG. A.15 ACCELERATION VELOCITY AND DISPLACEMENT HISTORIES FOR RECORD NO. 15.

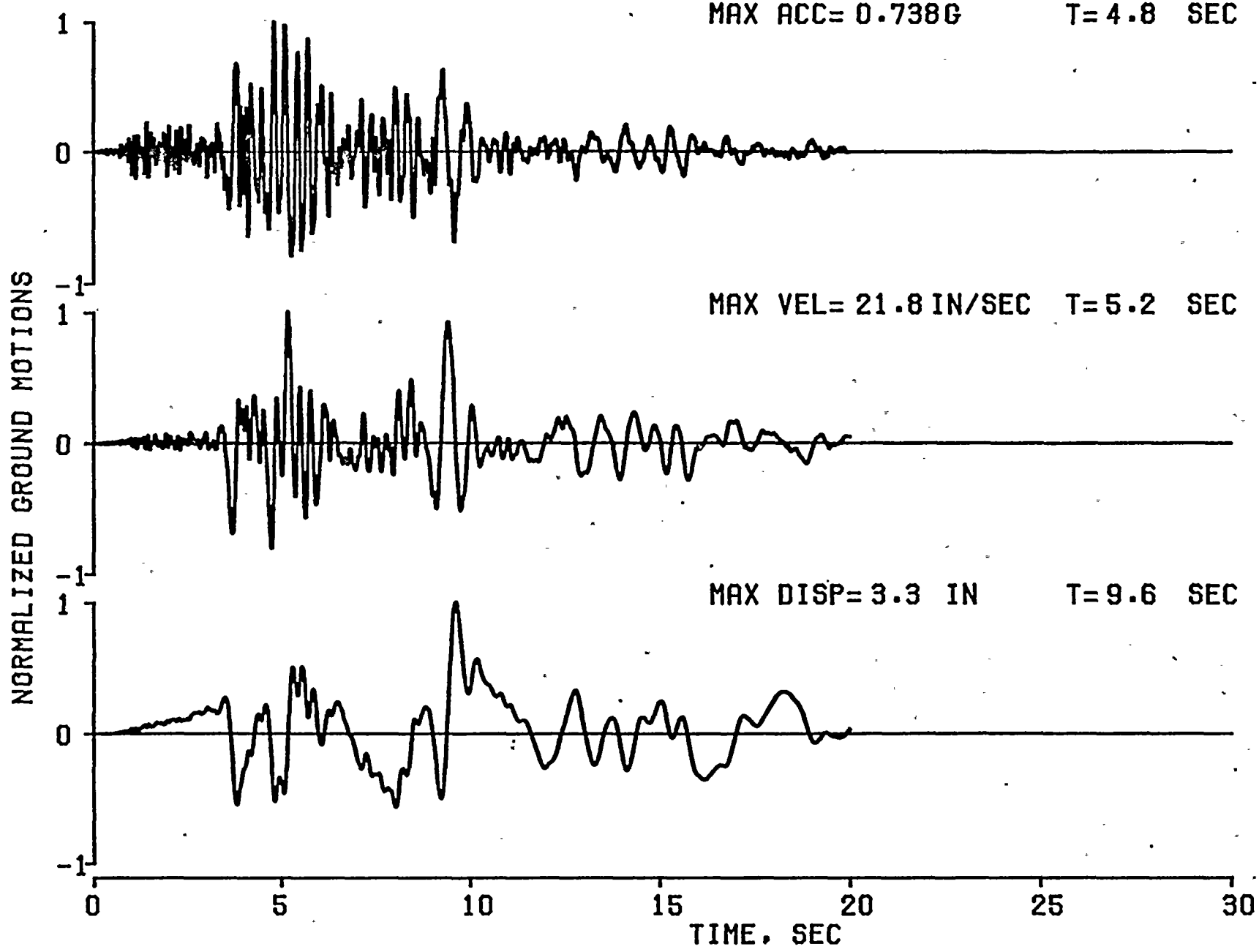

FIG. A.16 ACCELERATION VELOCITY AND DISPLACEMENT HISTORIES FOR RECORD NO. 16

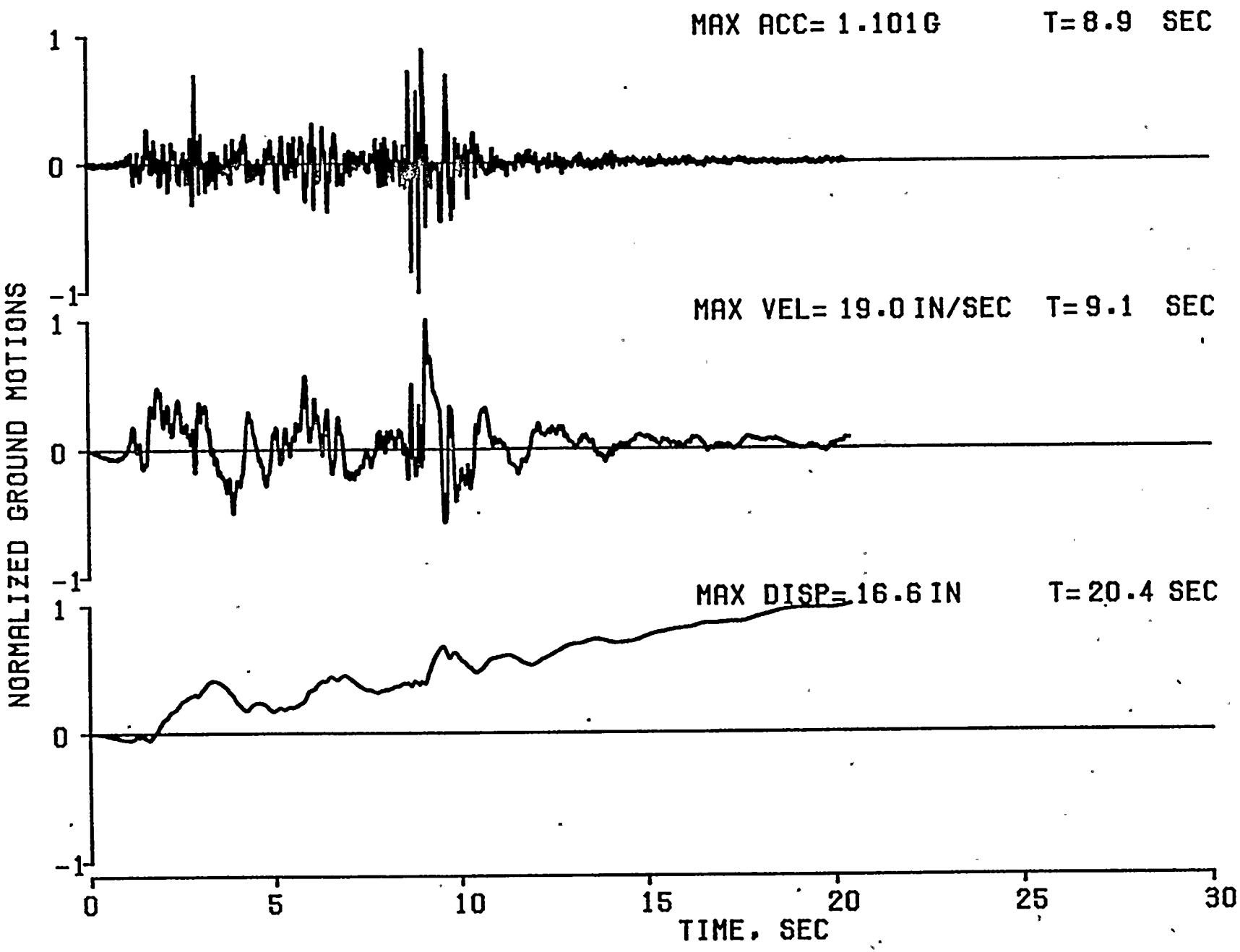

FIG. A.17 ACCELERATION VELOCITY AND DISPLACEMENT HISTORIES FOR RECORD NO. 17

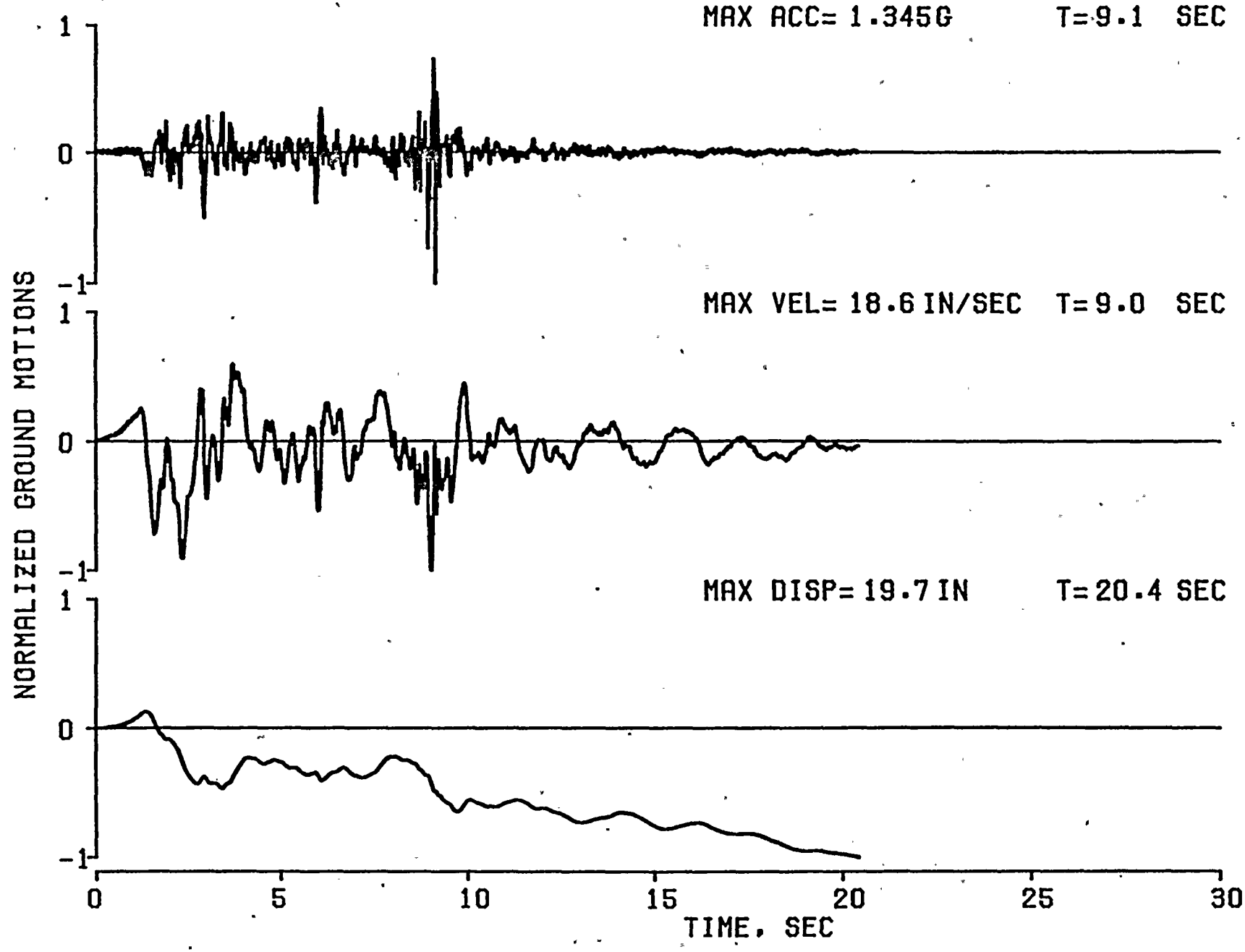

FIG. A.18 ACCELERATION VELOCITY AND DISPLACEMENT HISTORIES FOR RECORD NO. 18

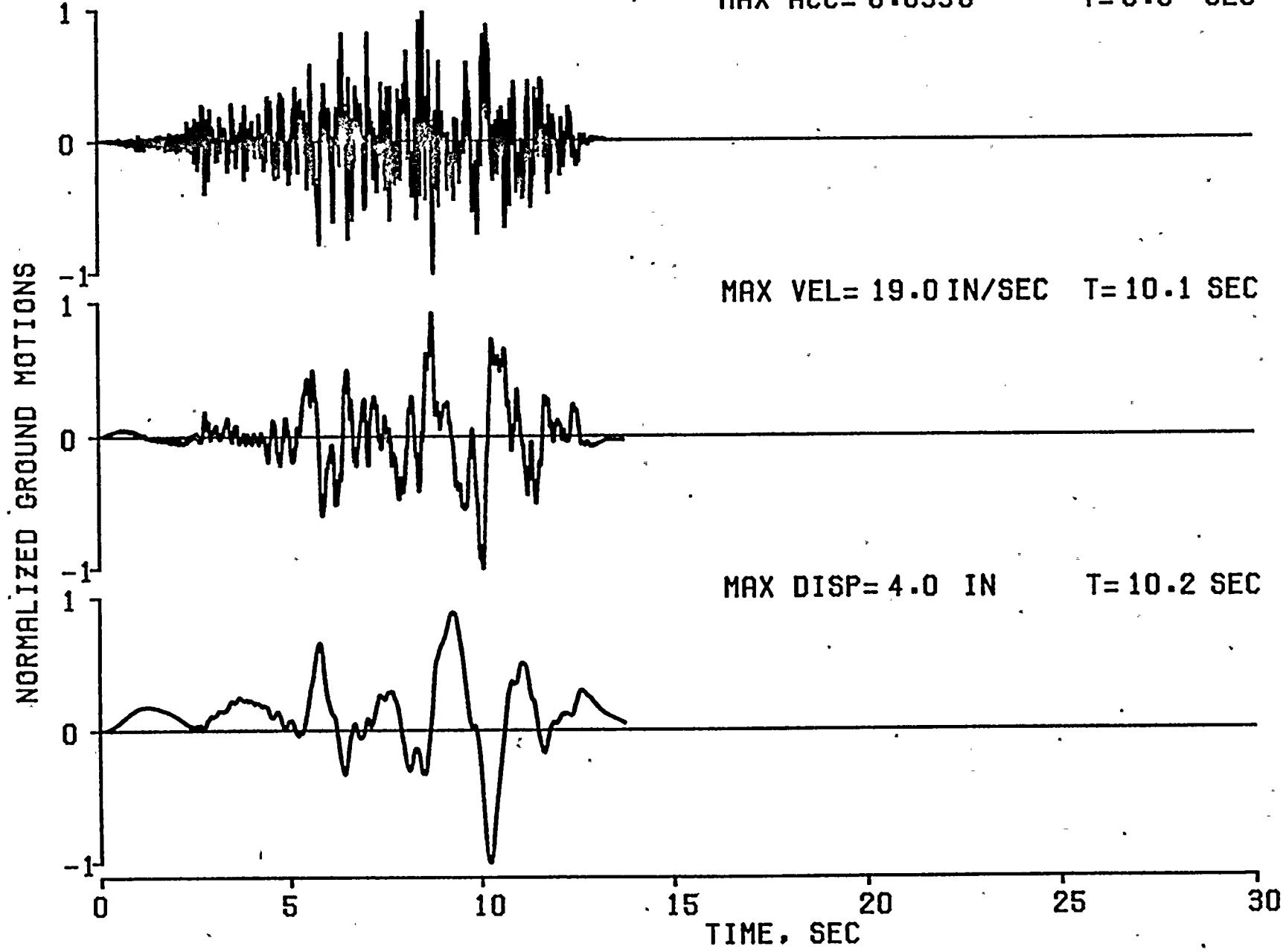

FIG. A.19 ACCELERATION VELOCITY AND DISPLACEMENT HISTORIES FOR RECORD NO. 19

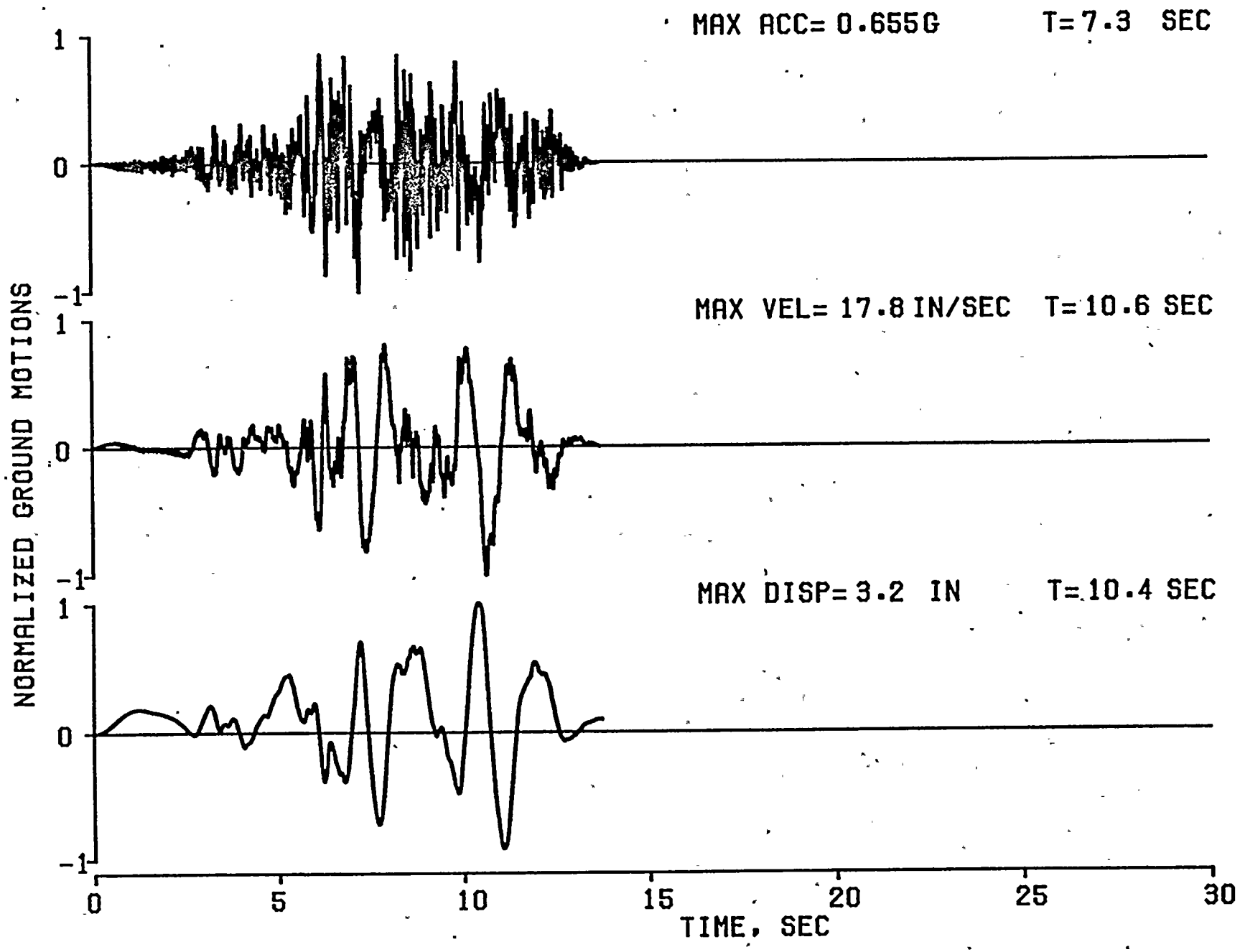

FIG. A.20 ACCELERATION VELOCITY AND DISPLACEMENT HISTORIES FOR RECORD NO. 20

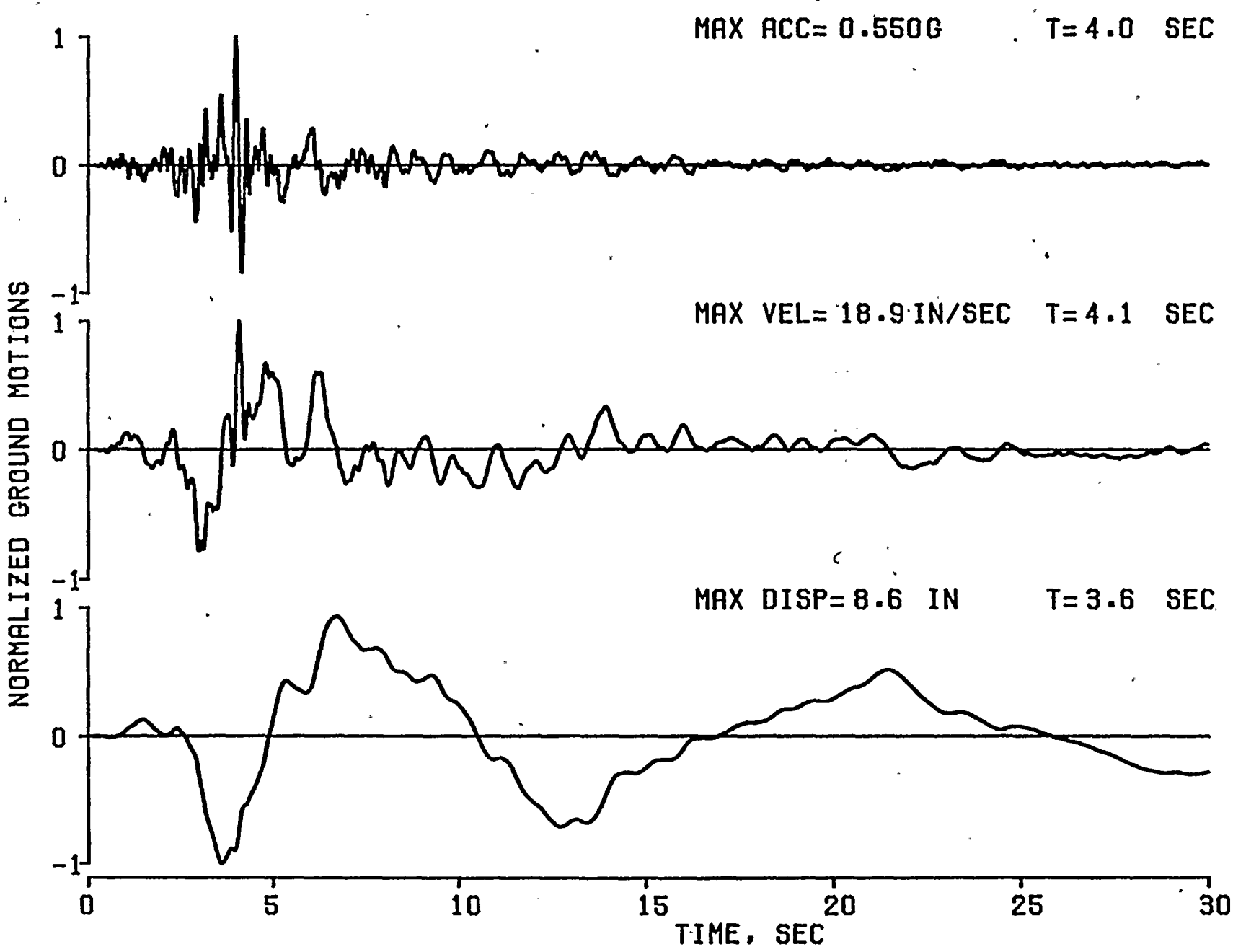

FIG. A.21 ACCELERATION VELOCITY AND DISPLACEMENT HISTORIES FOR RECORD NO. 21

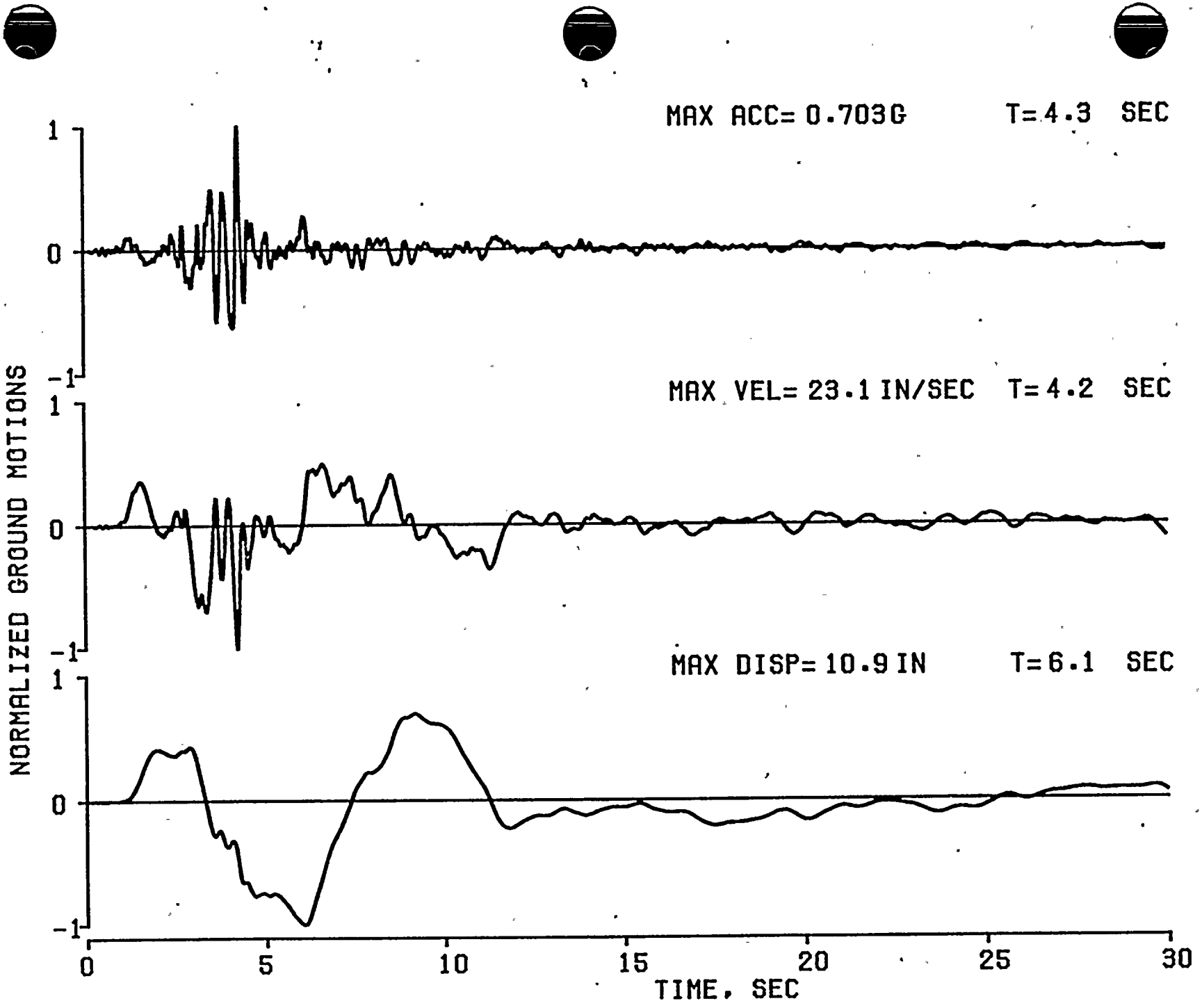

FIG. A.22 ACCELERATION VELOCITY AND DISPLACEMENT HISTORIES FOR RECORD NO. 22

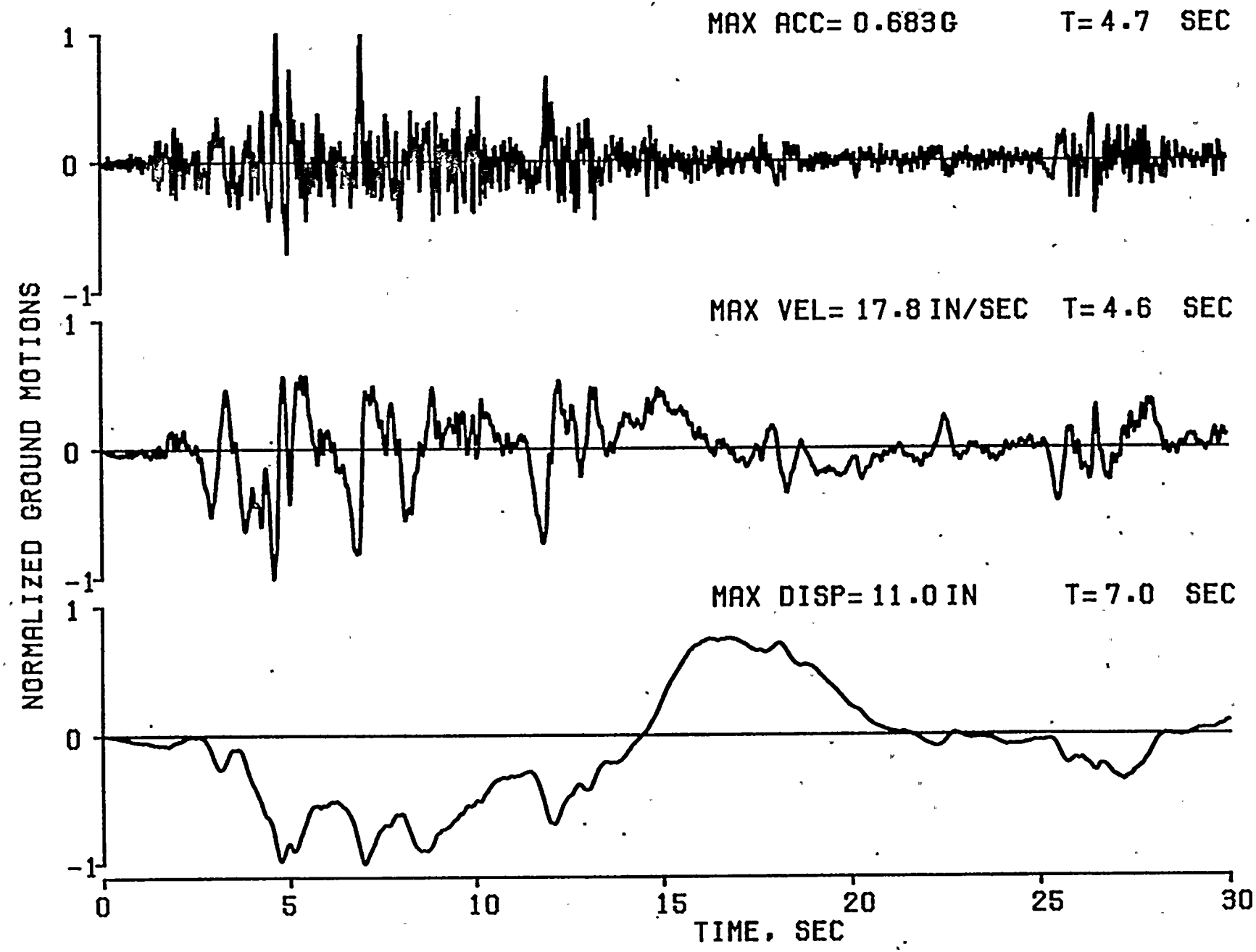

FIG. A.23 ACCELERATION VELOCITY AND DISPLACEMENT HISTORIES FOR RECORD NO. 23

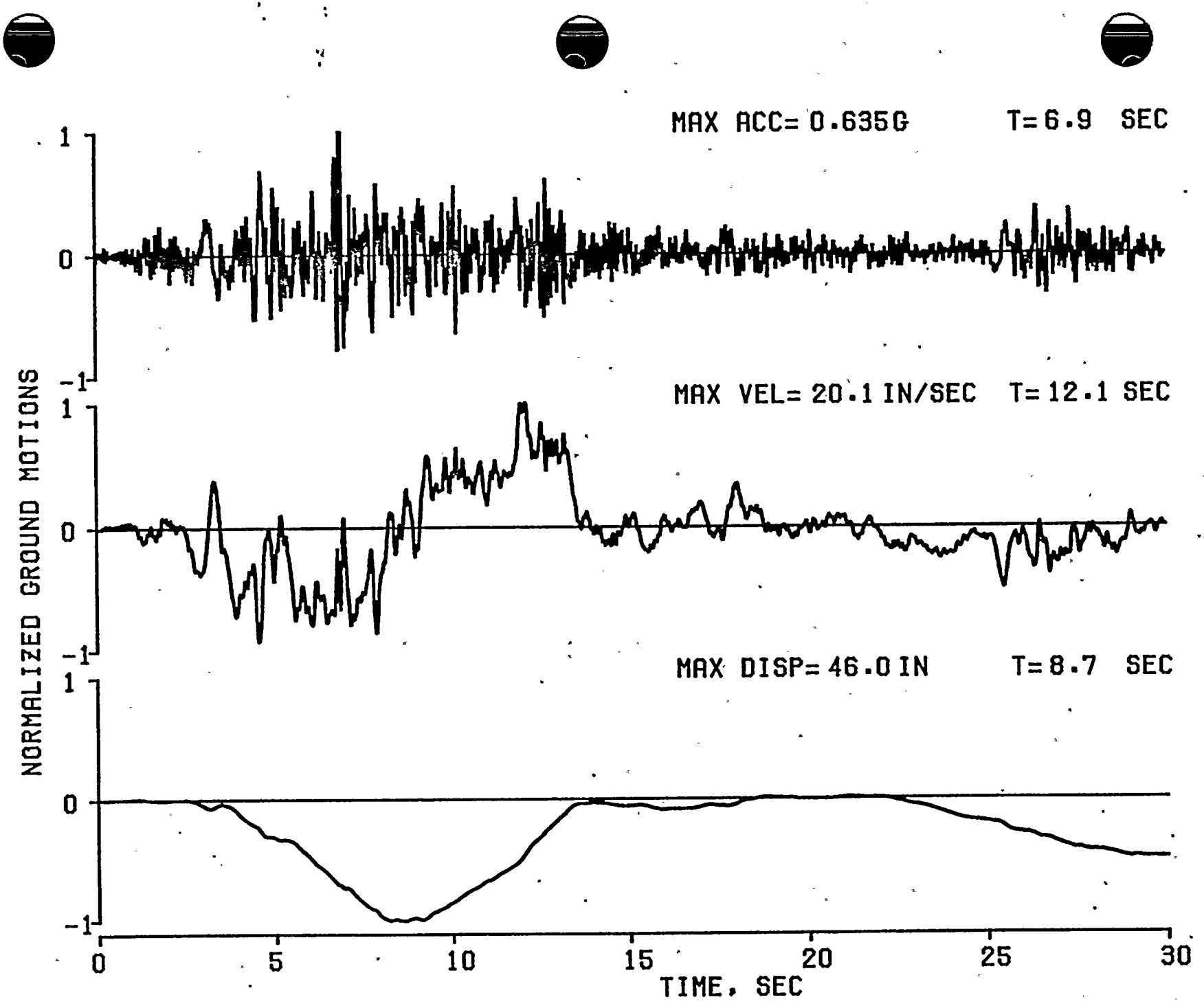

FIG. A.24 ACCELERATION VELOCITY AND DISPLACEMENT HISTORIES FOR RECORD NO. 24

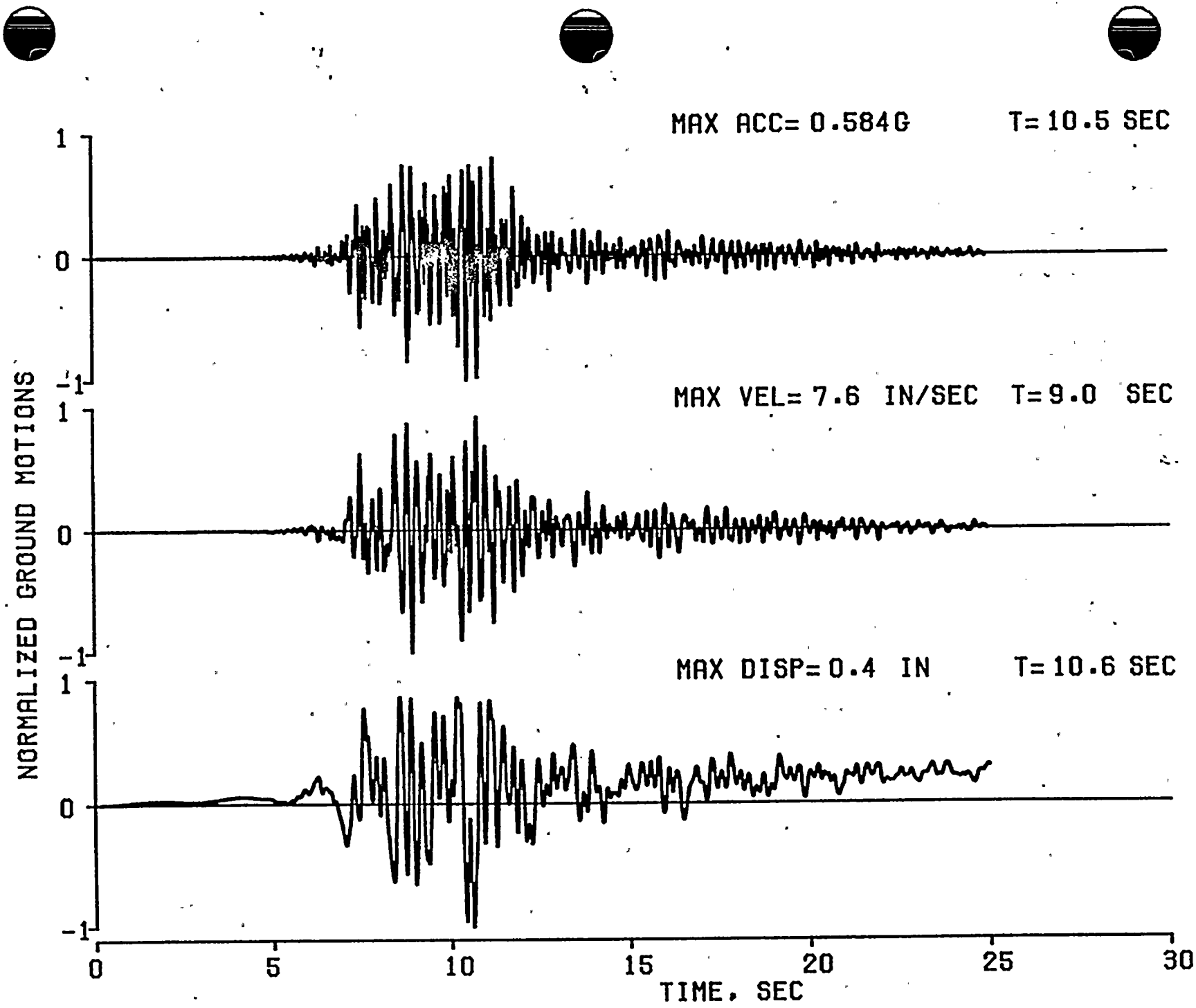

FIG. A.25 ACCELERATION VELOCITY AND DISPLACEMENT HISTORIES FOR RECORD NO. 25

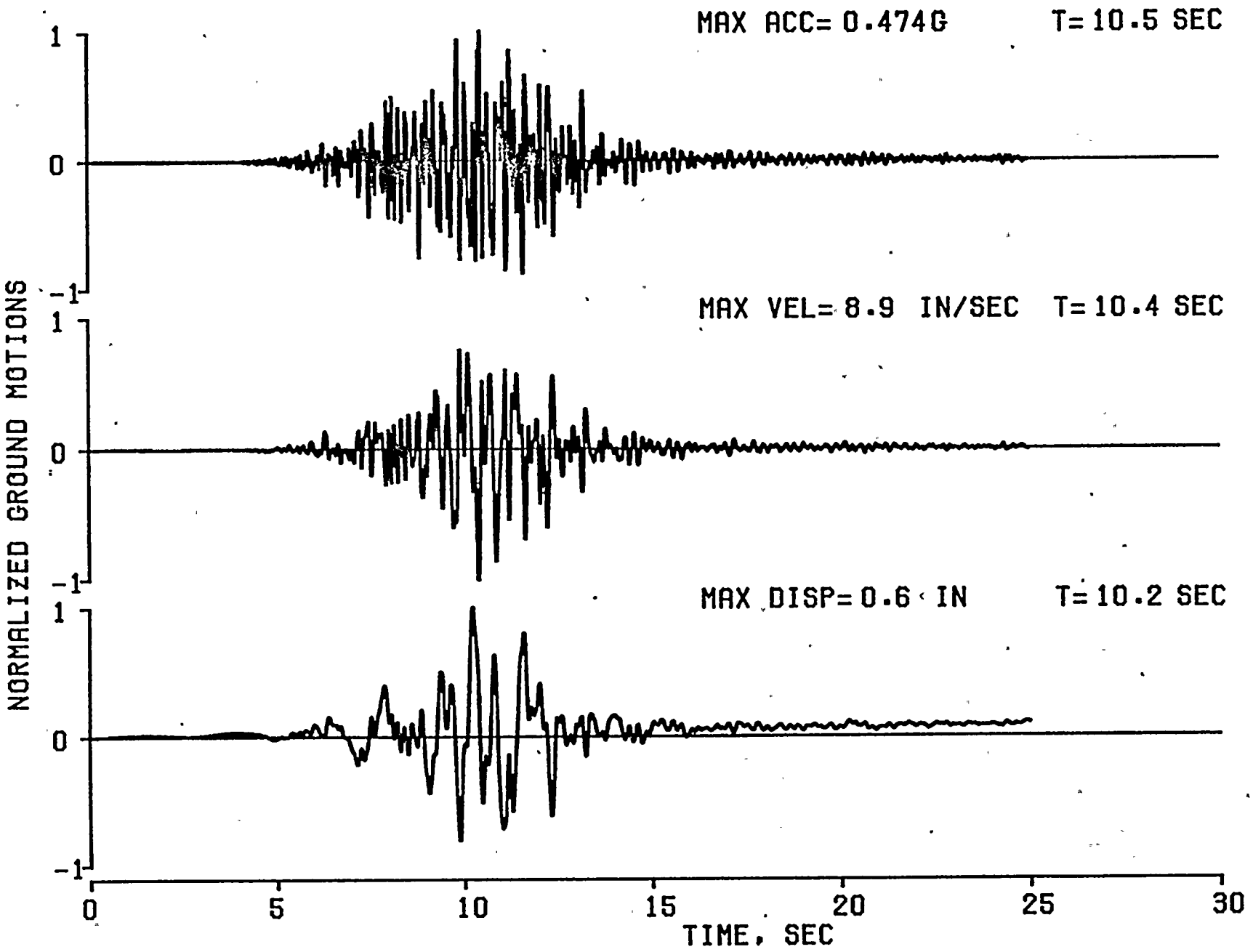

FIG. A.26 ACCELERATION VELOCITY AND DISPLACEMENT HISTORIES FOR RECORD NO. 26

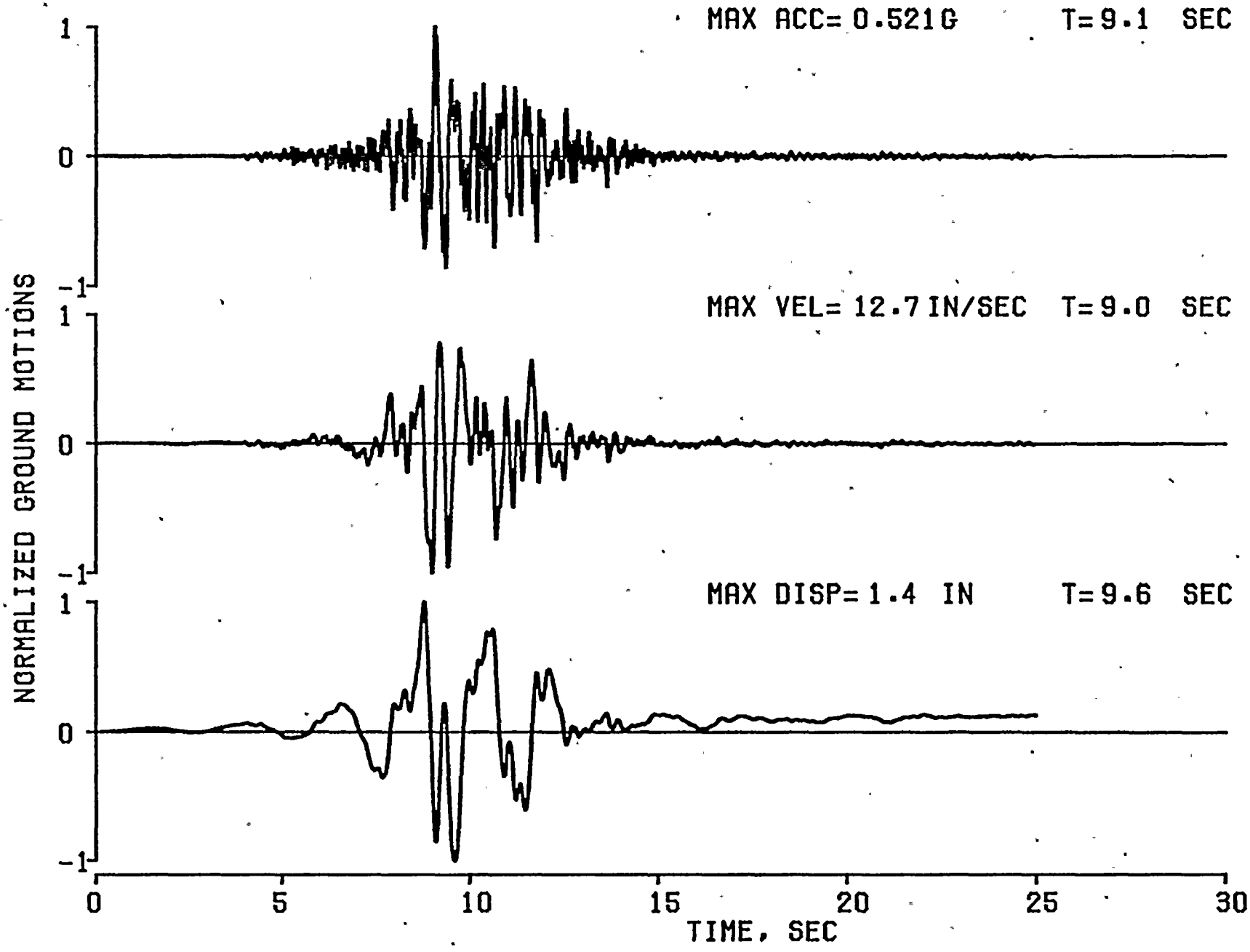

FIG. A.27 ACCELERATION VELOCITY AND DISPLACEMENT HISTORIES FOR RECORD NO. 27

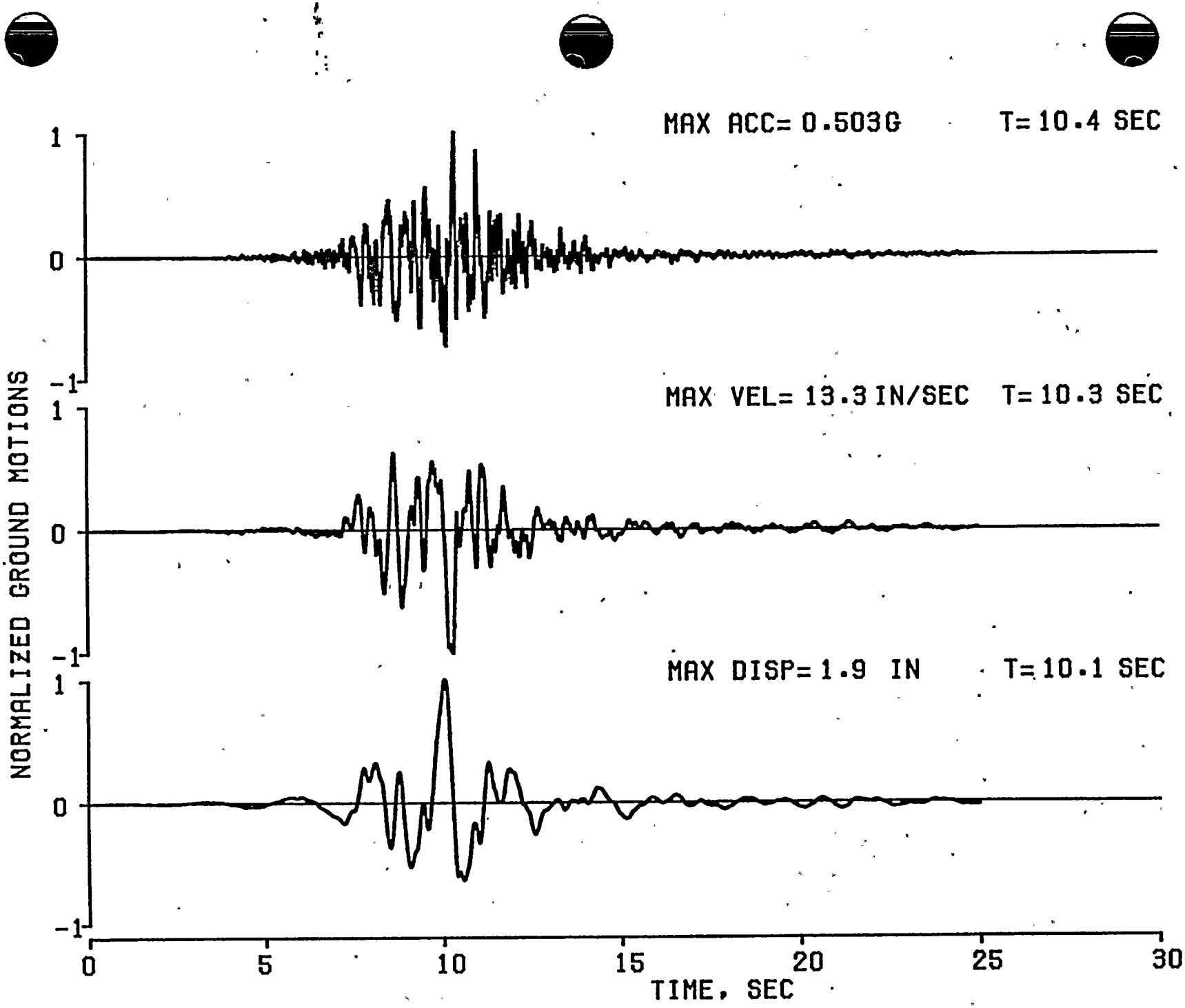

FIG. A.28 ACCELERATION VELOCITY AND DISPLACEMENT HISTORIES FOR RECORD NO. 28

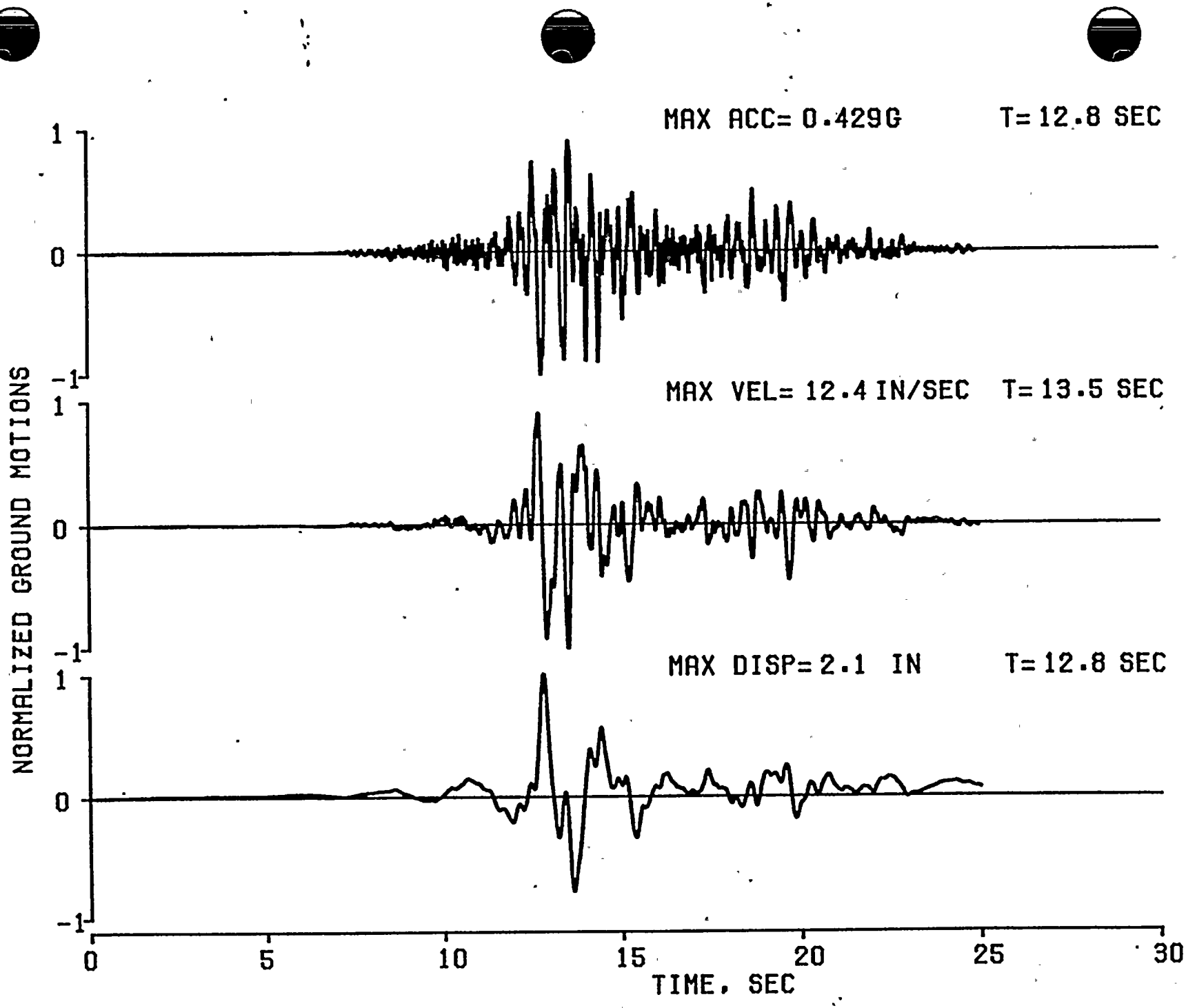

FIG. A.29 ACCELERATION VELOCITY AND DISPLACEMENT HISTORIES FOR RECORD NO. 29

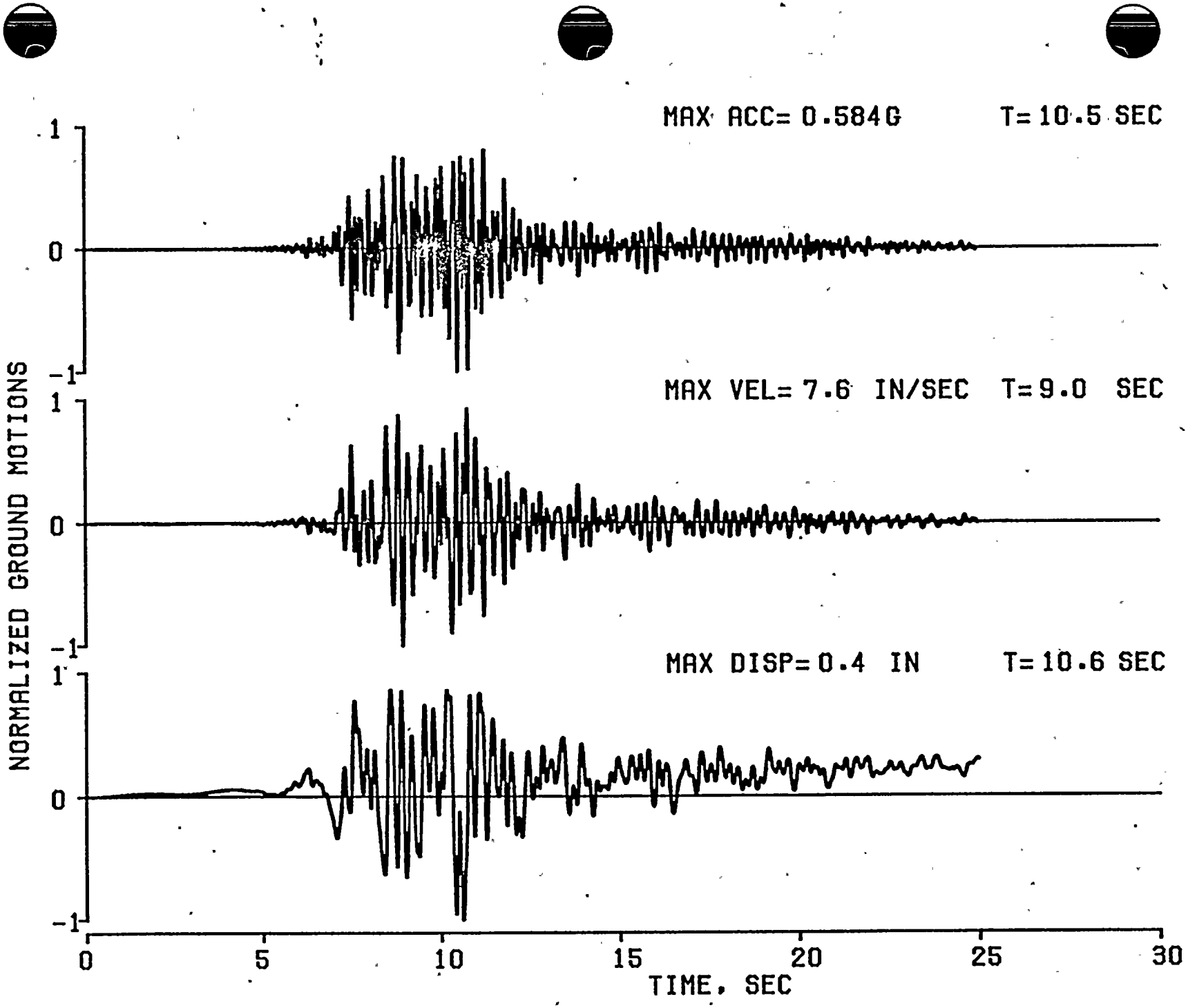

FIG. A.30 ACCELERATION VELOCITY AND DISPLACEMENT HISTORIES FOR RECORD NO. 30

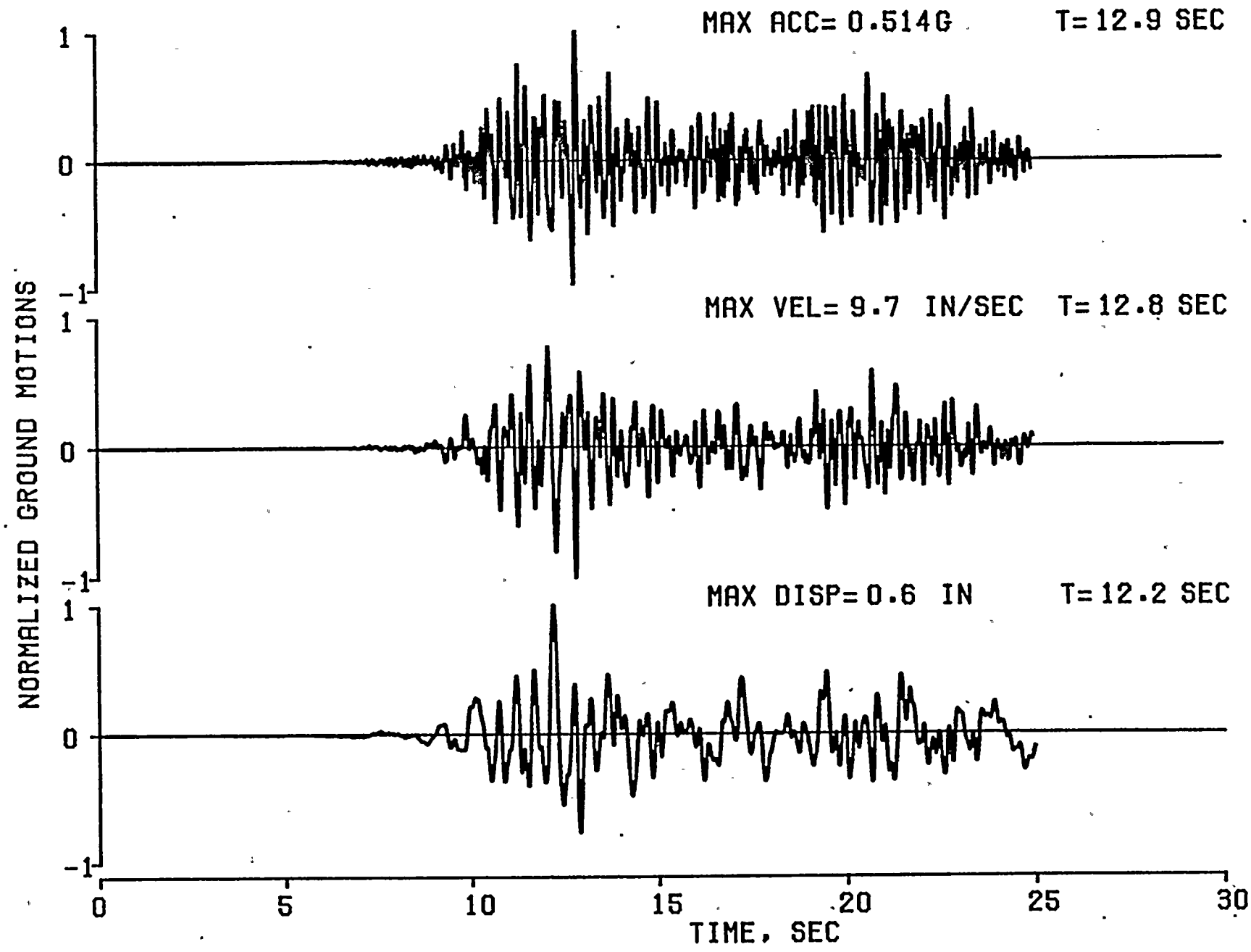

FIG. A.31 ACCELERATION VELOCITY AND DISPLACEMENT HISTORIES FOR RECORD NO. 31

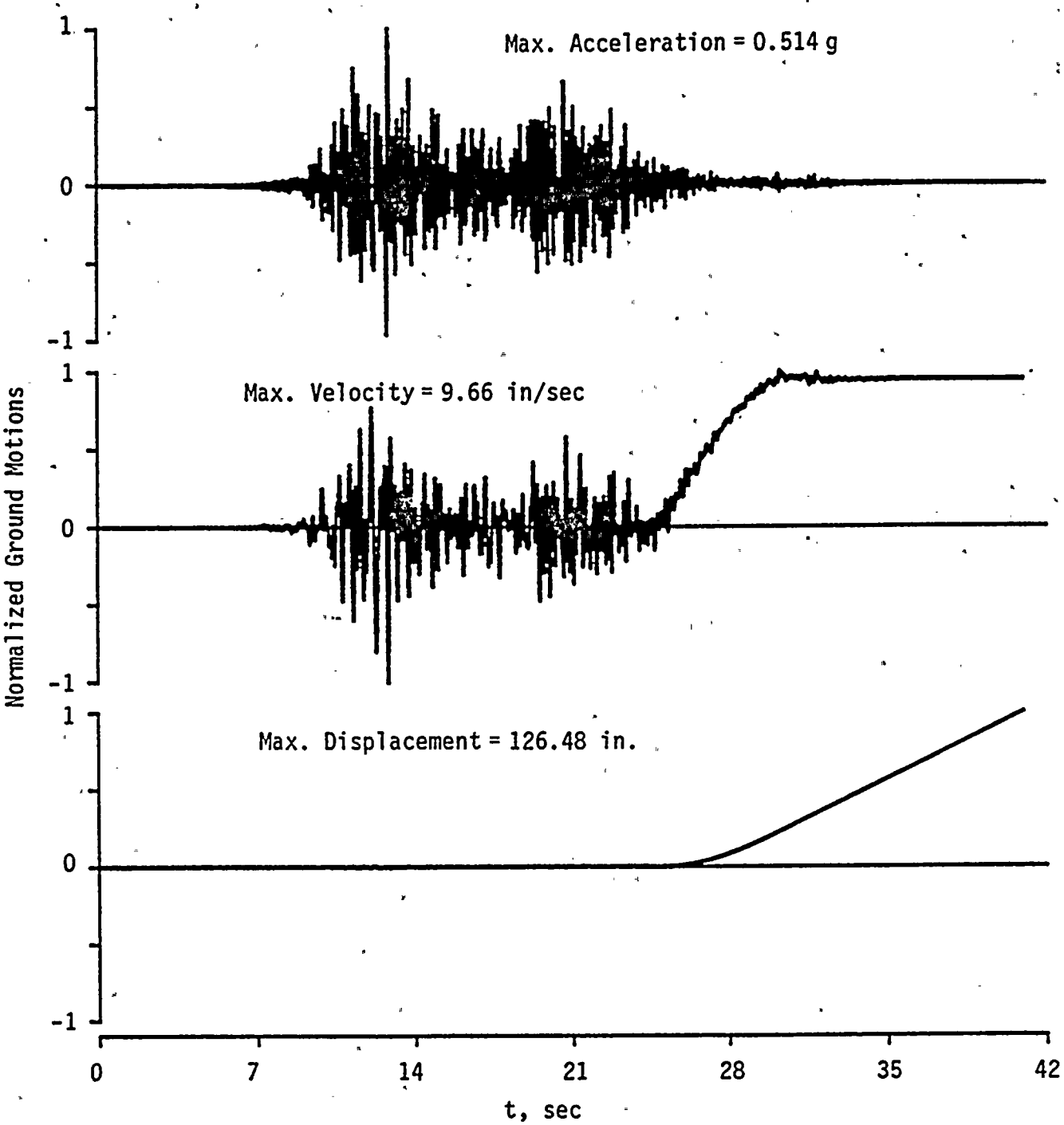

FIG. A.31b Acceleration, Velocity and Displacement Histories for Complete Records No. 31

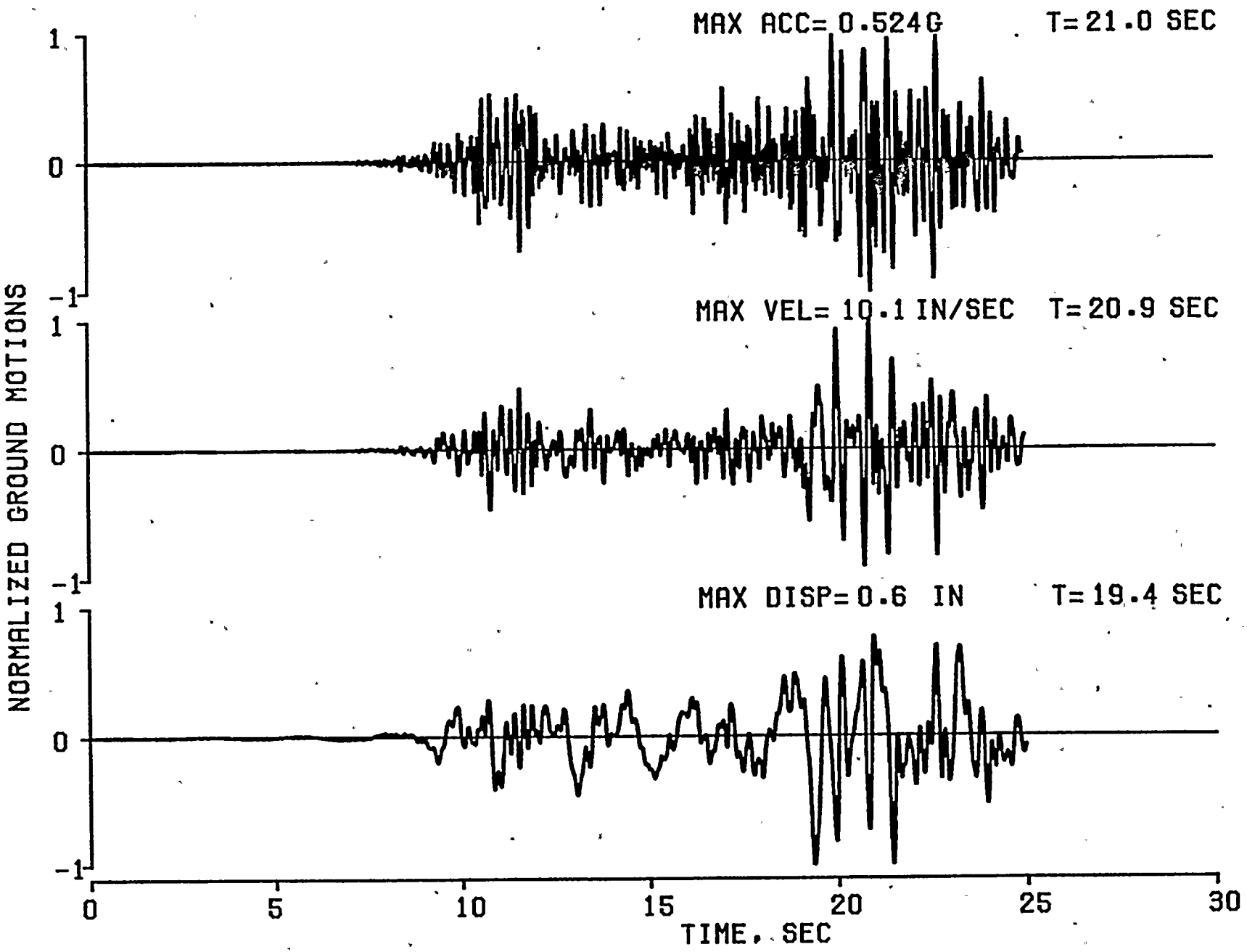

FIG. A.32 ACCELERATION VELOCITY AND DISPLACEMENT HISTORIES FOR RECORD NO. 32

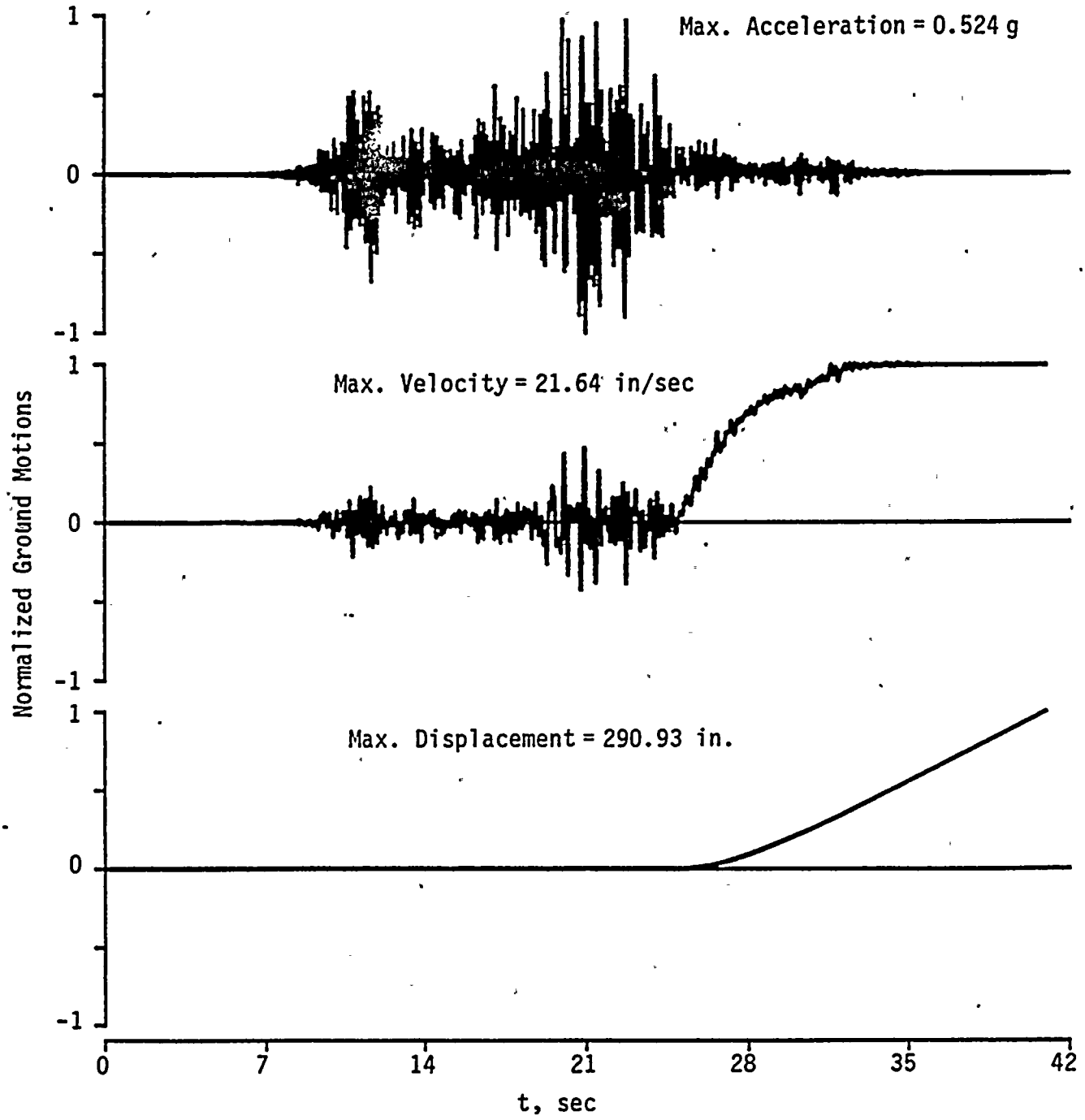

FIG. A.32b Acceleration, Velocity and Displacement Histories for Complete Record No. 32

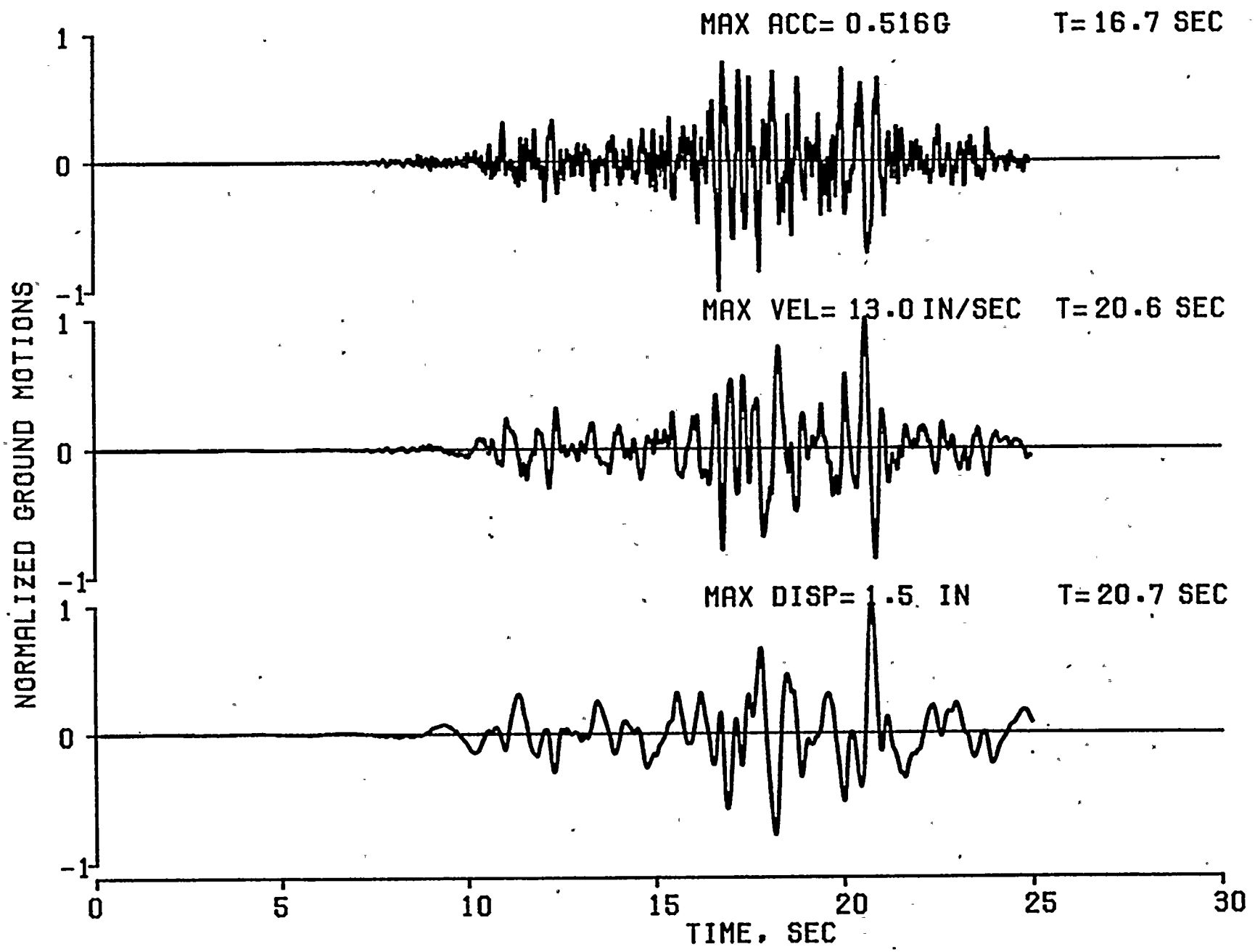

FIG. A.33 ACCELERATION VELOCITY AND DISPLACEMENT HISTORIES FOR RECORD NO. 33

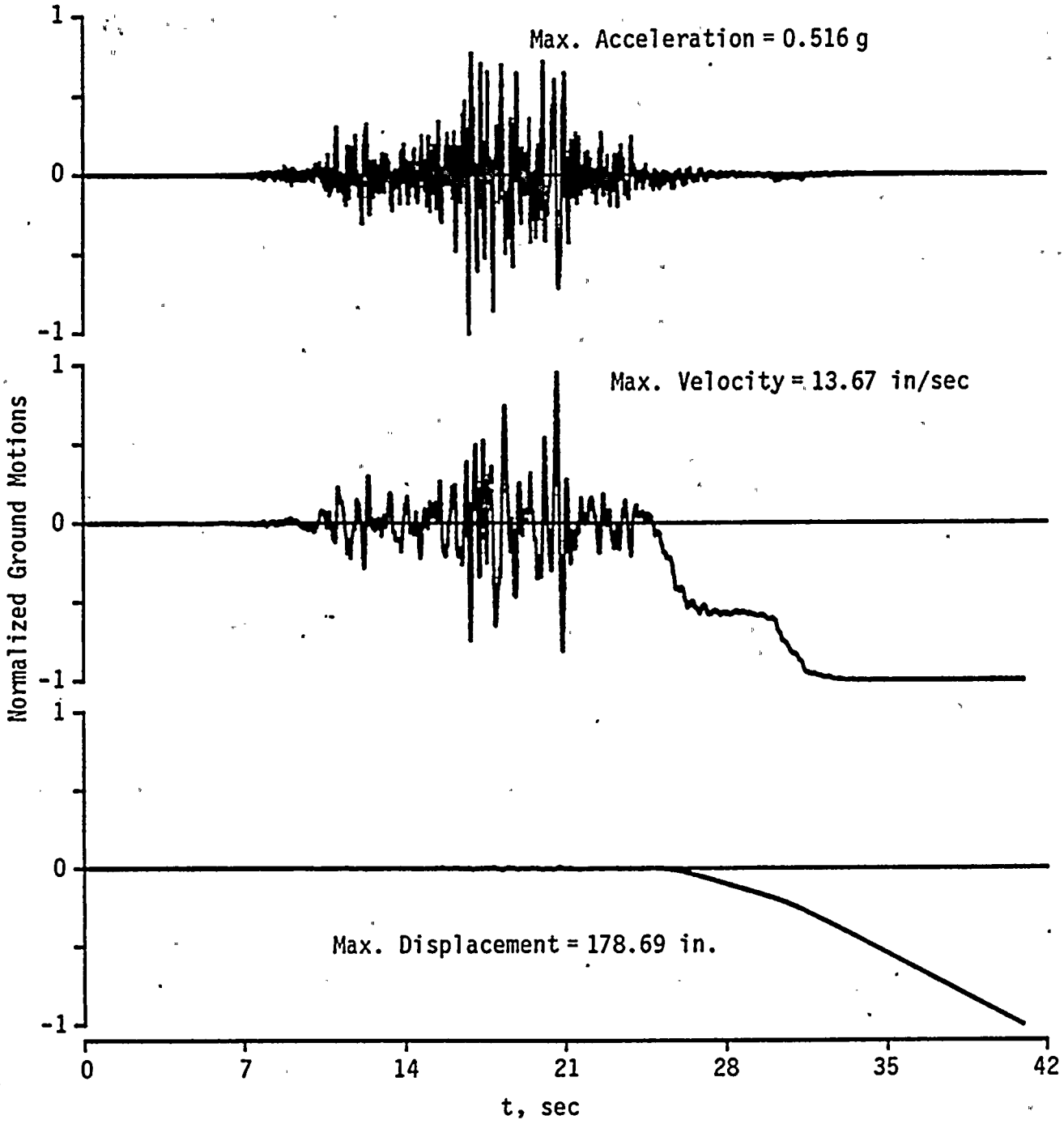

FIG. A.33b Acceleration, Velocity and Displacement Histories for Complete Record No. 33

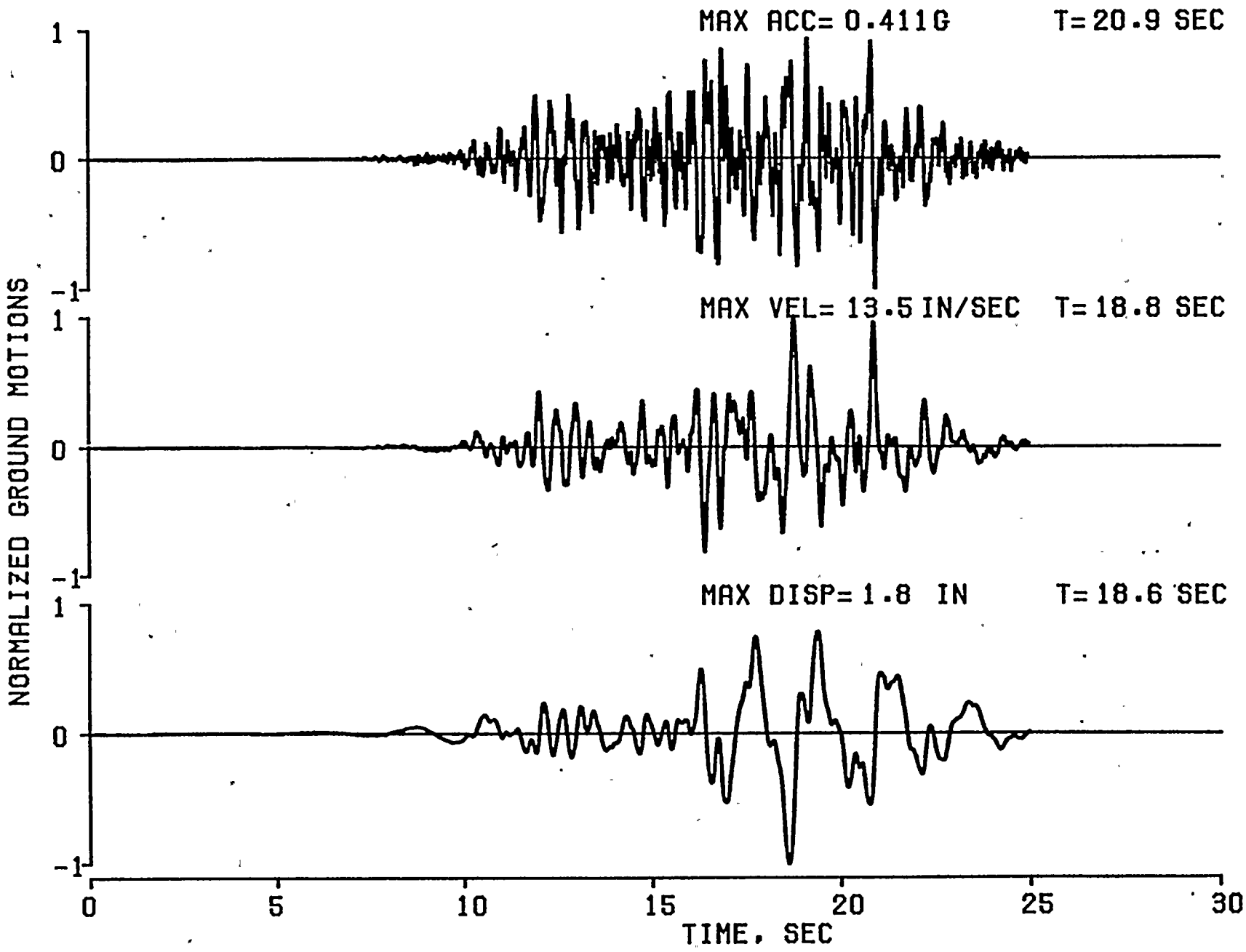

FIG. A.34 ACCELERATION VELOCITY AND DISPLACEMENT HISTORIES FOR RECORD NO. 34

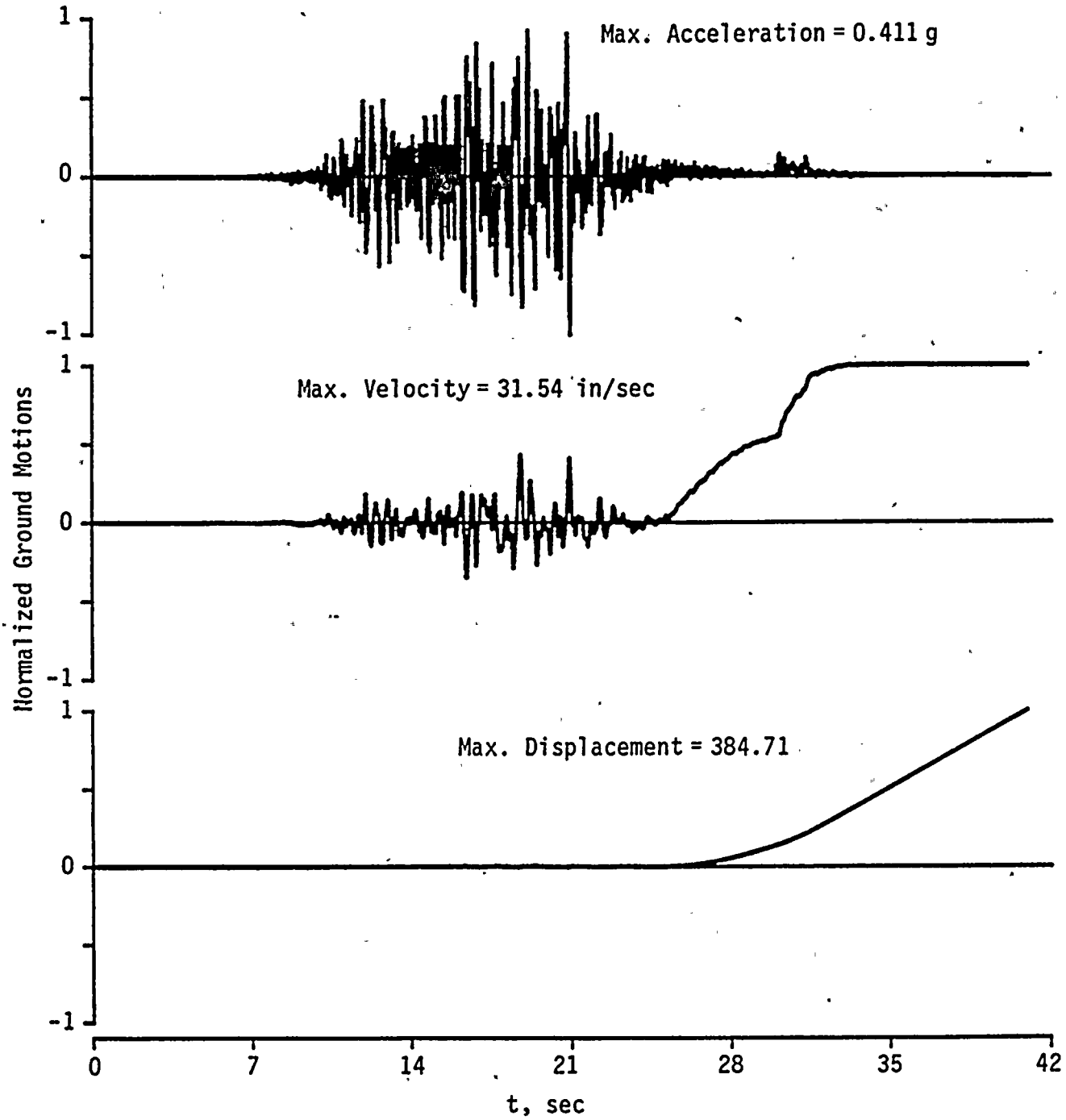

FIG. A.34b Acceleration, Velocity and Displacement Histories for Complete Record No. 34

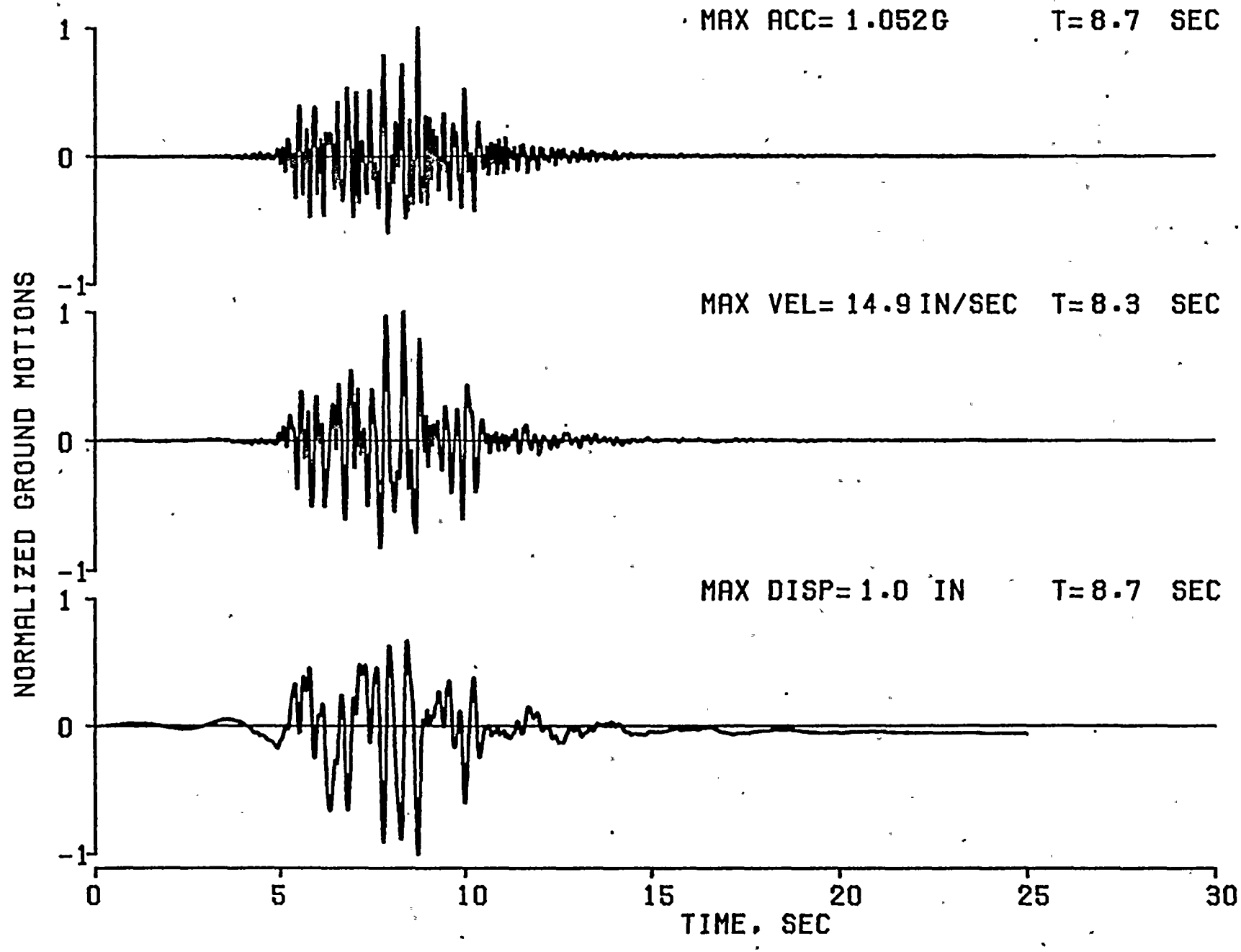

FIG. A.35 ACCELERATION VELOCITY AND DISPLACEMENT HISTORIES FOR RECORD NO. 35

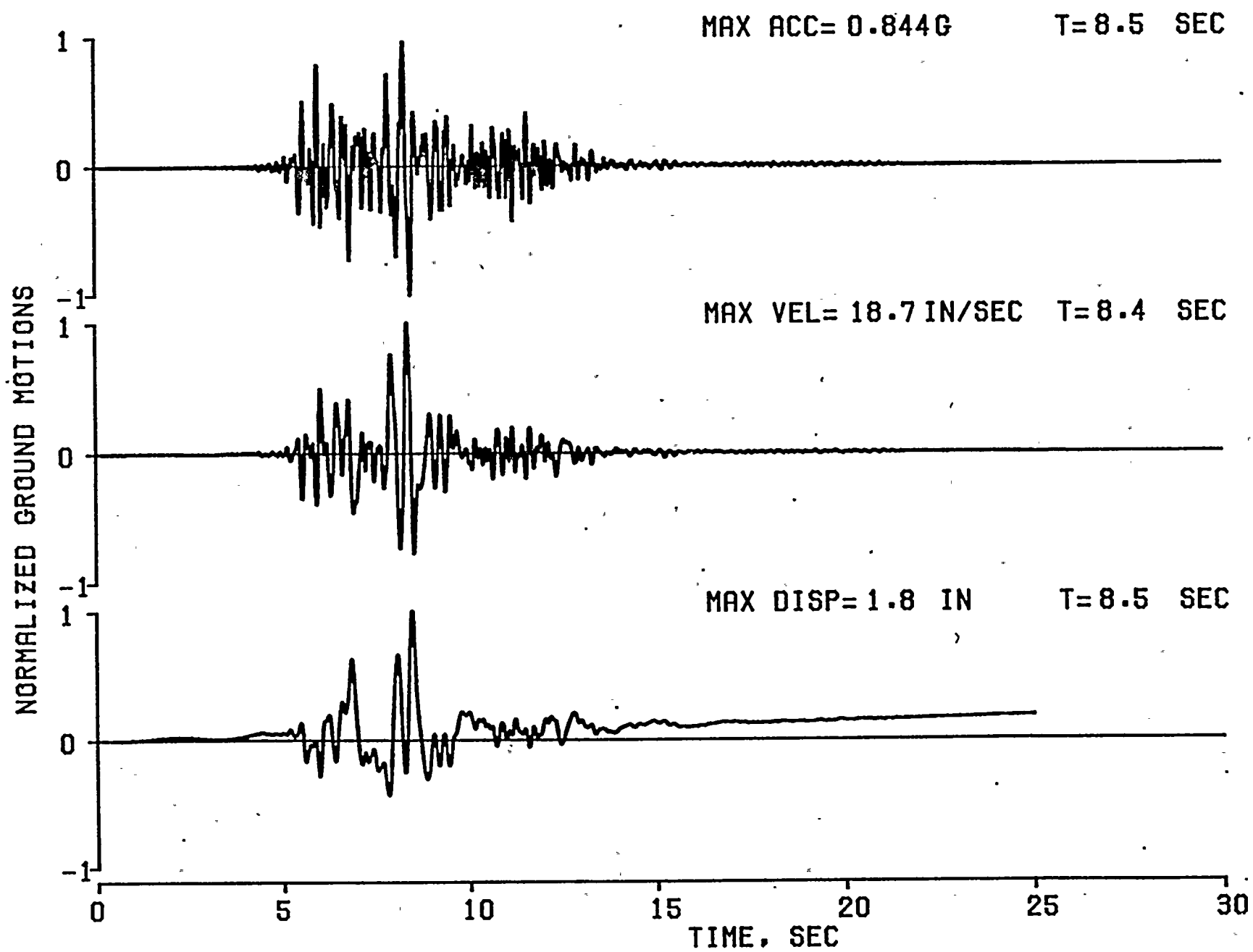

FIG. A.36 ACCELERATION VELOCITY AND DISPLACEMENT HISTORIES FOR RECORD NO. 36

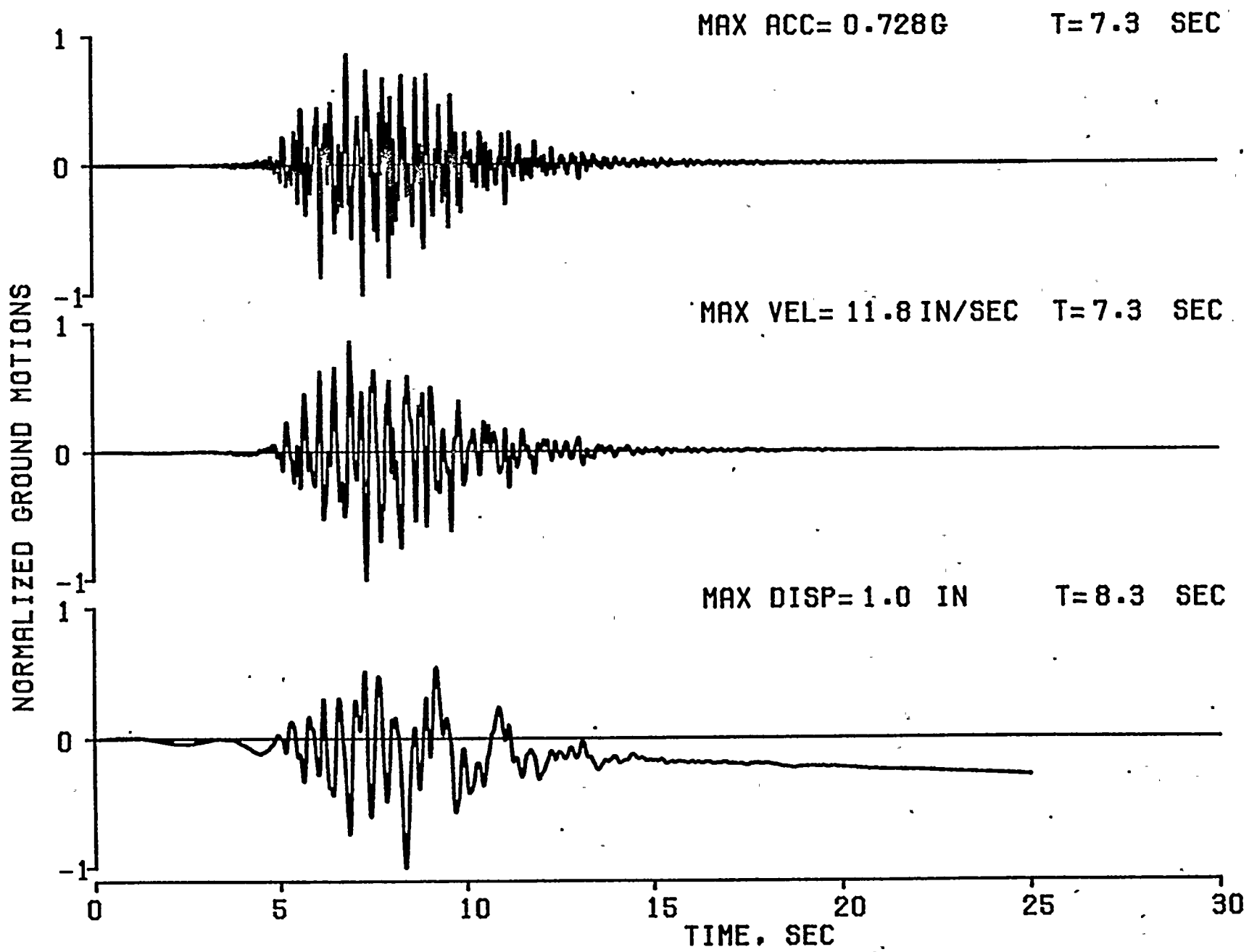

FIG. A.37 ACCELERATION VELOCITY AND DISPLACEMENT HISTORIES FOR RECORD NO. 37

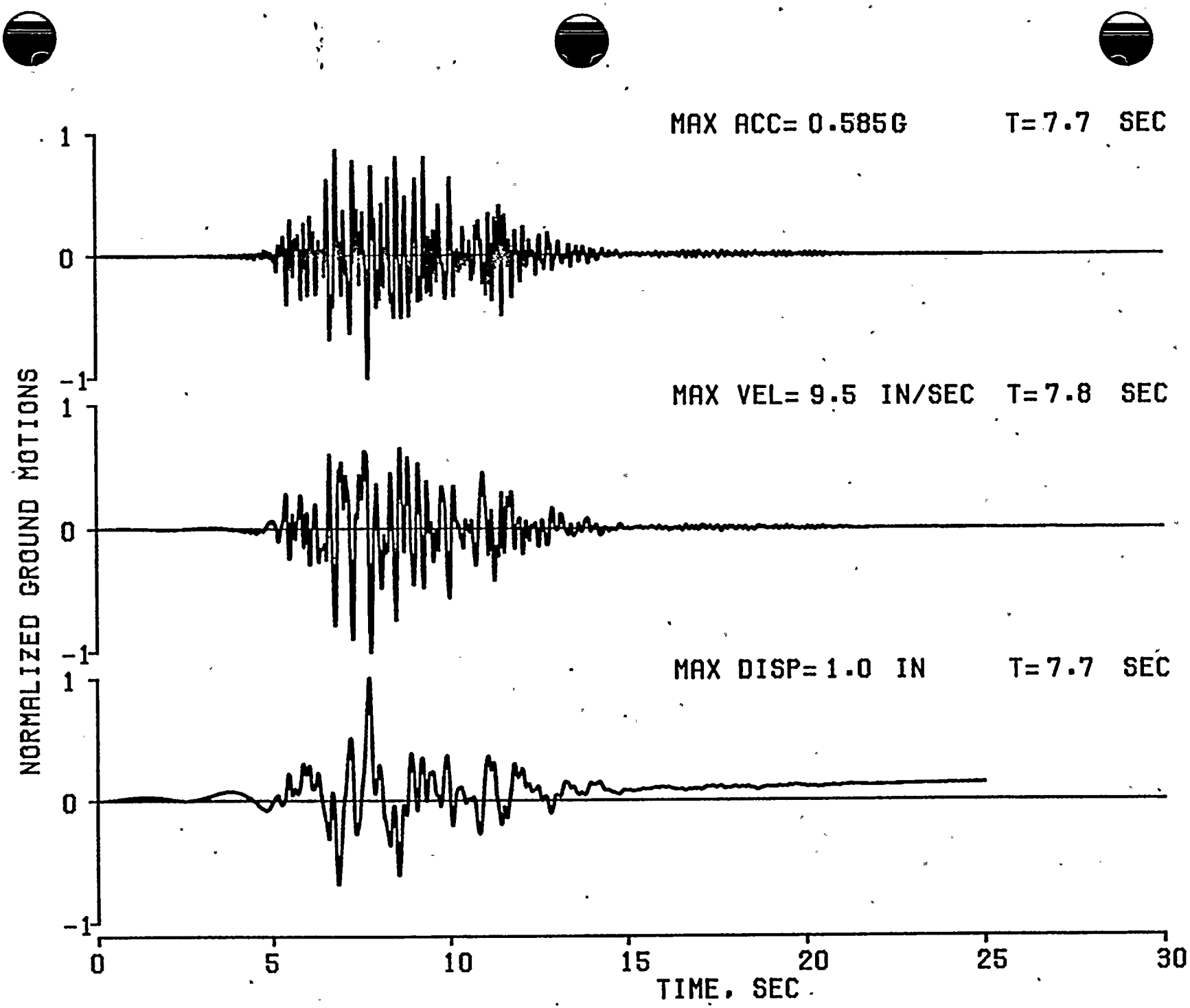

FIG. A.38 ACCELERATION VELOCITY AND DISPLACEMENT HISTORIES FOR RECORD NO. 38

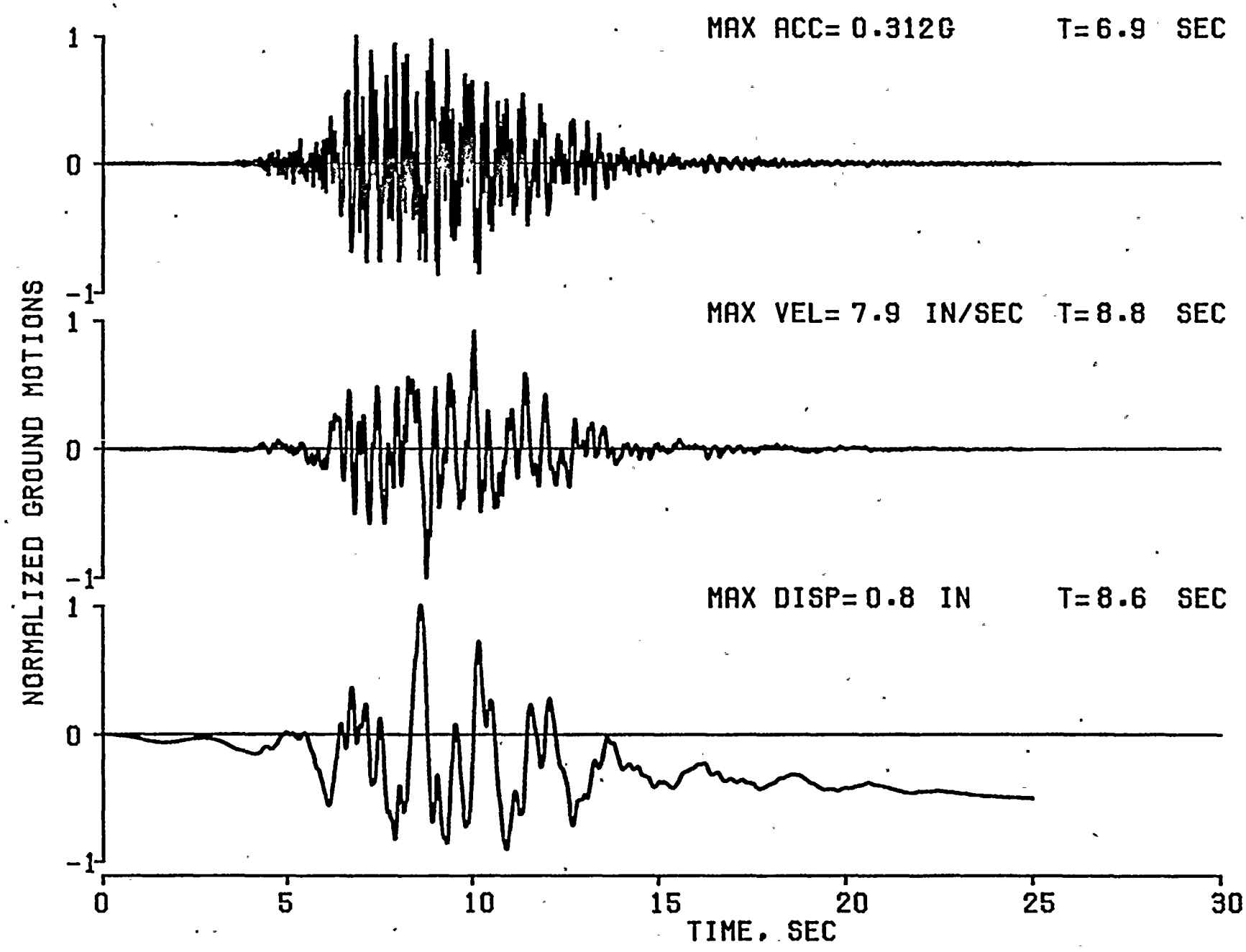

FIG. A.39 ACCELERATION VELOCITY AND DISPLACEMENT HISTORIES FOR RECORD NO. 39

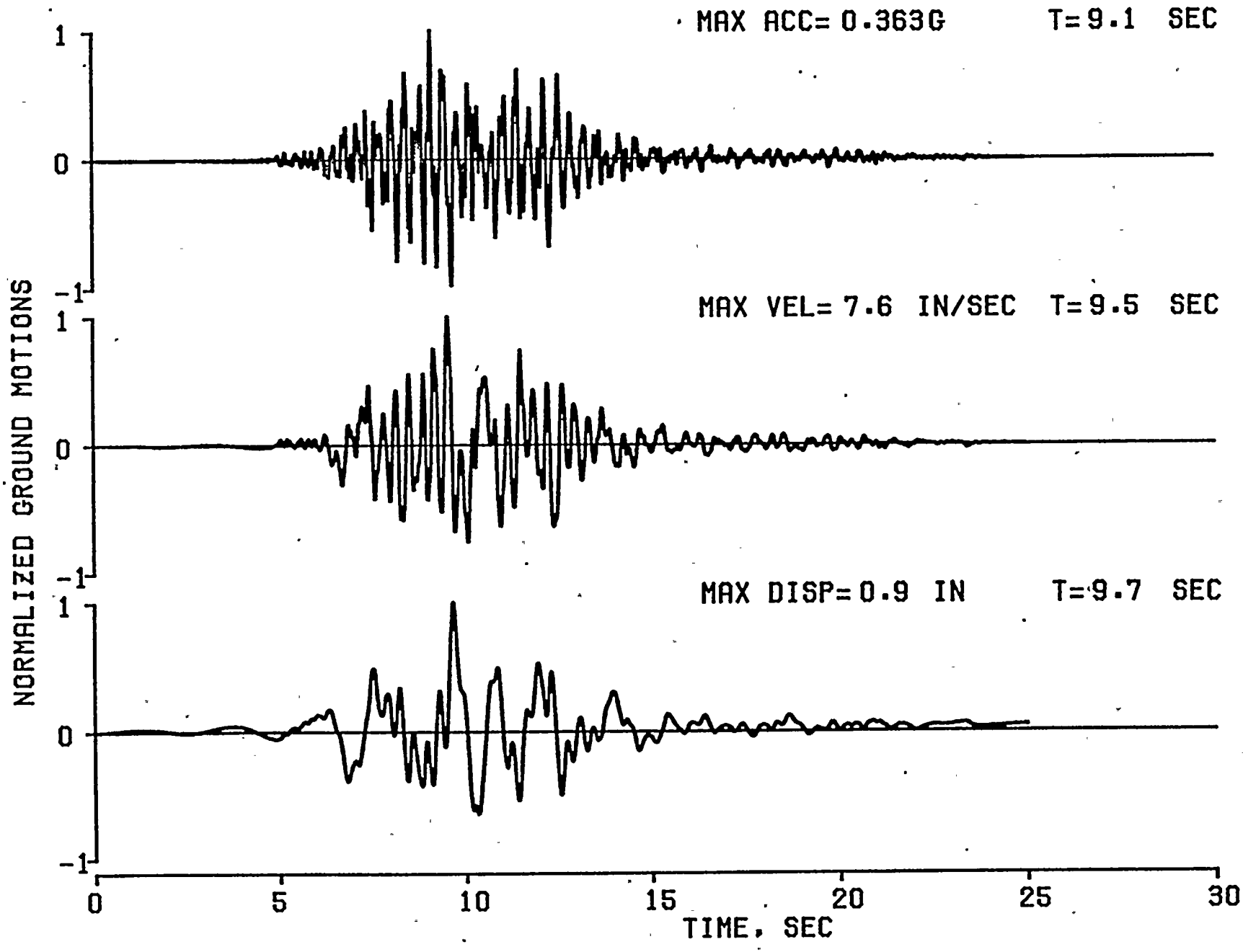

FIG. A.40 ACCELERATION VELOCITY AND DISPLACEMENT HISTORIES FOR RECORD NO. 40

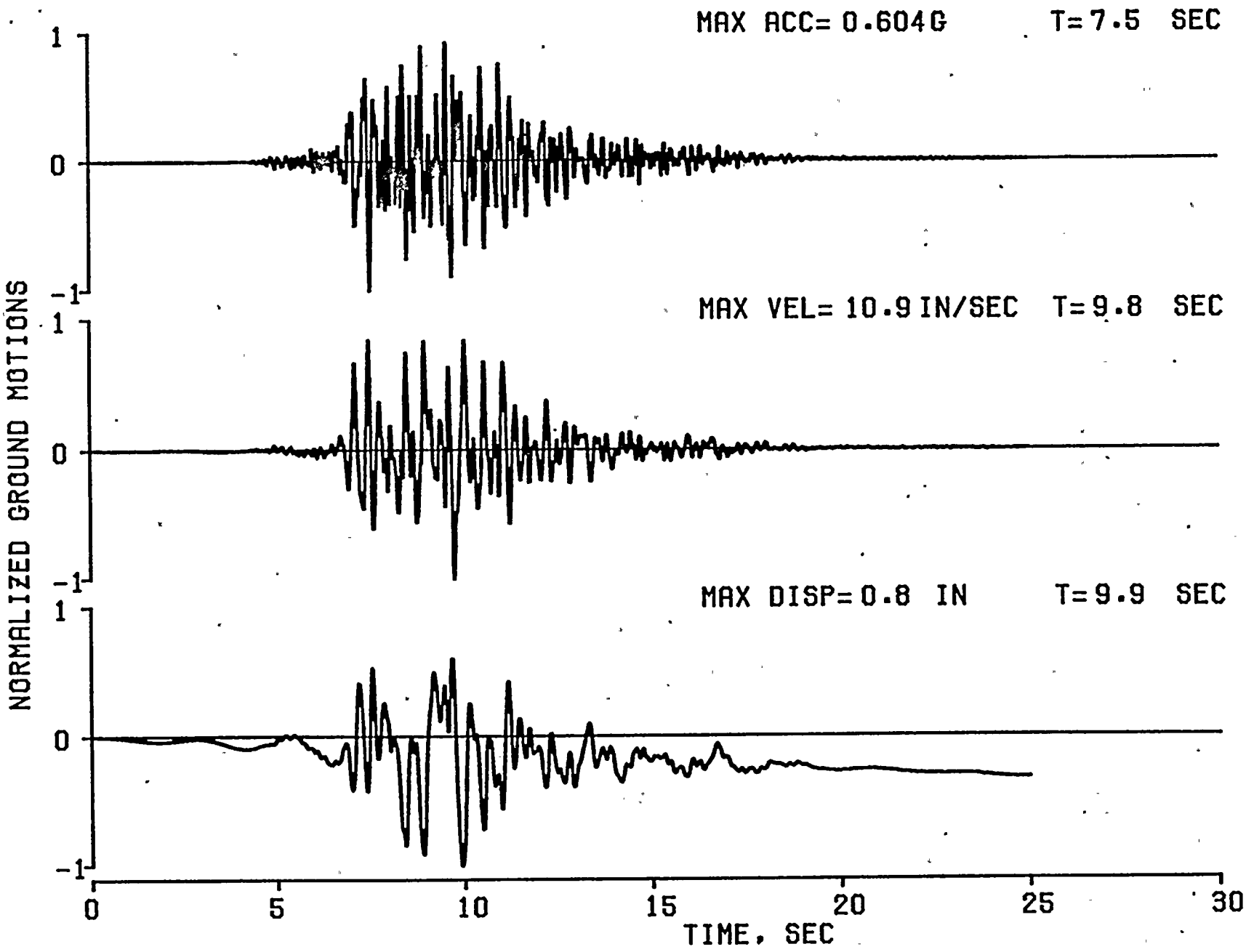

FIG. A.41 ACCELERATION VELOCITY AND DISPLACEMENT HISTORIES FOR RECORD NO. 41

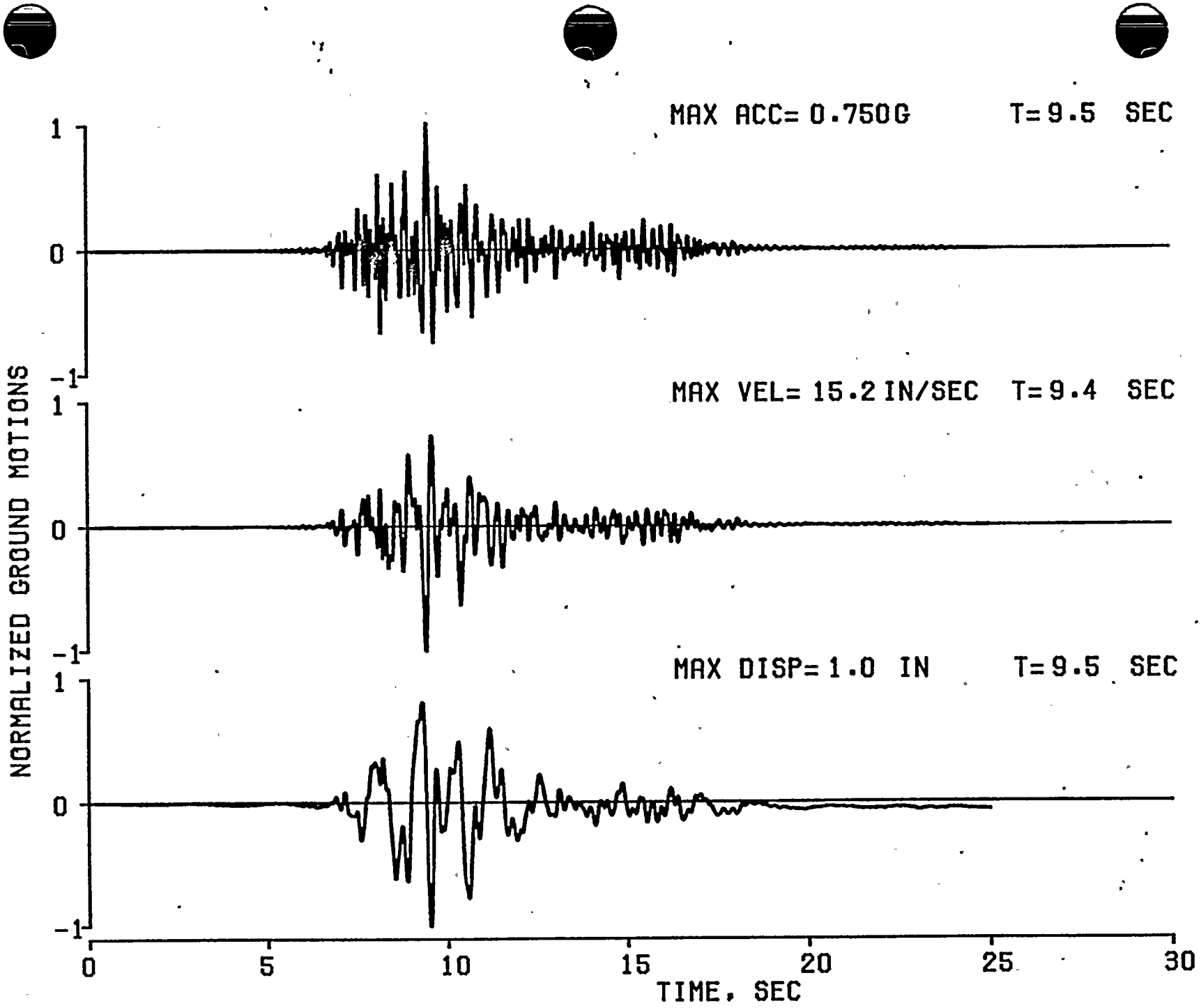

FIG. A.42 ACCELERATION VELOCITY AND DISPLACEMENT HISTORIES FOR RECORD NO. 42

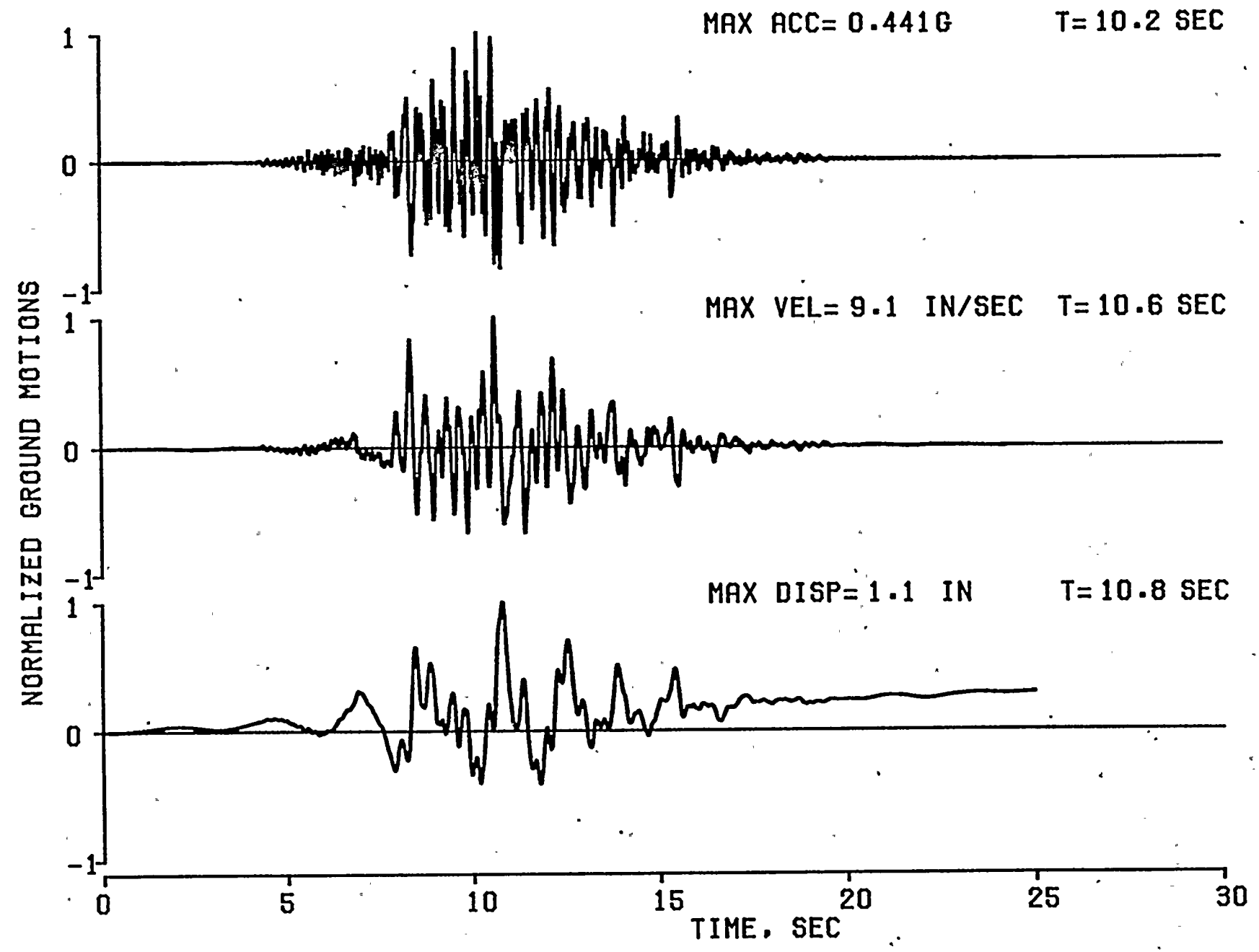

FIG. A.43 ACCELERATION VELOCITY AND DISPLACEMENT HISTORIES FOR RECORD NO. 43

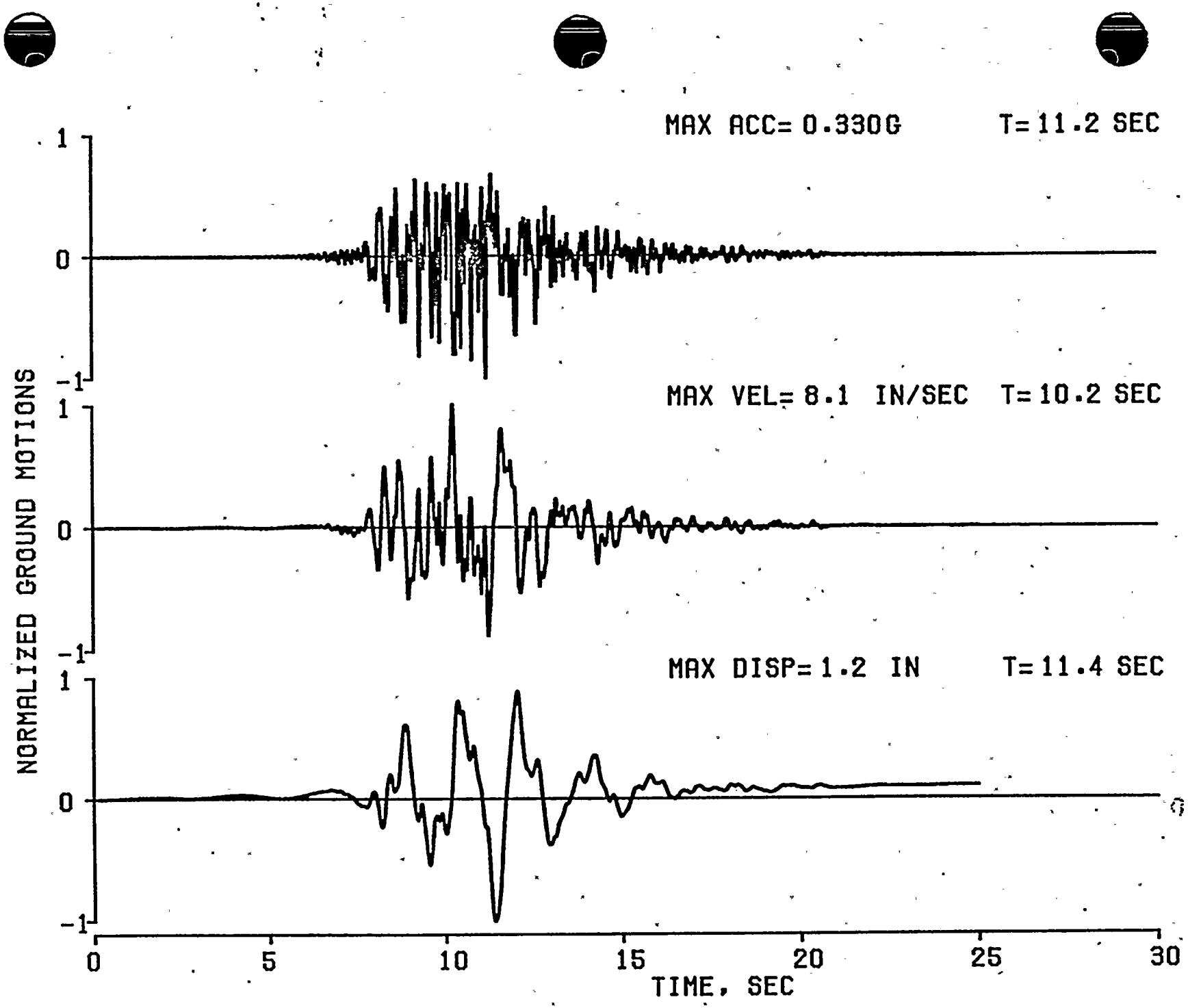

FIG. A.44 ACCELERATION VELOCITY AND DISPLACEMENT HISTORIES FOR RECORD NO. 44

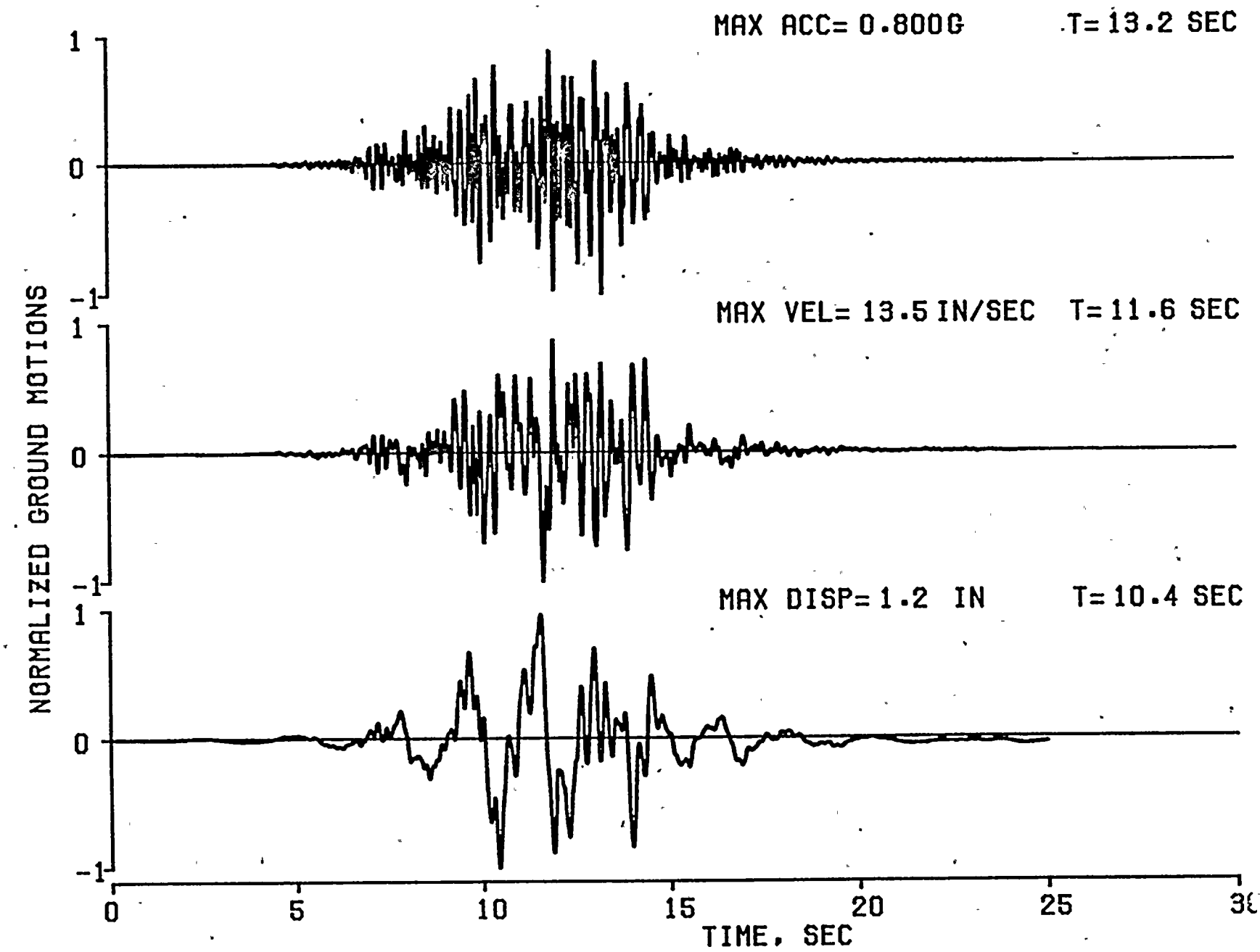

FIG. A.45 ACCELERATION VELOCITY AND DISPLACEMENT HISTORIES FOR RECORD NO. 45

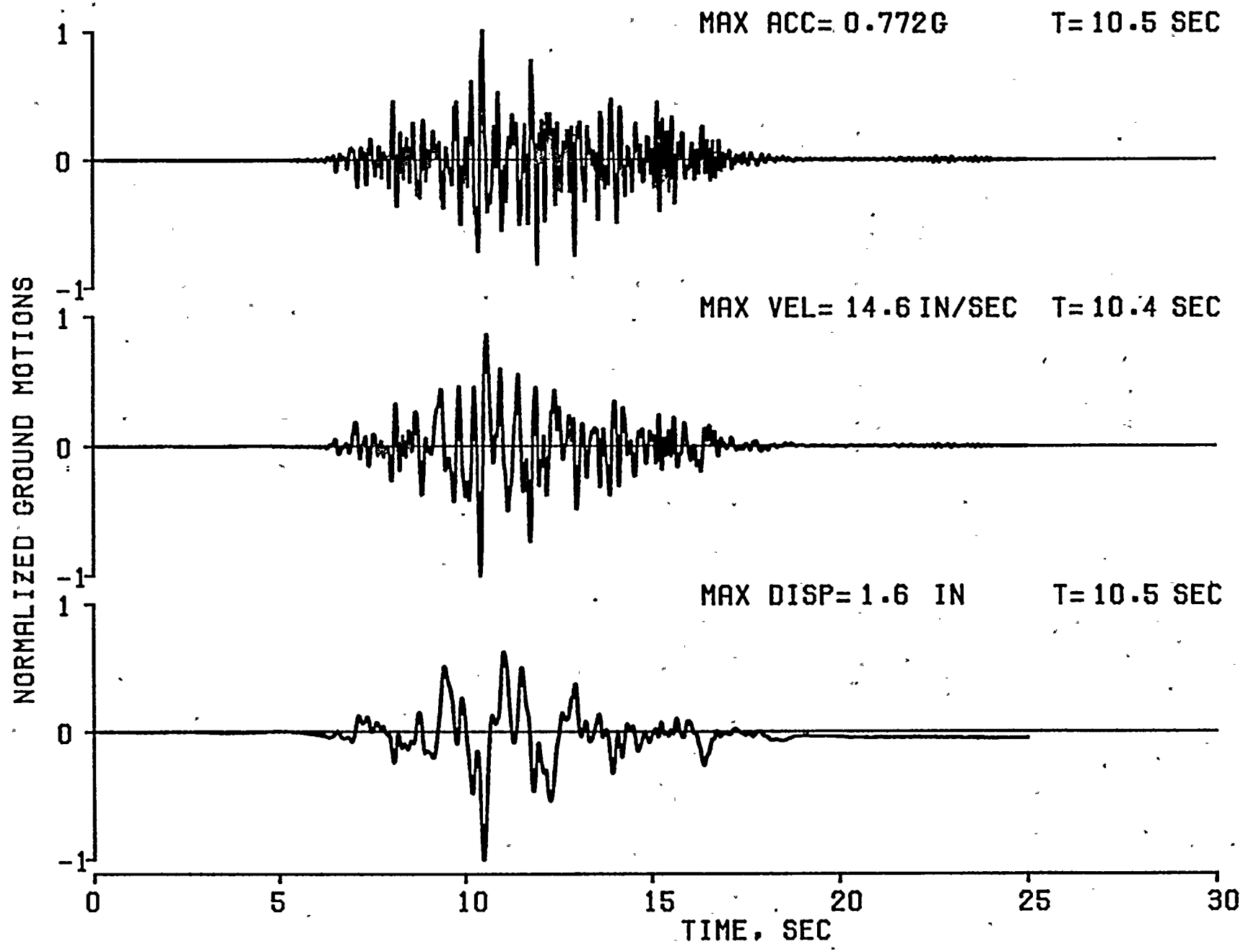

FIG. A.46 ACCELERATION VELOCITY AND DISPLACEMENT HISTORIES FOR RECORD NO. 46

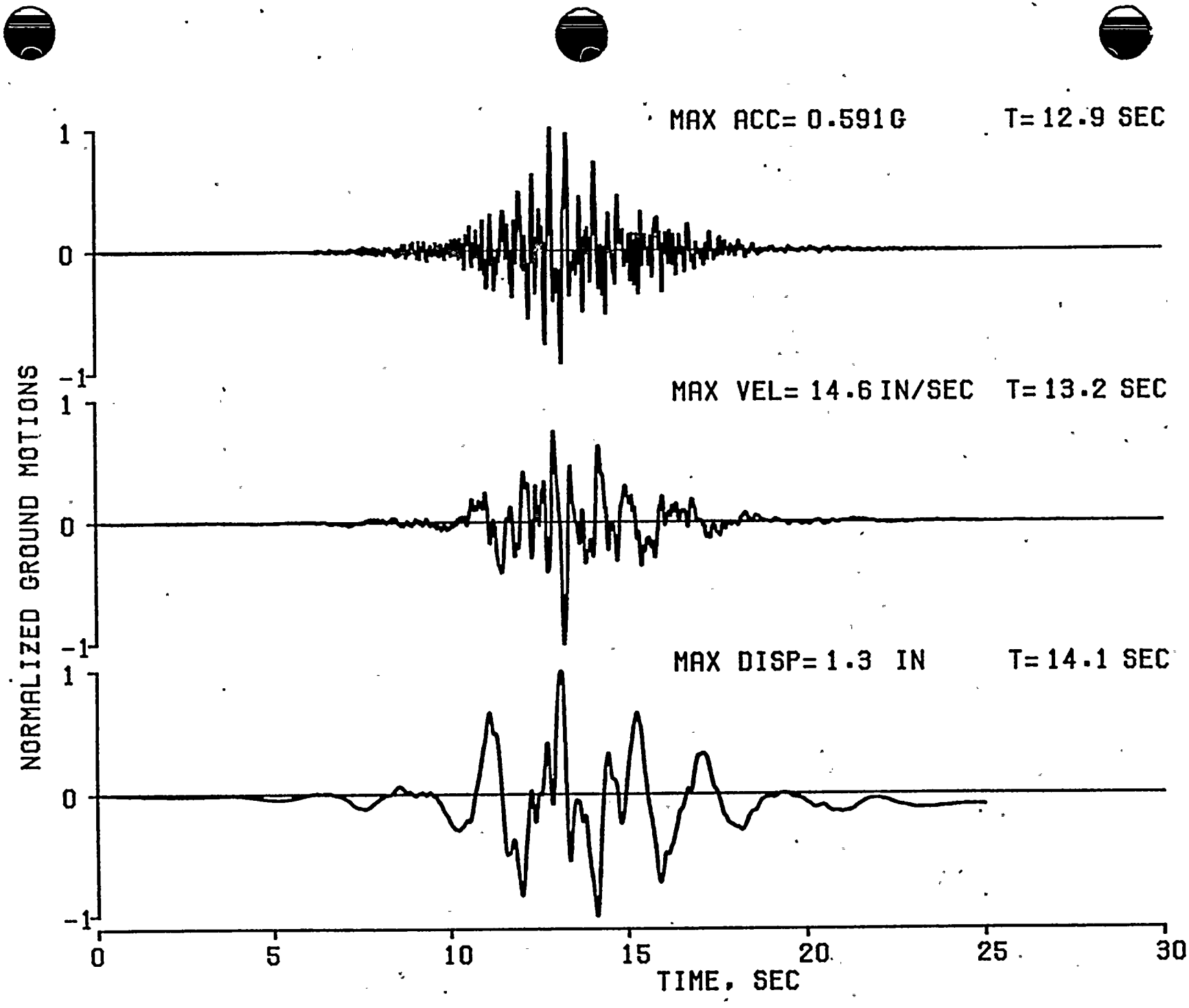

FIG. A.47 ACCELERATION VELOCITY AND DISPLACEMENT HISTORIES FOR RECORD NO. 47

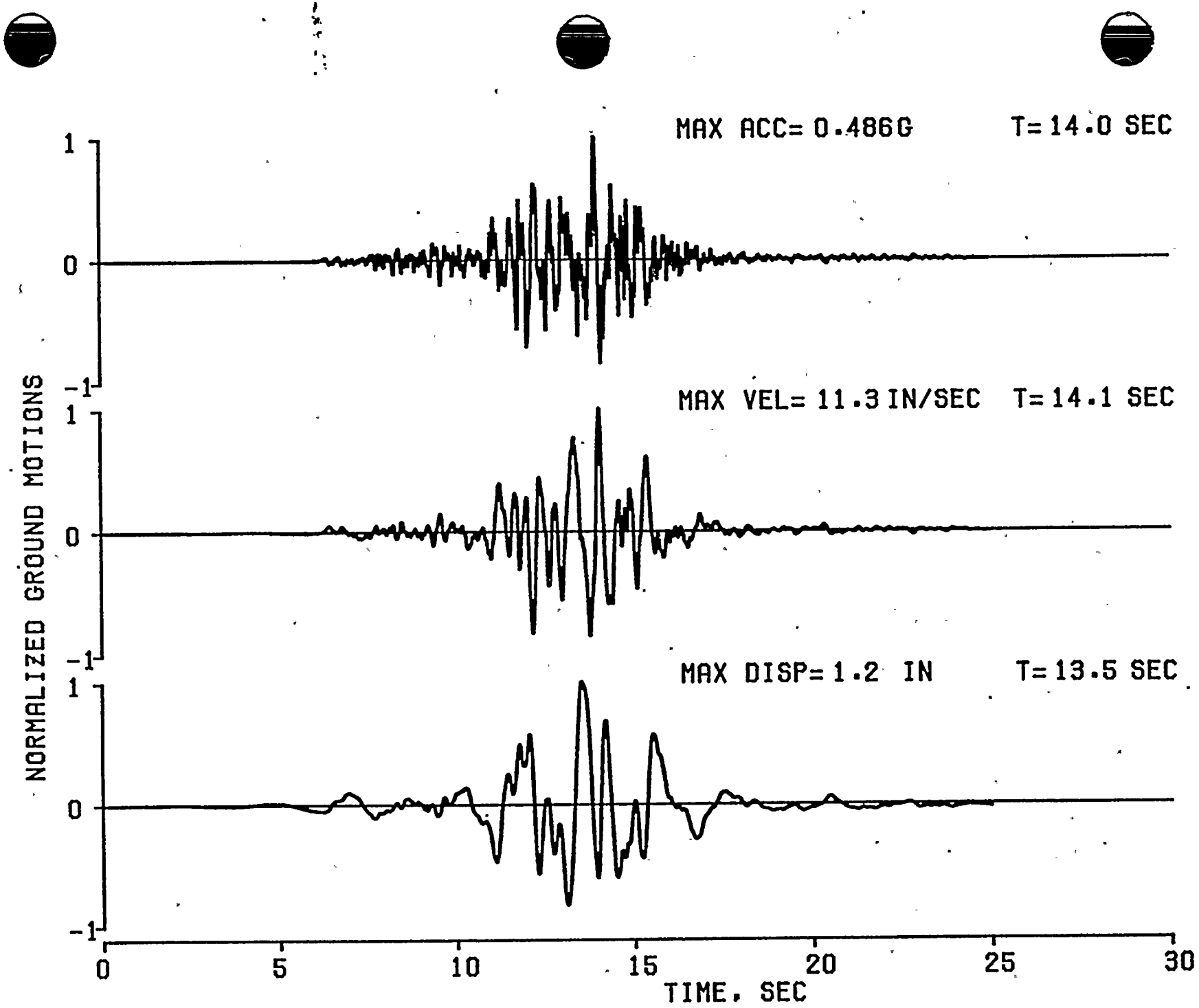

FIG. A.48 ACCELERATION VELOCITY AND DISPLACEMENT HISTORIES FOR RECORD NO. 48

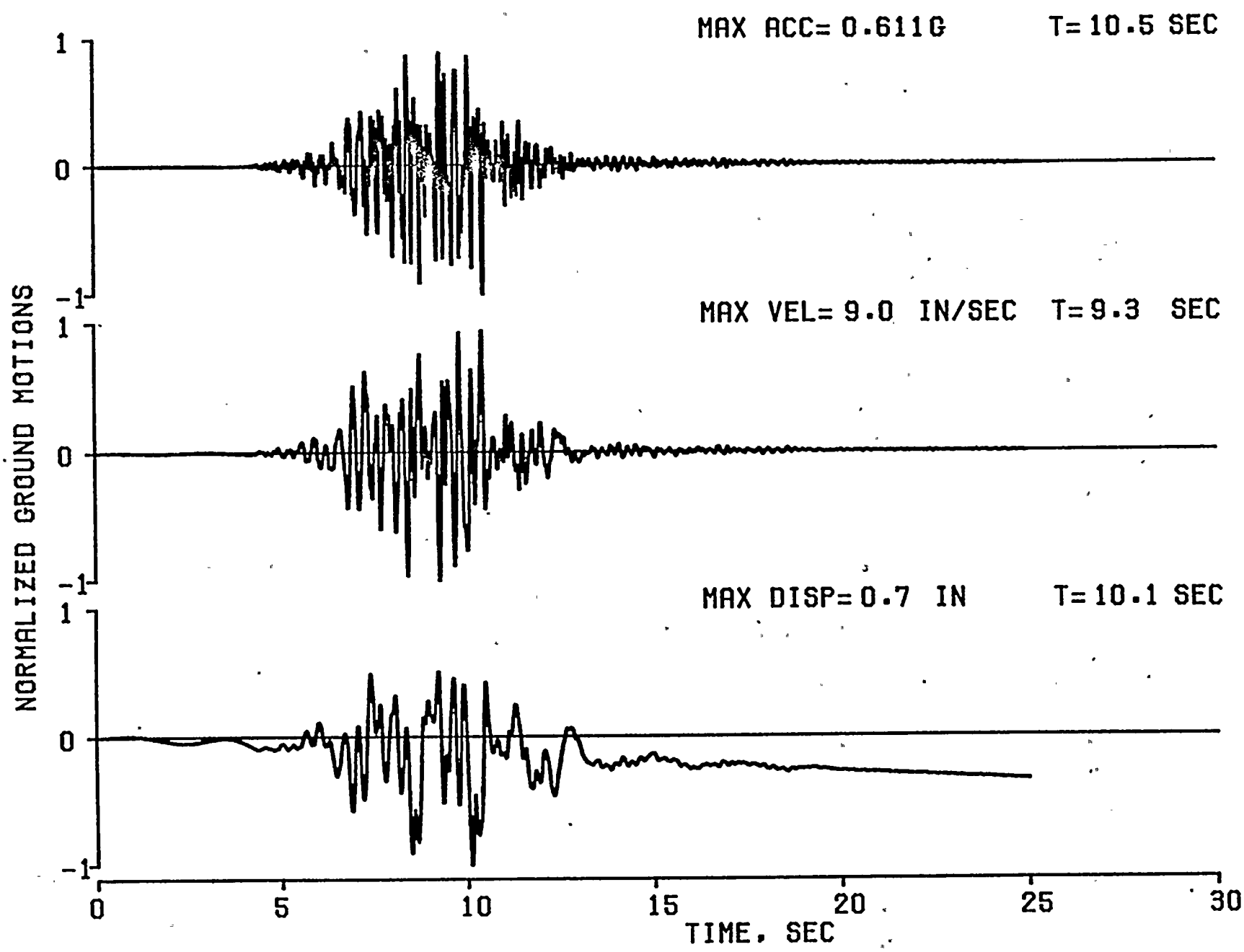

FIG. A.49 ACCELERATION VELOCITY AND DISPLACEMENT HISTORIES FOR RECORD NO. 49

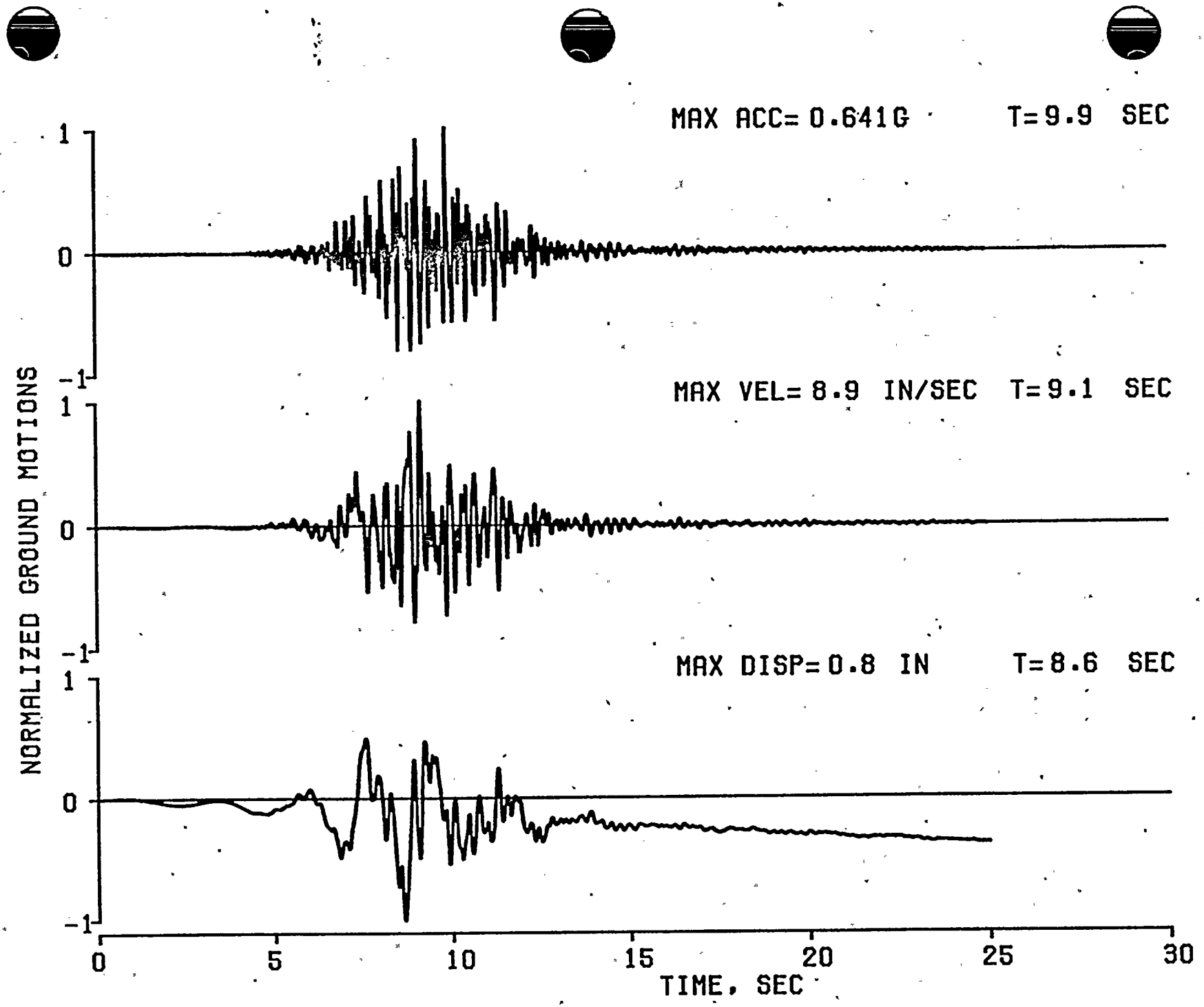

FIG. A.50 ACCELERATION VELOCITY AND DISPLACEMENT HISTORIES FOR RECORD NO. 50

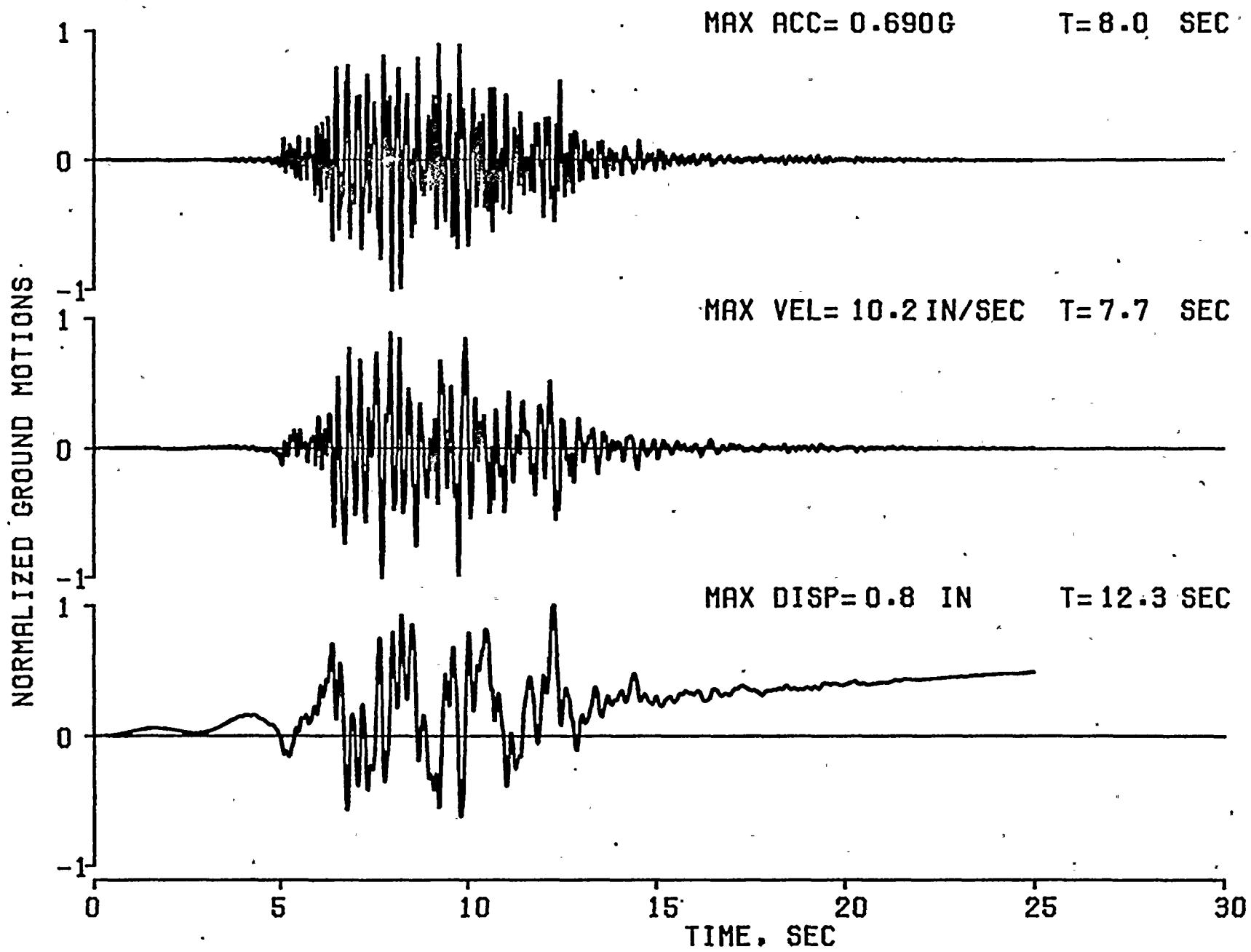

FIG. A.51 ACCELERATION VELOCITY AND DISPLACEMENT HISTORIES FOR RECORD NO. 51

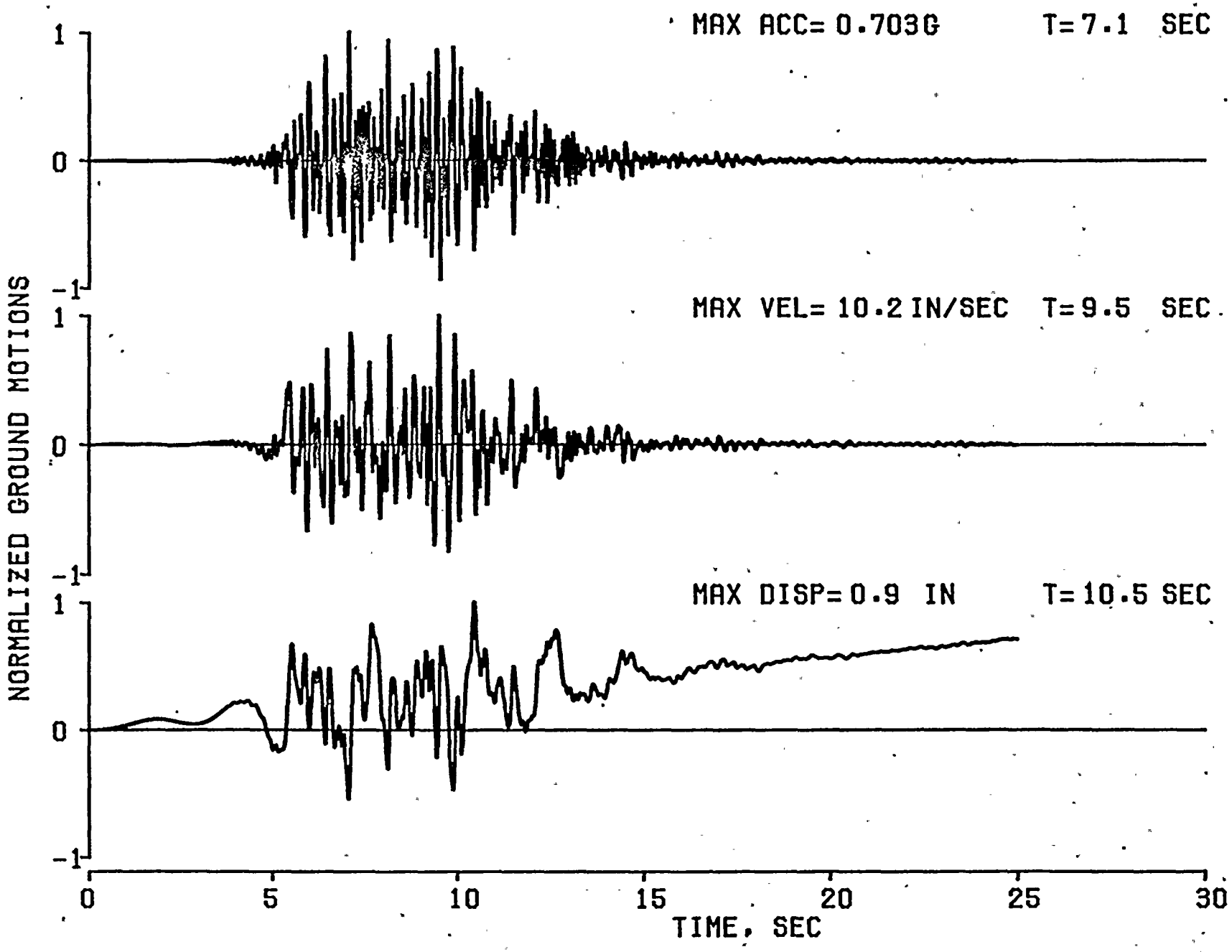

FIG. A.52 ACCELERATION VELOCITY AND DISPLACEMENT HISTORIES FOR RECORD NO. 52

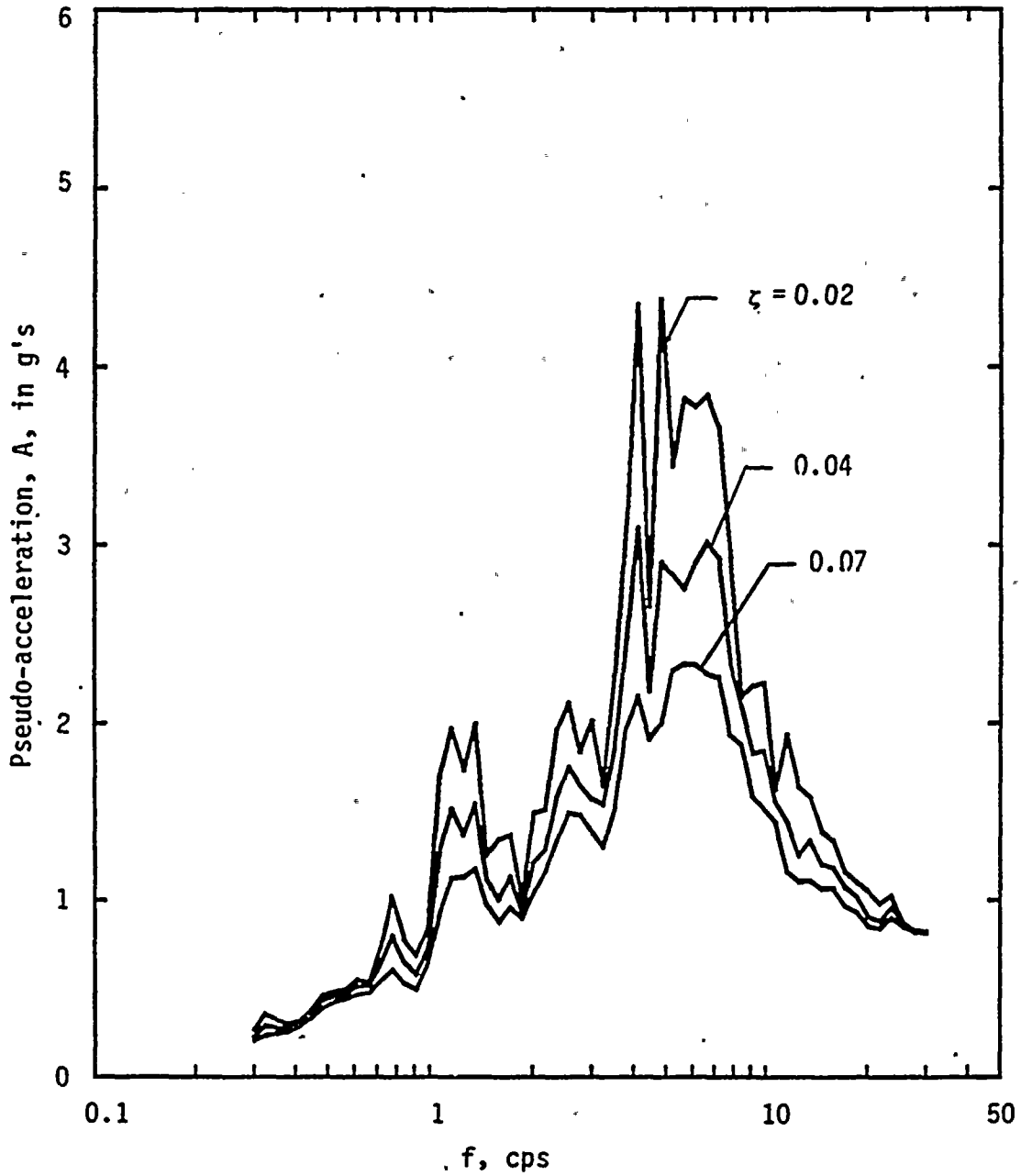

FIG. B.1 Pseudo-acceleration Response Spectra for Systems Subjected to Empirical Ground Motion Record No. 1

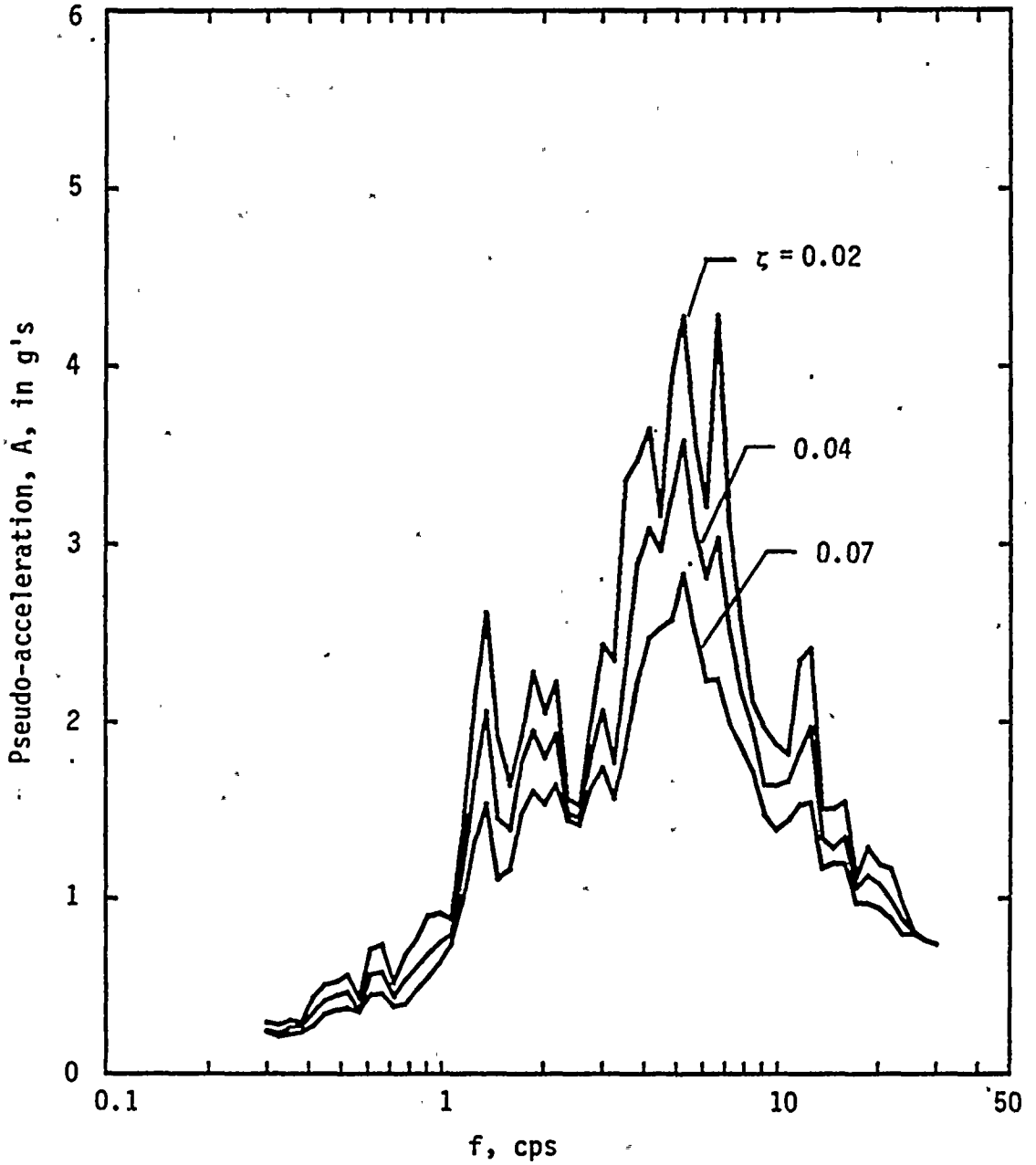

FIG. B.2 Pseudo-acceleration Response Spectra for Systems Subjected to Empirical Ground Motion Record No. 2

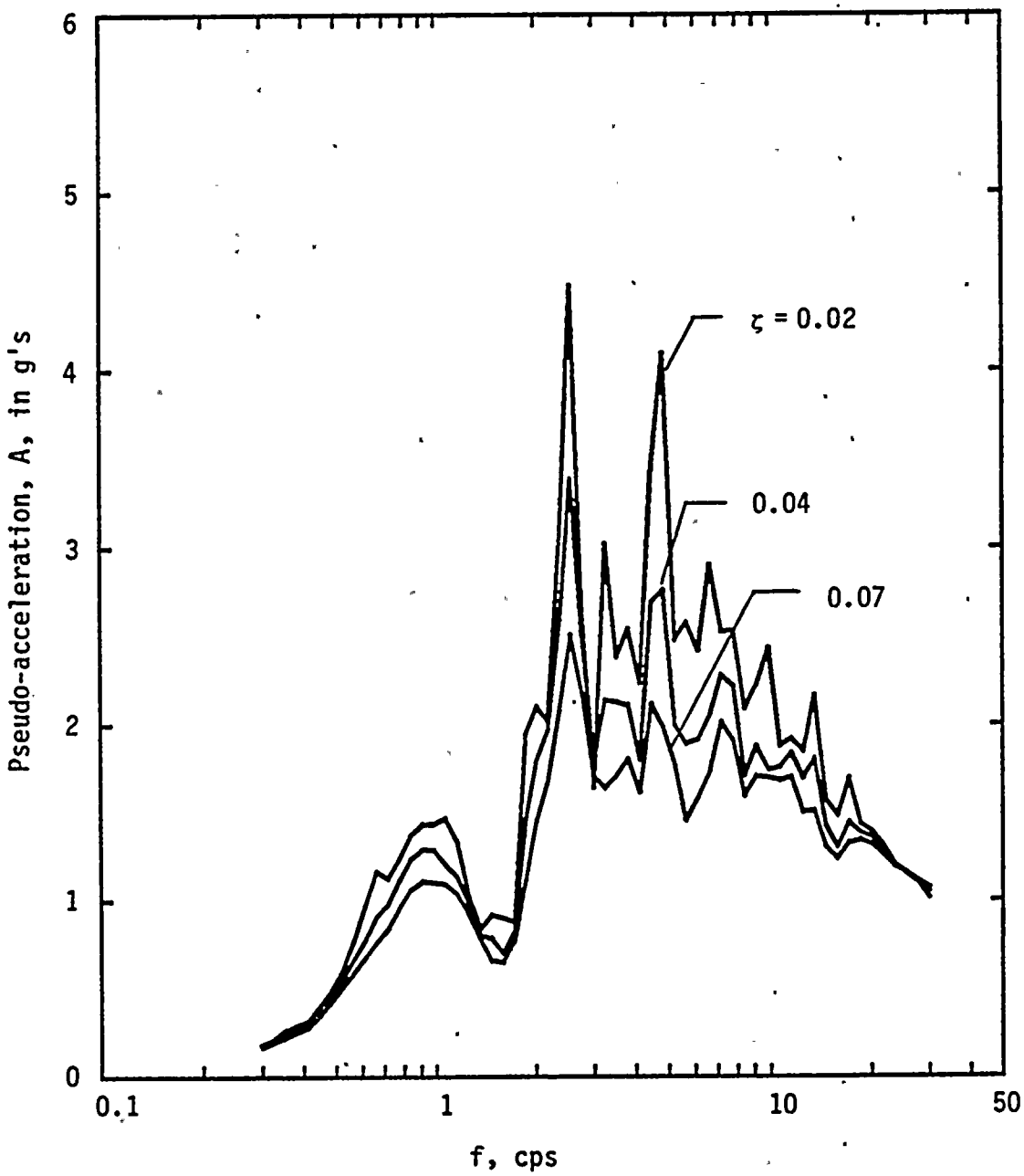

FIG. B.3 Pseudo-acceleration Response Spectra for Systems Subjected to Empirical Ground Motion Record No. 3

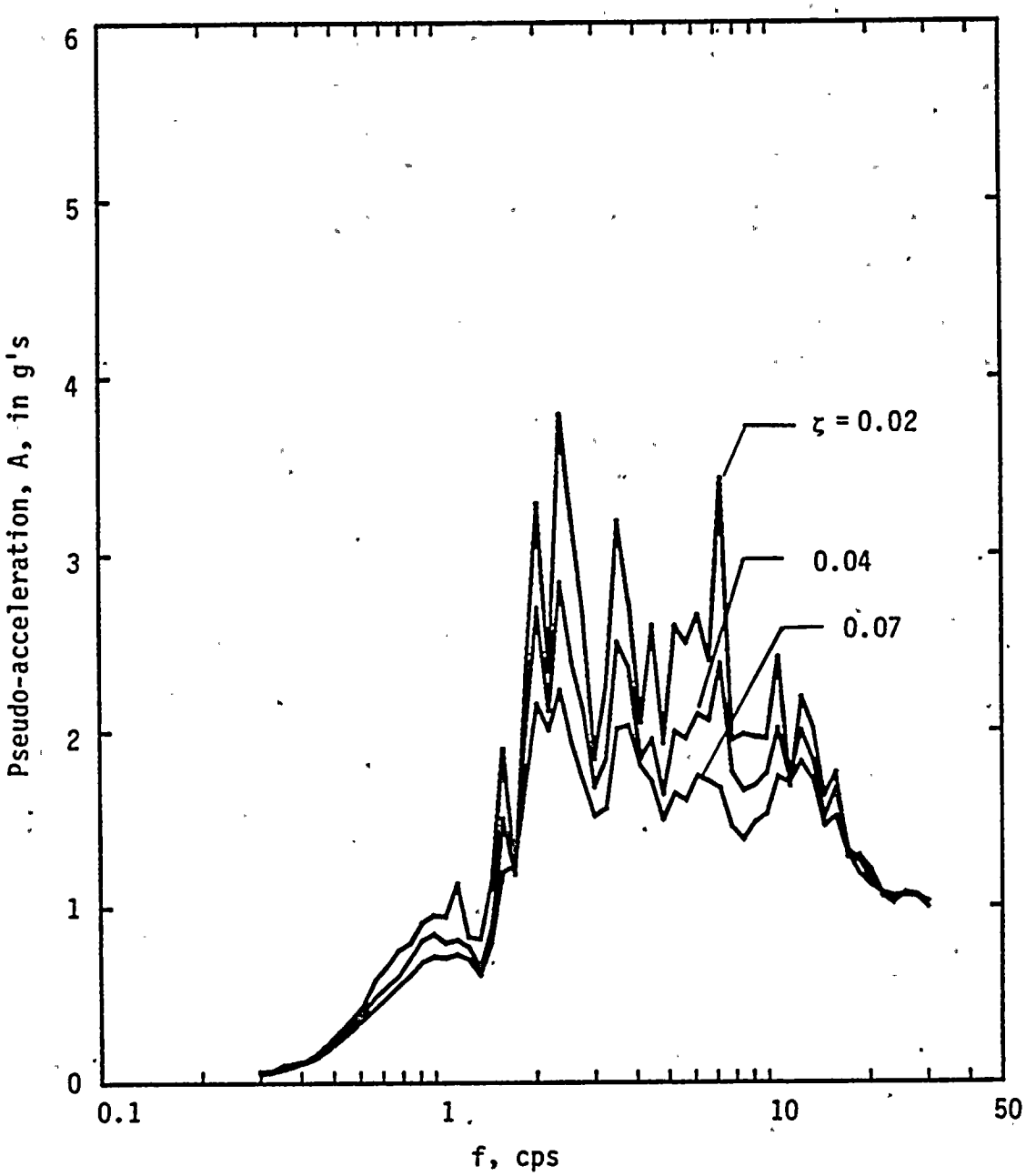

FIG. B.4 Pseudo-acceleration Response Spectra for Systems Subjected to Empirical Ground Motion Record No. 4

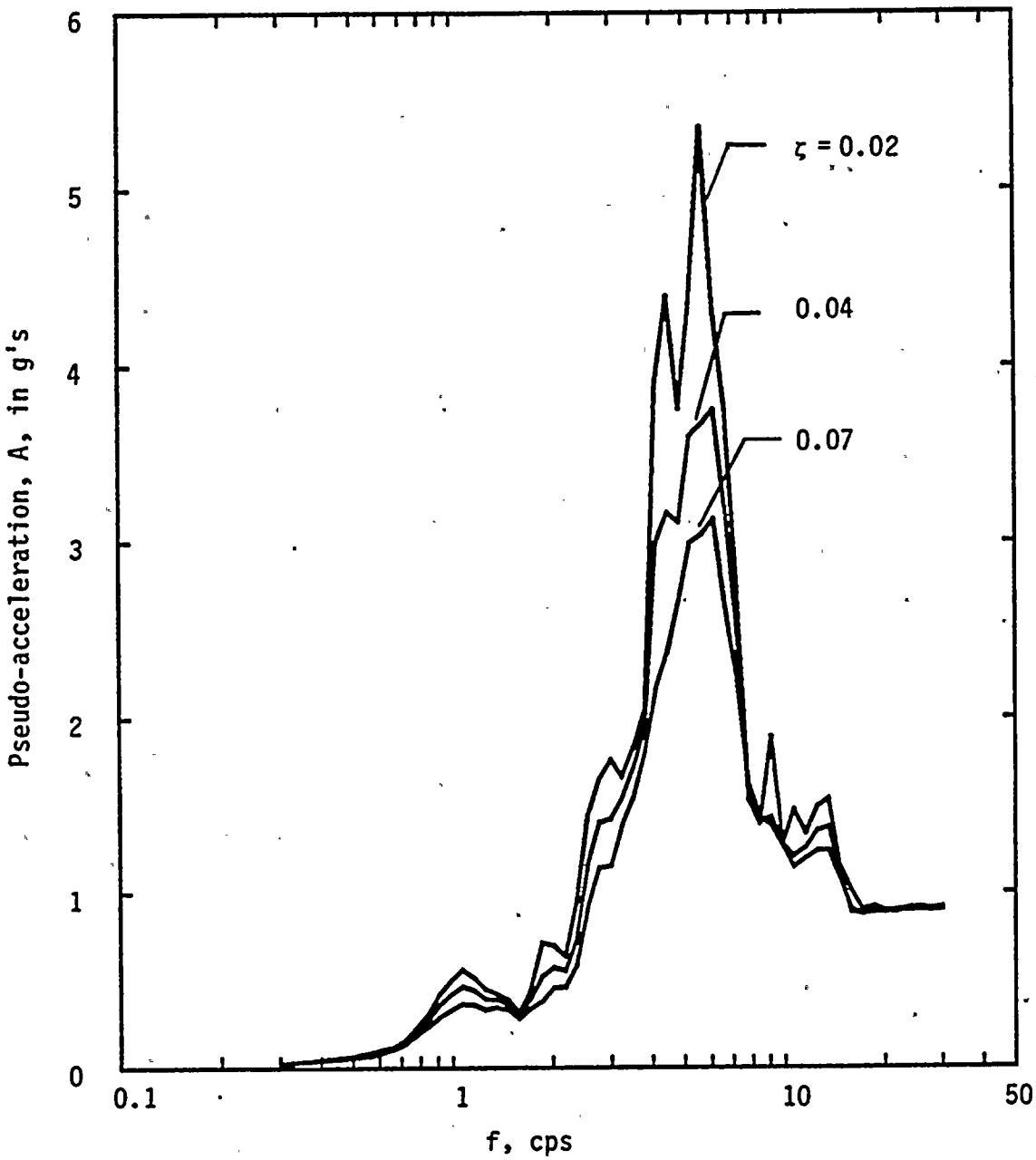

FIG. B.5 Pseudo-acceleration Response Spectra for Systems Subjected to Empirical Ground Motion Record No. 5

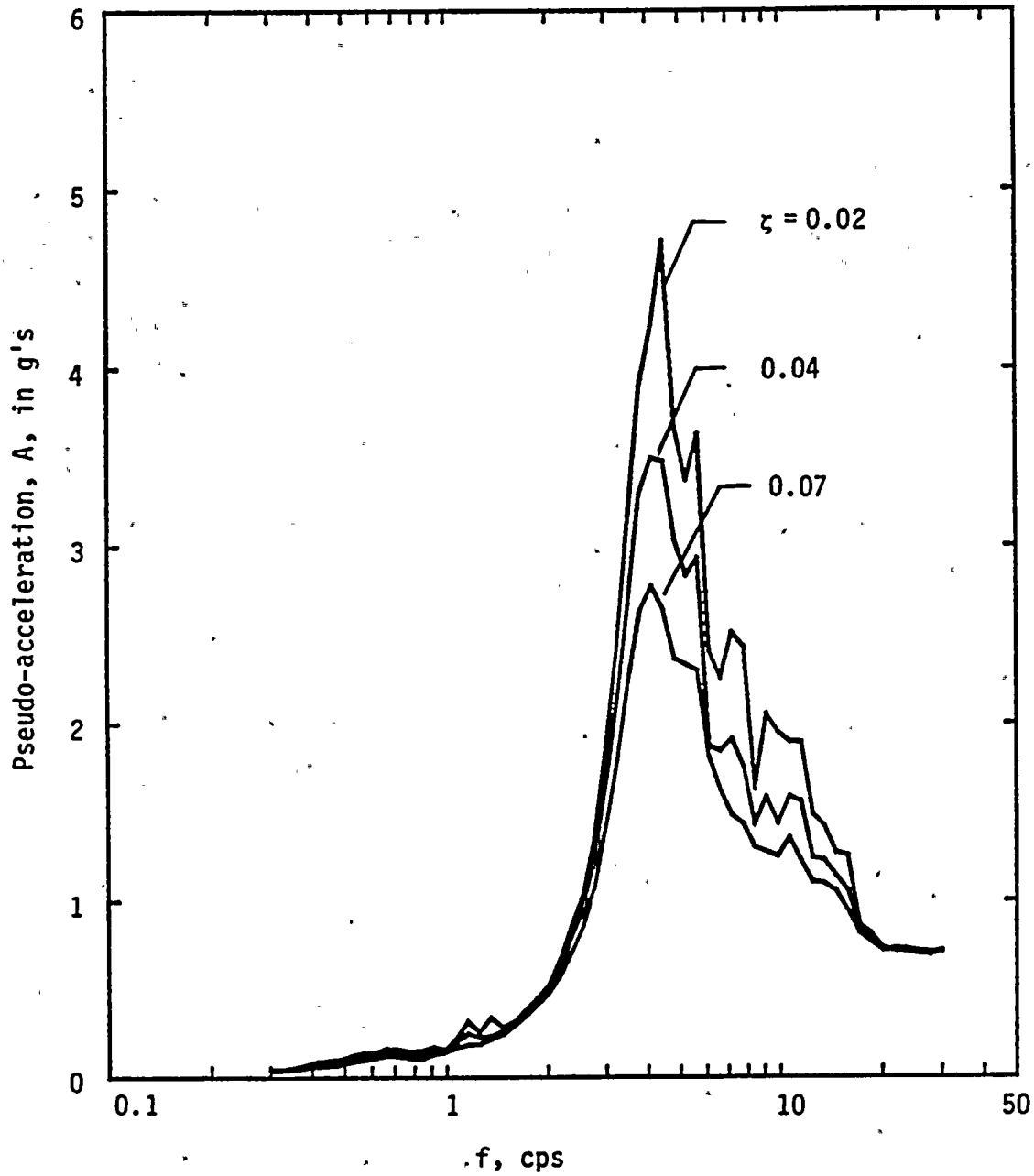

FIG. B.6 Pseudo-acceleration Response Spectra for Systems Subjected to Empirical Ground Motion Record No. 6

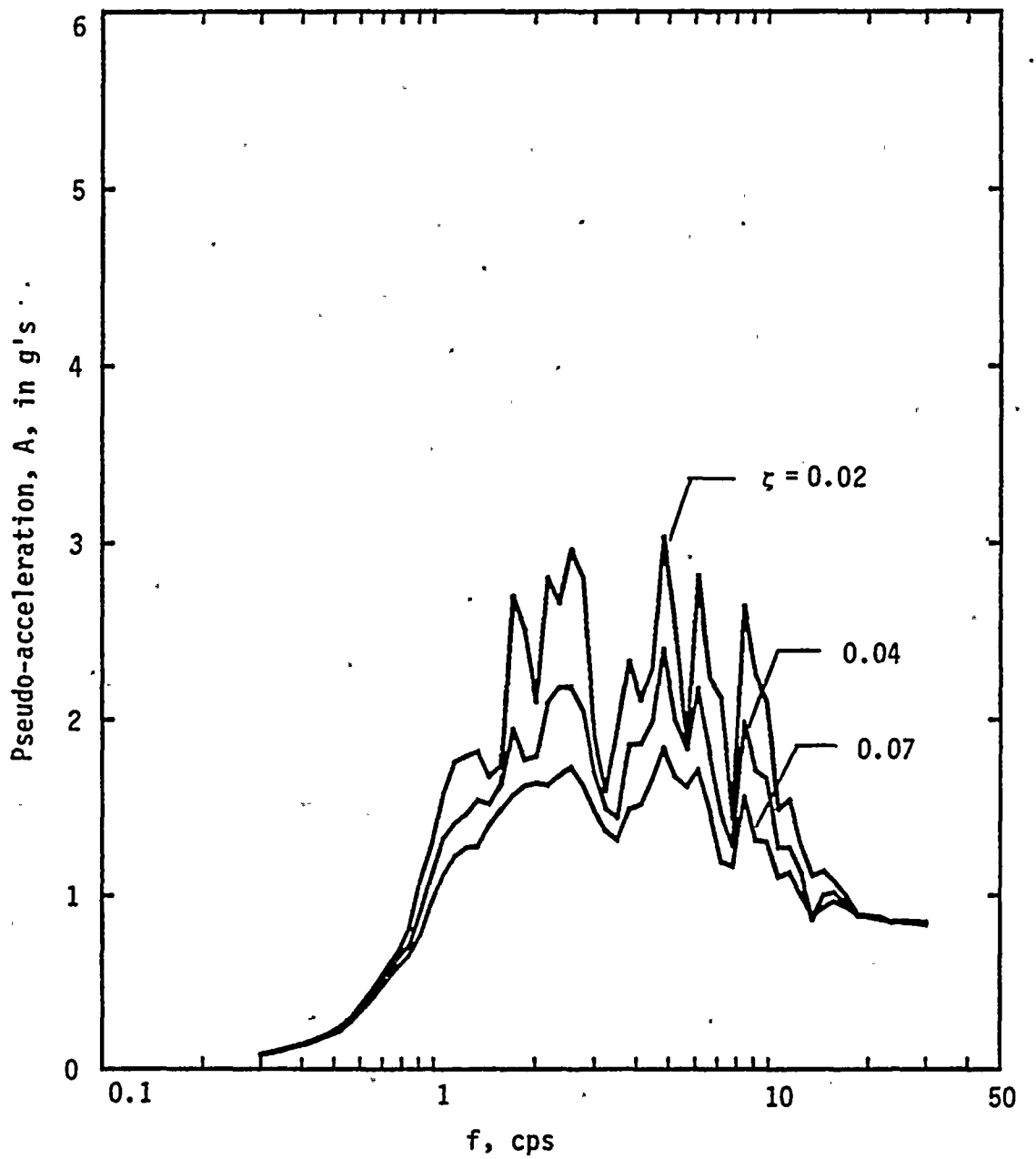

FIG. B.7 Pseudo-acceleration Response Spectra for Systems Subjected to Empirical Ground Motion Record No. 7

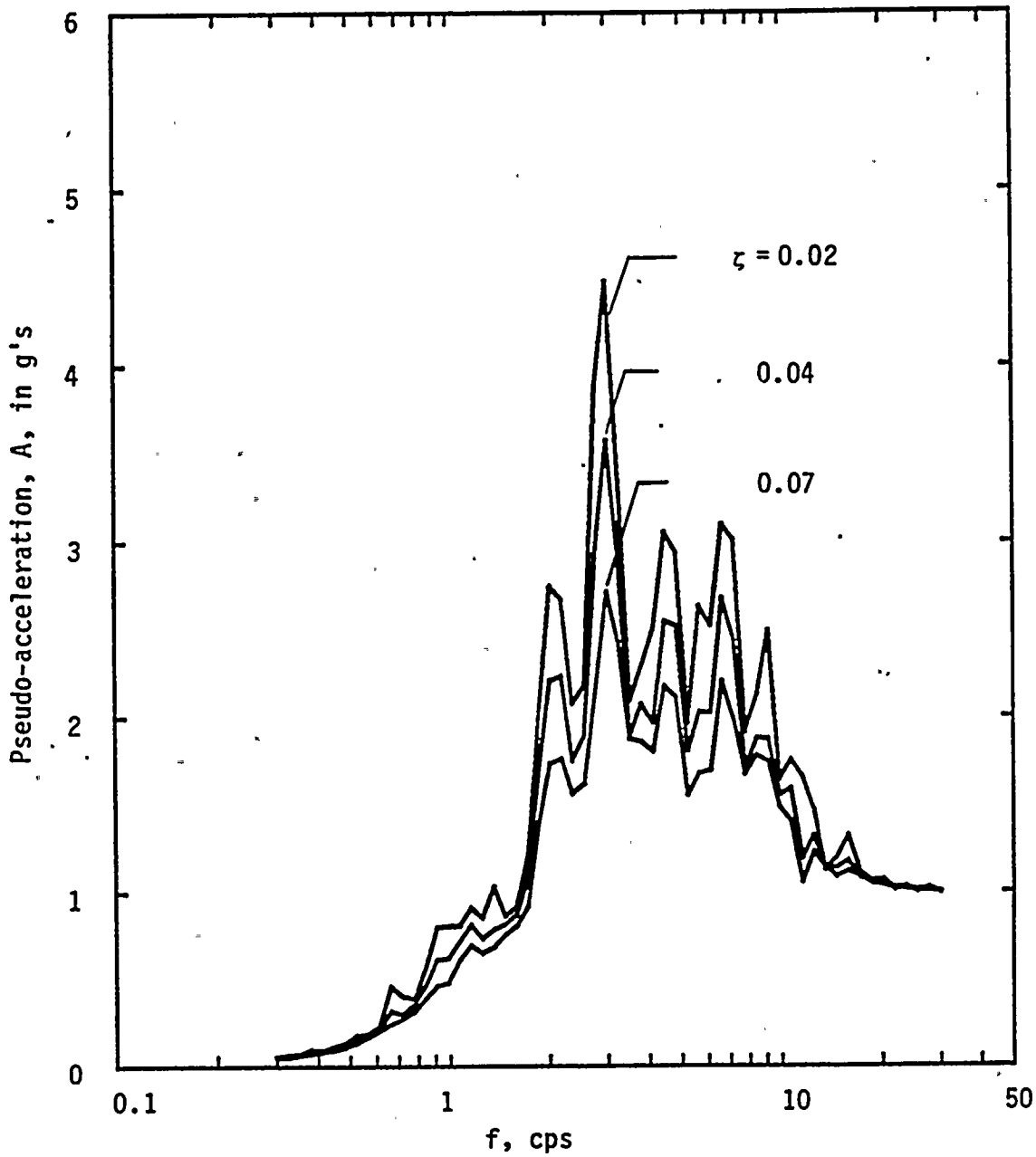

FIG. B.8 Pseudo-acceleration Response Spectra for Systems Subjected to Empirical Ground Motion Record No. 8

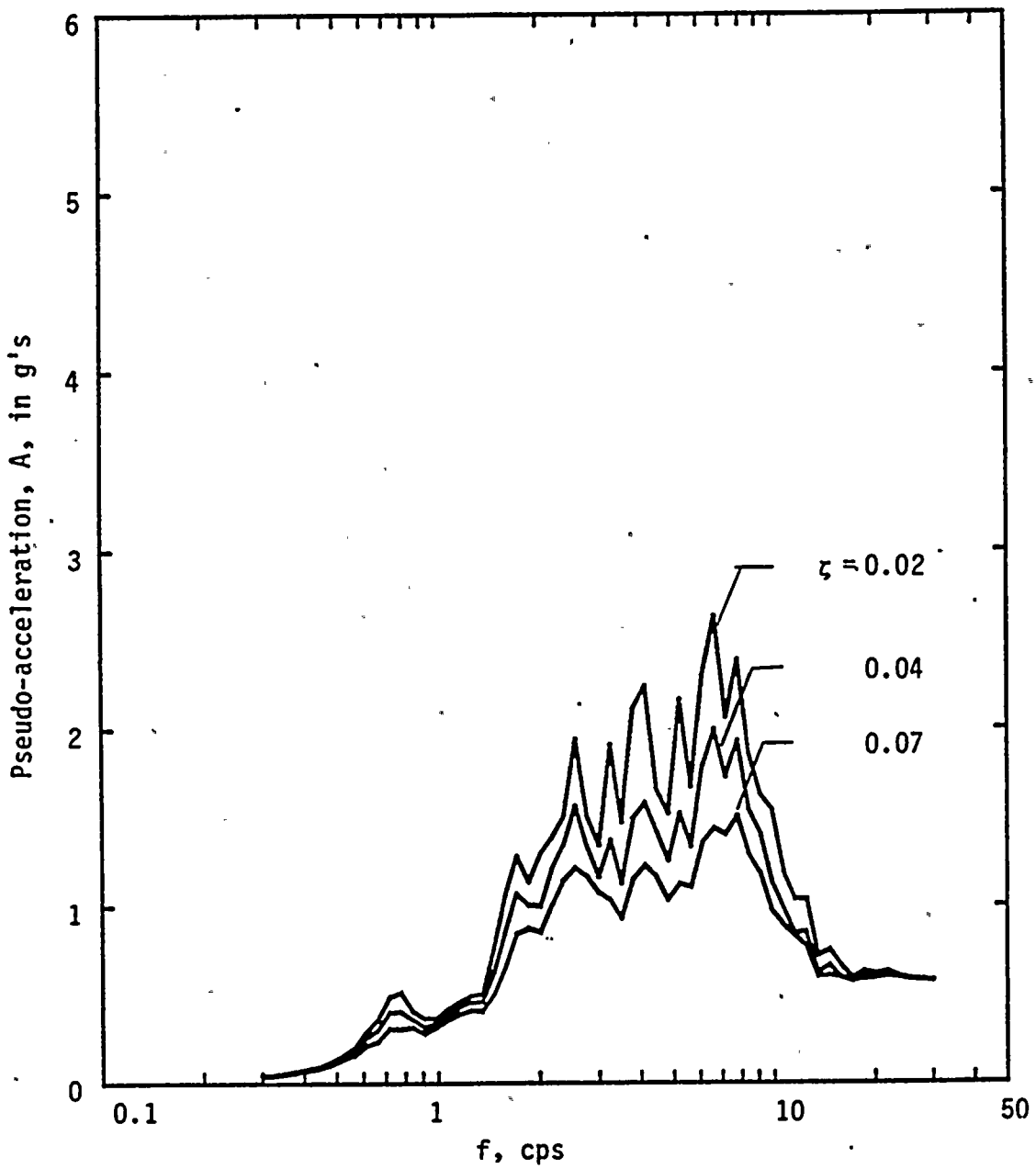

FIG. B.9 Pseudo-acceleration Response Spectra for Systems Subjected to Empirical Ground Motion Record No. 9

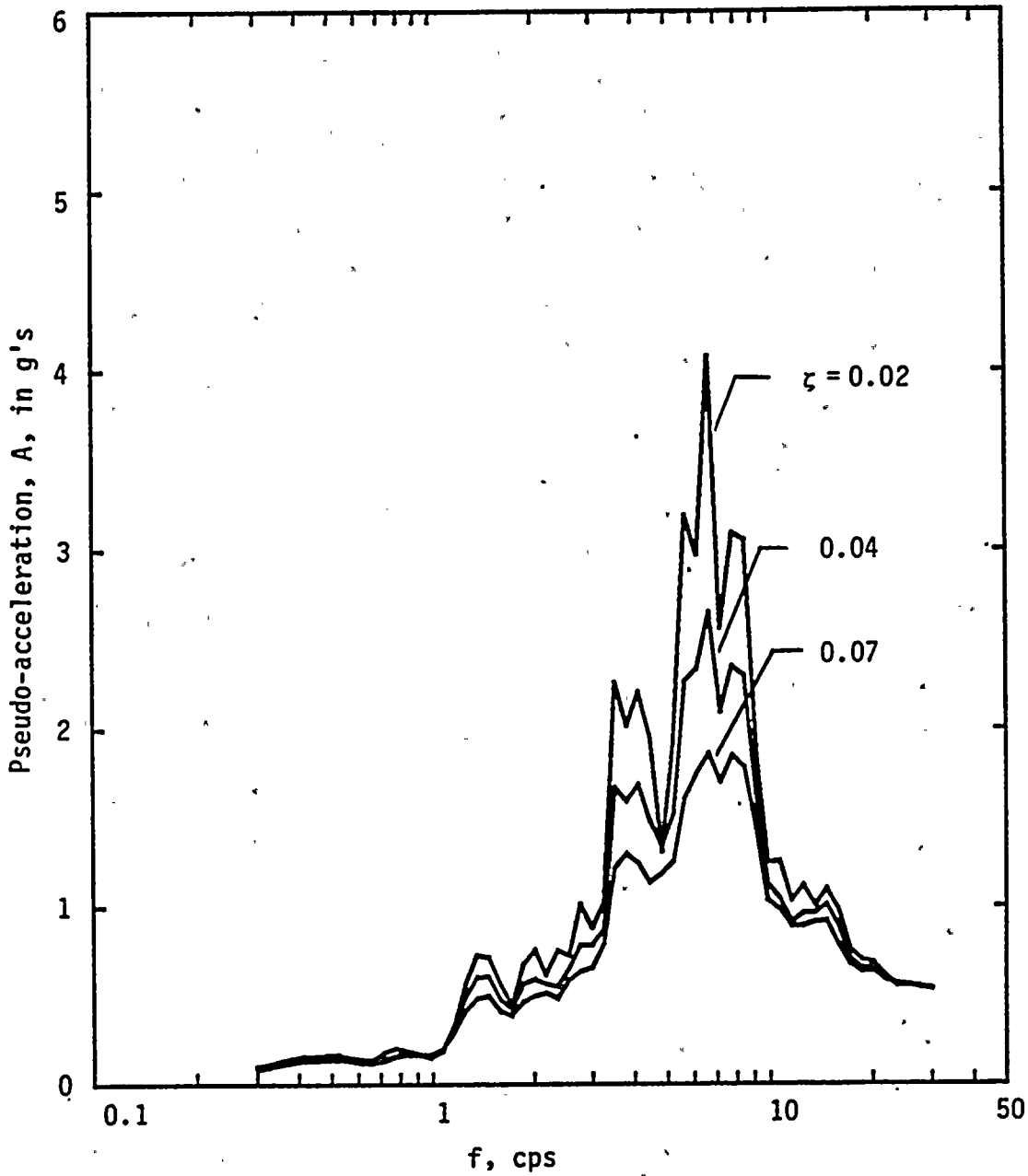

FIG. B.10 Pseudo-acceleration Response Spectra for Systems Subjected to Empirical Ground Motion Record No. 10

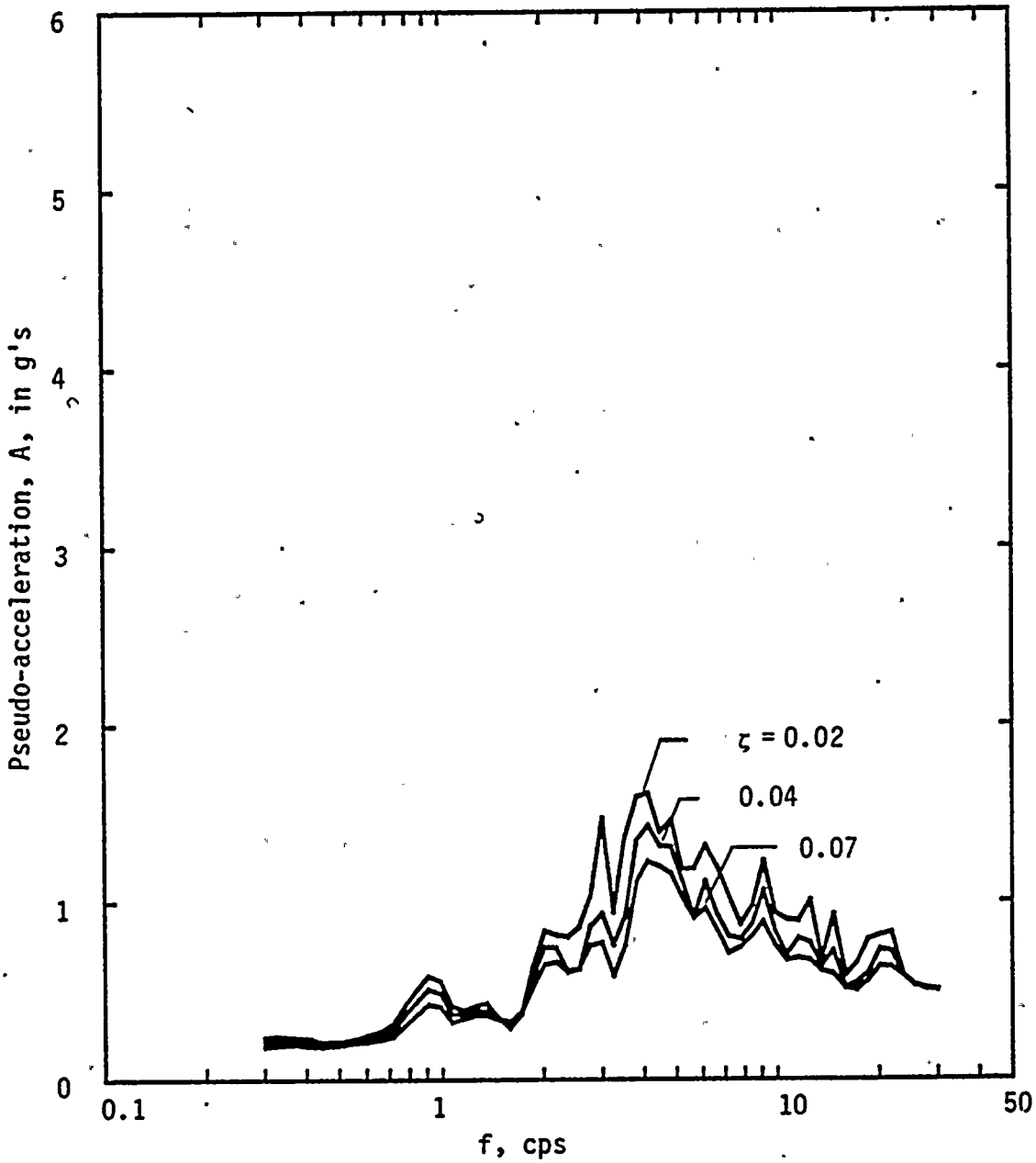

FIG. B.11 Pseudo-acceleration Response Spectra for Systems Subjected to Empirical Ground Motion Record No. 11

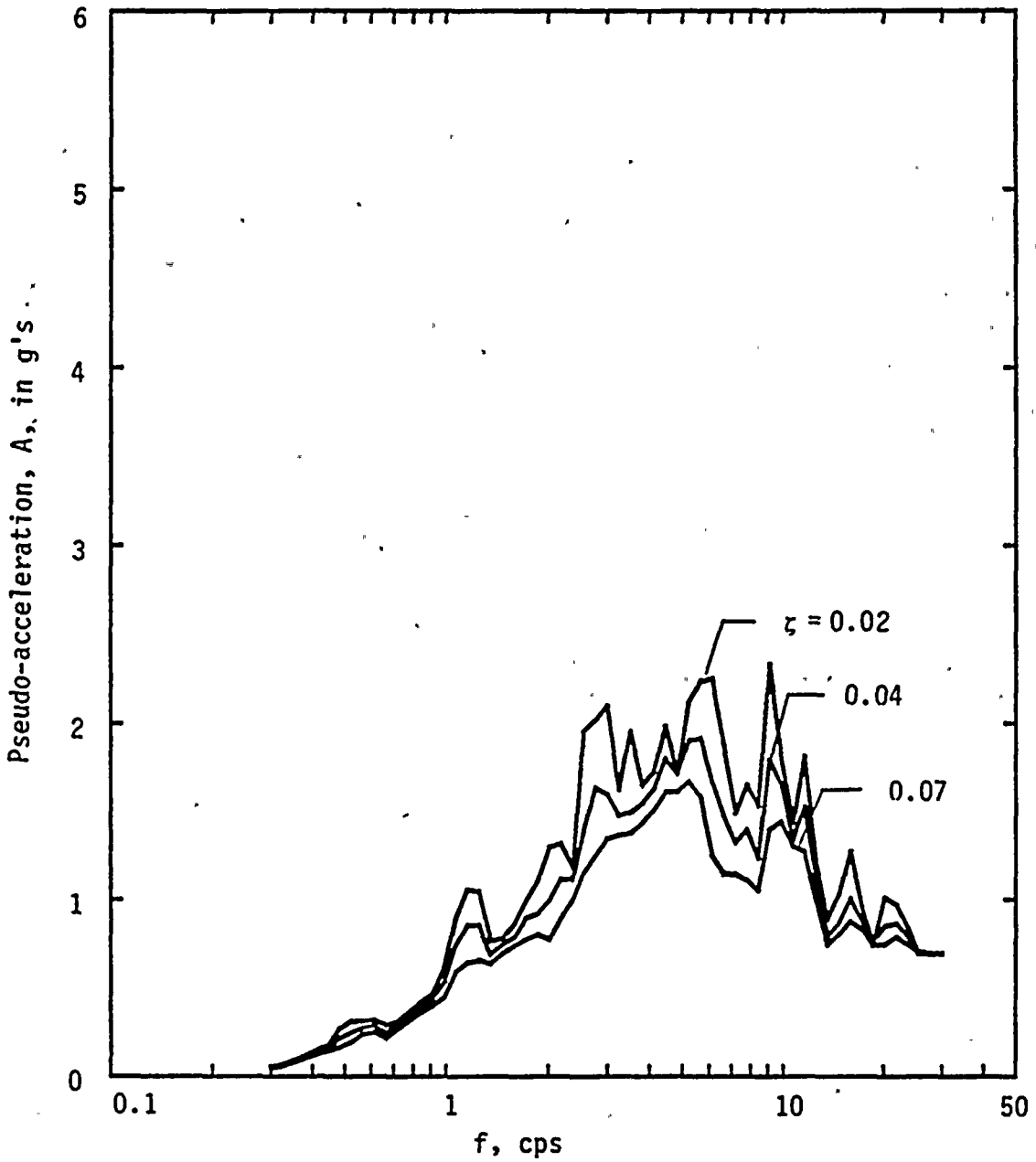

FIG. B.12 Pseudo-acceleration Response Spectra for Systems Subjected to Empirical Ground Motion Record No. 12

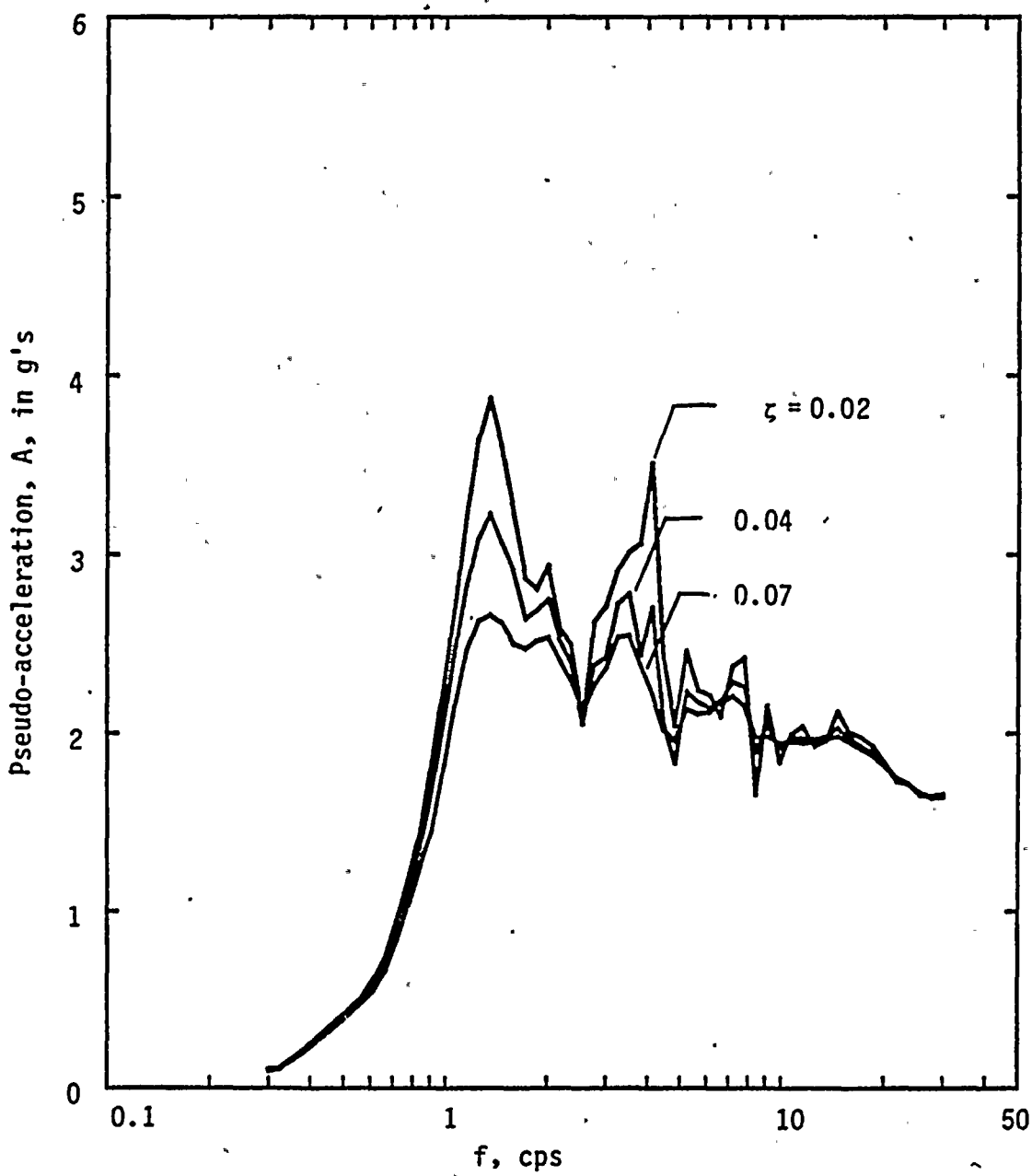

FIG. B.13 Pseudo-acceleration Response Spectra for Systems Subjected to Empirical Ground Motion Record No. 13

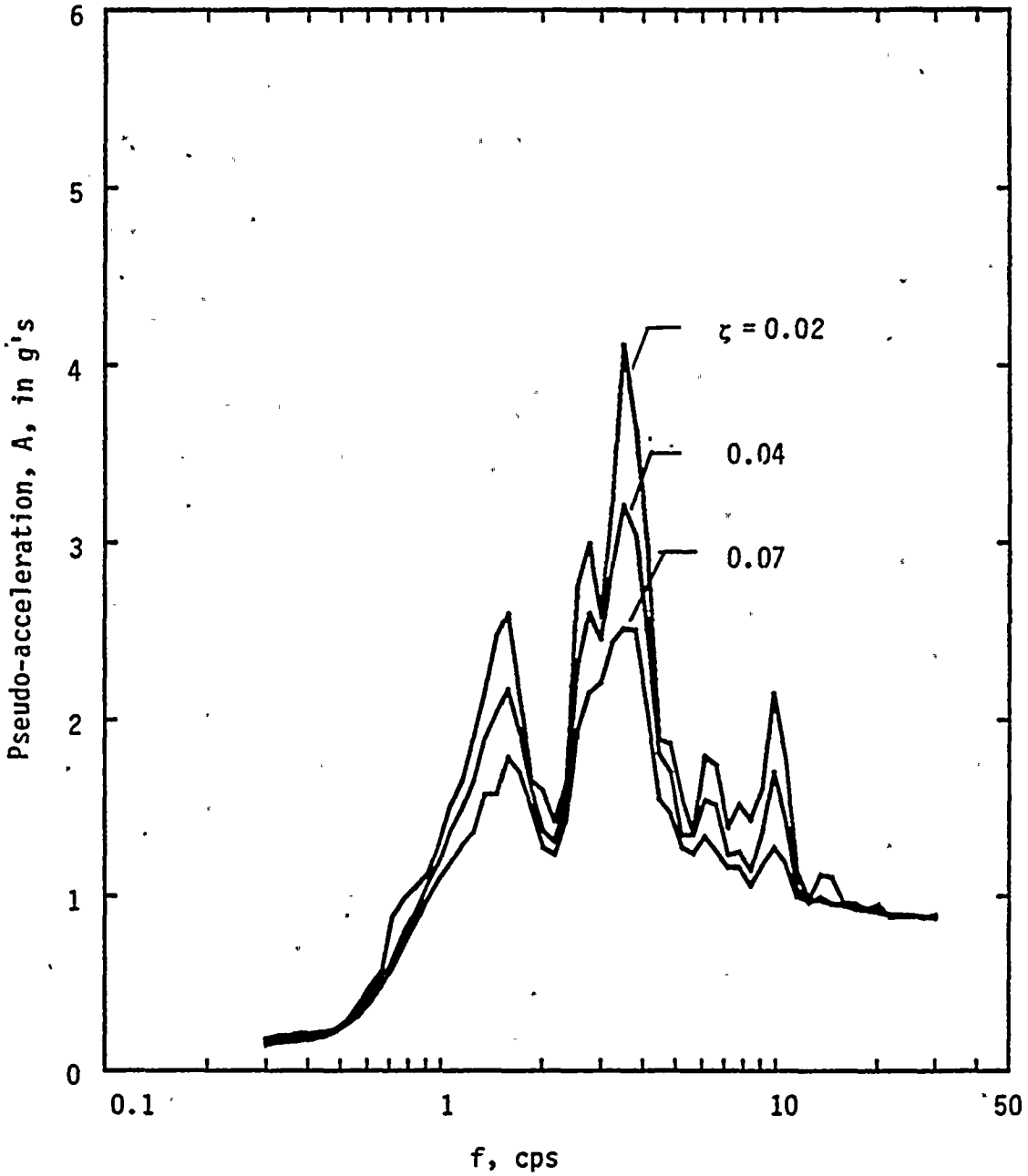

FIG. B.14 Pseudo-acceleration Response Spectra for Systems Subjected to Empirical Ground Motion Record No. 14

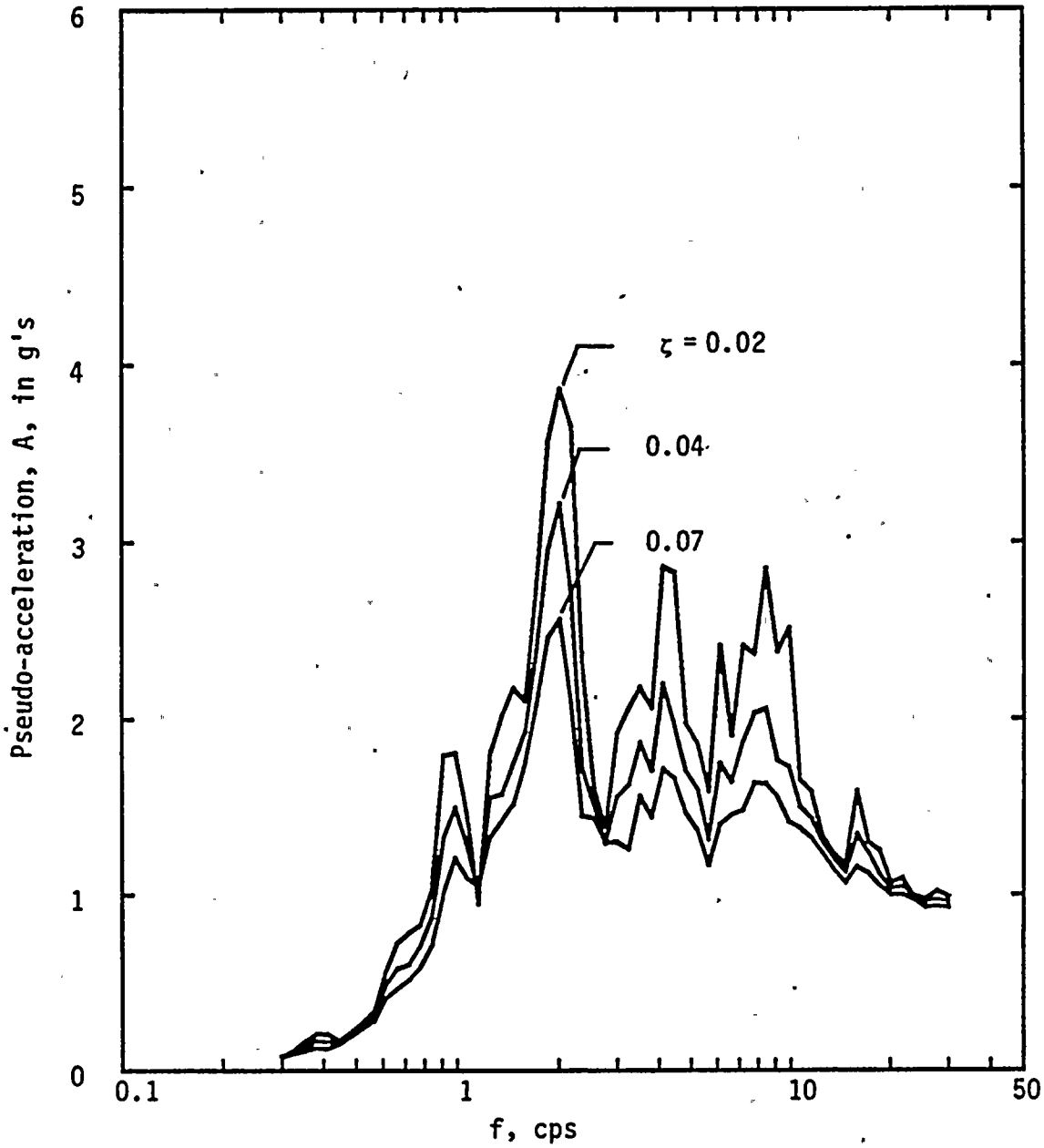

FIG. B.15 Pseudo-acceleration Response Spectra for Systems Subjected to Empirical Ground Motion Record No. 15

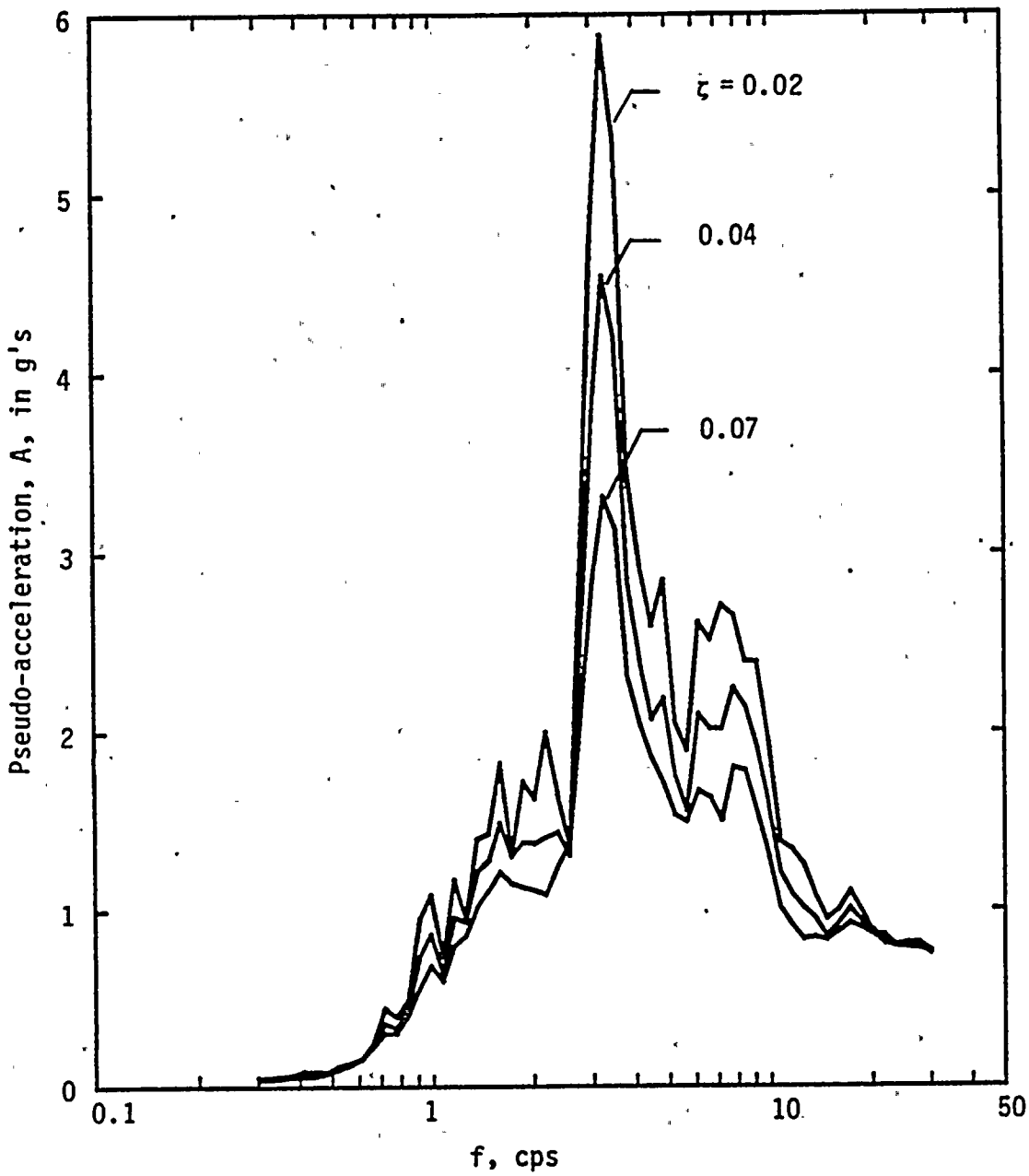

FIG. B.16 Pseudo-acceleration Response Spectra for Systems Subjected to Empirical Ground Motion Record No. 16

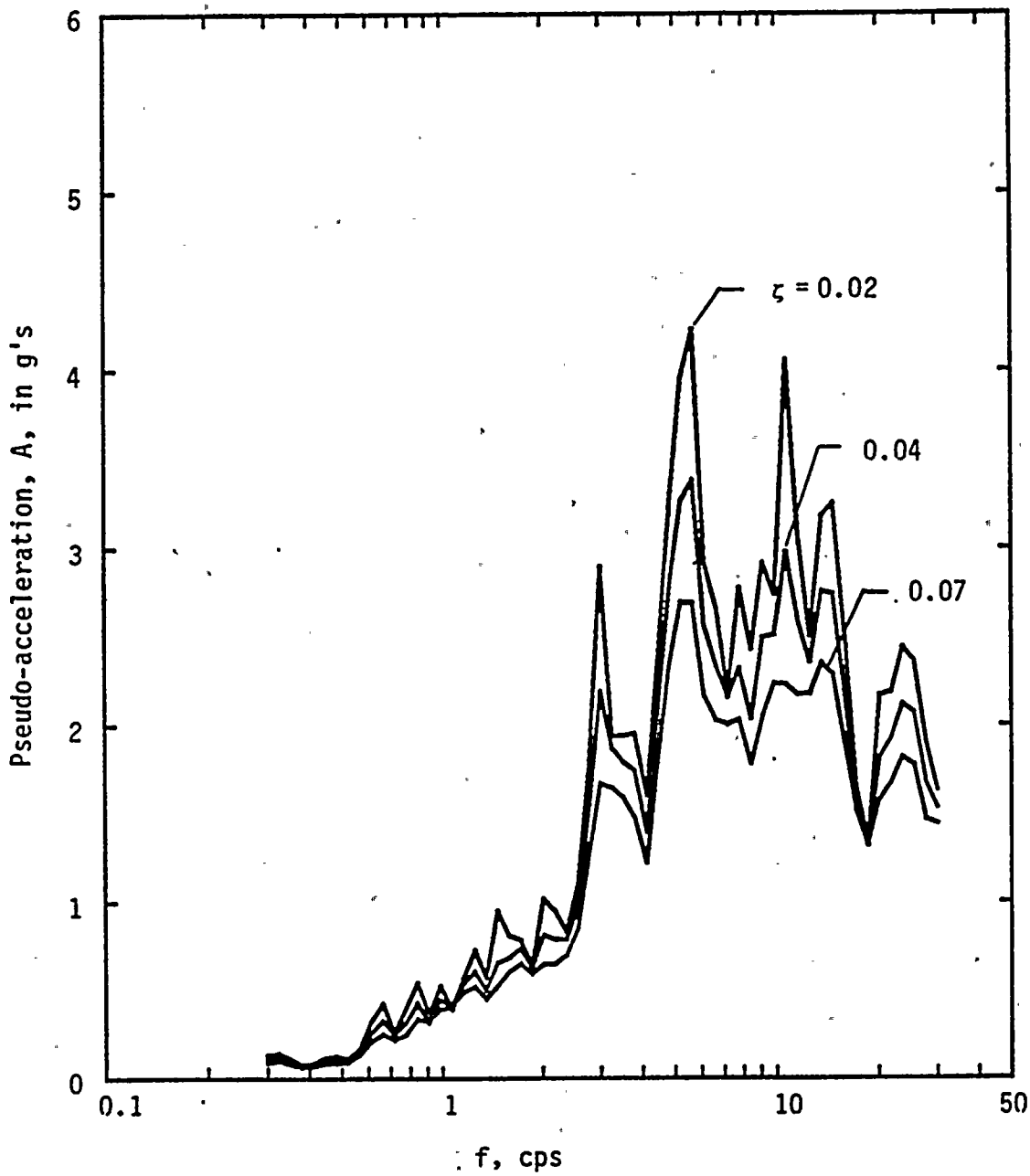

FIG. B.17 Pseudo-acceleration Response Spectra for Systems Subjected to Empirical Ground Motion Record No. 17

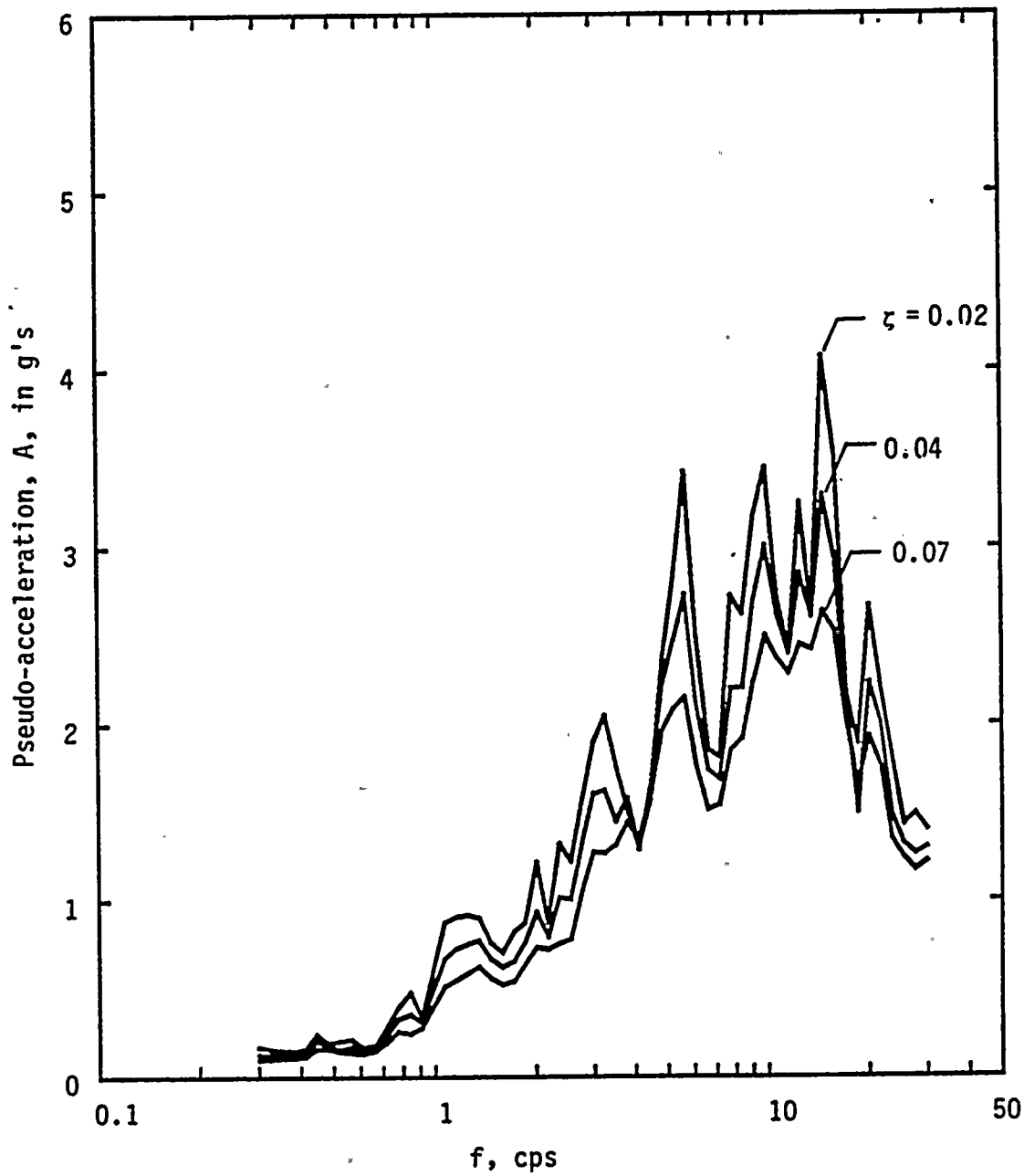

FIG. B.18 Pseudo-acceleration Response Spectra for Systems Subjected to Empirical Ground Motion Record No. 18

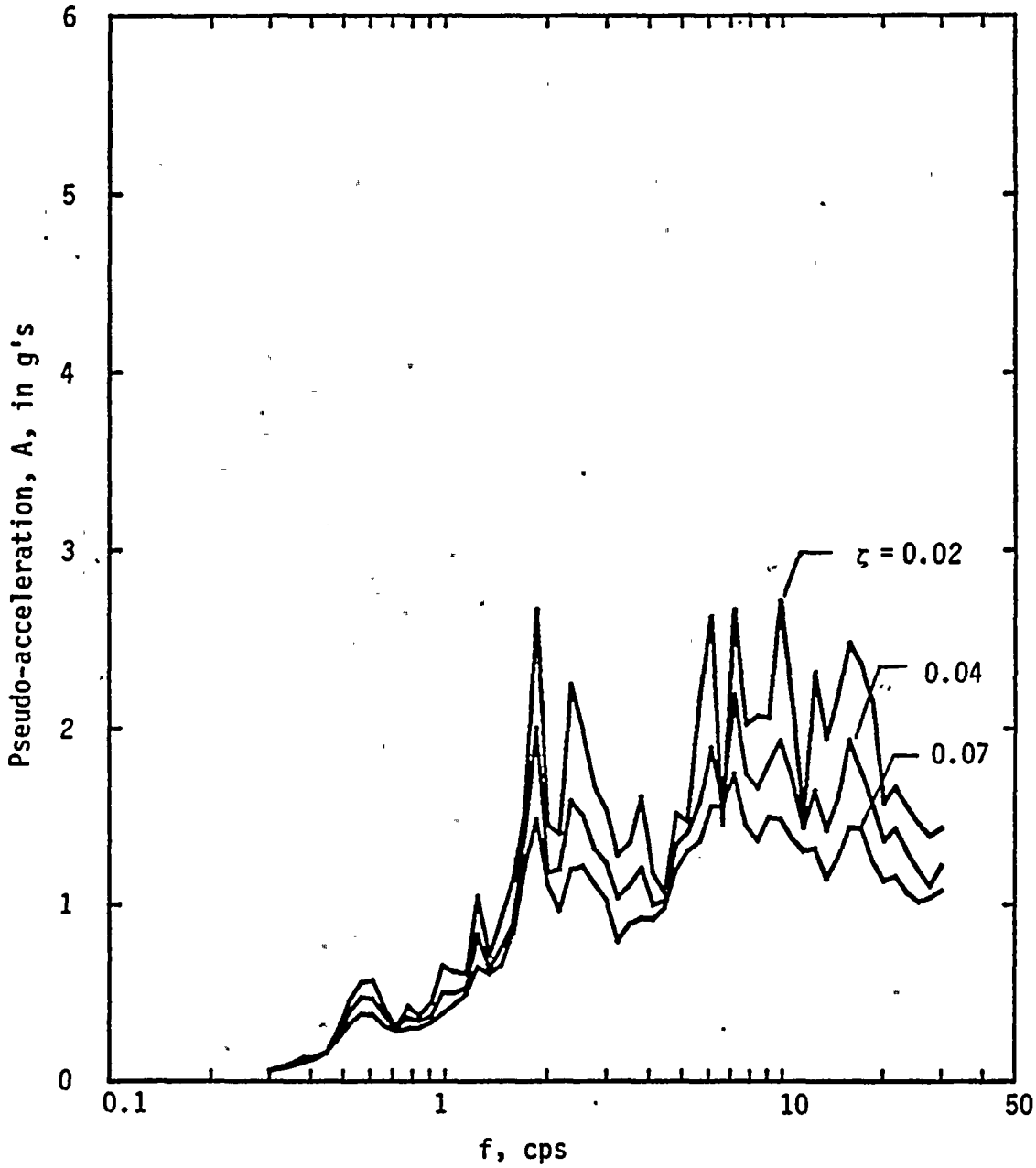

FIG. B.19 Pseudo-acceleration Response Spectra for Systems Subjected to Empirical Ground Motion Record No. 19

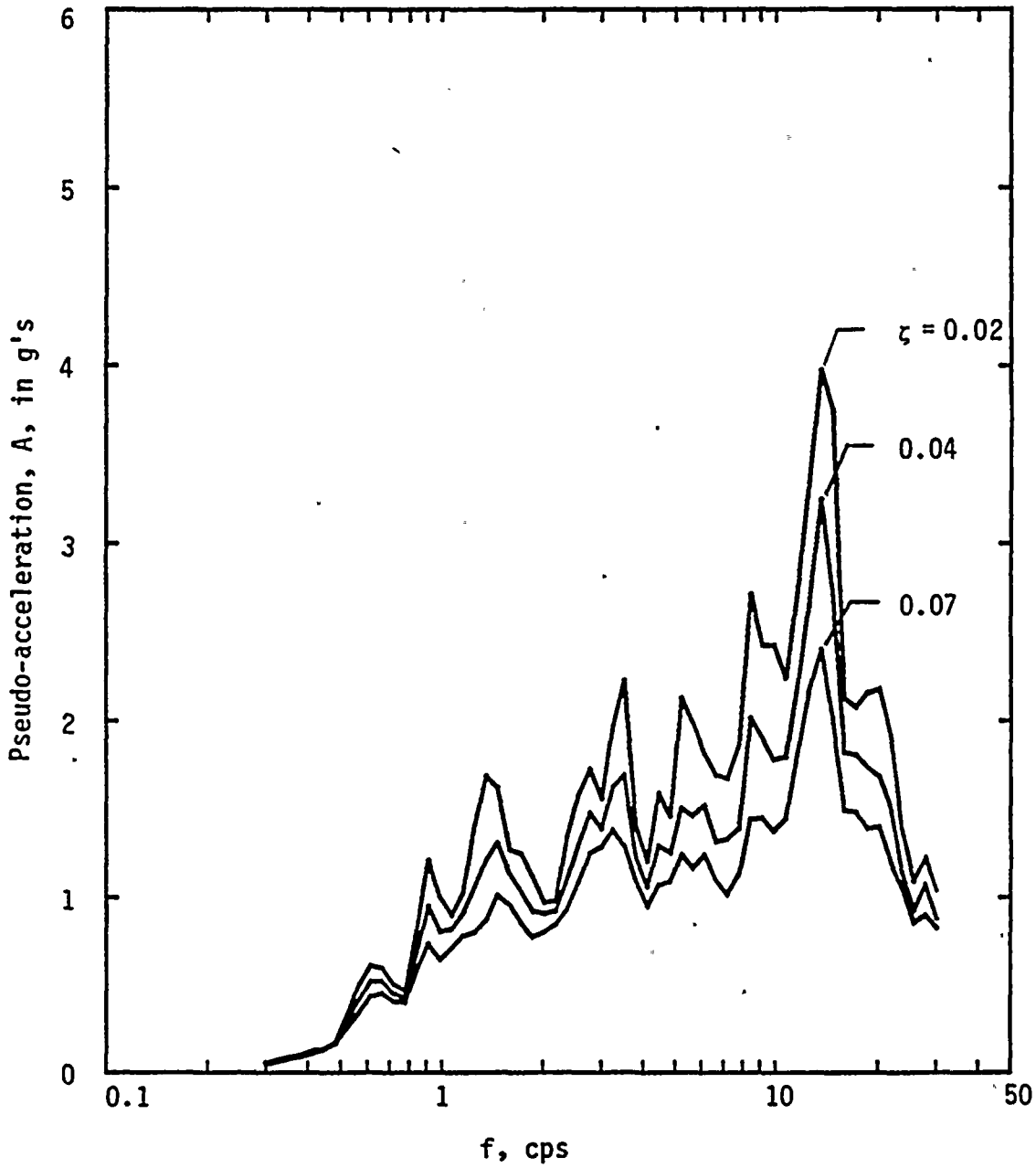

FIG. B.20 Pseudo-acceleration Response Spectra for Systems Subjected to Empirical Ground Motion Record No. 20

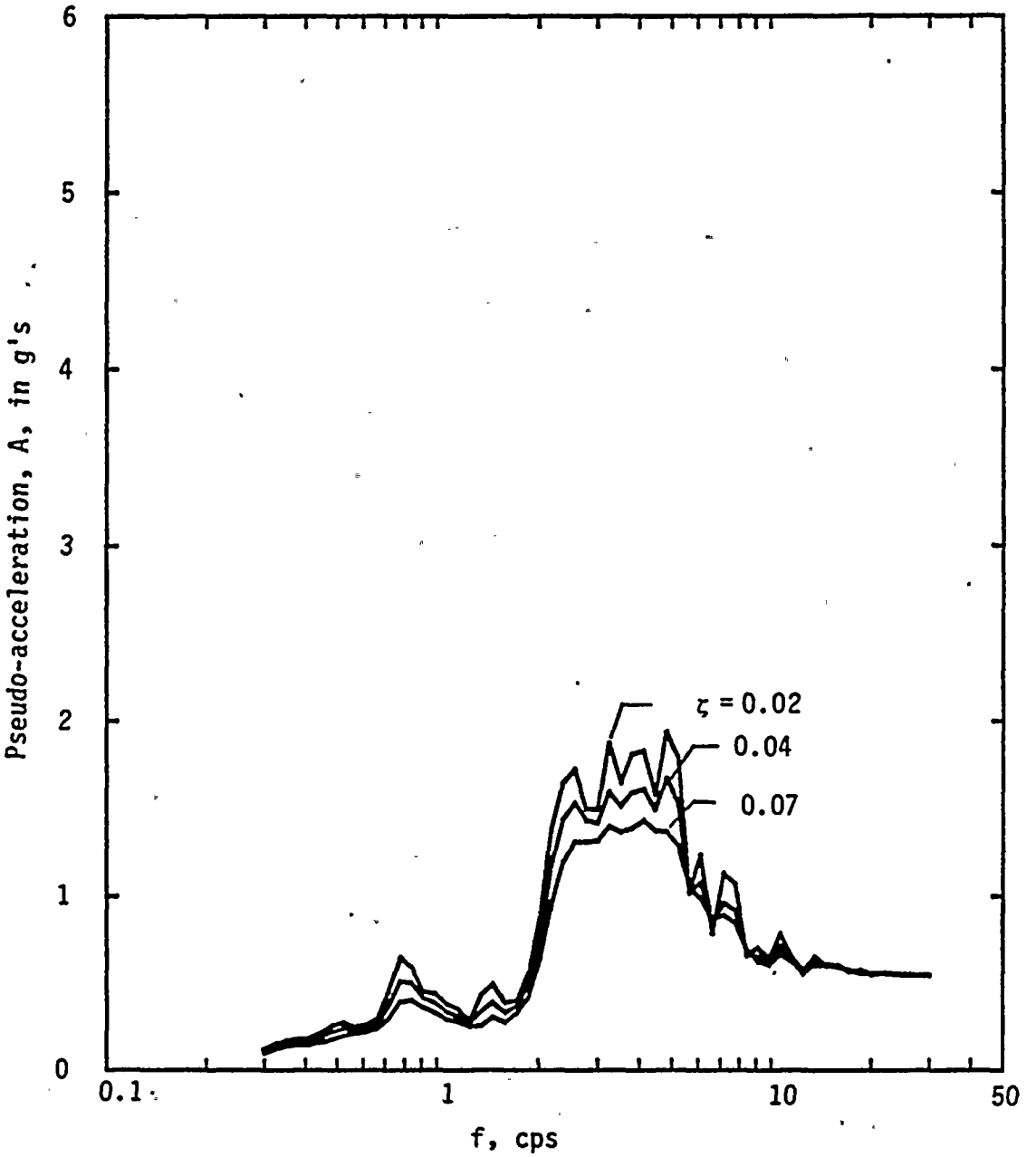

FIG. B.21 Pseudo-acceleration Response Spectra for Systems Subjected to Empirical Ground Motion Record No. 21

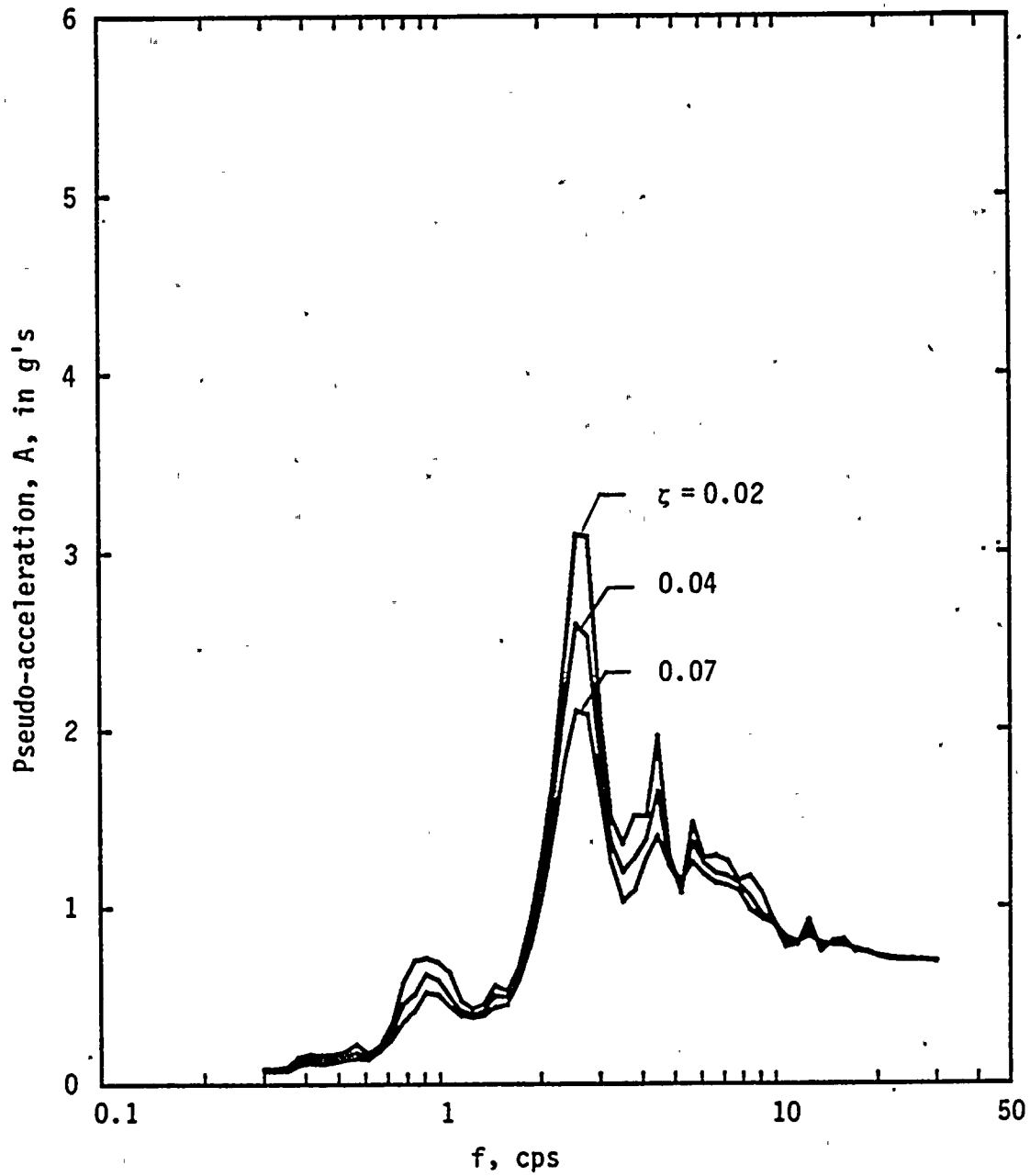

FIG. B.22 Pseudo-acceleration Response Spectra for Systems Subjected to Empirical Ground Motion Record No. 22

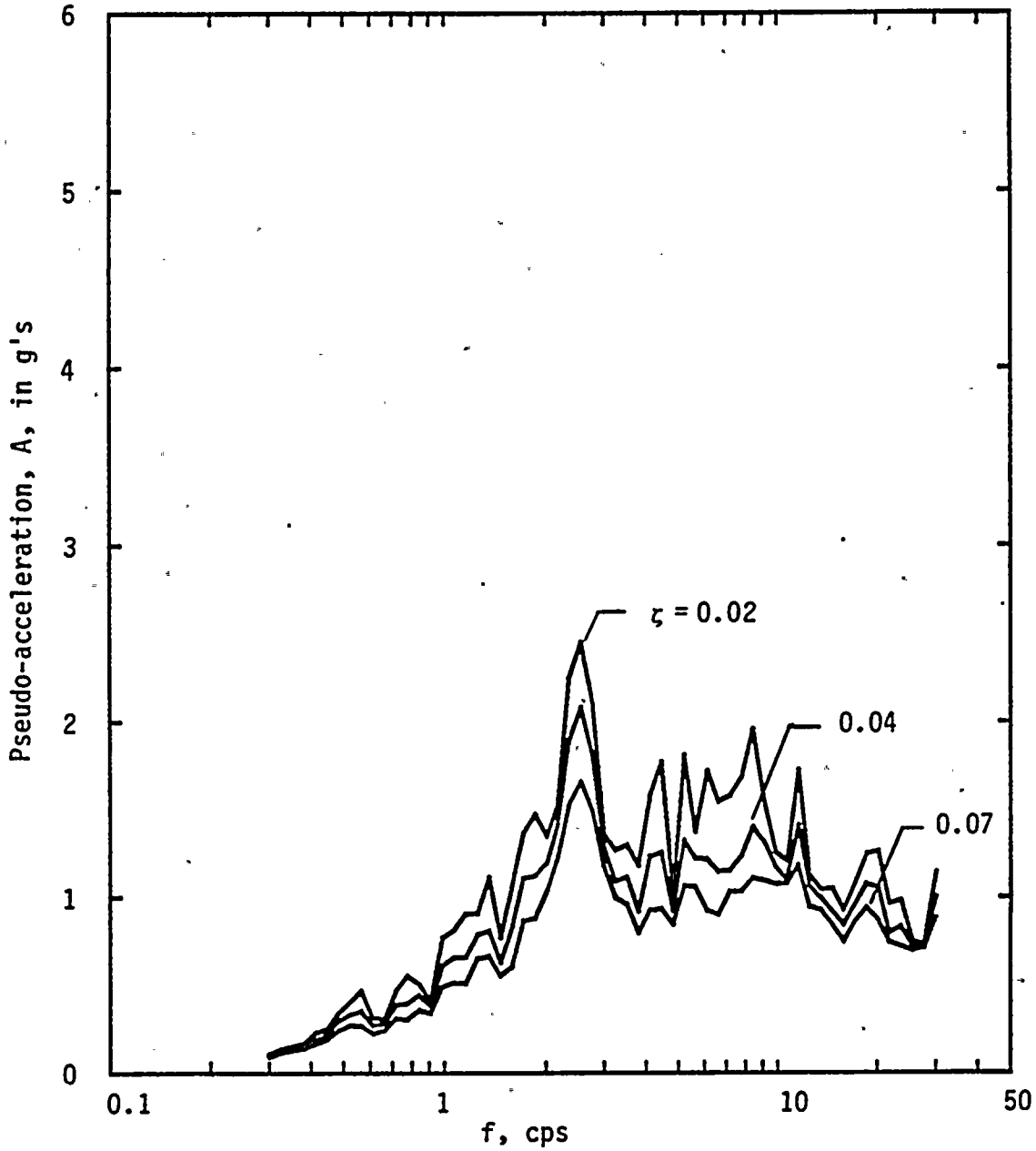

FIG. B.23 Pseudo-acceleration Response Spectra for Systems Subjected to Empirical Ground Motion Record No. 23

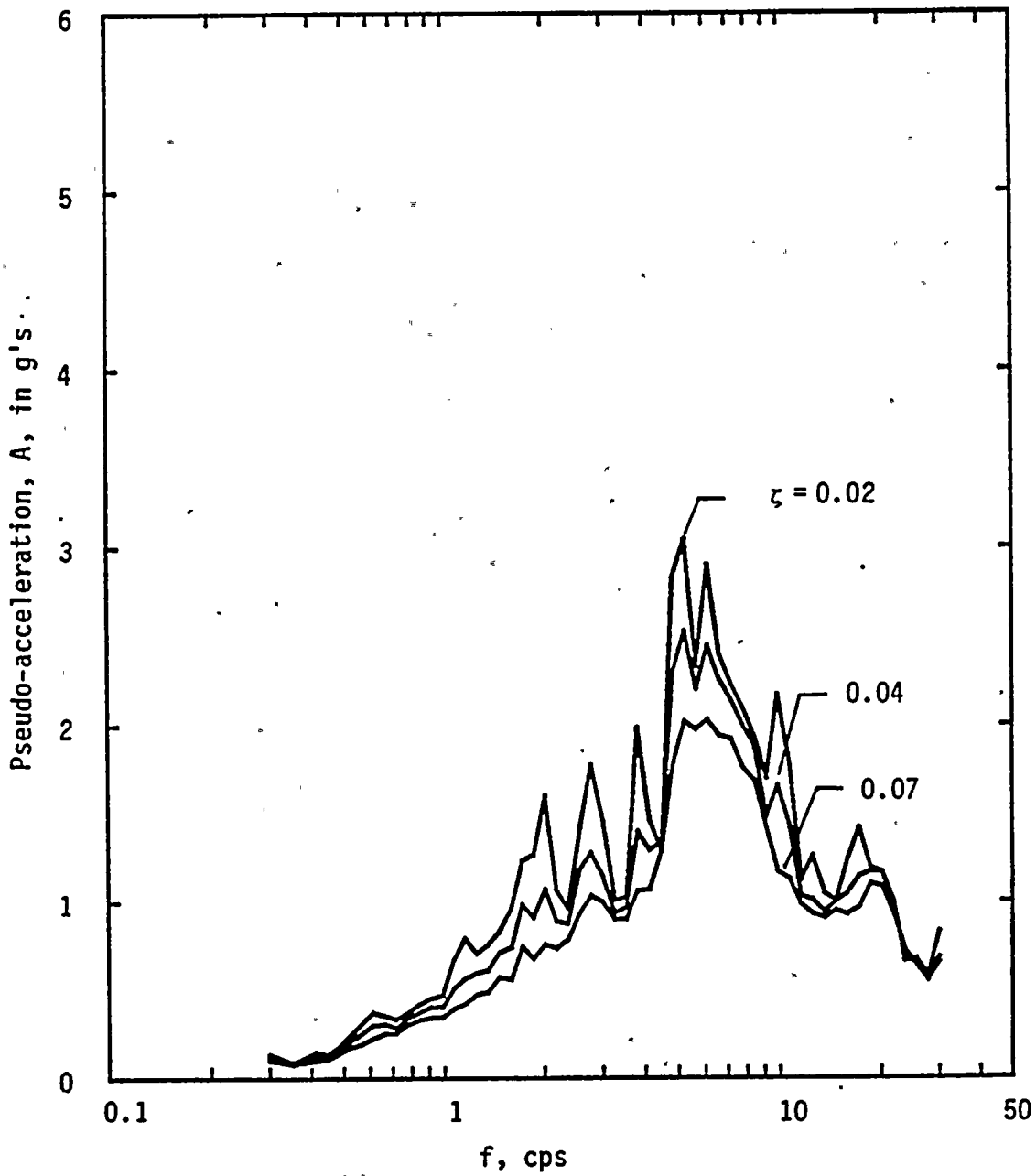

FIG. B.24 Pseudo-acceleration Response Spectra for Systems Subjected to Empirical Ground Motion Record No. 24

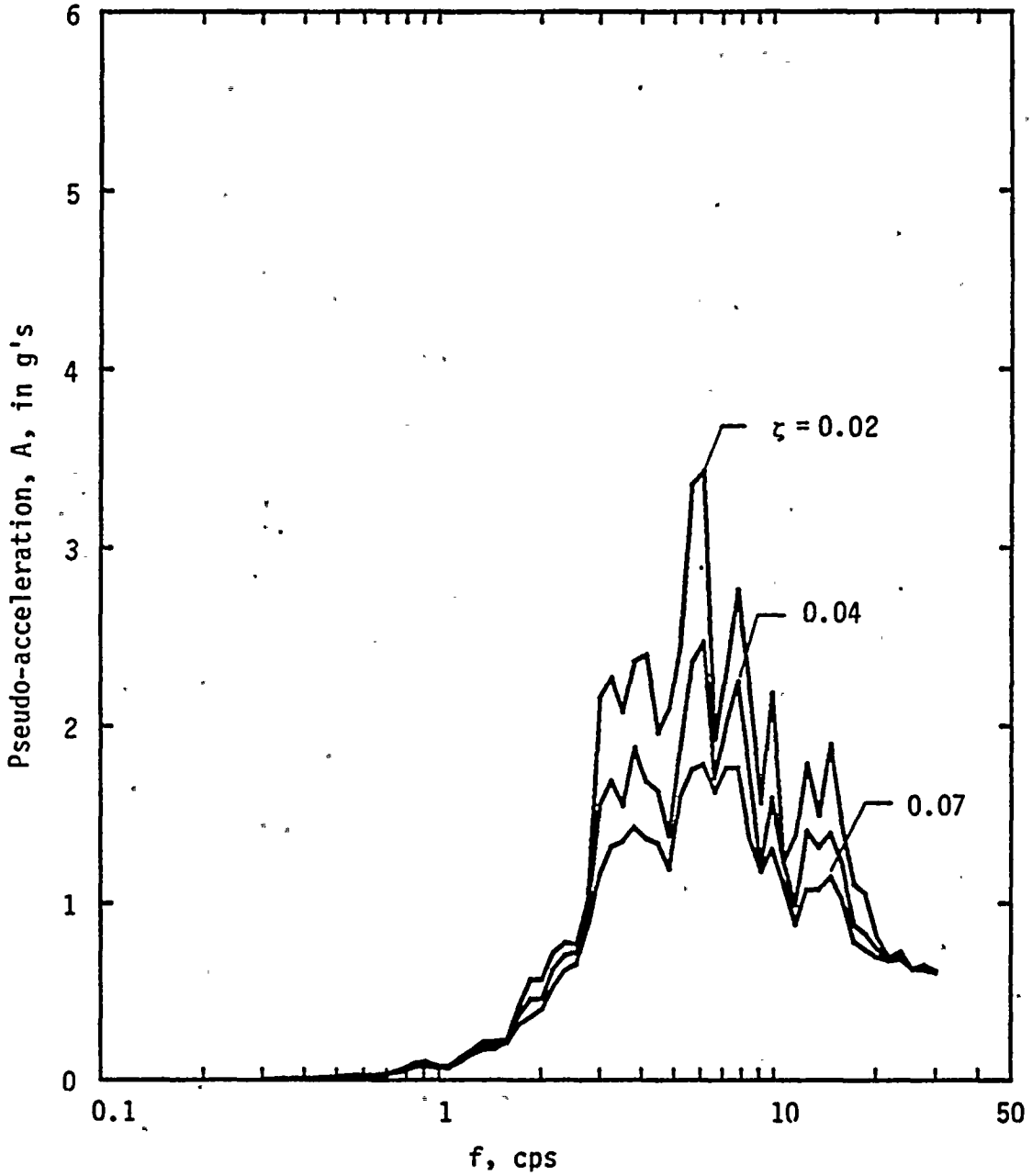

FIG. B.25 Pseudo-acceleration Response Spectra for Systems Subjected to Numerically Generated Ground Motion Record No. 25

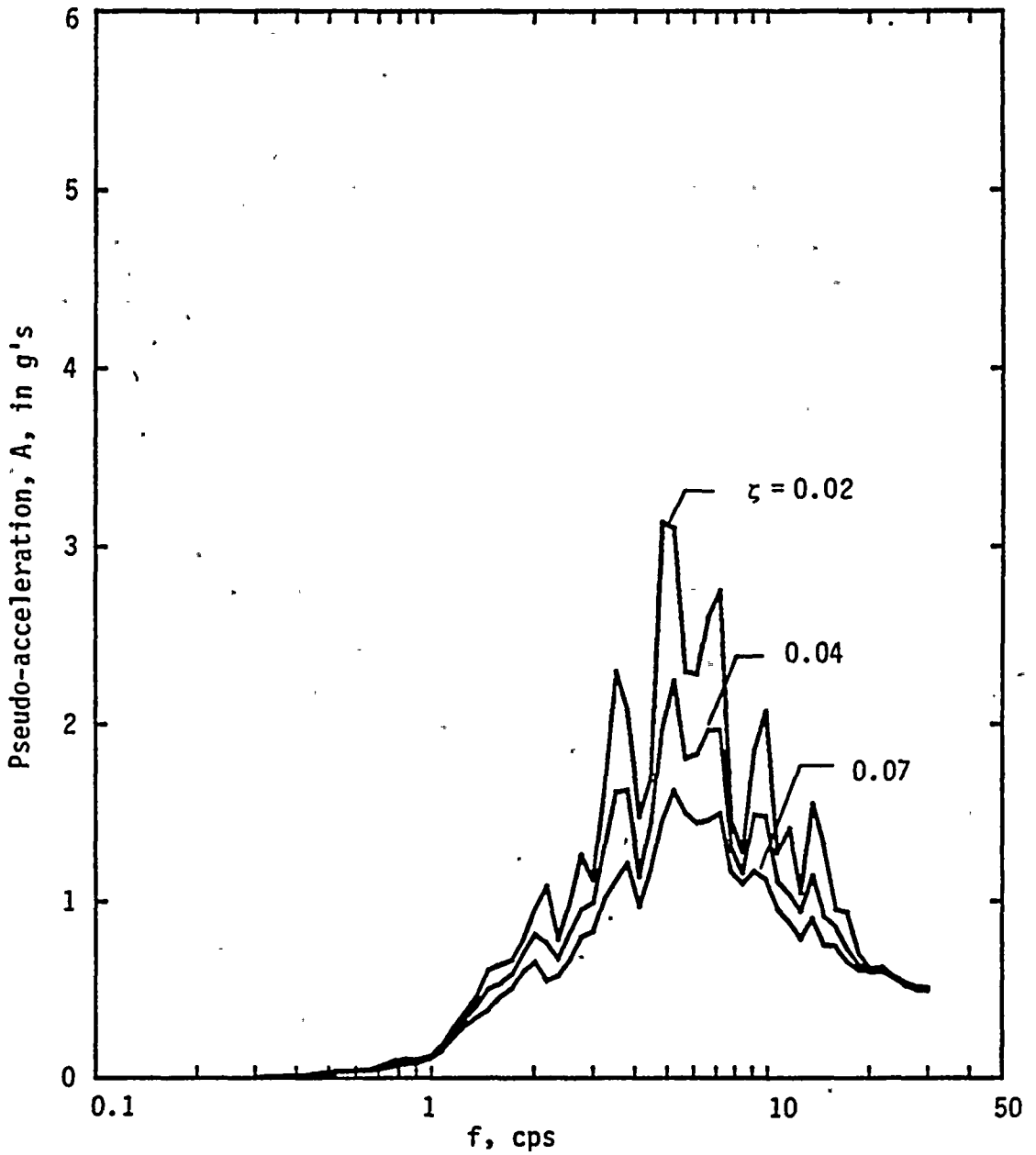

FIG. B.26 Pseudo-acceleration Response Spectra for Systems Subjected to Numerically Generated Ground Motion Record No. 26

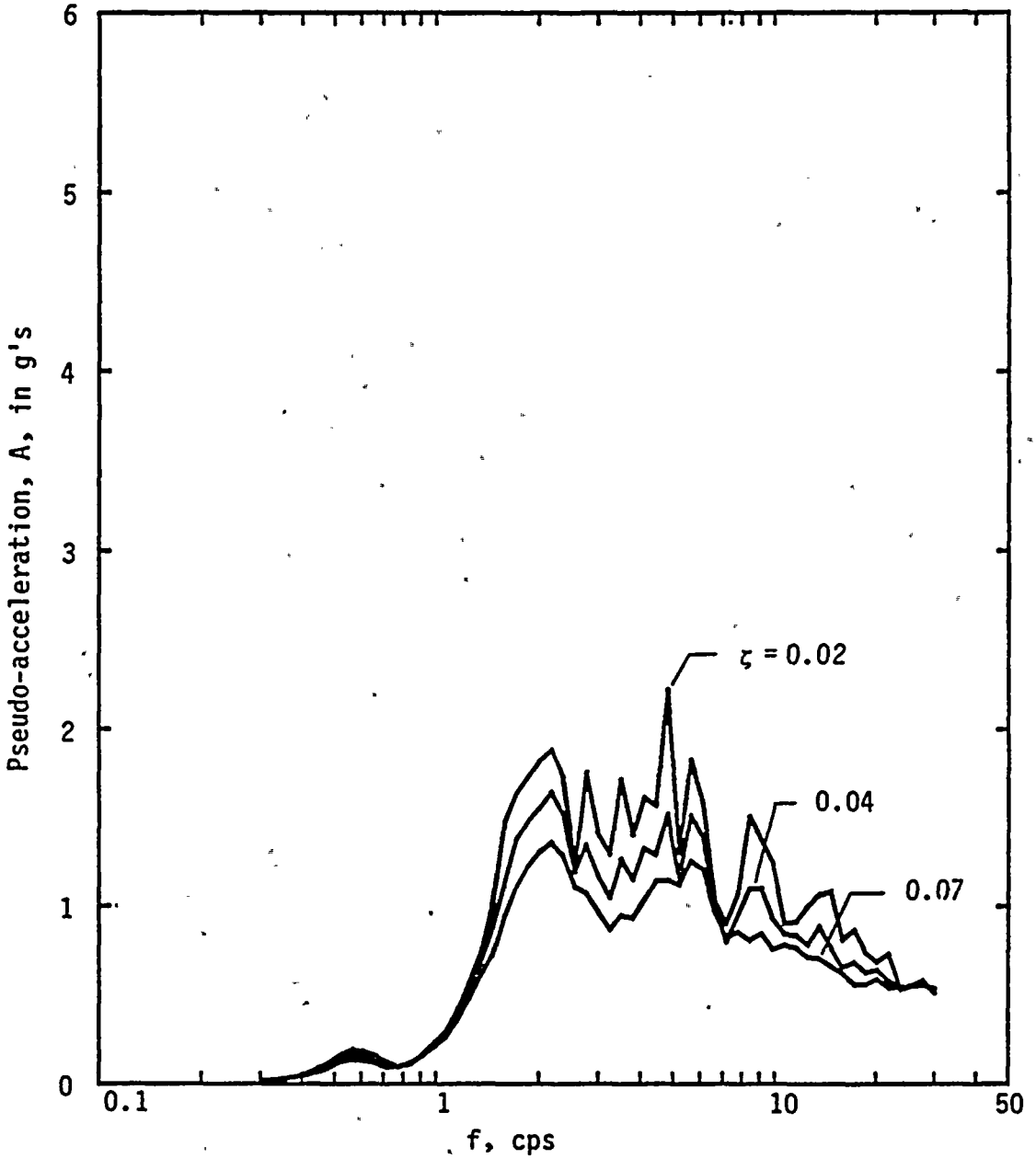

FIG. B.27 Pseudo-acceleration Response Spectra for Systems Subjected to Numerically Generated Ground Motion Record No. 27

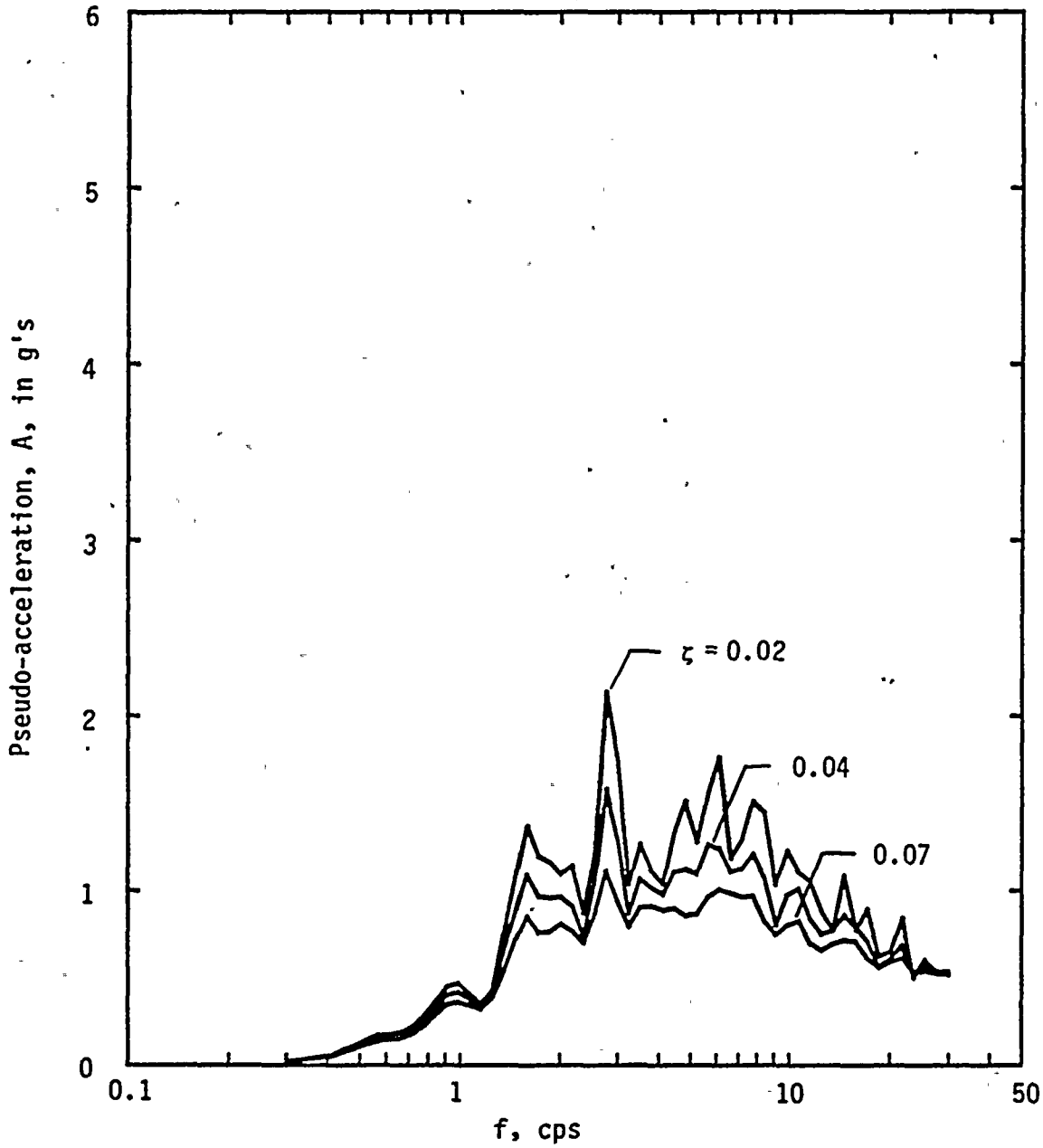

FIG. B.28 Pseudo-acceleration Response Spectra for Systems Subjected to Numerically Generated Ground Motion Record No. 28

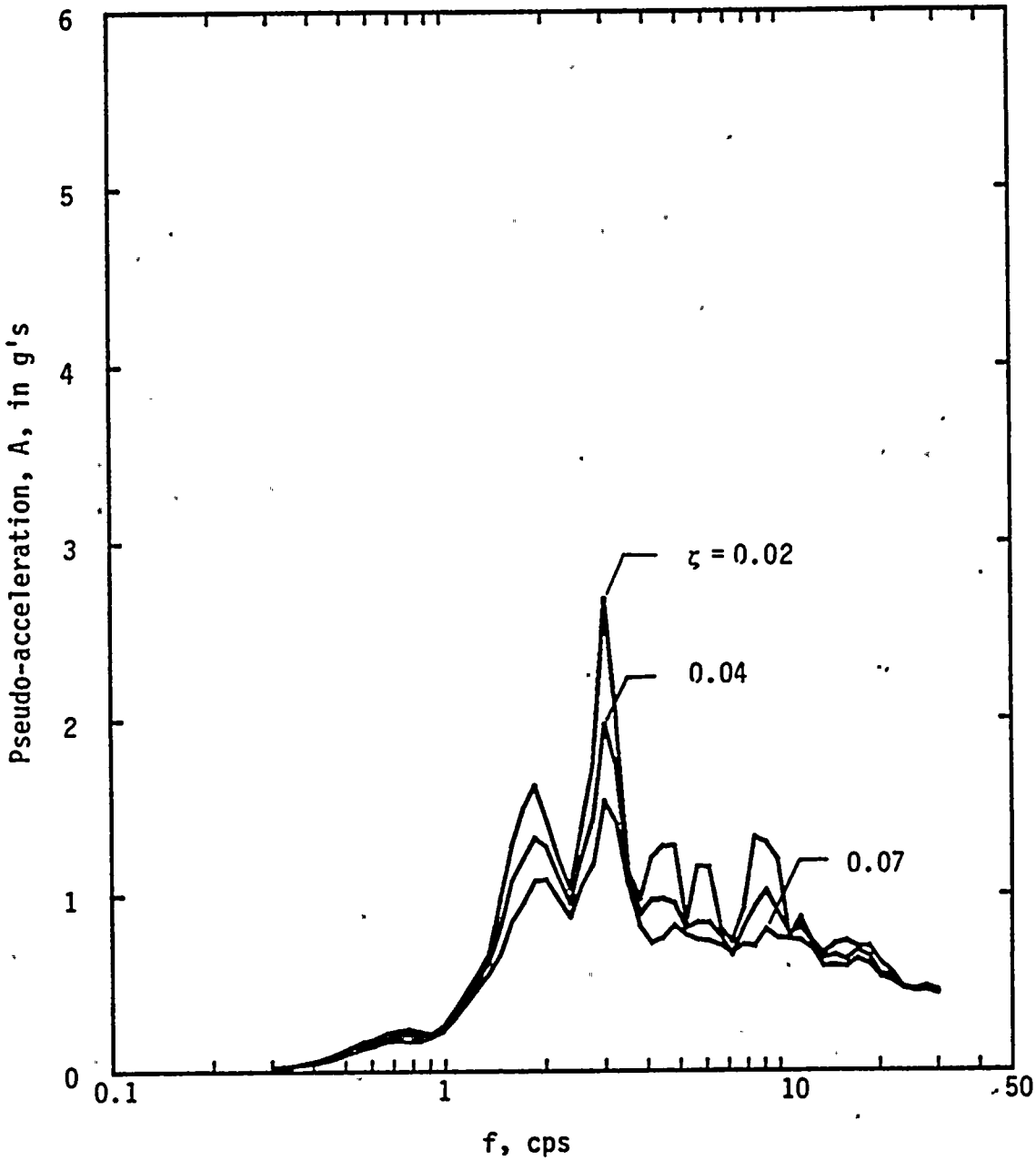

FIG. B.29 Pseudo-acceleration Response Spectra for Systems Subjected to Numerically Generated Ground Motion Record No. 29

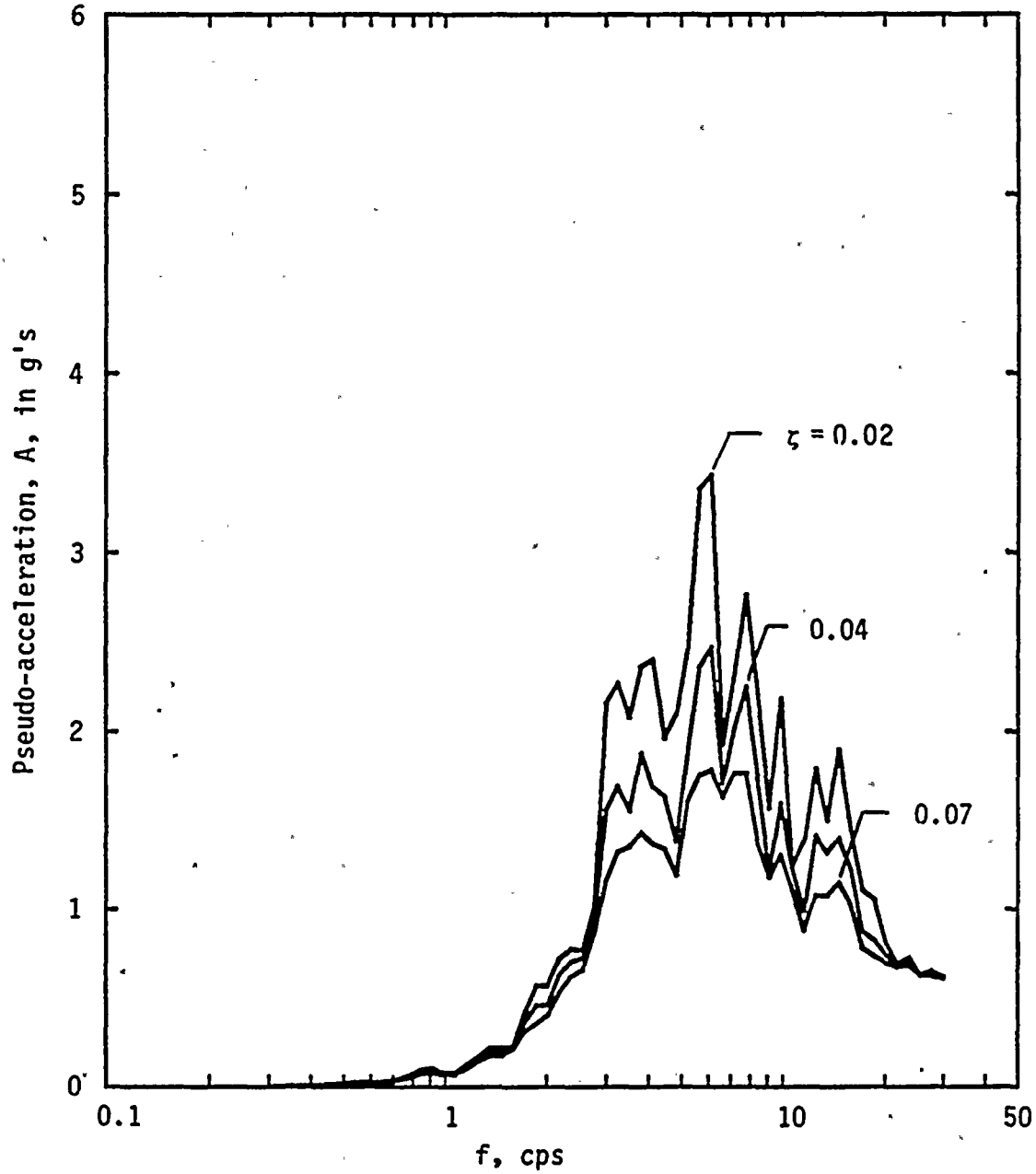

FIG. B.30 Pseudo-acceleration Response Spectra for Systems Subjected to Numerically Generated Ground Motion Record No. 30

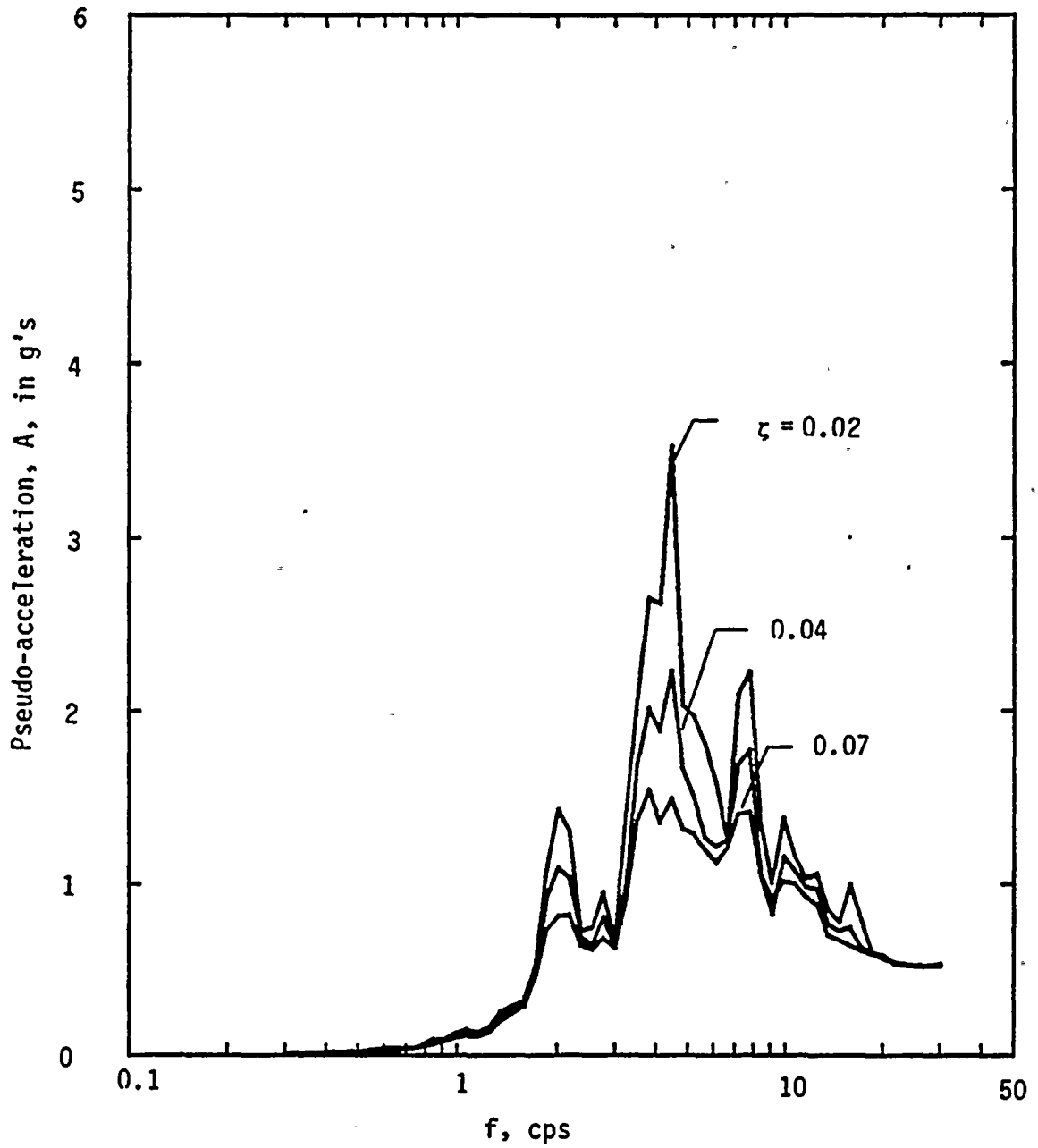

FIG. B.31 Pseudo-acceleration Response Spectra for Systems Subjected to Numerically Generated Ground Motion Record No. 31

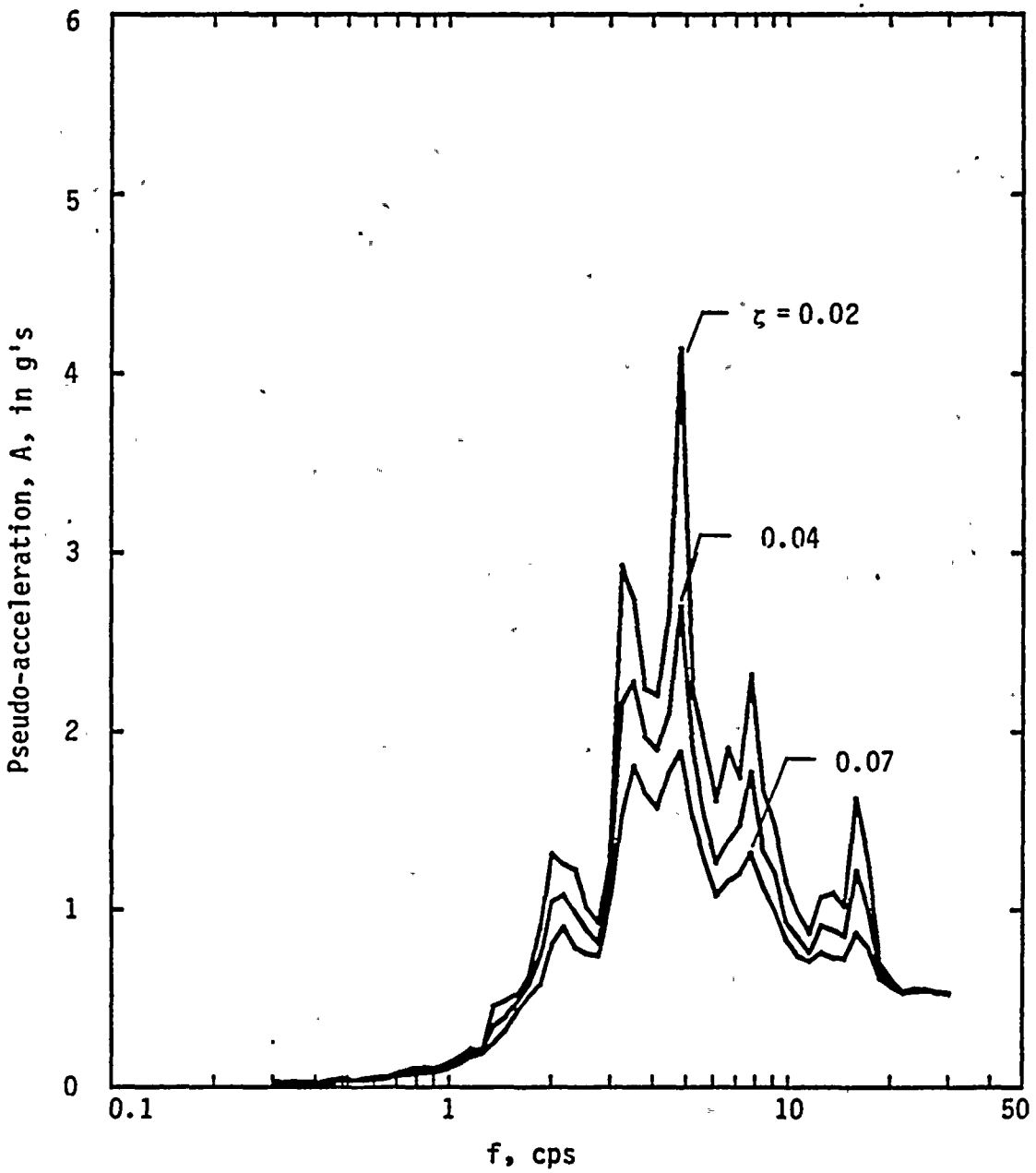

FIG. B.32 Pseudo-acceleration Response Spectra for Systems Subjected to Numerically Generated Ground Motion Record No. 32

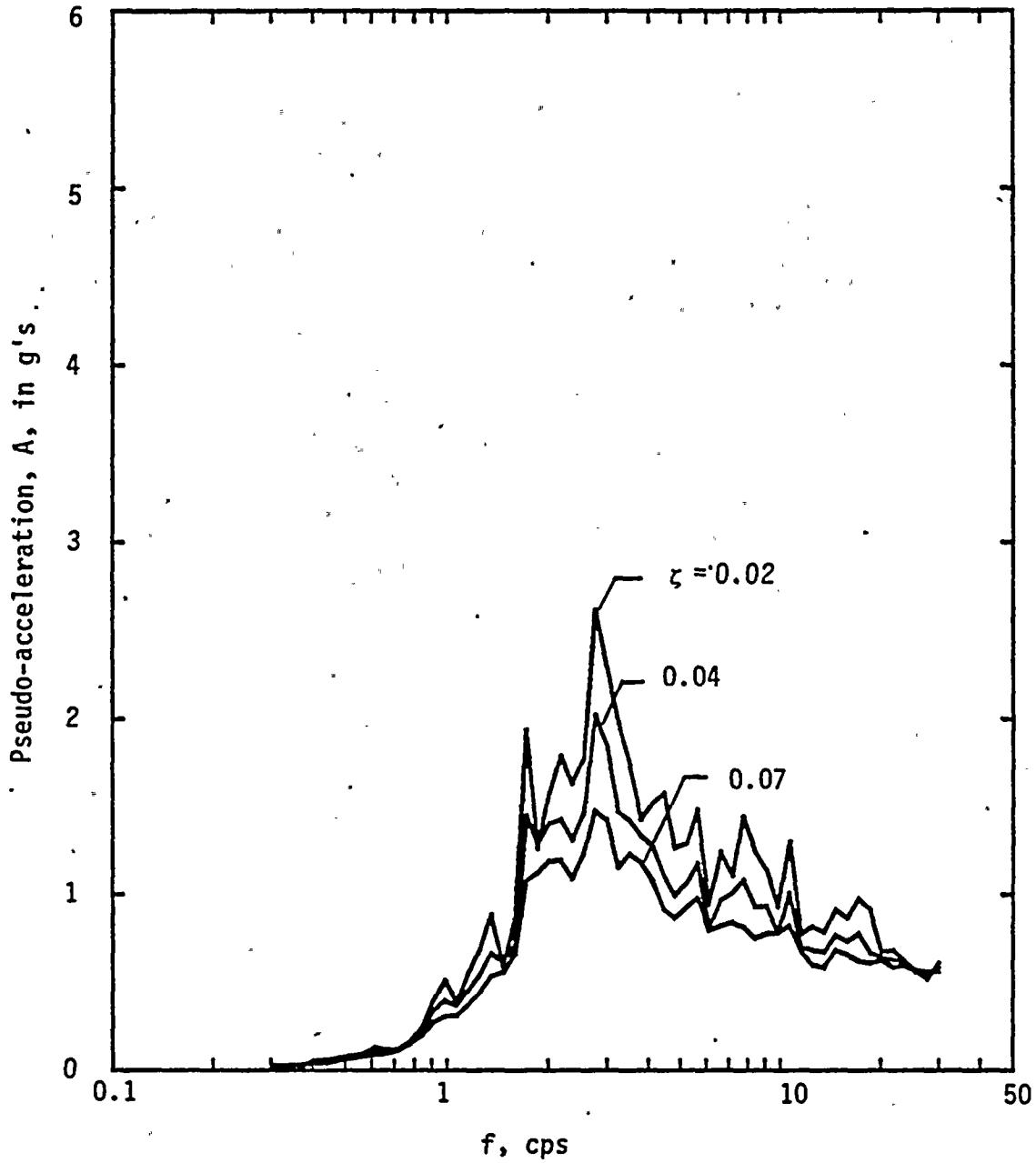

FIG. B.33 Pseudo-acceleration Response Spectra for Systems Subjected to Numerically Generated Ground Motion Record No. 33

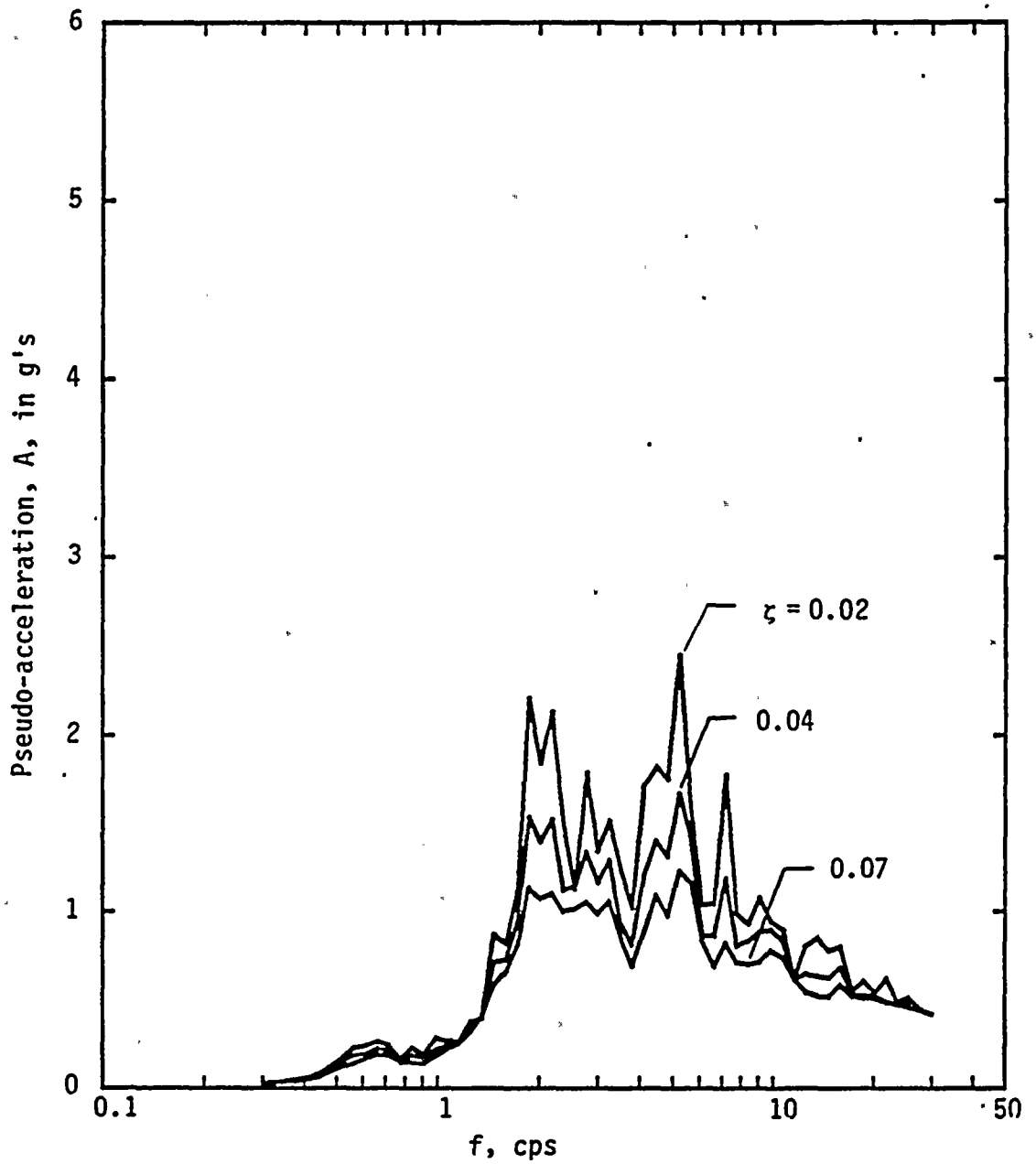

FIG. B.34 Pseudo-acceleration Response Spectra for Systems Subjected to Numerically Generated Ground Motion Record No. 34

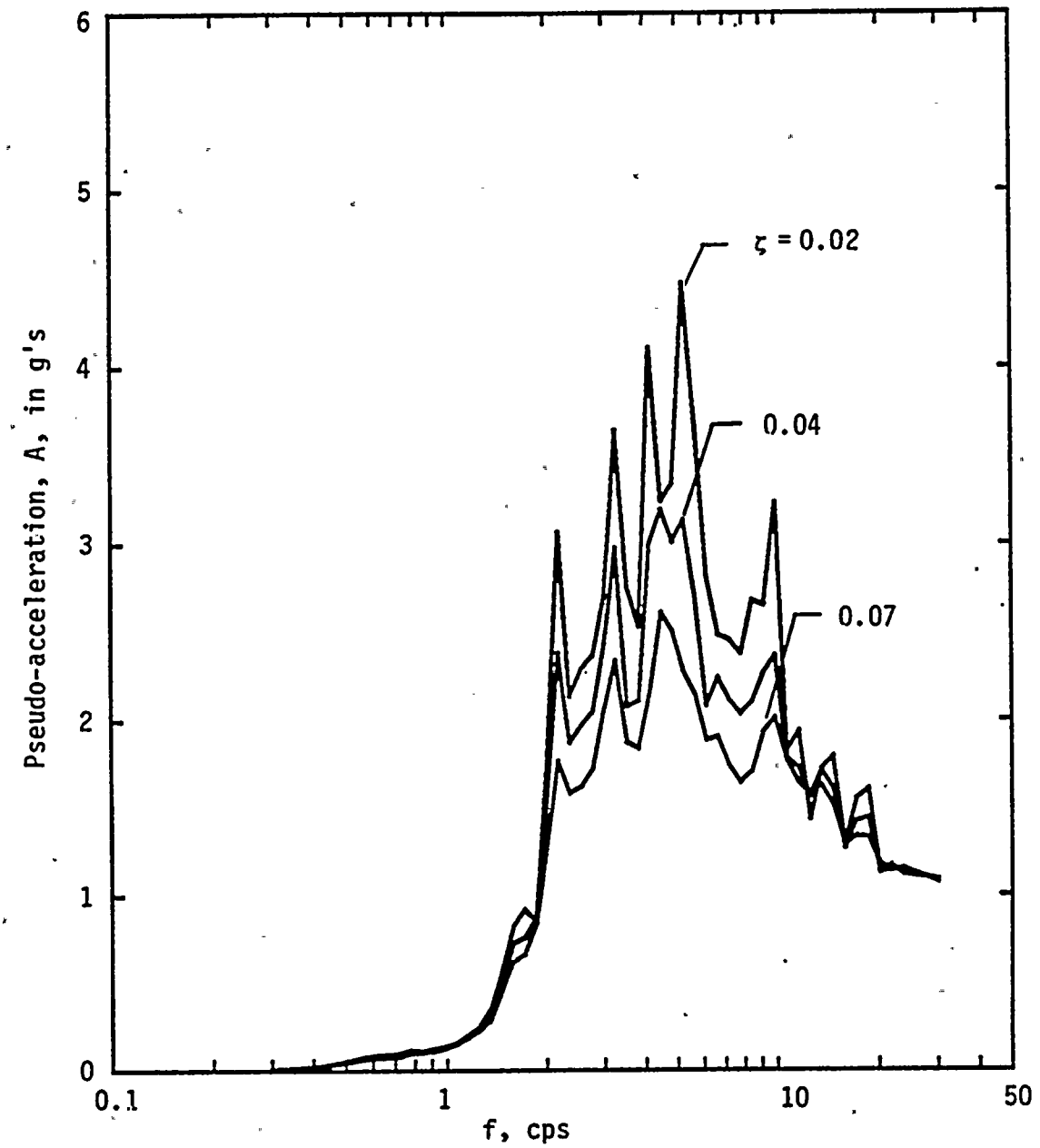

FIG. B.35 Pseudo-acceleration Response Spectra for Systems Subjected to Numerically Generated Ground Motion Record No. 35

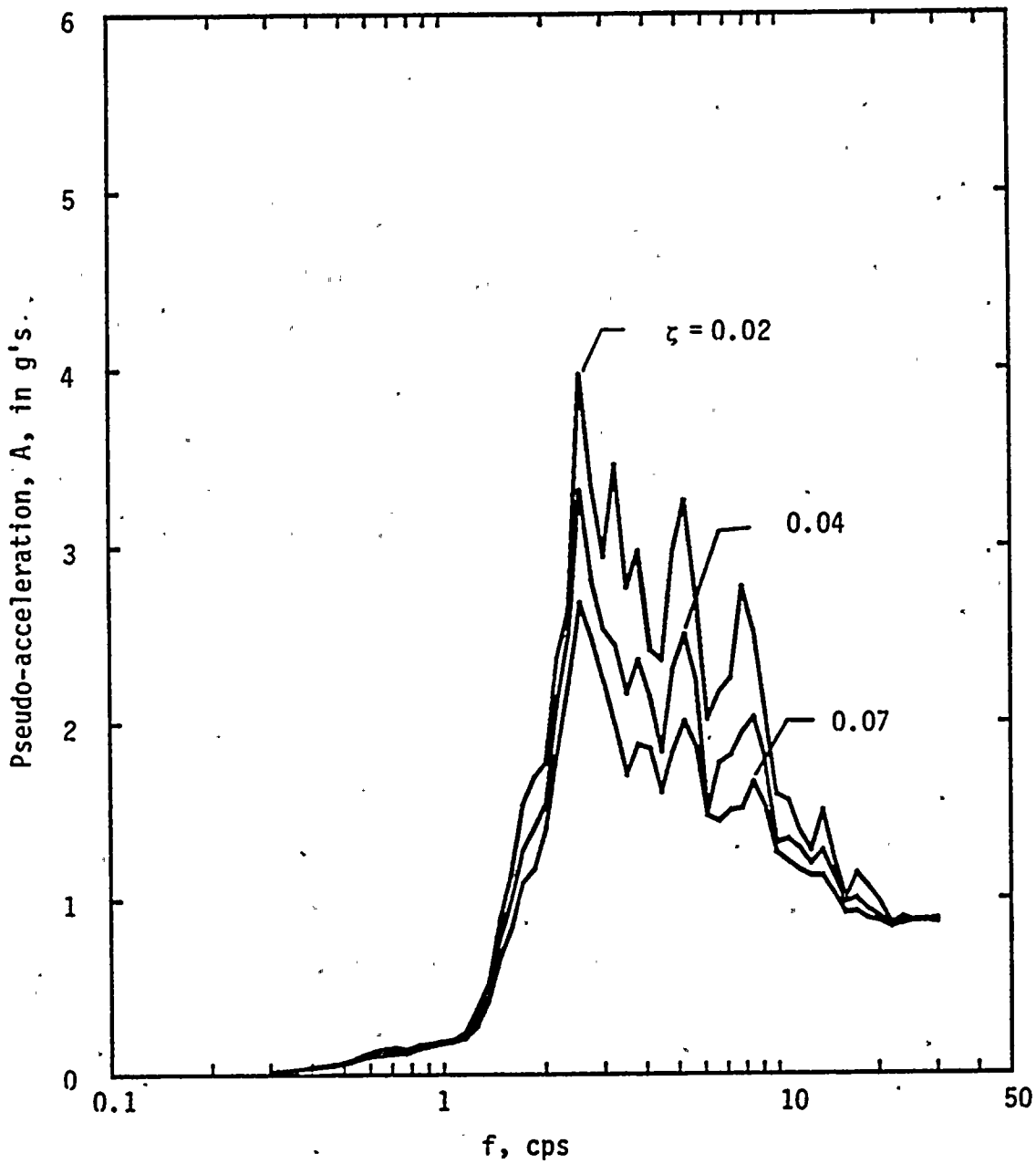

FIG. B.36 Pseudo-acceleration Response Spectra for Systems Subjected to Numerically Generated Ground Motion Record No. 36

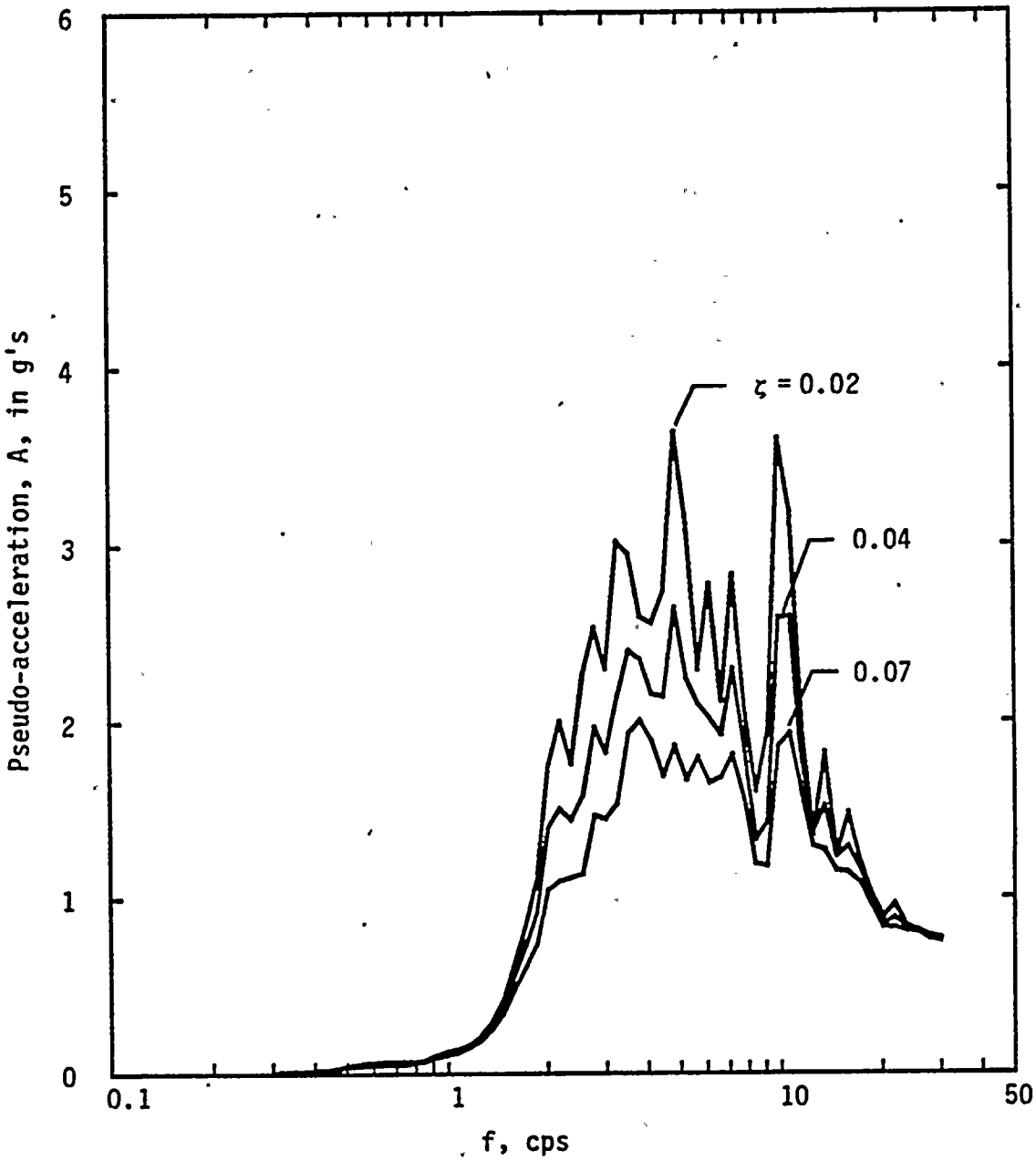

FIG. B.37 Pseudo-acceleration Response Spectra for Systems Subjected to Numerically Generated Ground Motion Record No. 37

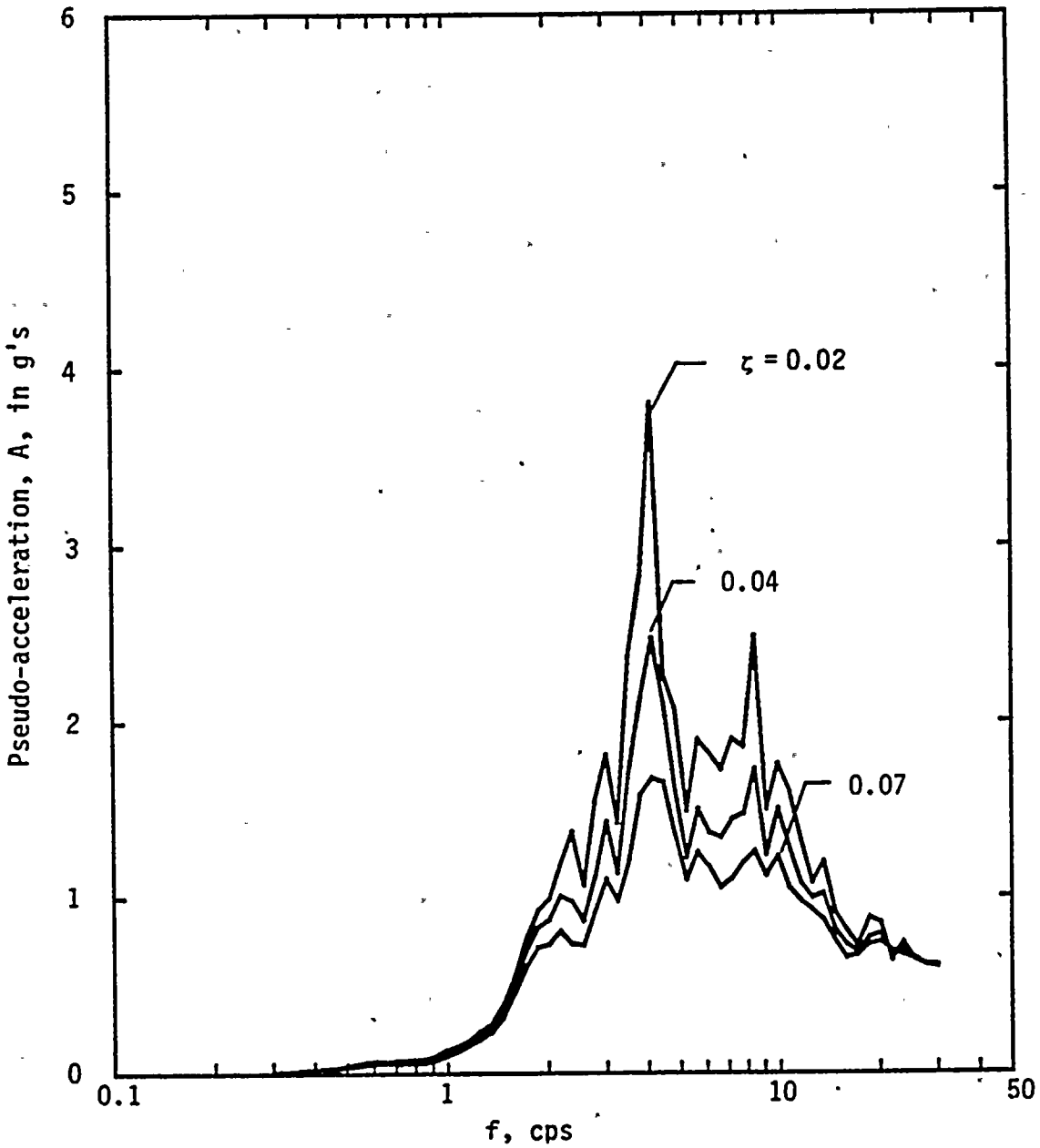

FIG. B.38 Pseudo-acceleration Response Spectra for Systems Subjected to Numerically Generated Ground Motion Record No. 38

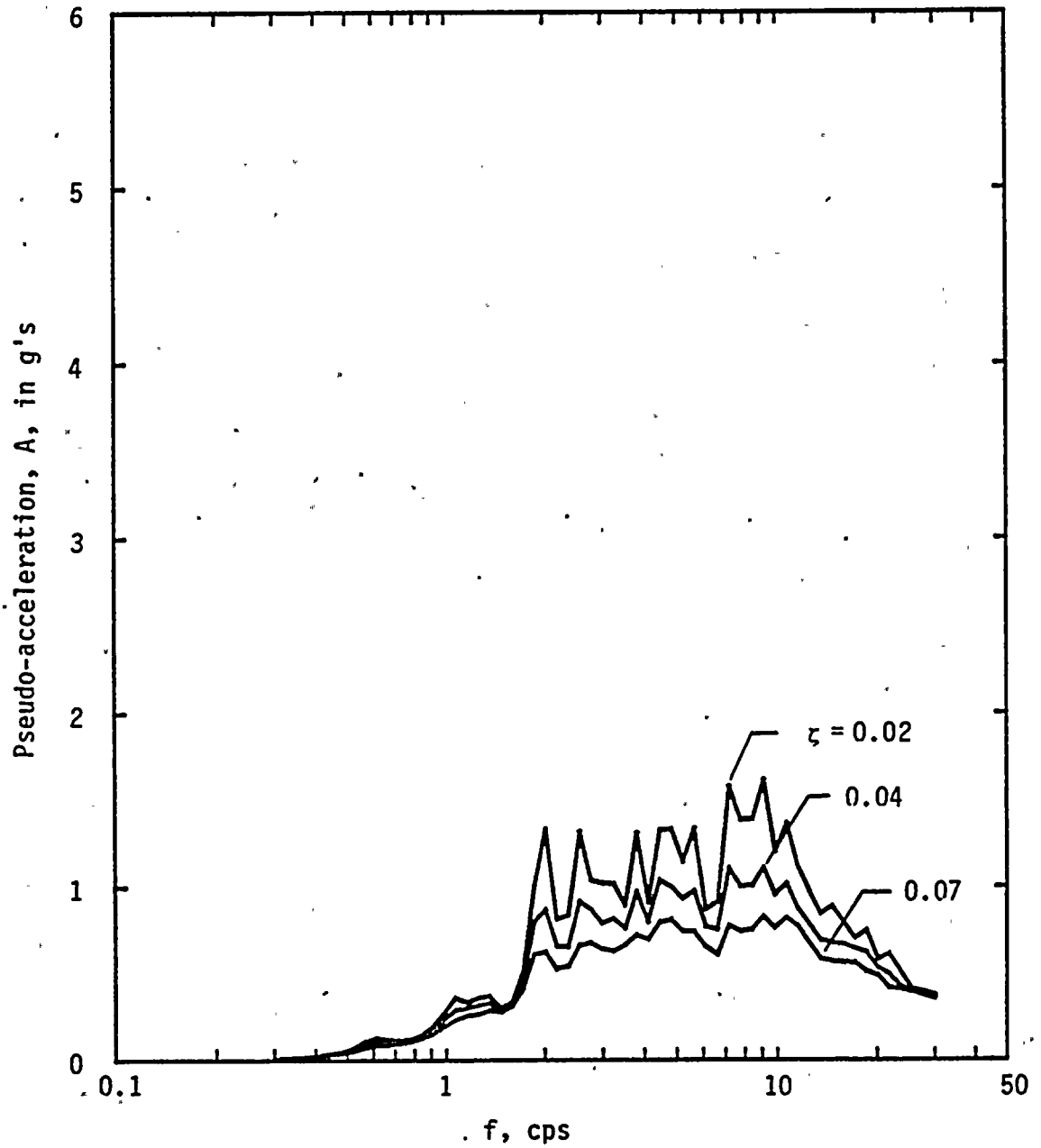

FIG. B.39 Pseudo-acceleration Response Spectra for Systems Subjected to Numerically Generated Ground Motion Record No. 39

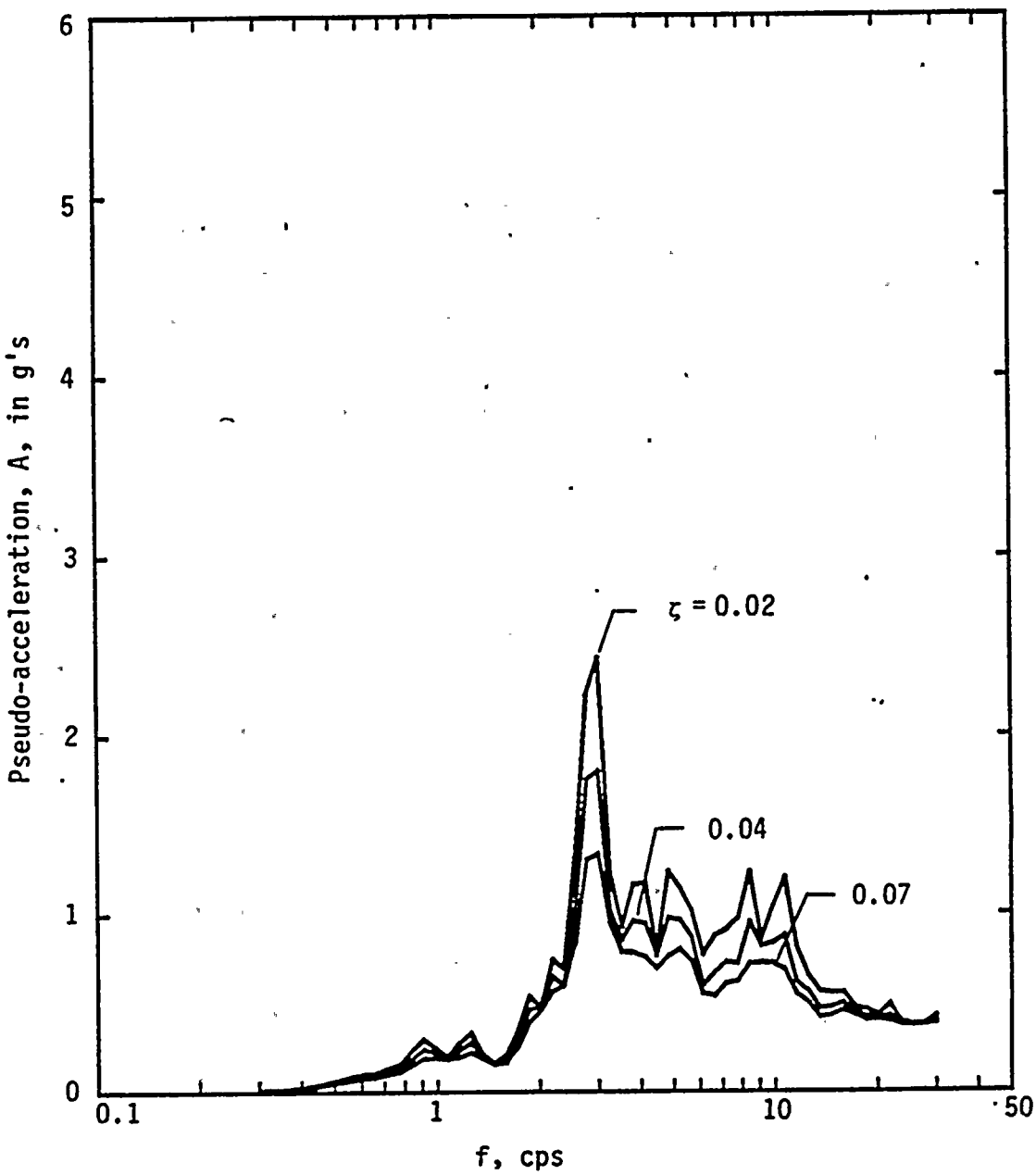

FIG. B.40 Pseudo-acceleration Response Spectra for Systems Subjected to Numerically Generated Ground Motion Record No. 40

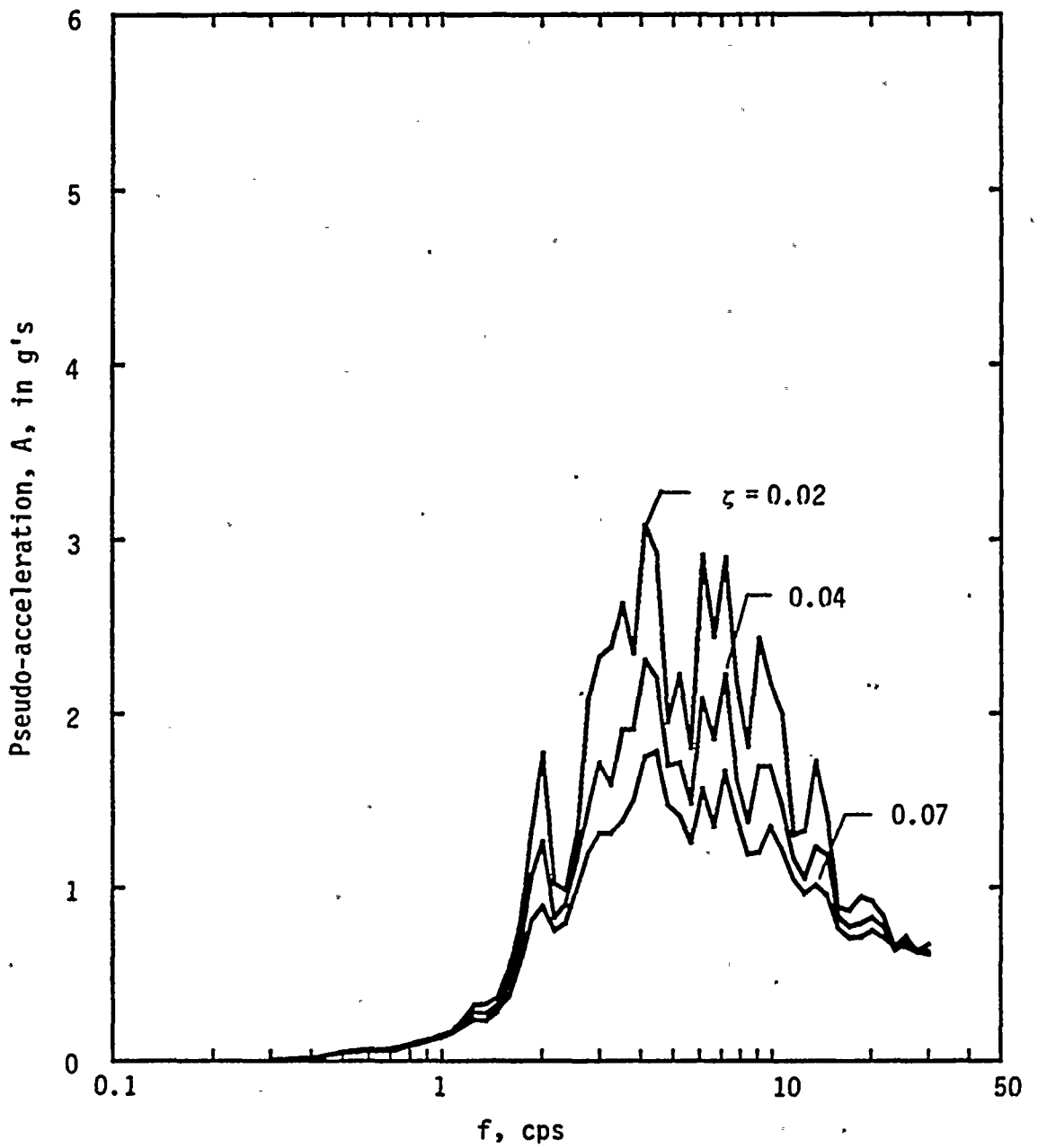

FIG. B.41 Pseudo-acceleration Response Spectra for Systems Subjected to Numerically Generated Ground Motion Record No. 41

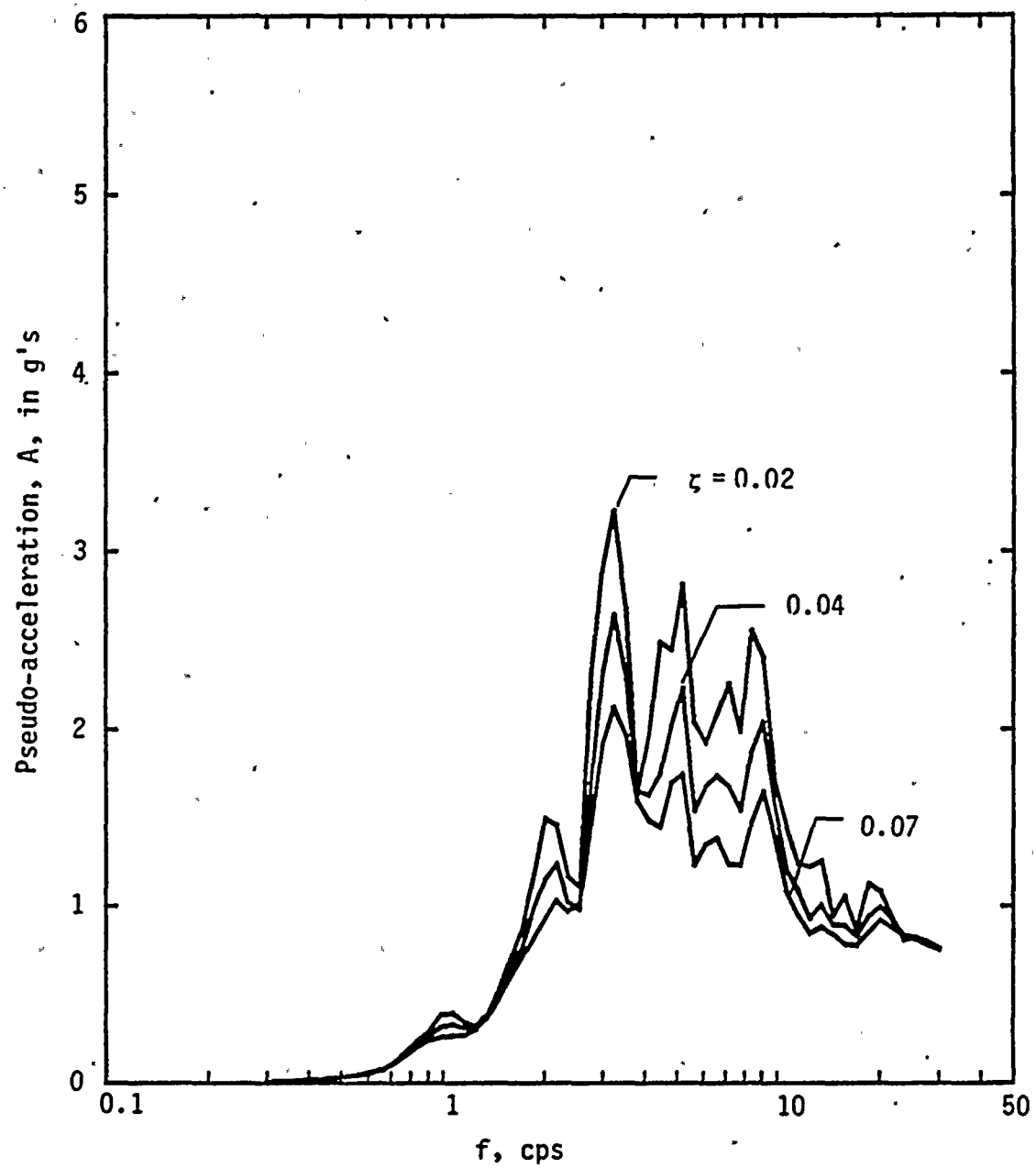

FIG. B.42 Pseudo-acceleration Response Spectra for Systems Subjected to Numerically Generated Ground Motion Record No. 42

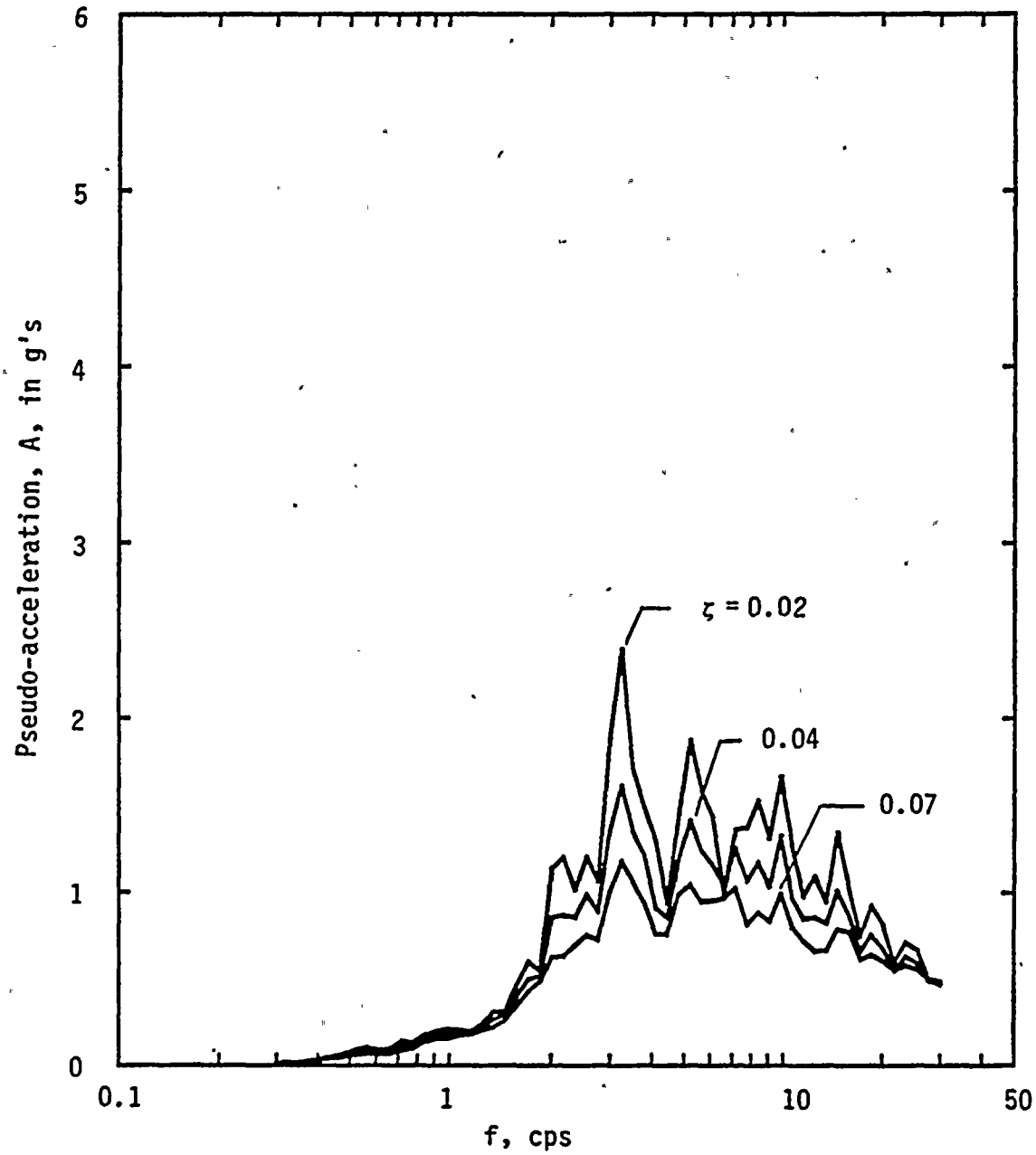

FIG. B.43 Pseudo-acceleration Response Spectra for Systems Subjected to Numerically Generated Ground Motion Record No. 43

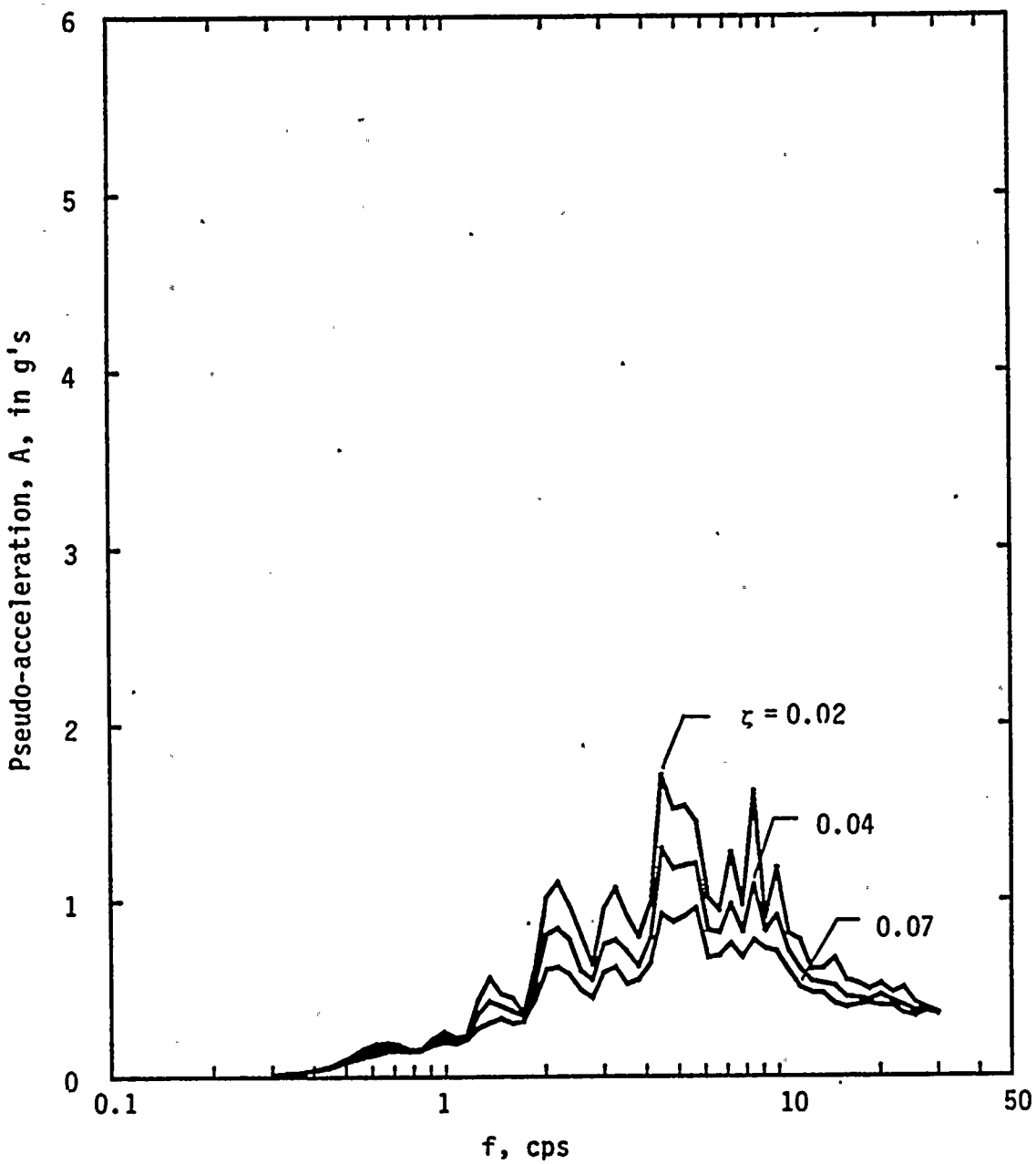

FIG. B.44 Pseudo-acceleration Response Spectra for Systems Subjected to Numerically Generated Ground Motion Record No. 44

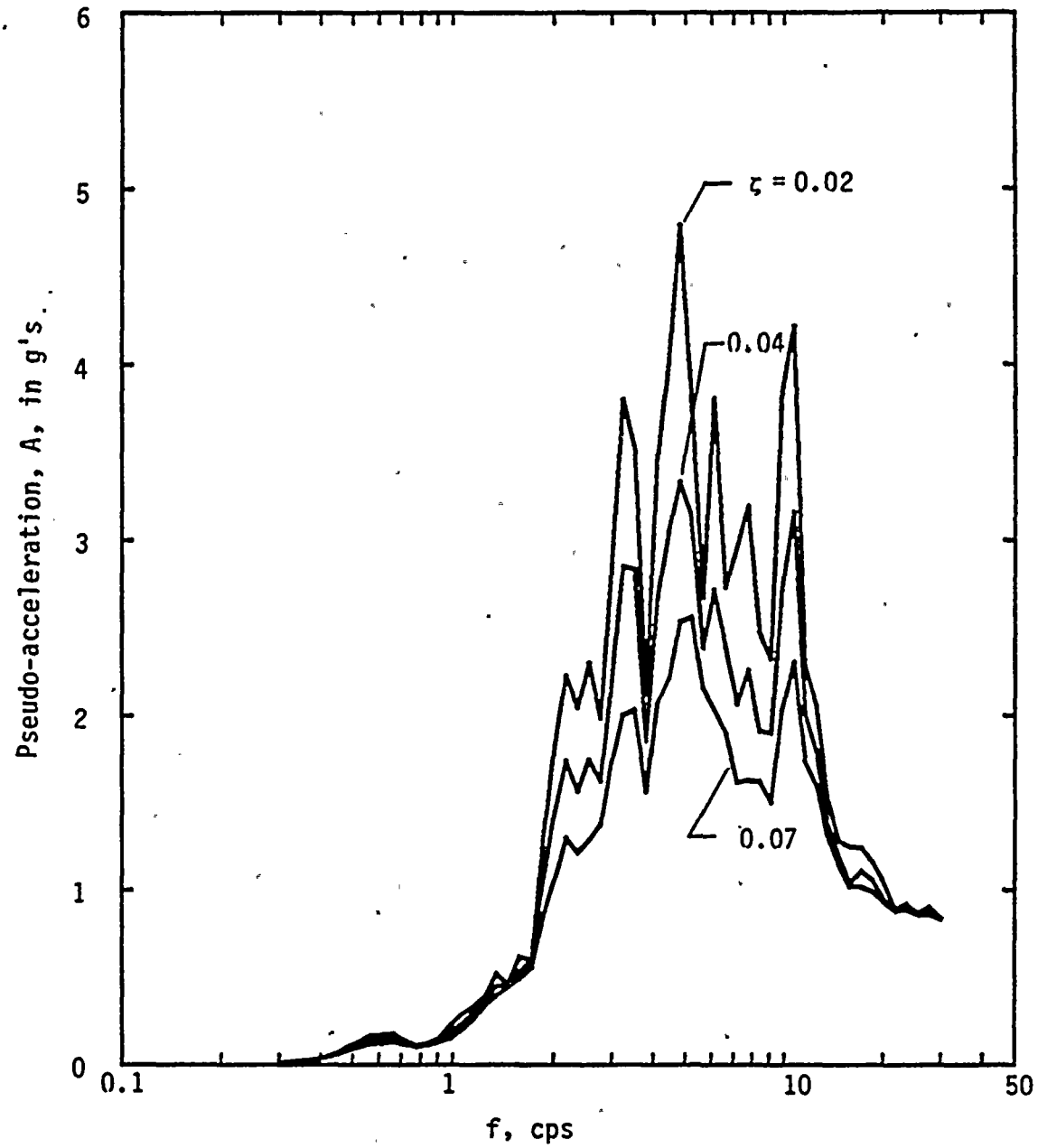

FIG. B.45 Pseudo-acceleration Response Spectra for Systems Subjected to Numerically Generated Ground Motion Record No. 45

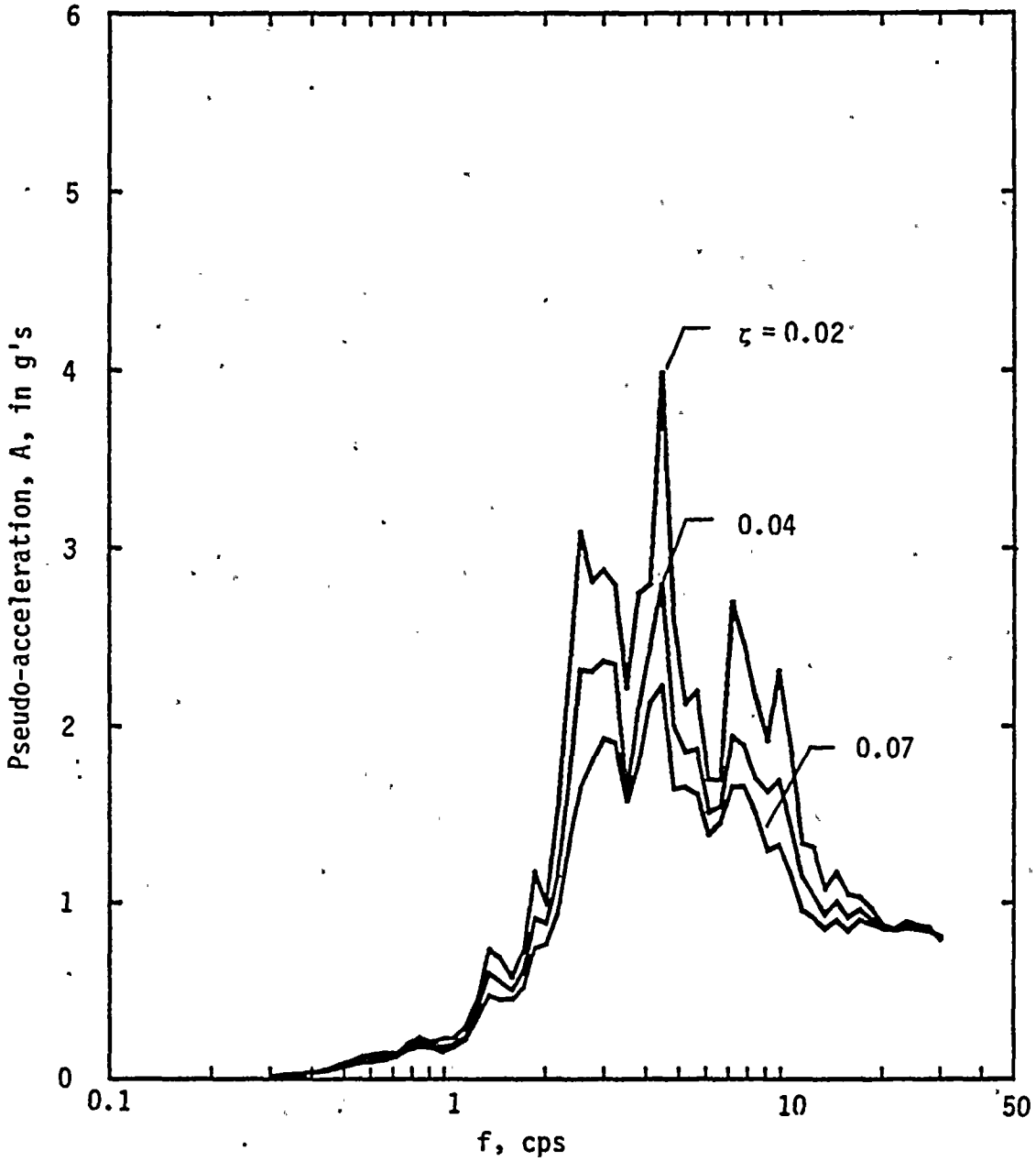

FIG. B.46 Pseudo-acceleration Response Spectra for Systems Subjected to Numerically Generated Ground Motion Record No. 46

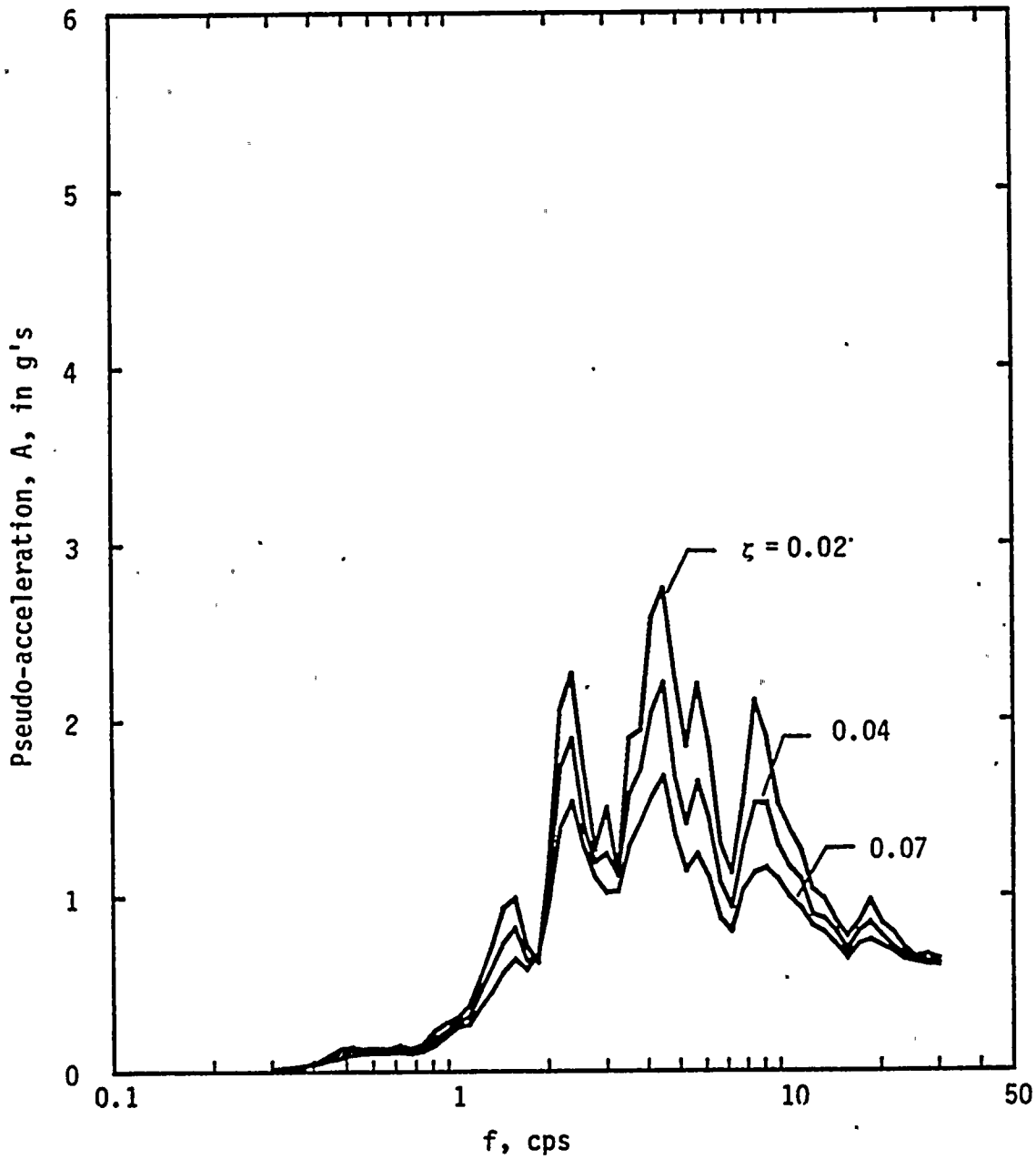

FIG. B.47 Pseudo-acceleration Response Spectra for Systems Subjected to Numerically Generated Ground Motion Record No. 47

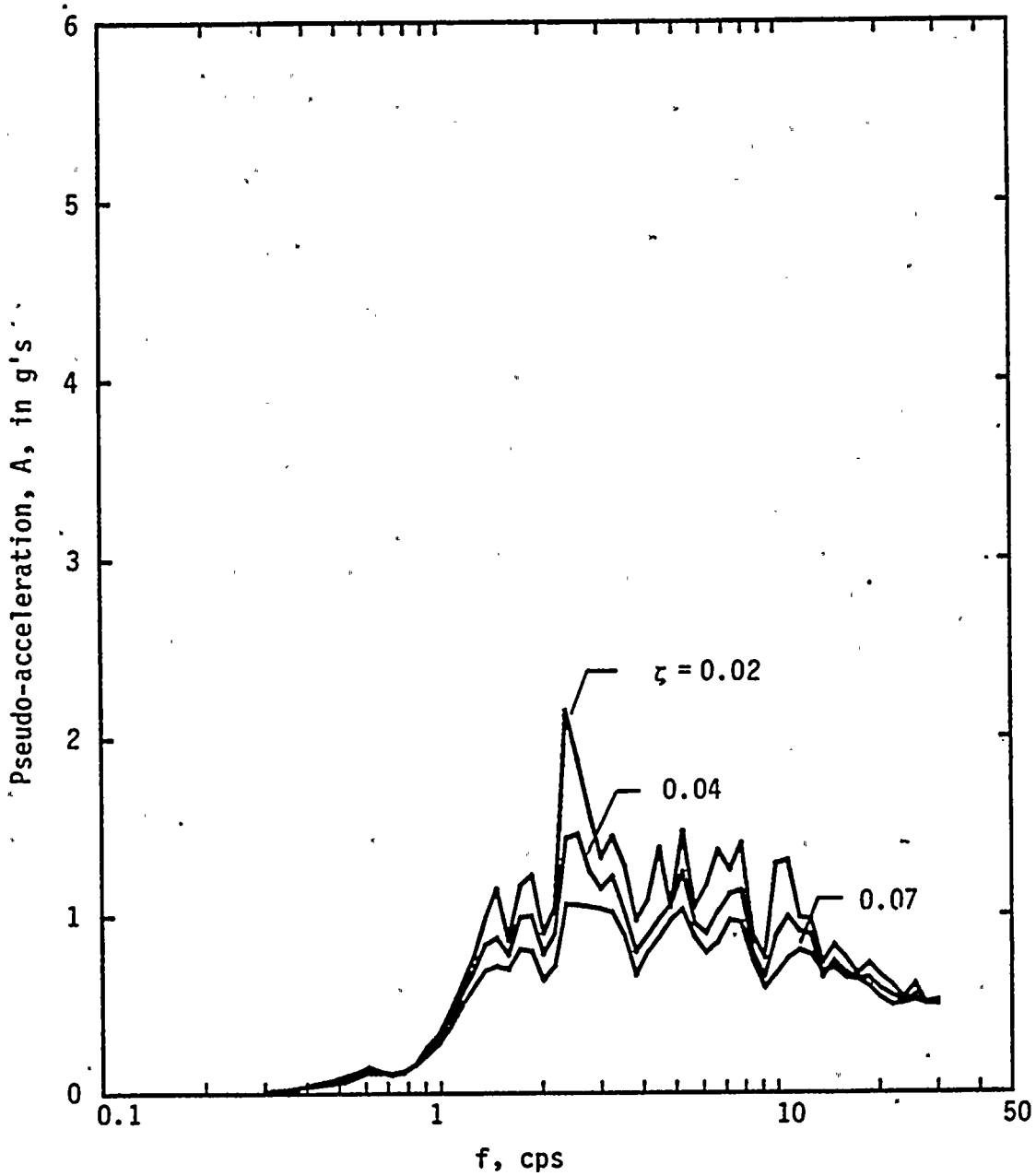

FIG. B.48 Pseudo-acceleration Response Spectra for Systems Subjected to Numerically Generated Ground Motion Record No. 48

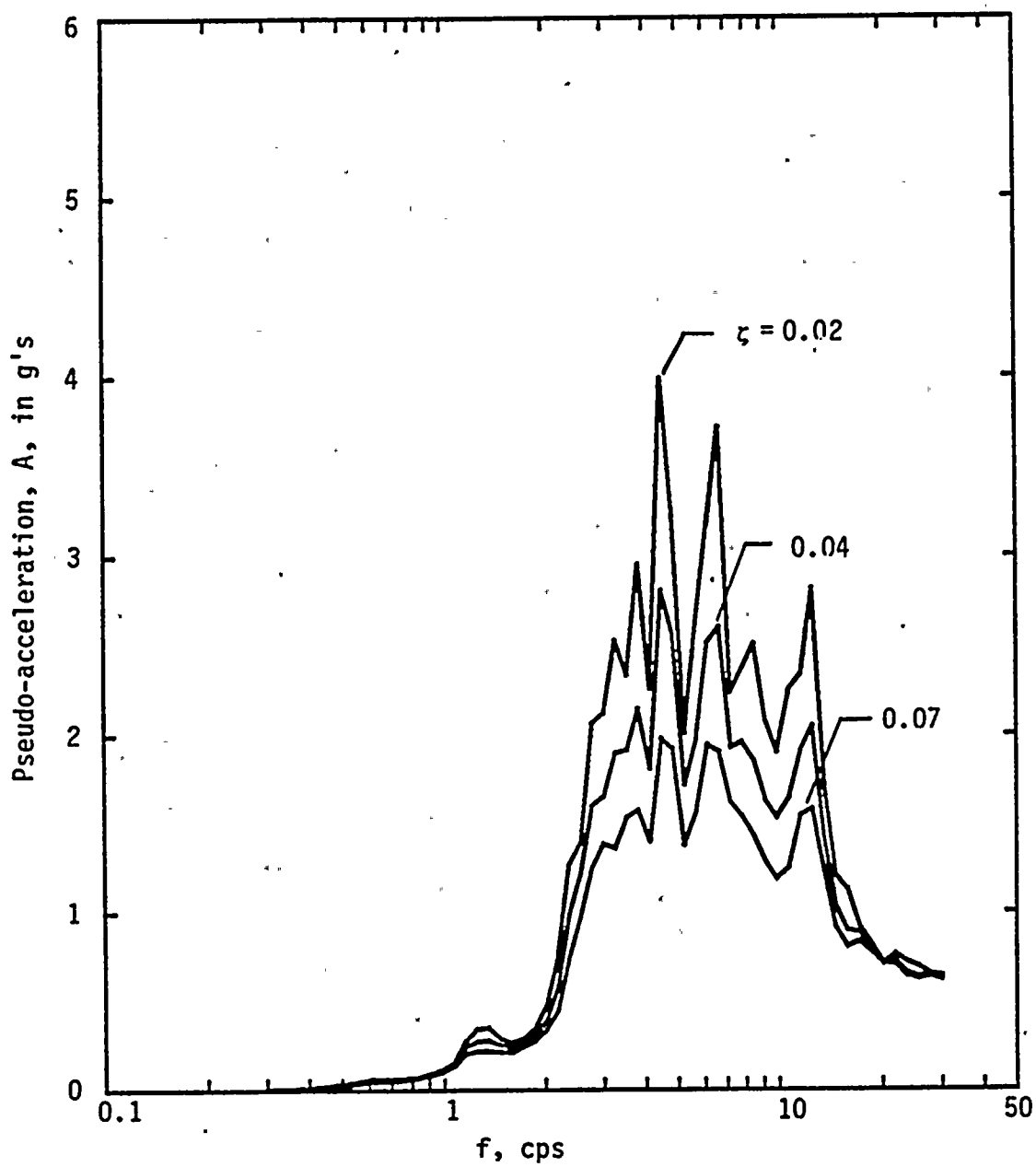

FIG. B.49 Pseudo-acceleration Response Spectra for Systems Subjected to Numerically Generated Ground Motion Record No. 49

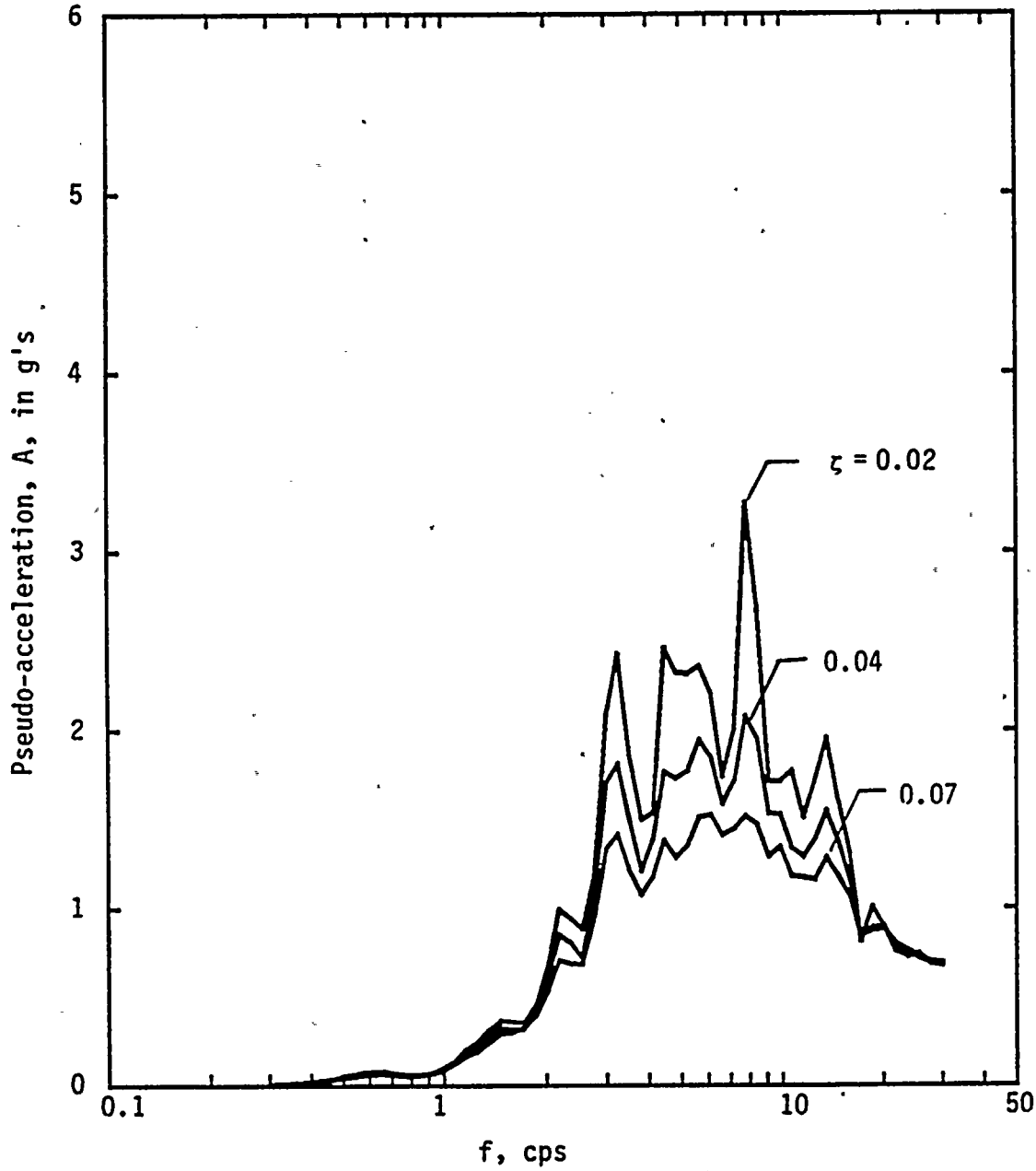

FIG. B.50 Pseudo-acceleration Response Spectra for Systems Subjected to Numerically Generated Ground Motion Record No. 50

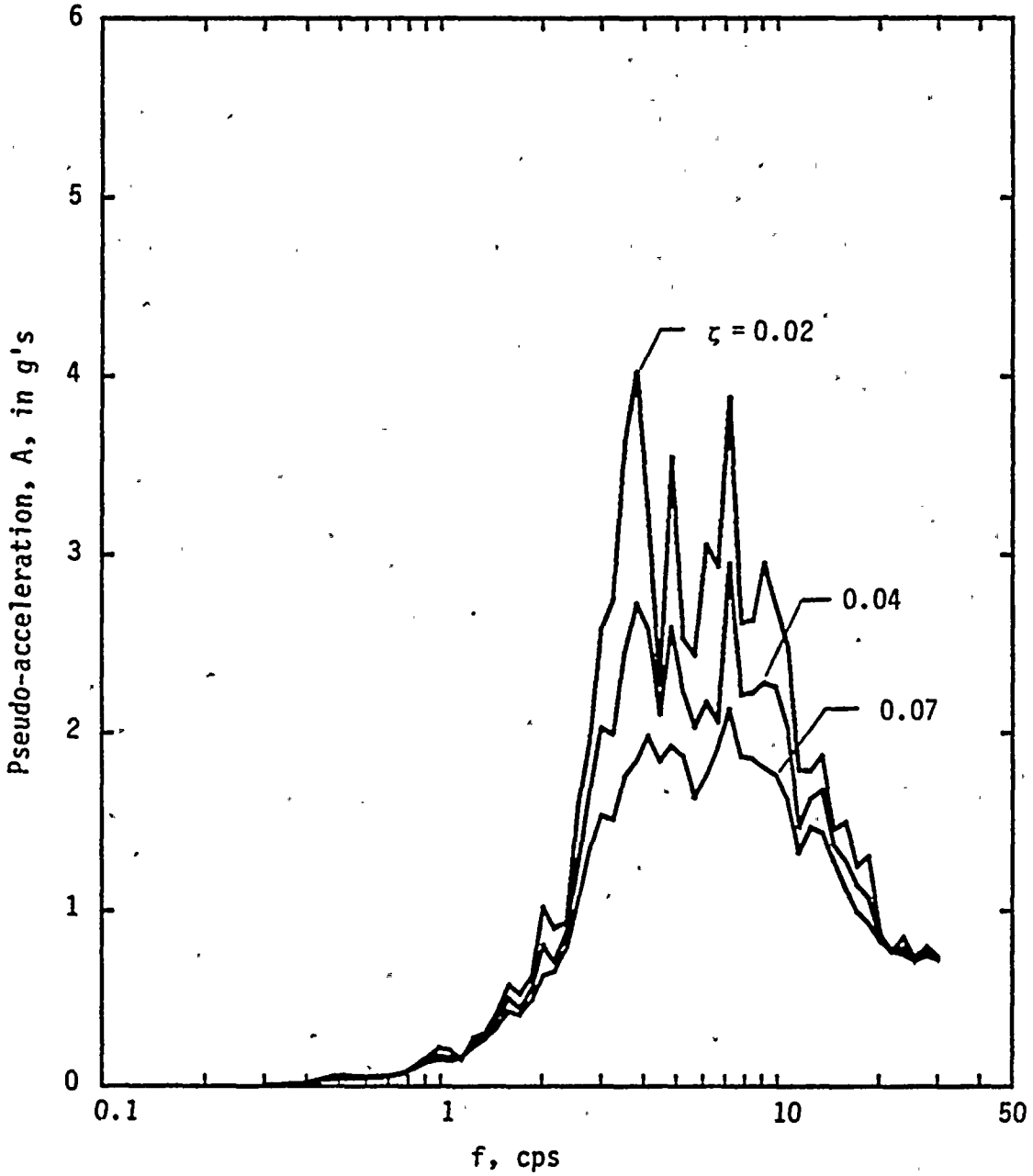

FIG. B.51 Pseudo-acceleration Response Spectra for Systems Subjected to Numerically Generated Ground Motion Record No. 51

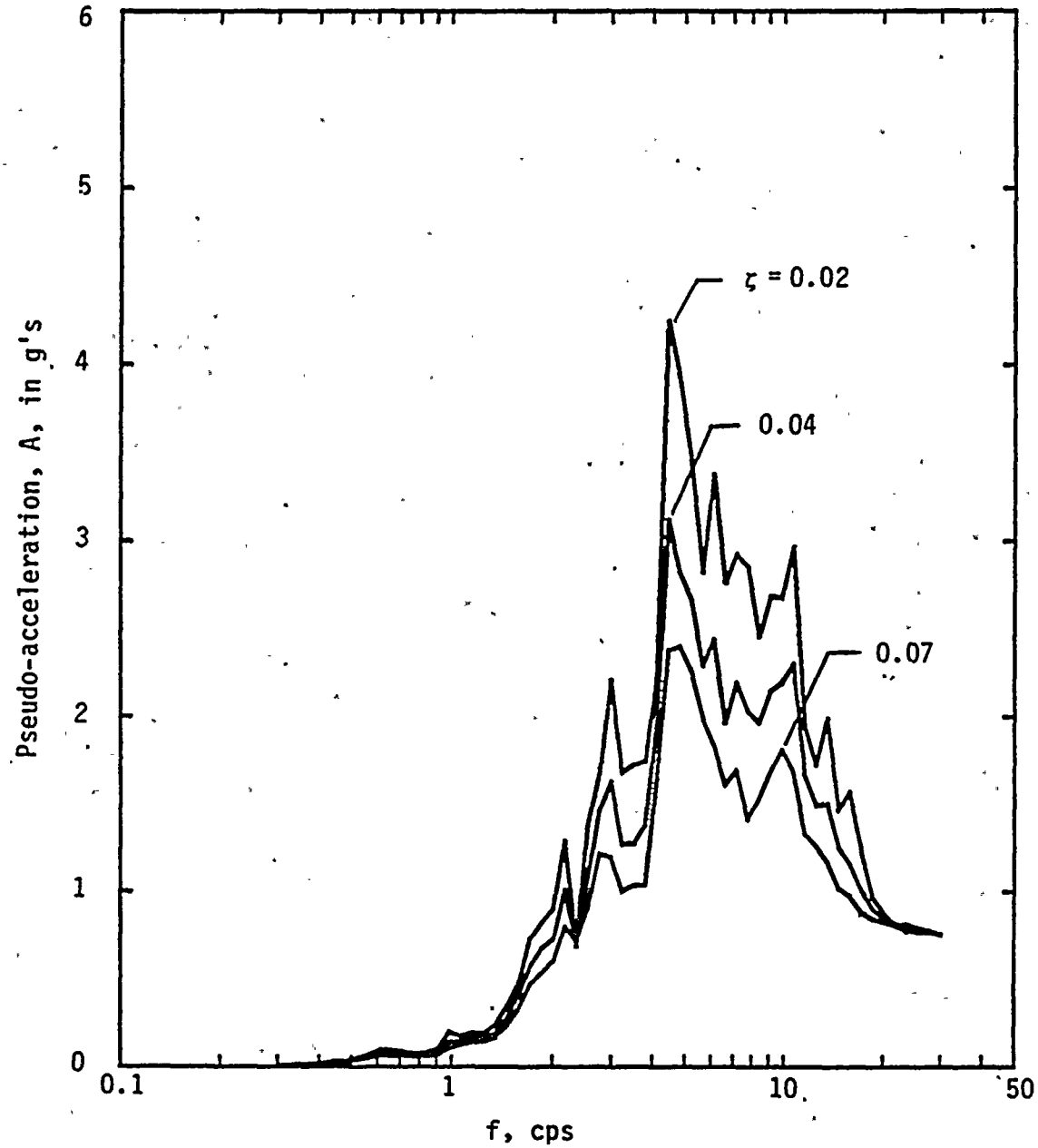

FIG. B.52 Pseudo-acceleration Response Spectra for Systems Subjected to Numerically Generated Ground Motion Record No. 52

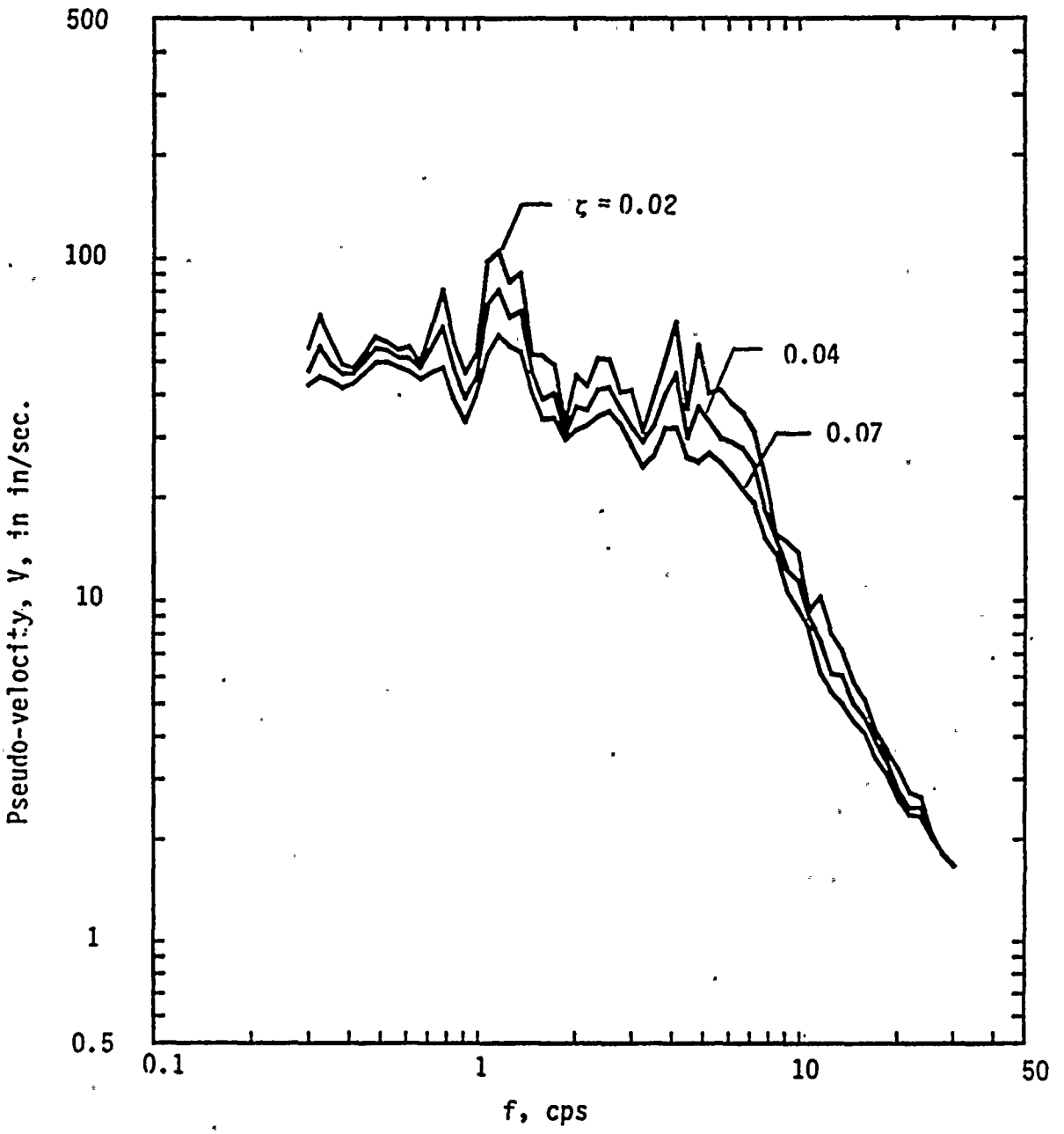

FIG. C.1 Pseudo-velocity Response Spectra for Systems Subjected to Empirical Ground Motion Record No. 1

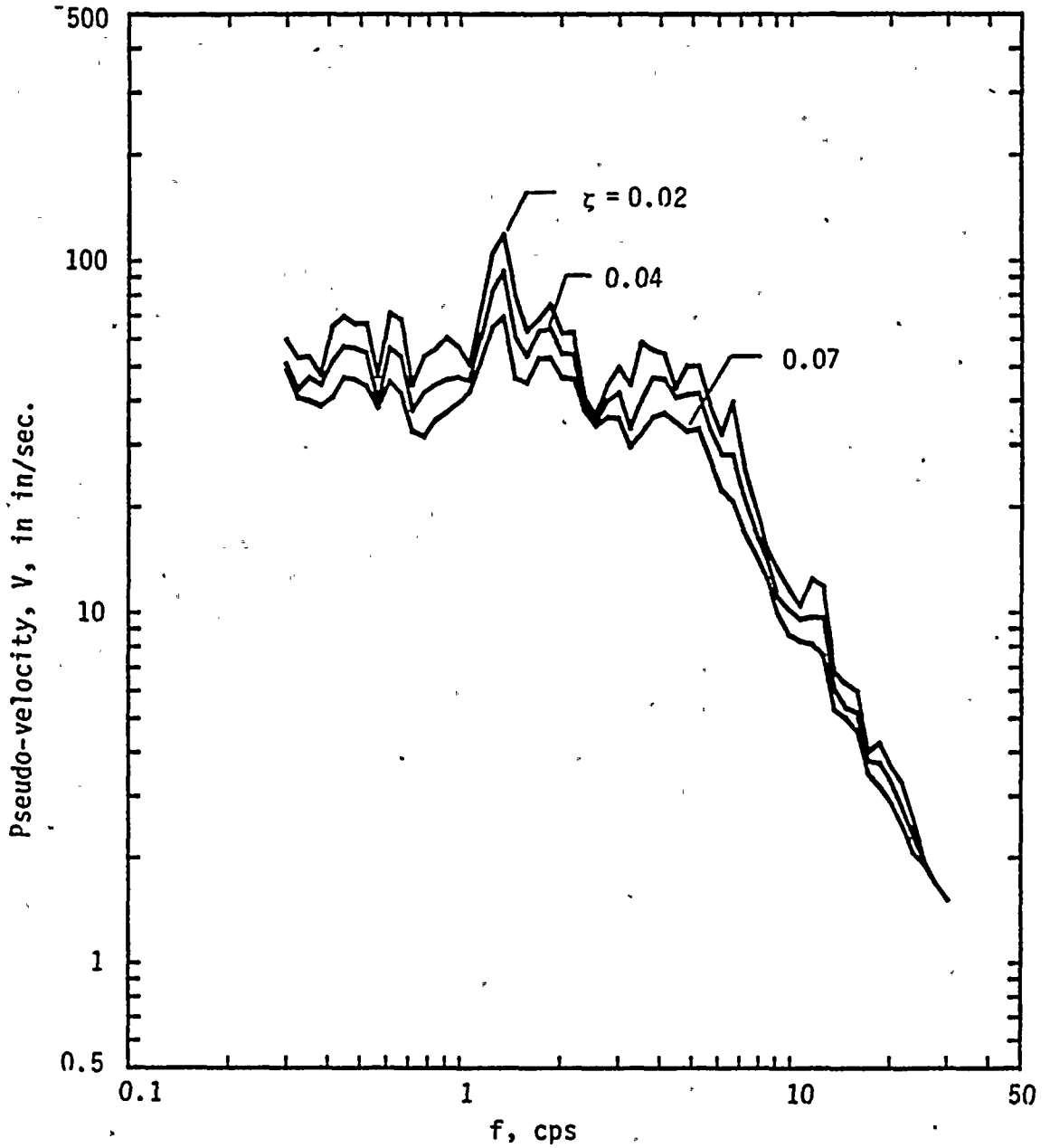

FIG. C.2 Pseudo-velocity Response Spectra for Systems Subjected to Empirical Ground Motion Record No. 2

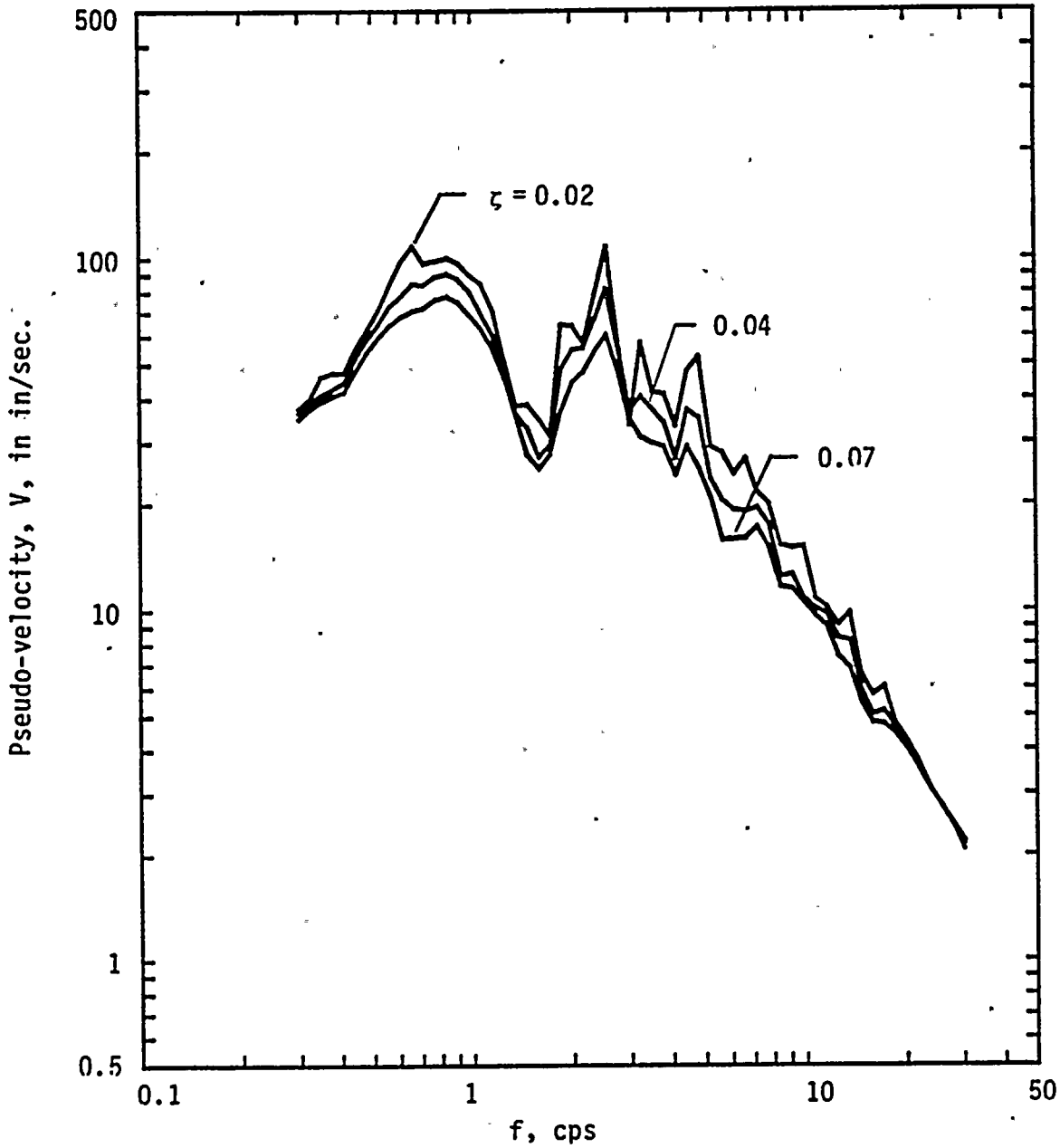

FIG. C.3 Pseudo-velocity Response Spectra for Systems Subjected to Empirical Ground Motion Record No. 3

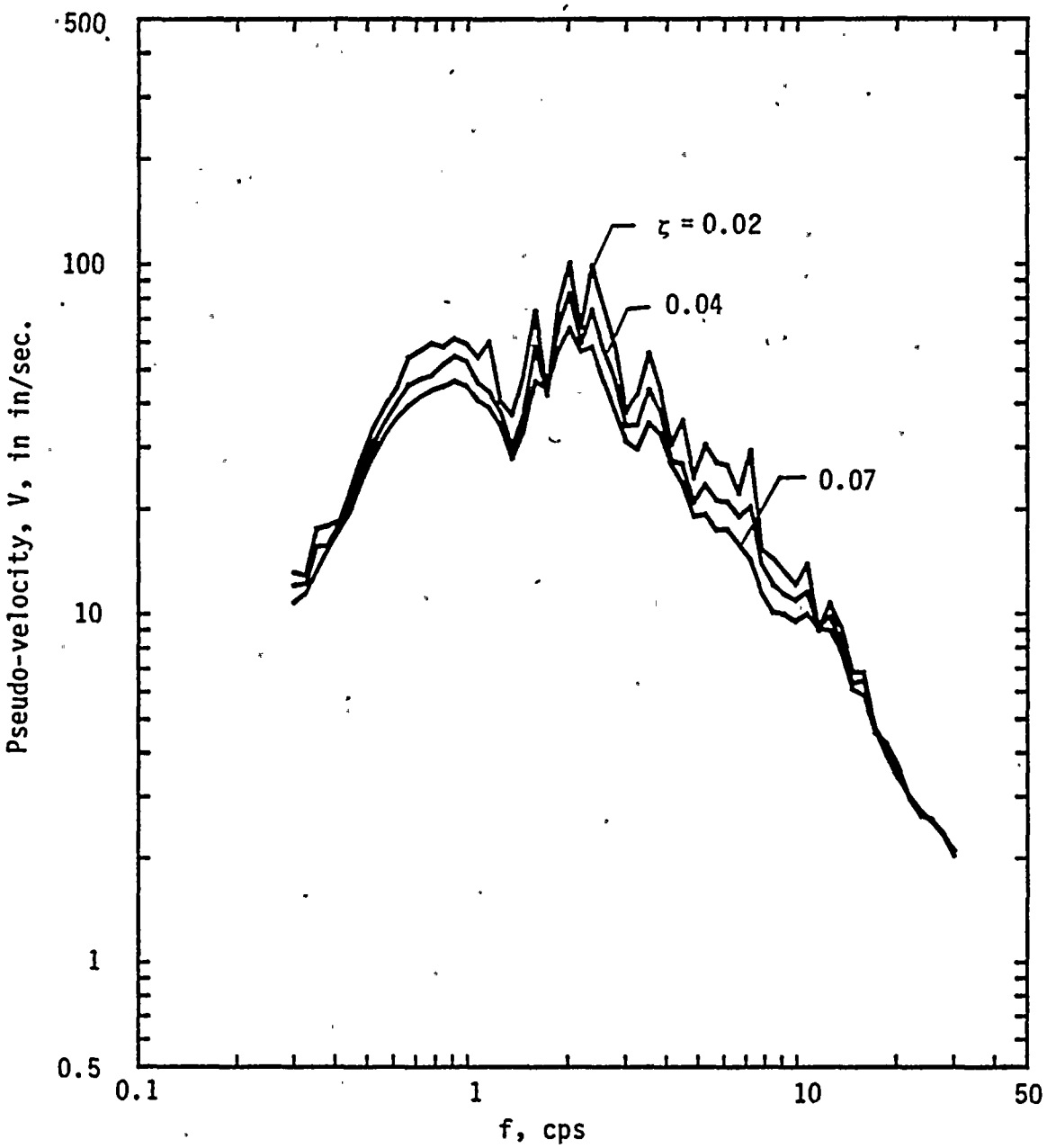

FIG. C.4 Pseudo-velocity Response Spectra for Systems Subjected to Empirical Ground Motion Record No. 4

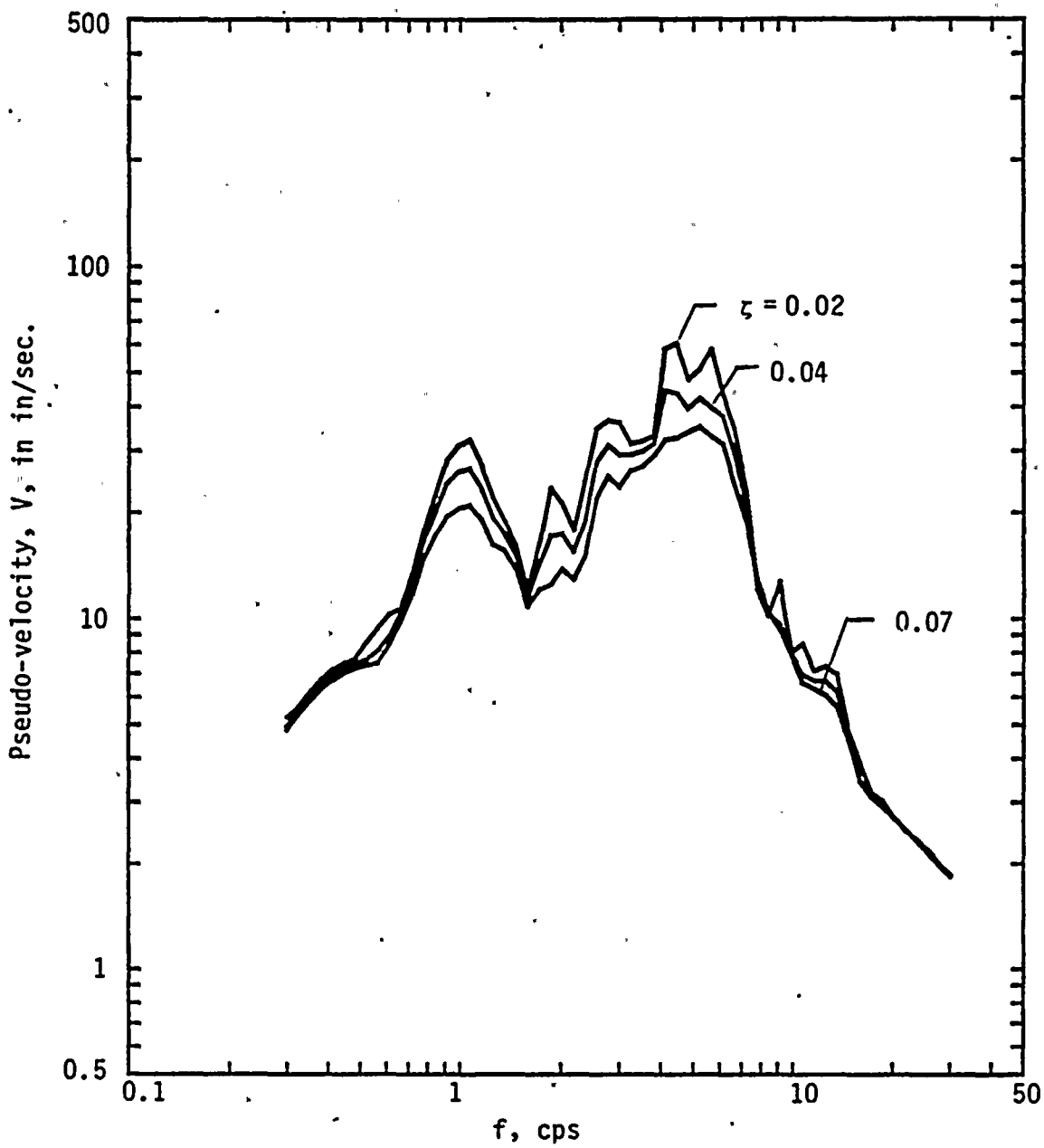

FIG. C.5 Pseudo-velocity Response Spectra for Systems Subjected to Empirical Ground Motion Record No. 5

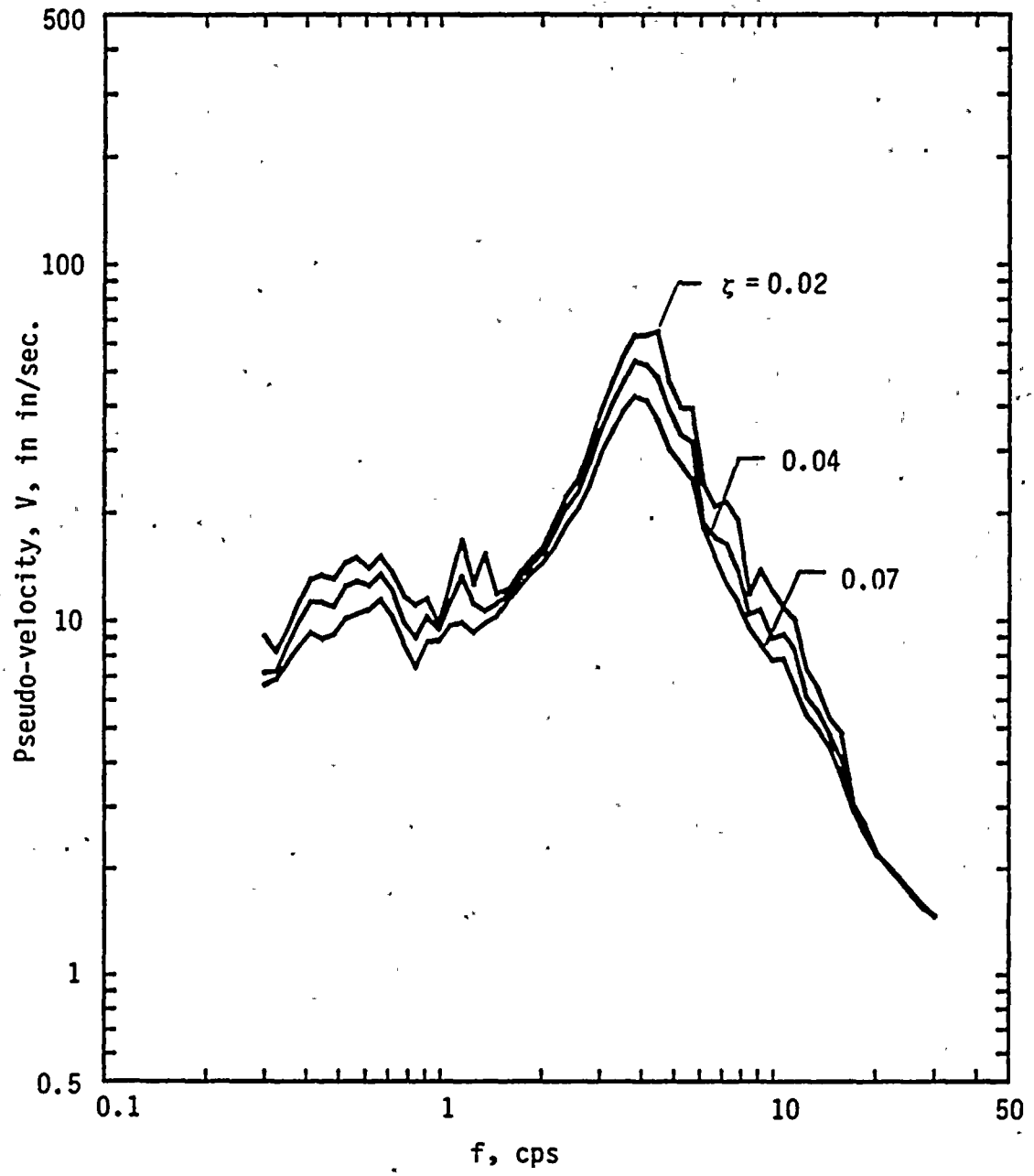

FIG. C.6 Pseudo-velocity Response Spectra for Systems Subjected to Empirical Ground Motion Record No. 6

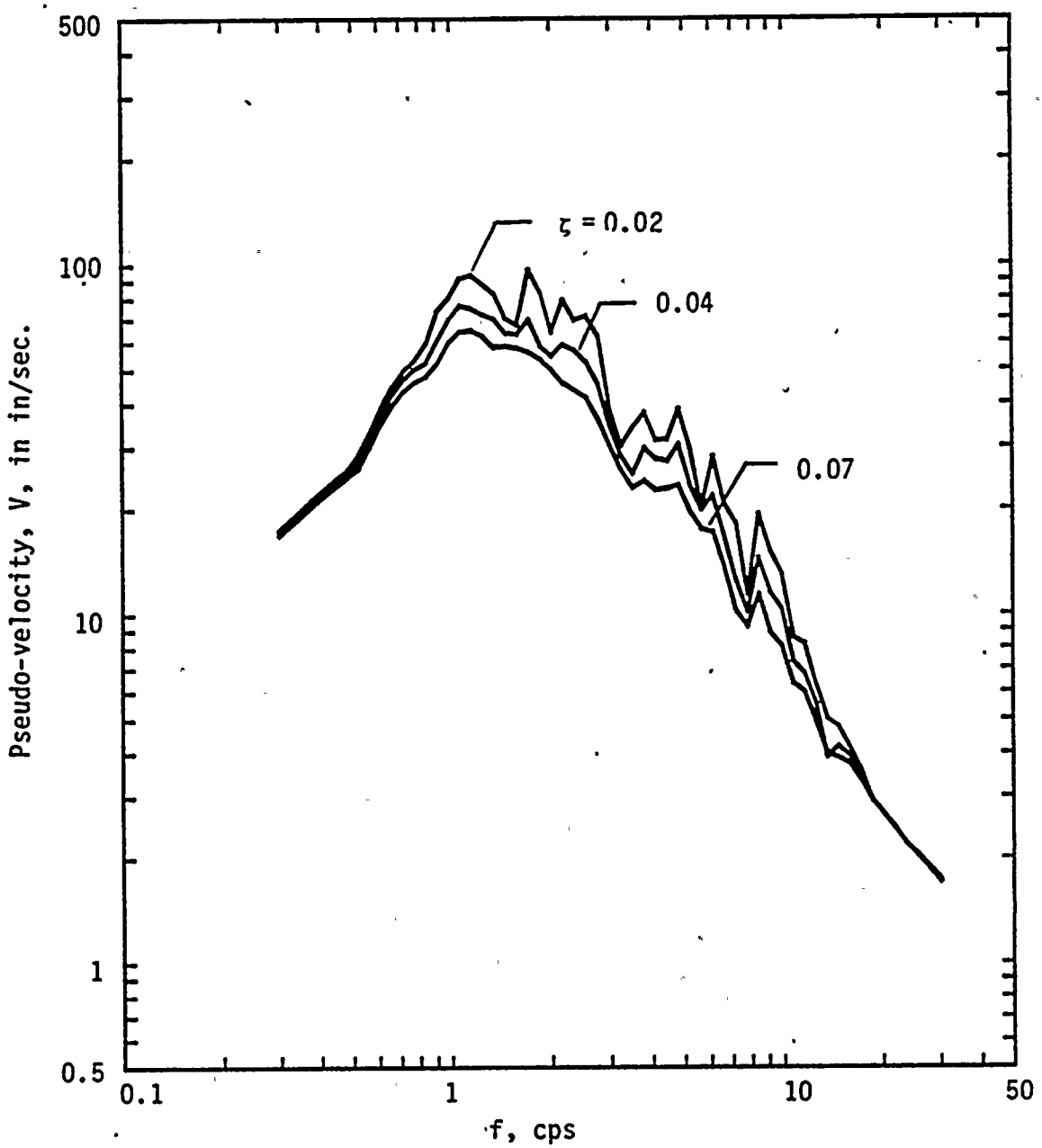

FIG. C.7 Pseudo-velocity Response Spectra for Systems Subjected to Empirical Ground Motion Record No. 7

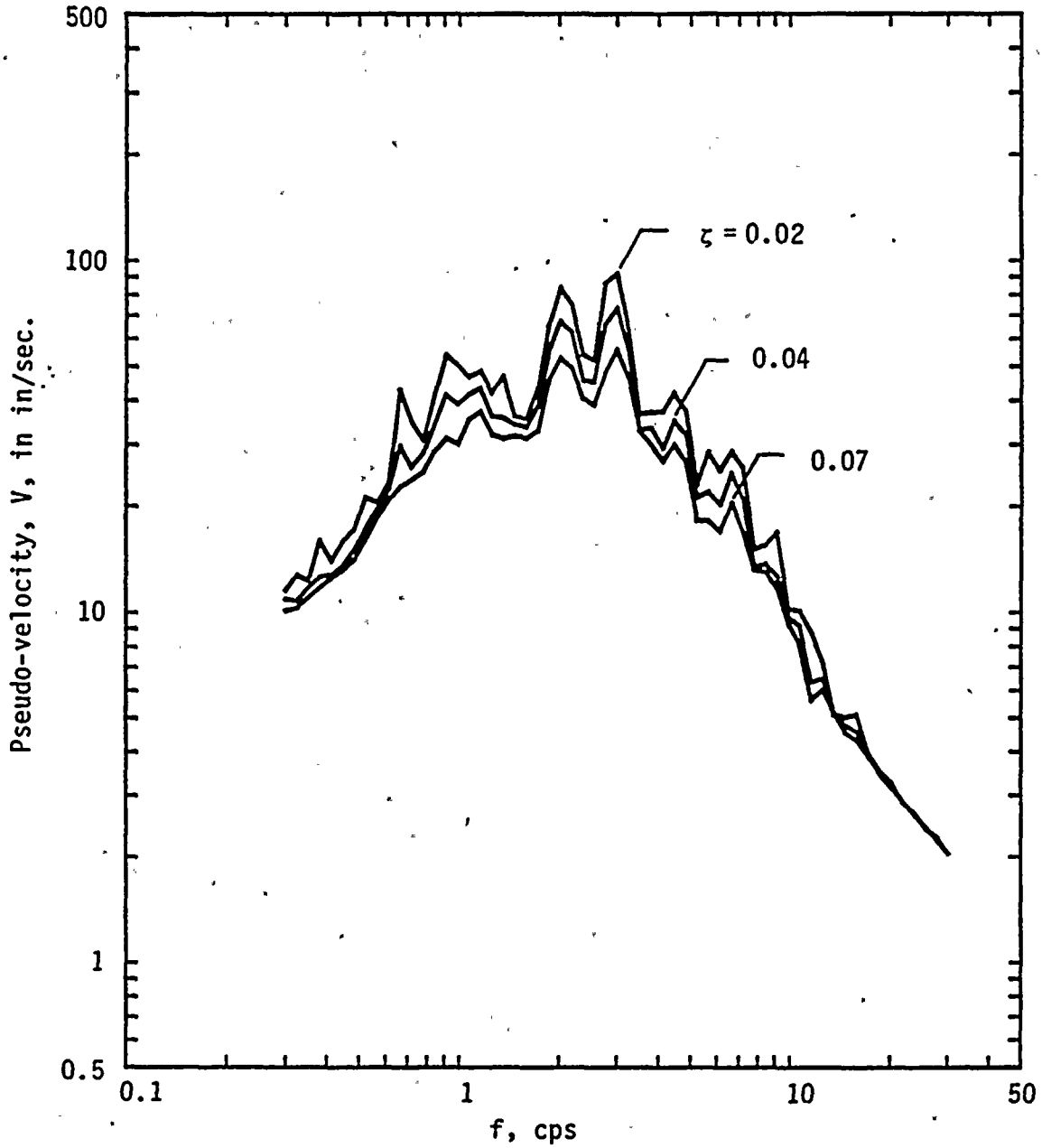

FIG. C.8 Pseudo-velocity Response Spectra for Systems Subjected to Empirical Ground Motion Record No. 8

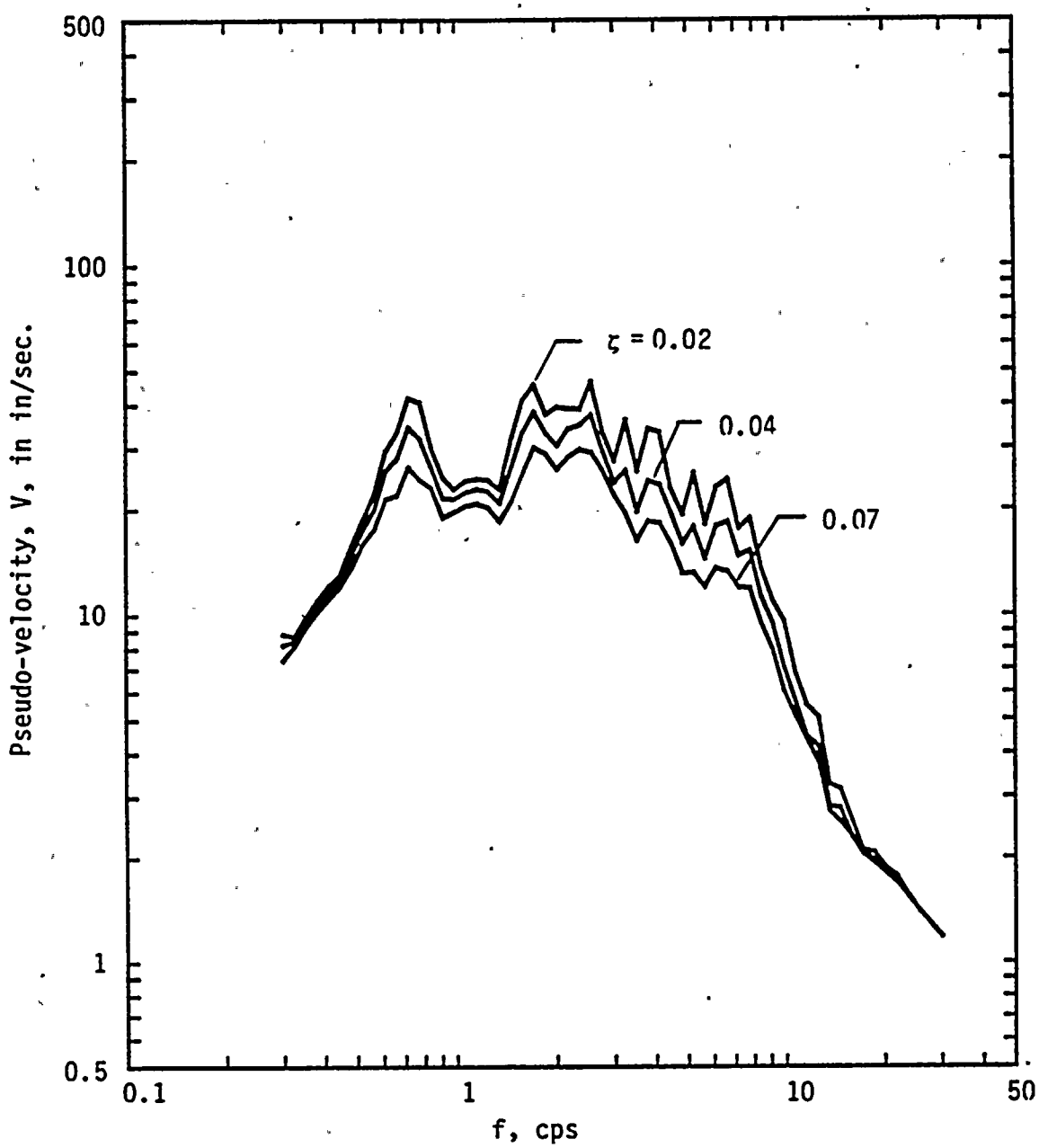

FIG. C.9 Pseudo-velocity Response Spectra for Systems Subjected to Empirical Ground Motion Record No. 9

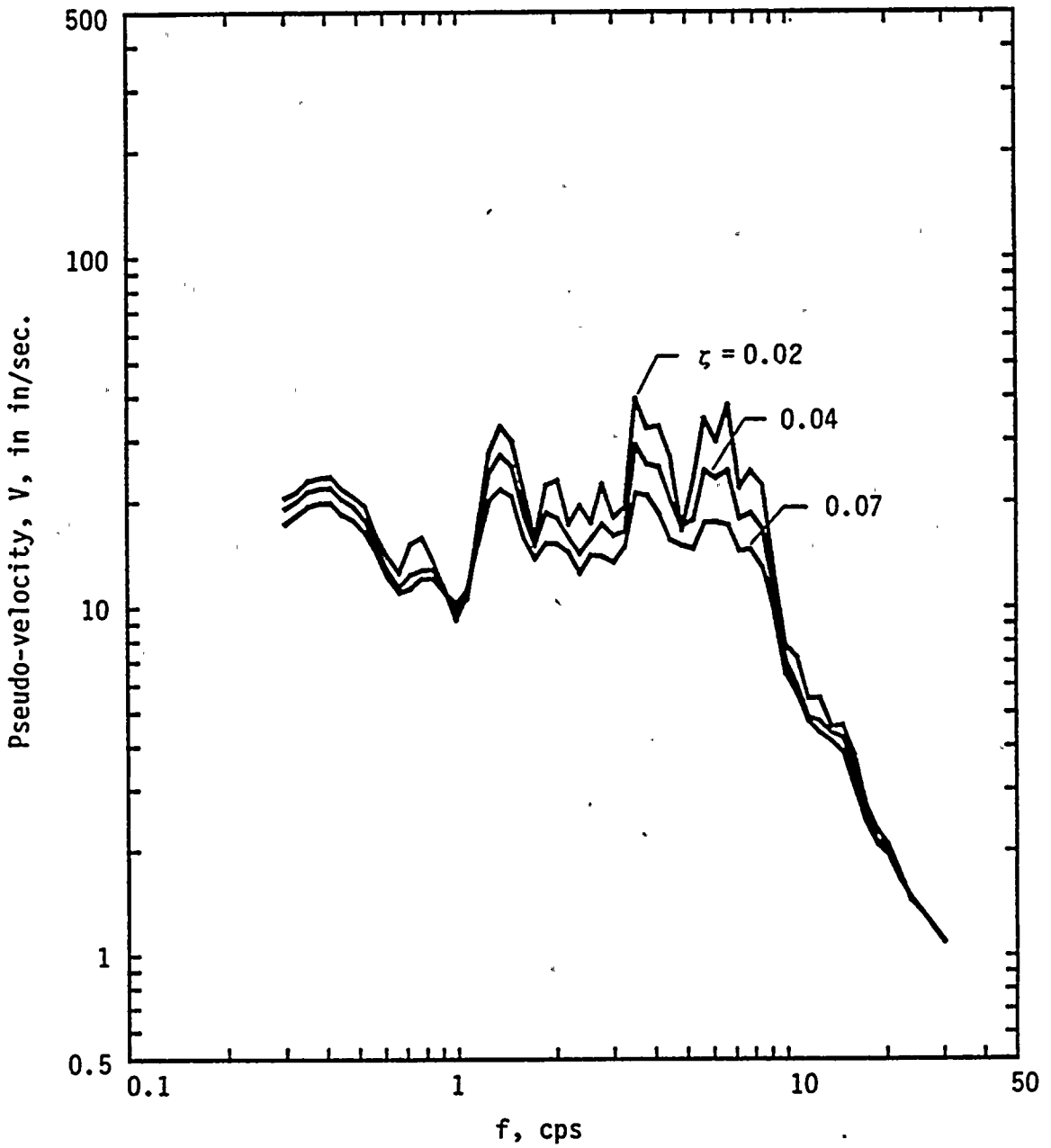

FIG. C.10 Pseudo-velocity Response Spectra for Systems Subjected to Empirical Ground Motion Record No. 10

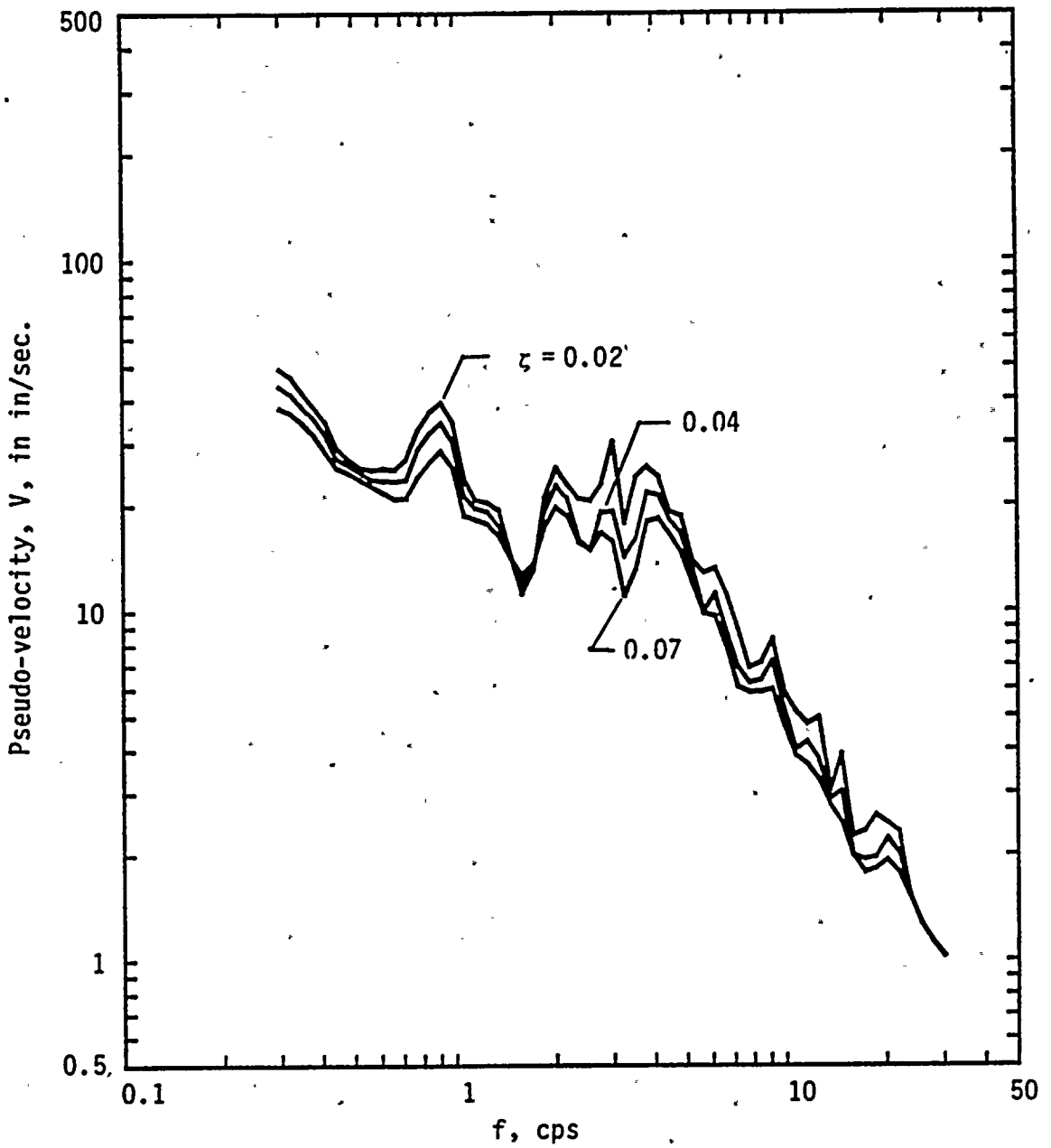

FIG. C.11 Pseudo-velocity Response Spectra for Systems Subjected to Empirical Ground Motion Record No. 11

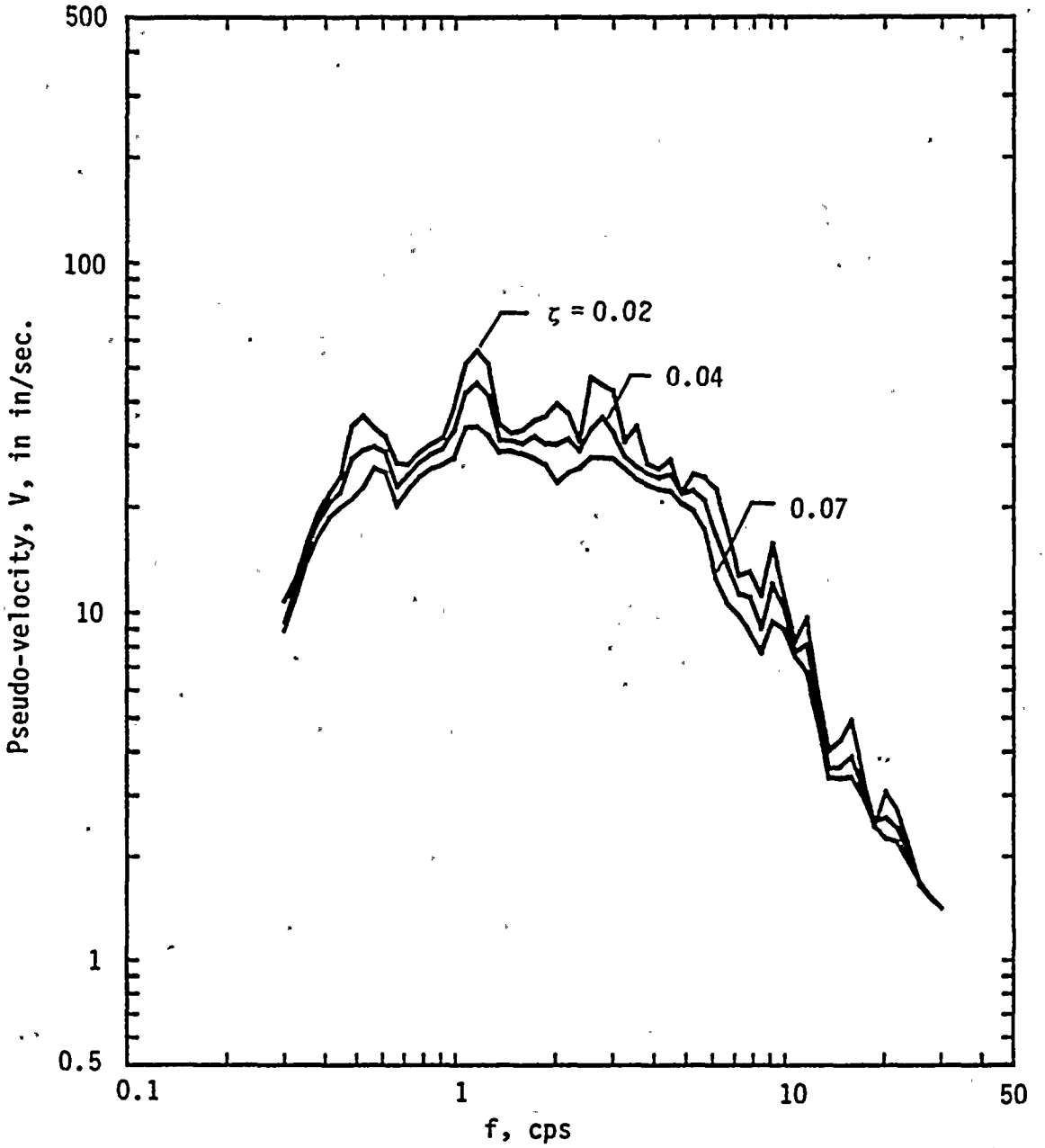

FIG. C.12 Pseudo-velocity Response Spectra for Systems Subjected to Empirical Ground Motion Record No. 12

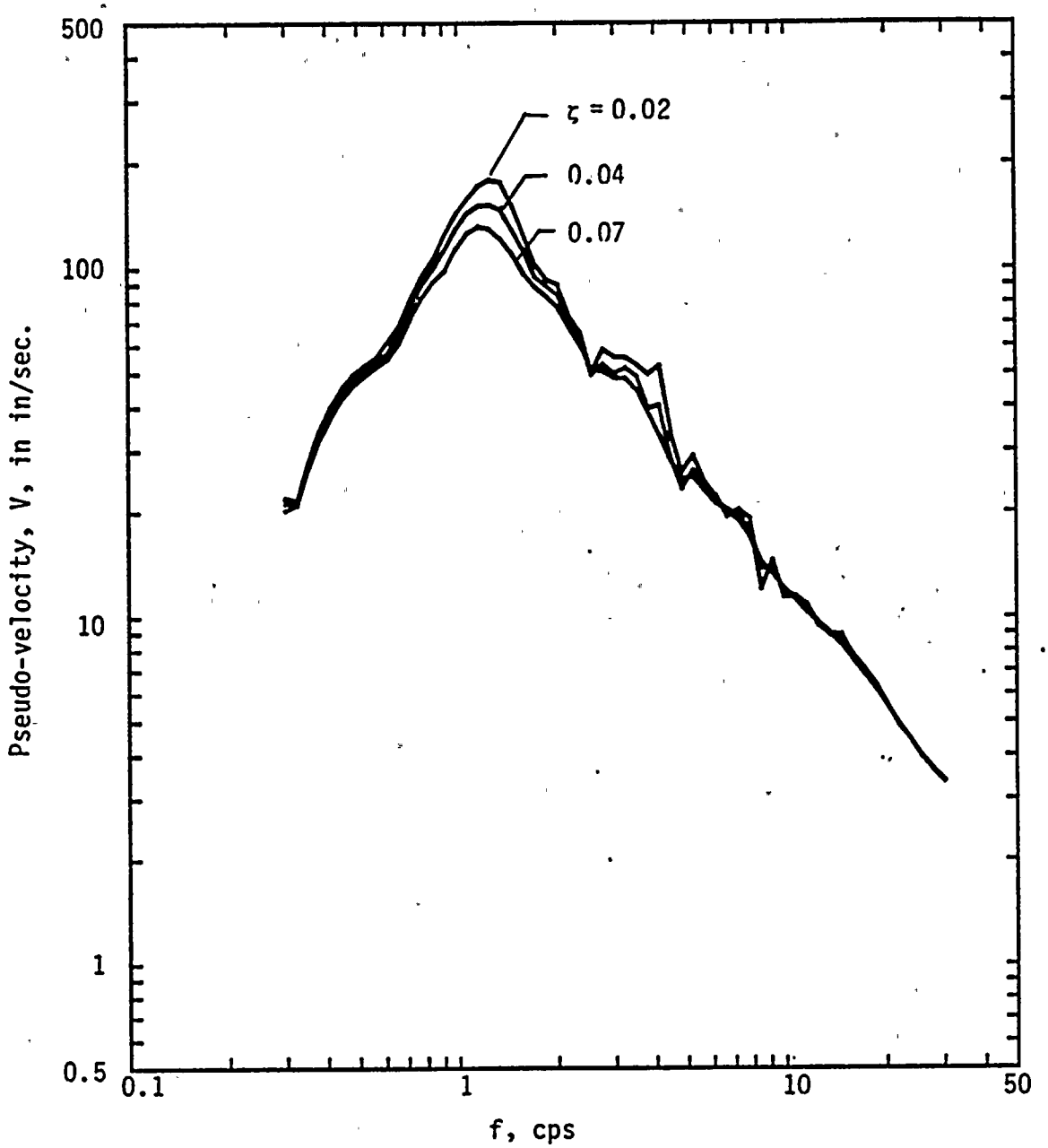

FIG. C.13 Pseudo-velocity Response Spectra for Systems Subjected to Empirical Ground Motion Record No. 13

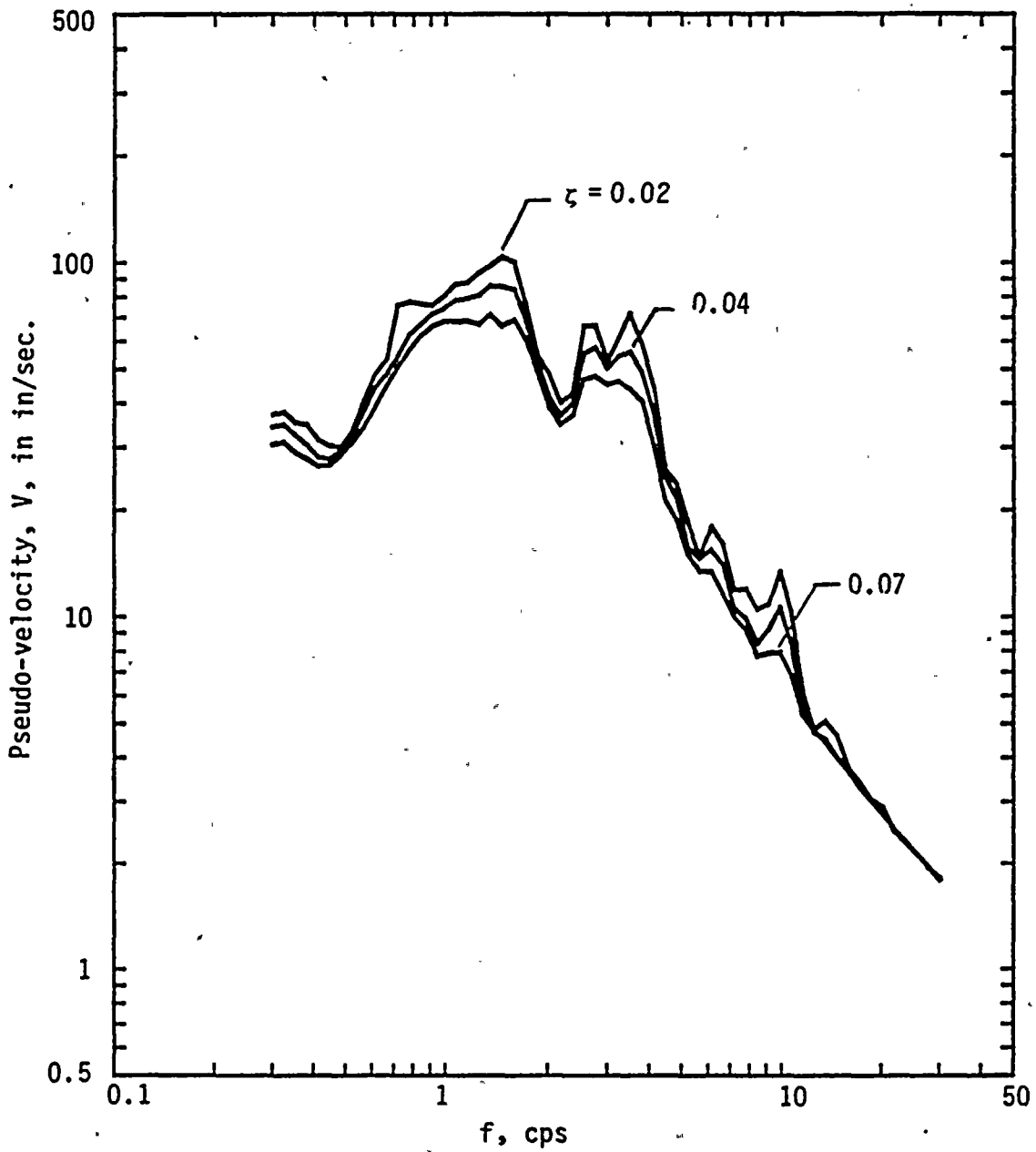

FIG. C.14 Pseudo-velocity Response Spectra for Systems Subjected to Empirical Ground Motion Record No. 14

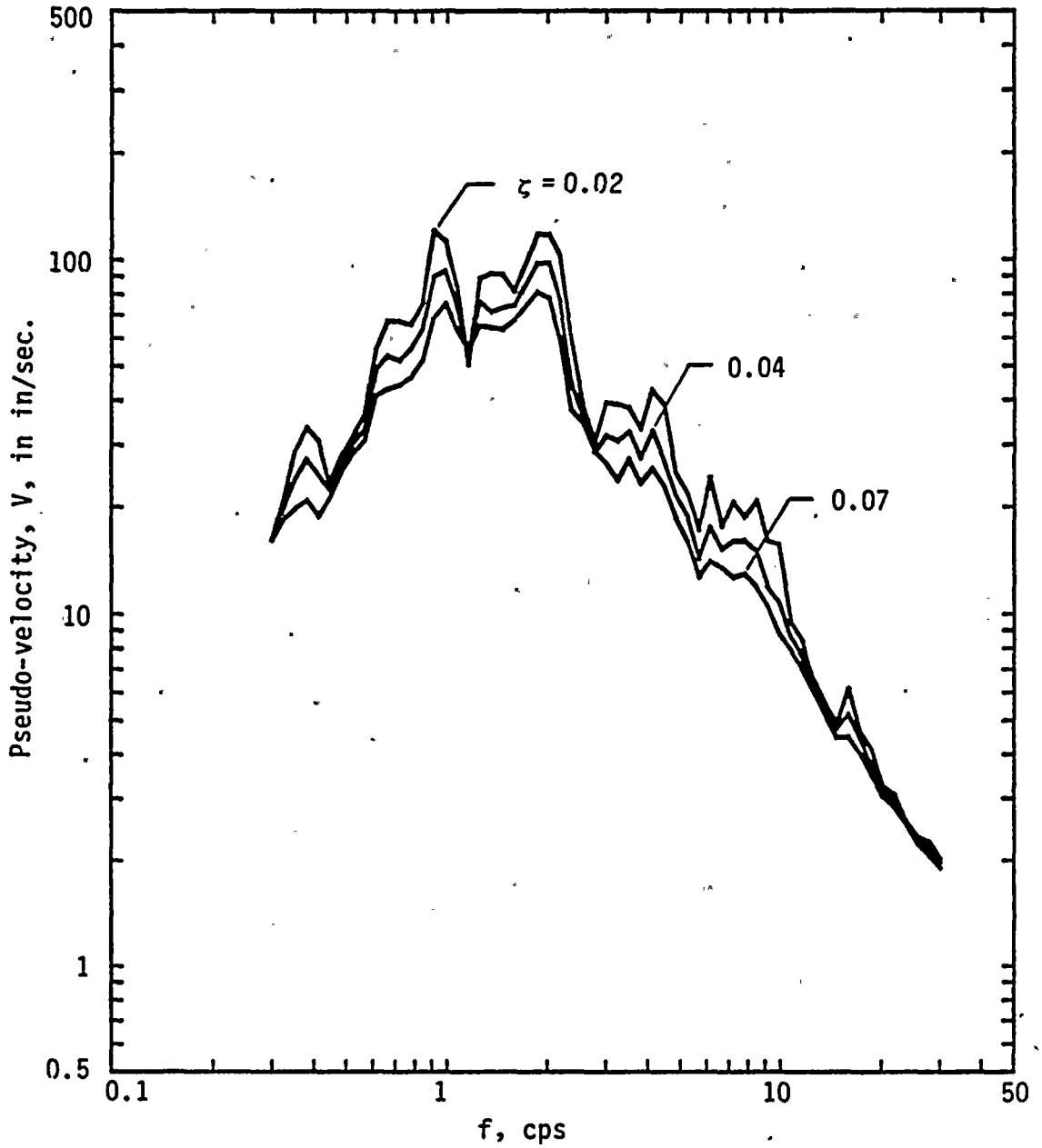

FIG. C.15 Pseudo-velocity Response Spectra for Systems Subjected to Empirical Ground Motion Record No. 15

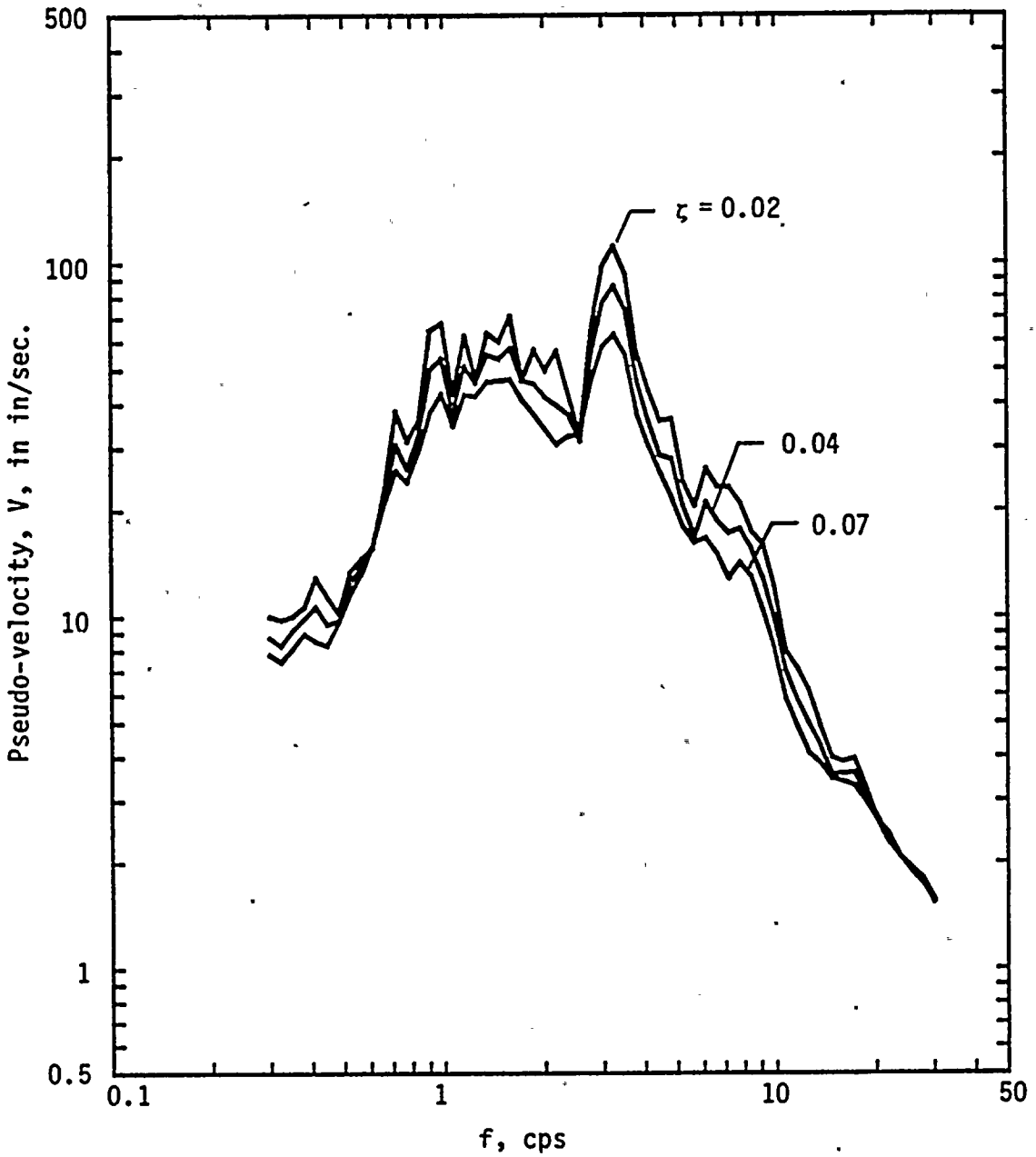

FIG. C.16 Pseudo-velocity Response Spectra for Systems Subjected to Empirical Ground Motion Record No. 16

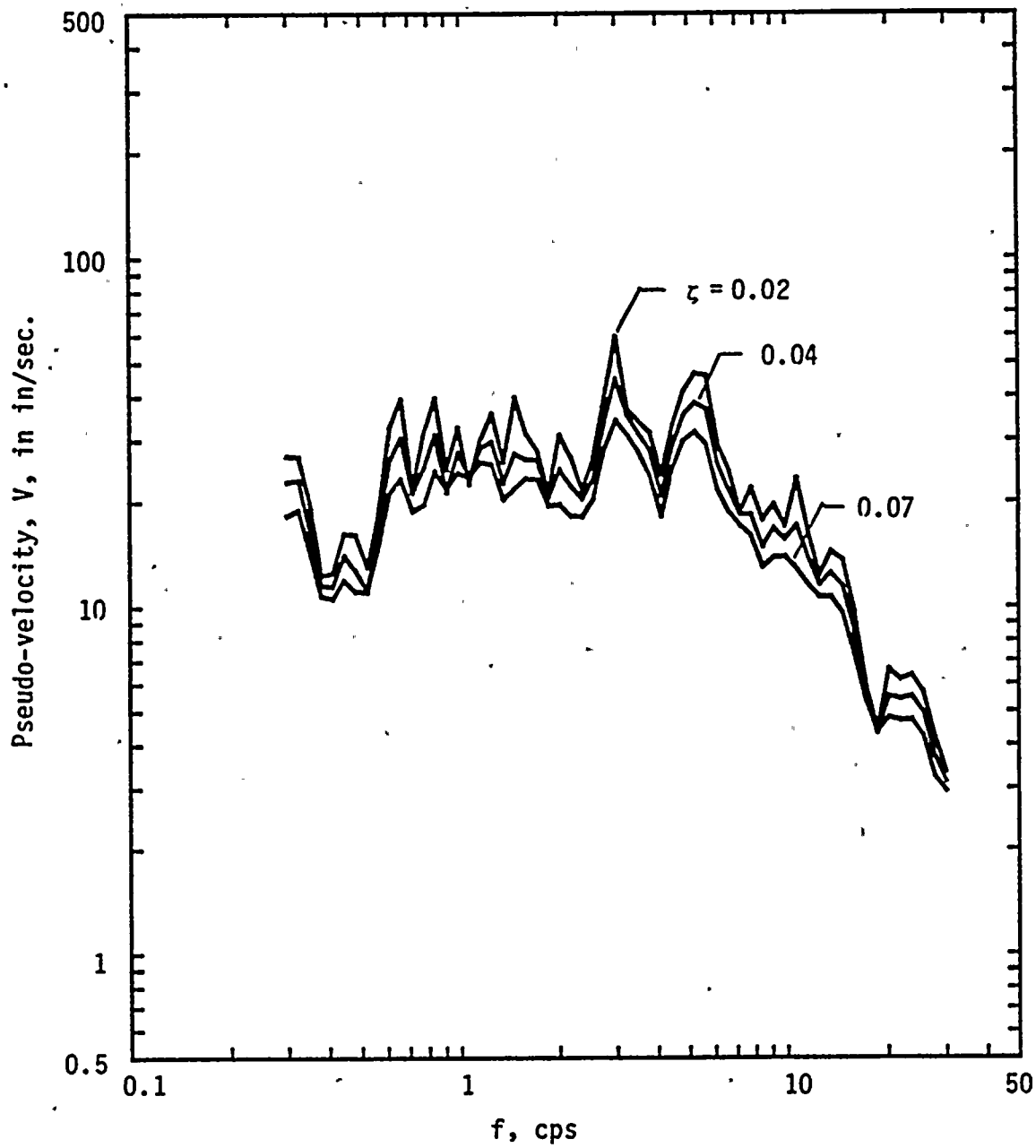

FIG. C.17 Pseudo-velocity Response Spectra for Systems Subjected to Empirical Ground Motion Record No. 17

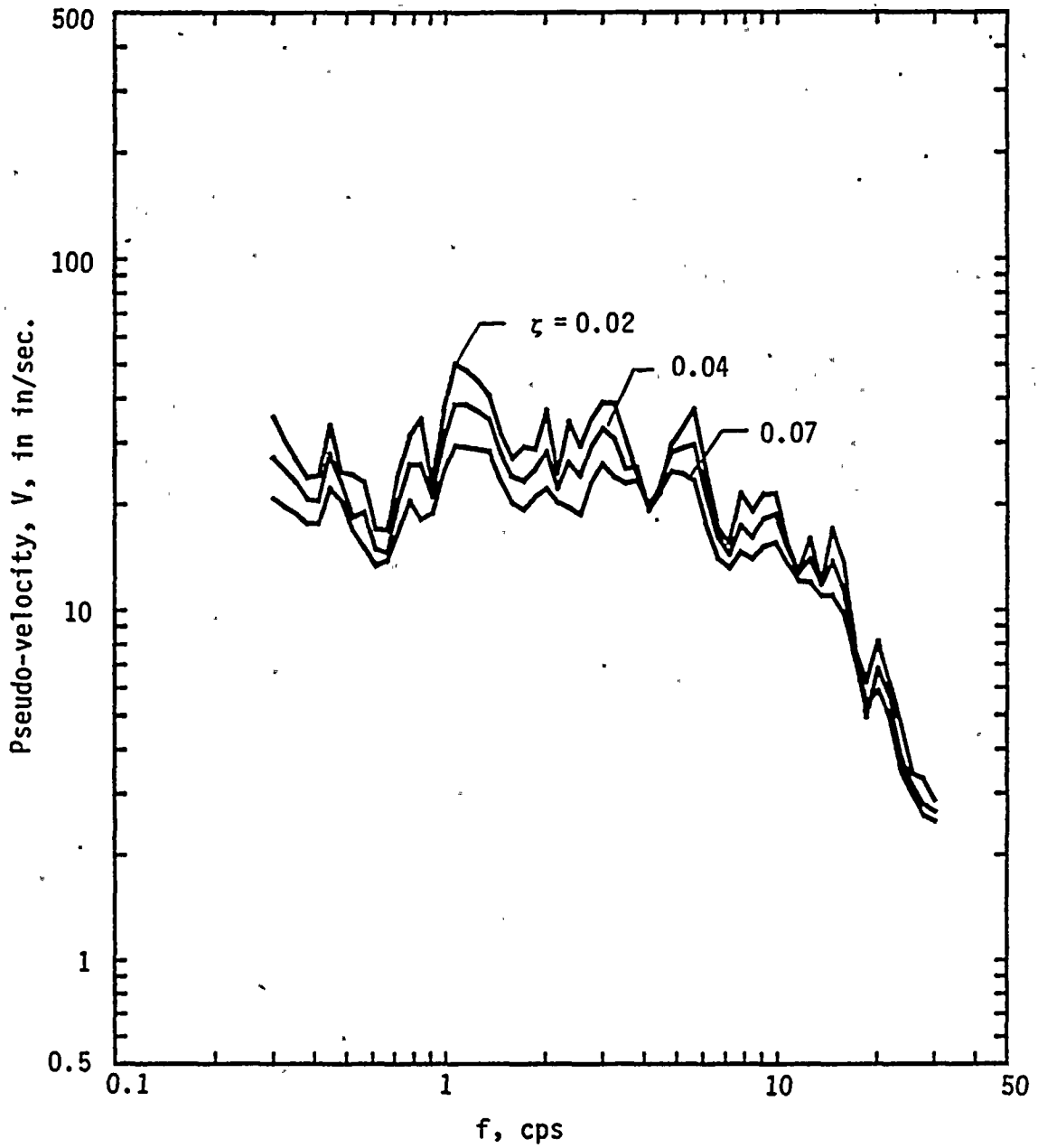

FIG. C.18 Pseudo-velocity Response Spectra for Systems Subjected to Empirical Ground Motion Record No. 18

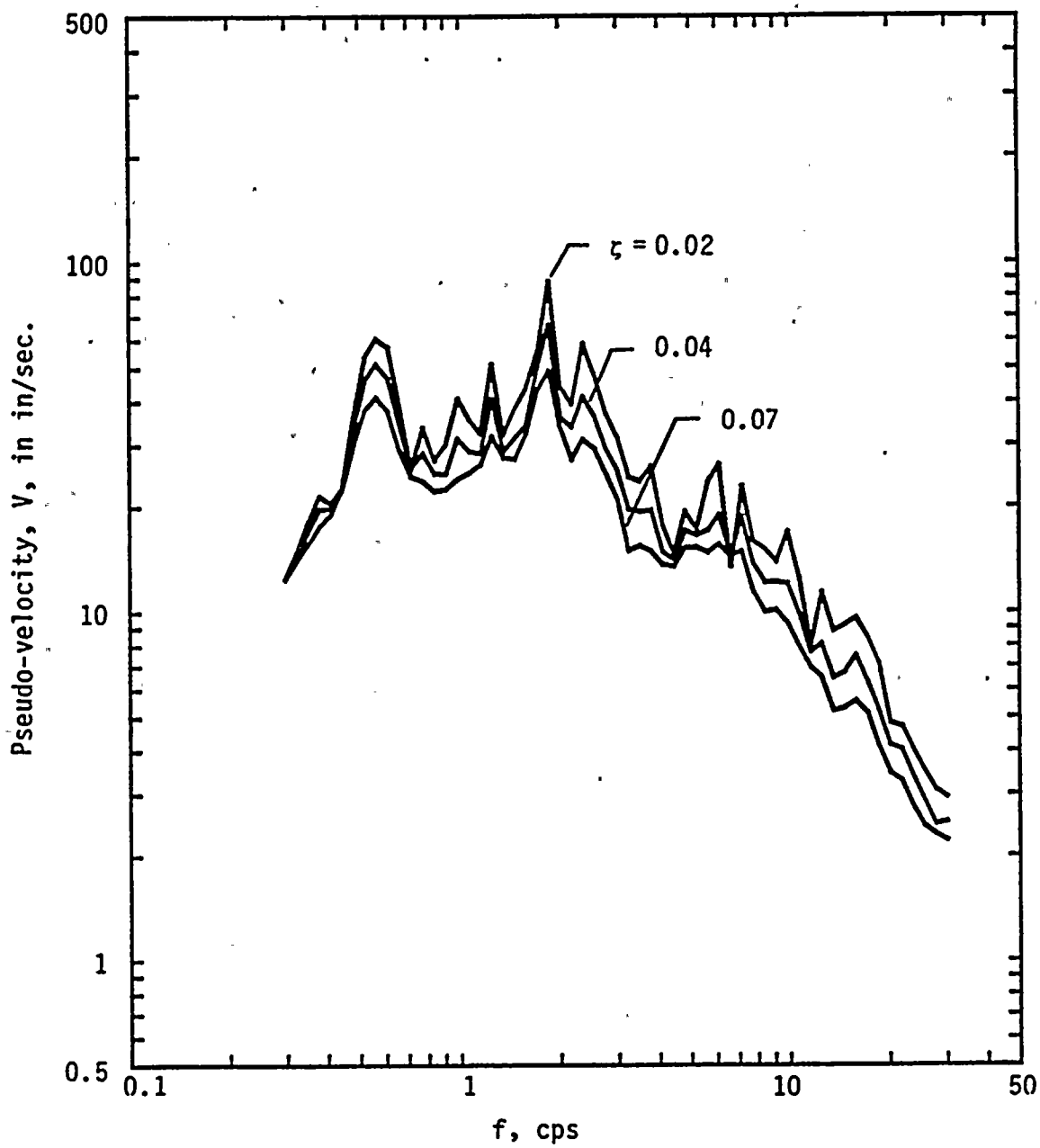

FIG. C.19 Pseudo-velocity Response Spectra for Systems Subjected to Empirical Ground Motion Record No. 19

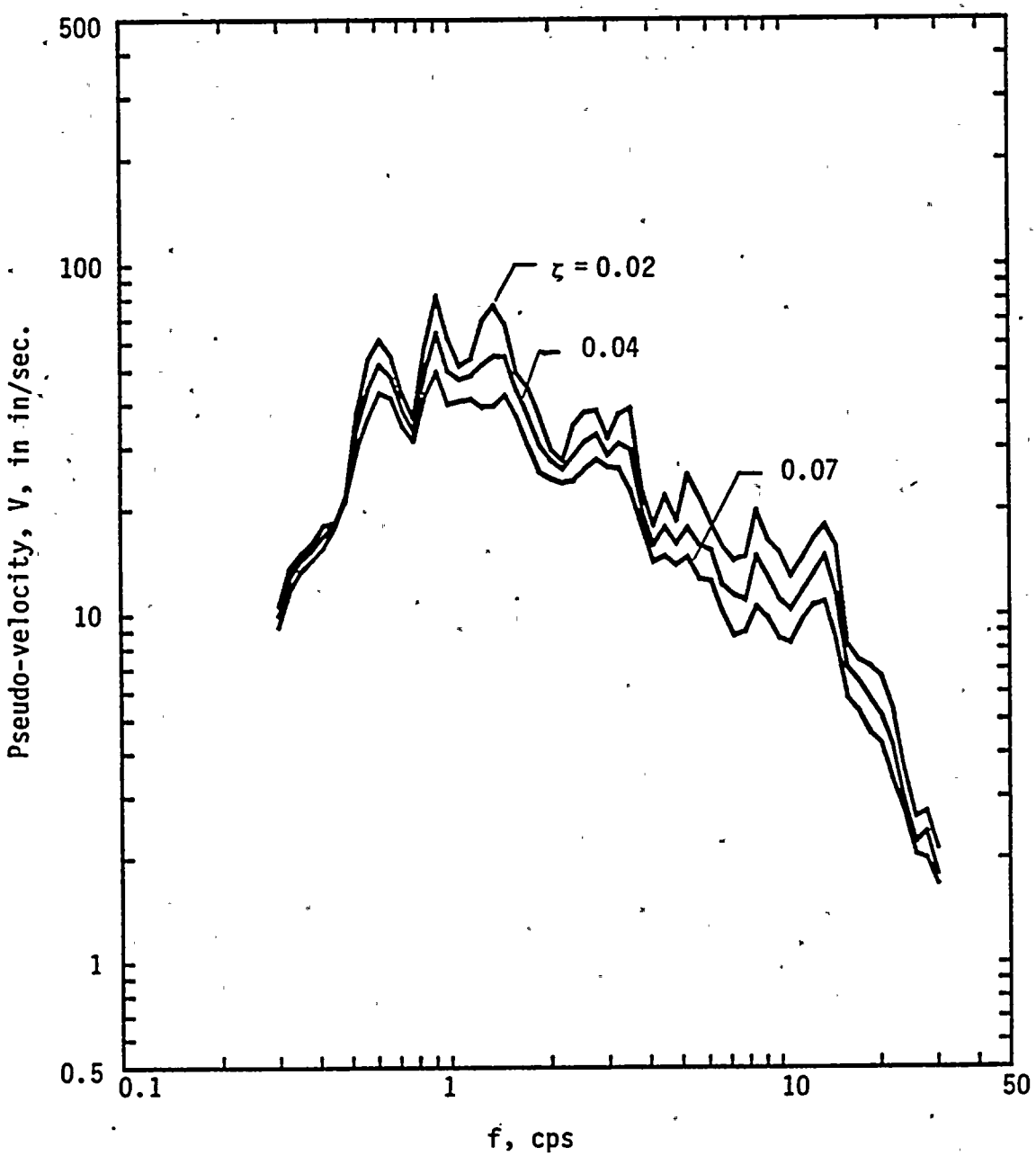

FIG. C.20 Pseudo-velocity Response Spectra for Systems Subjected to Empirical Ground Motion Record No. 20

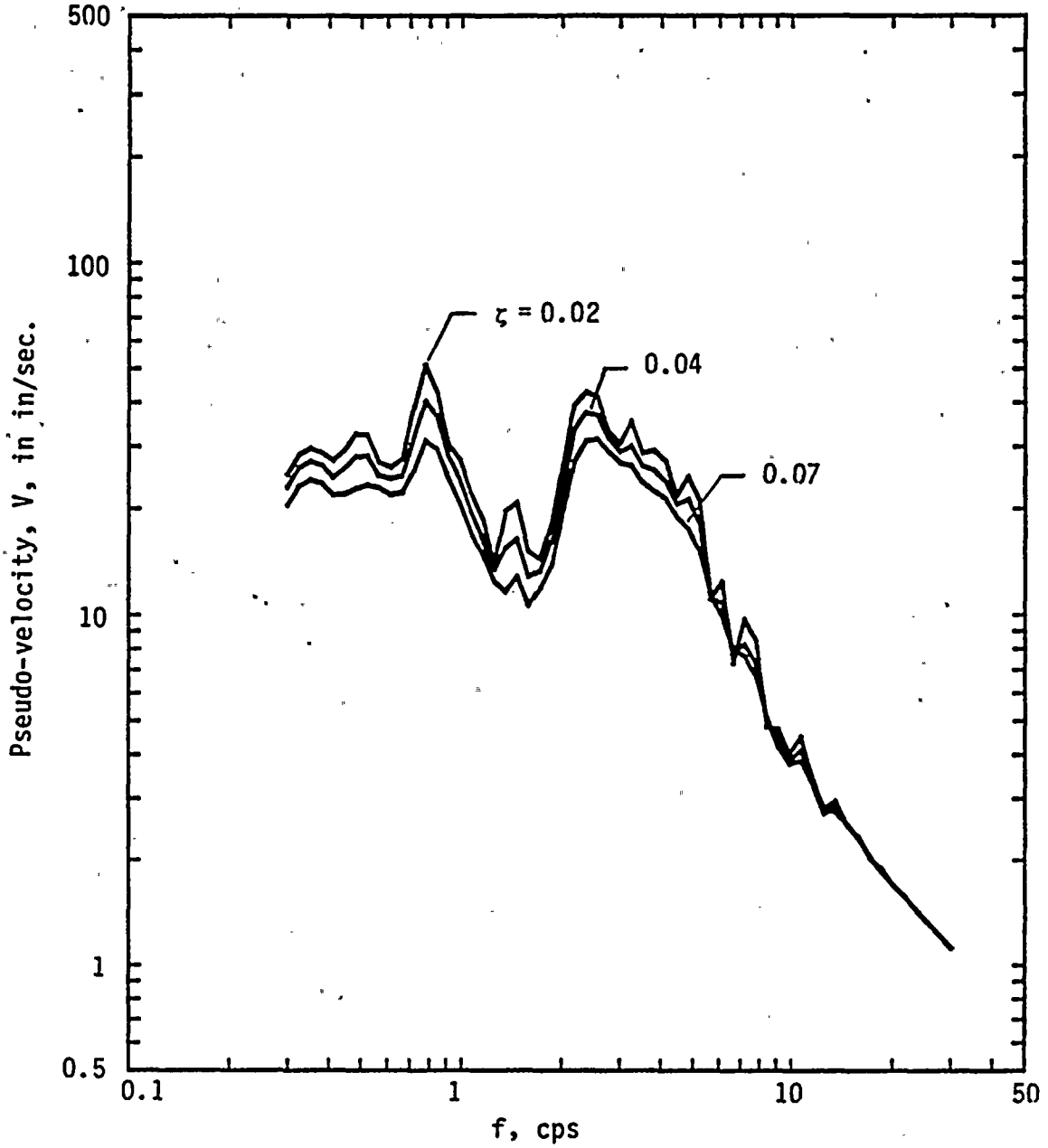

FIG. C.21 Pseudo-velocity Response Spectra for Systems Subjected to Empirical Ground Motion Record No. 21

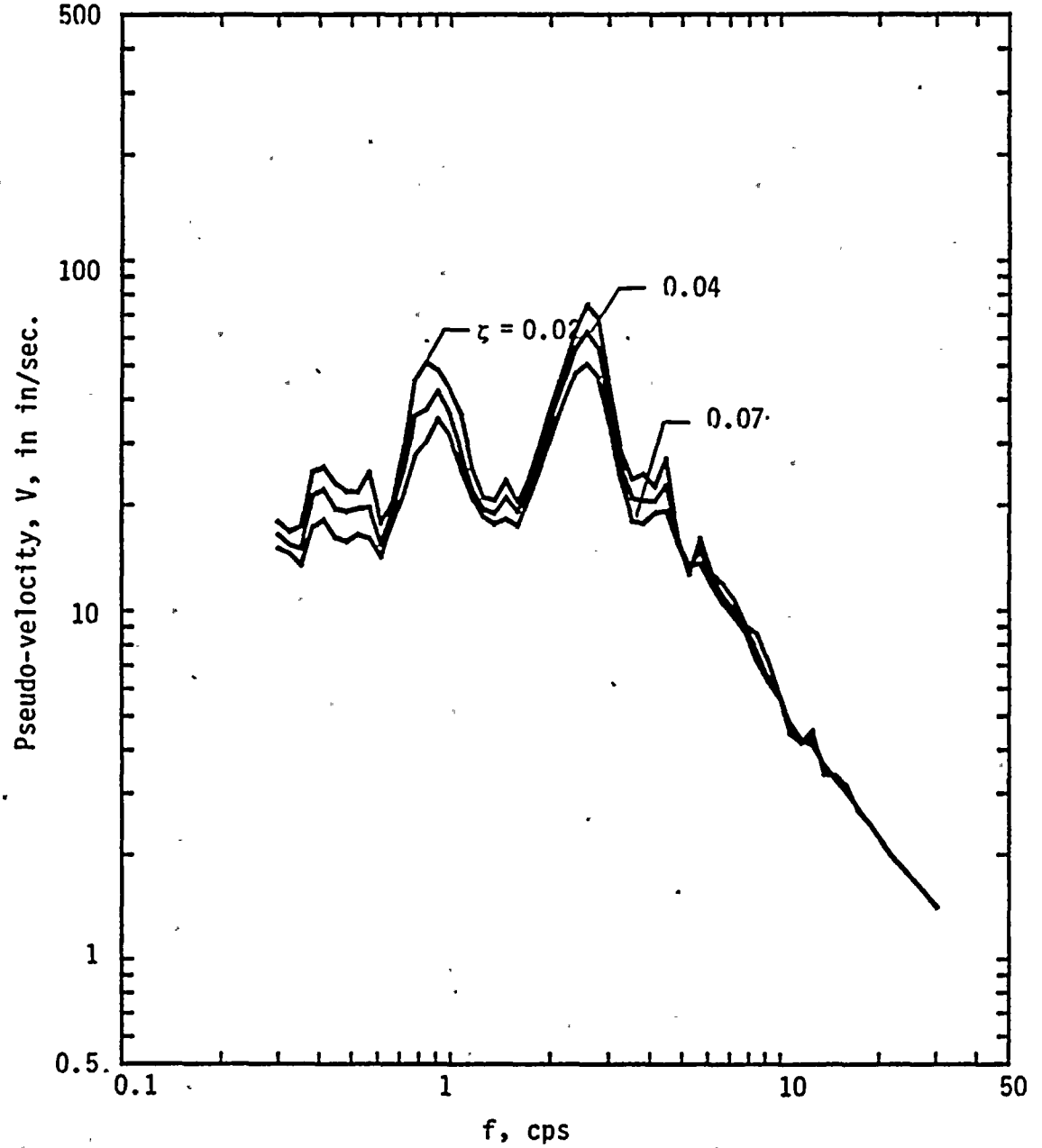

FIG. C.22 Pseudo-velocity Response Spectra for Systems Subjected to Empirical Ground Motion Record No. 22

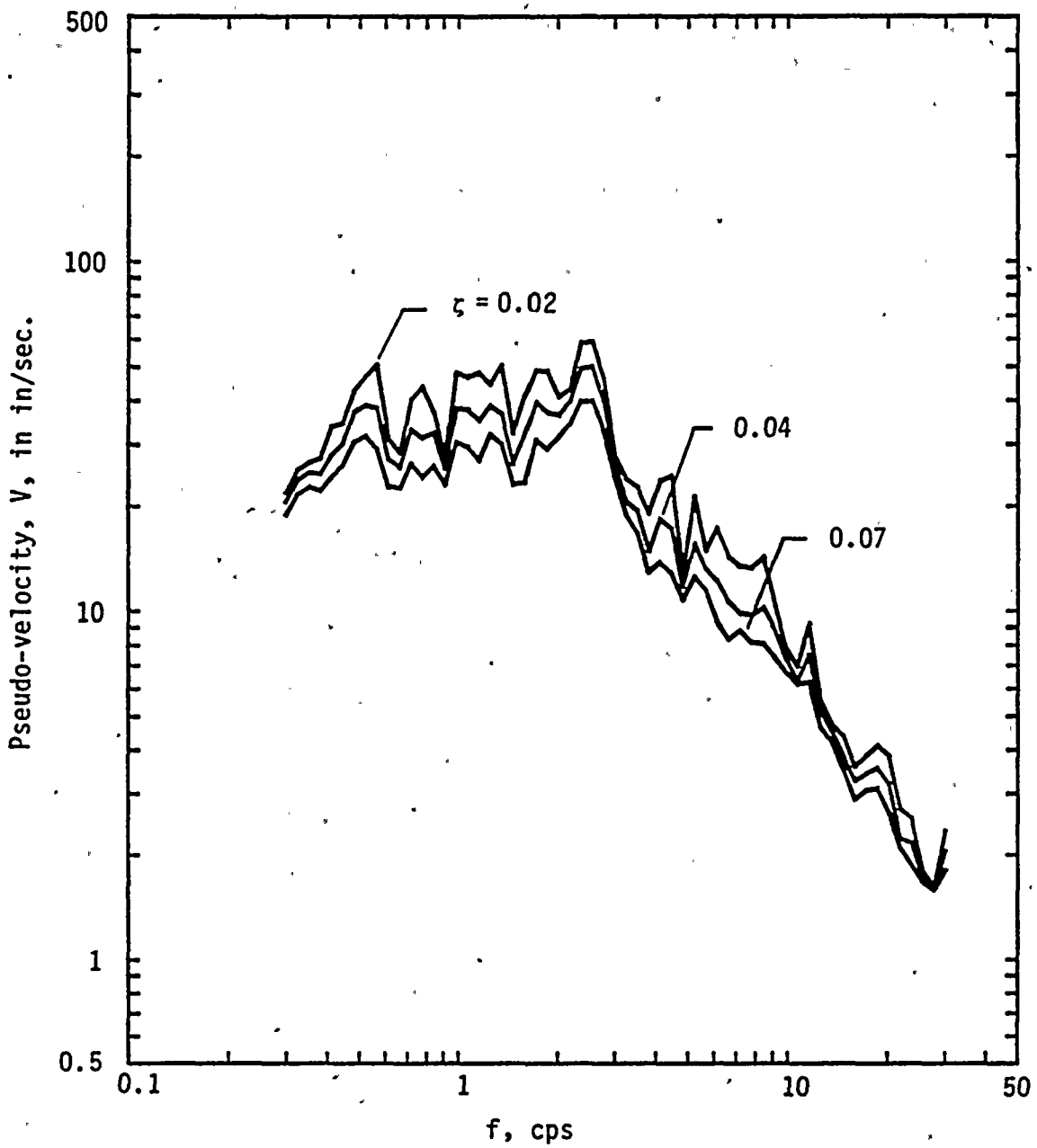

FIG. C.23 Pseudo-velocity Response Spectra for Systems Subjected to Empirical Ground Motion Record No. 23

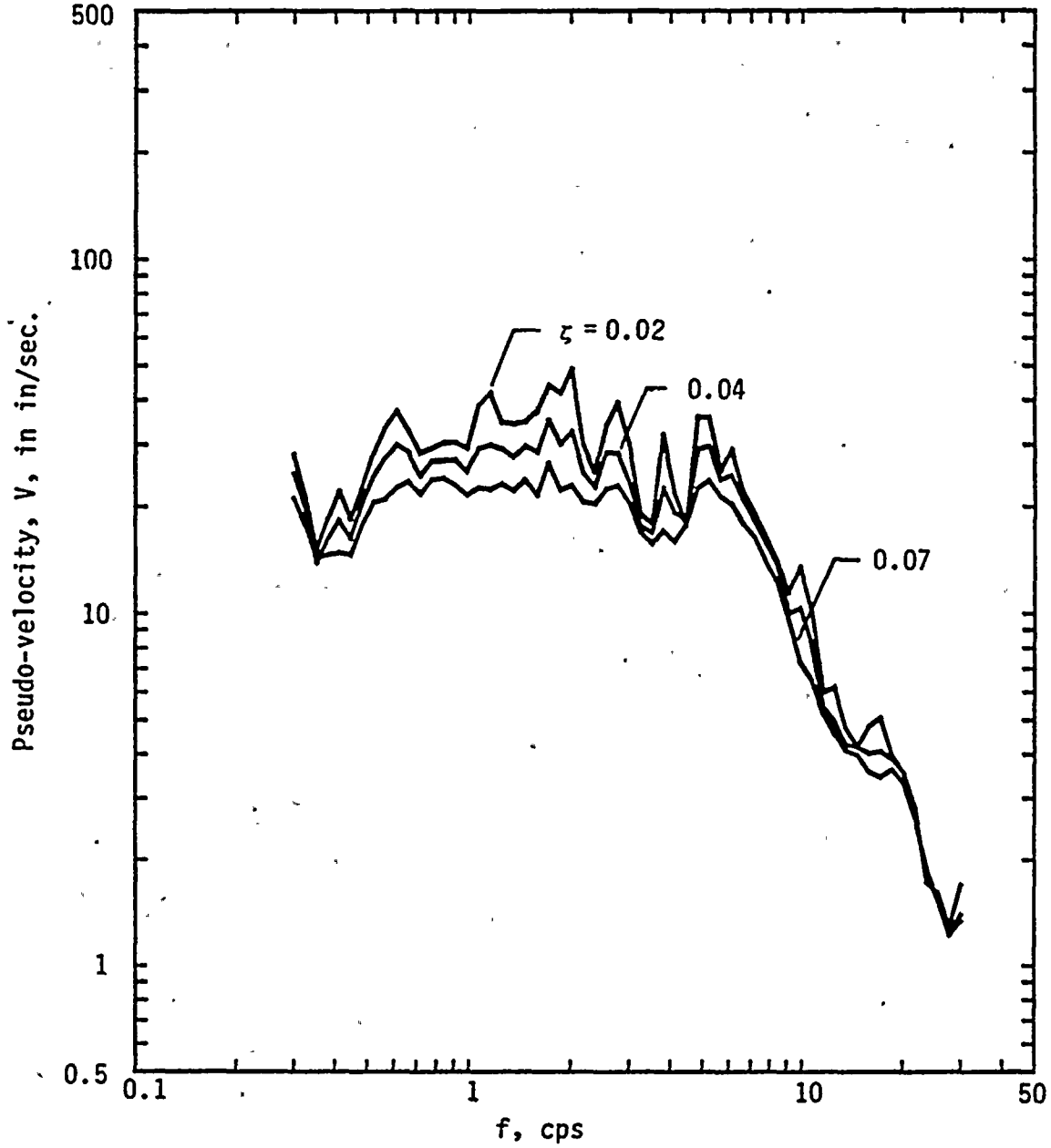

FIG. C.24 Pseudo-velocity Response Spectra for Systems Subjected to Empirical Ground Motion Record No. 24

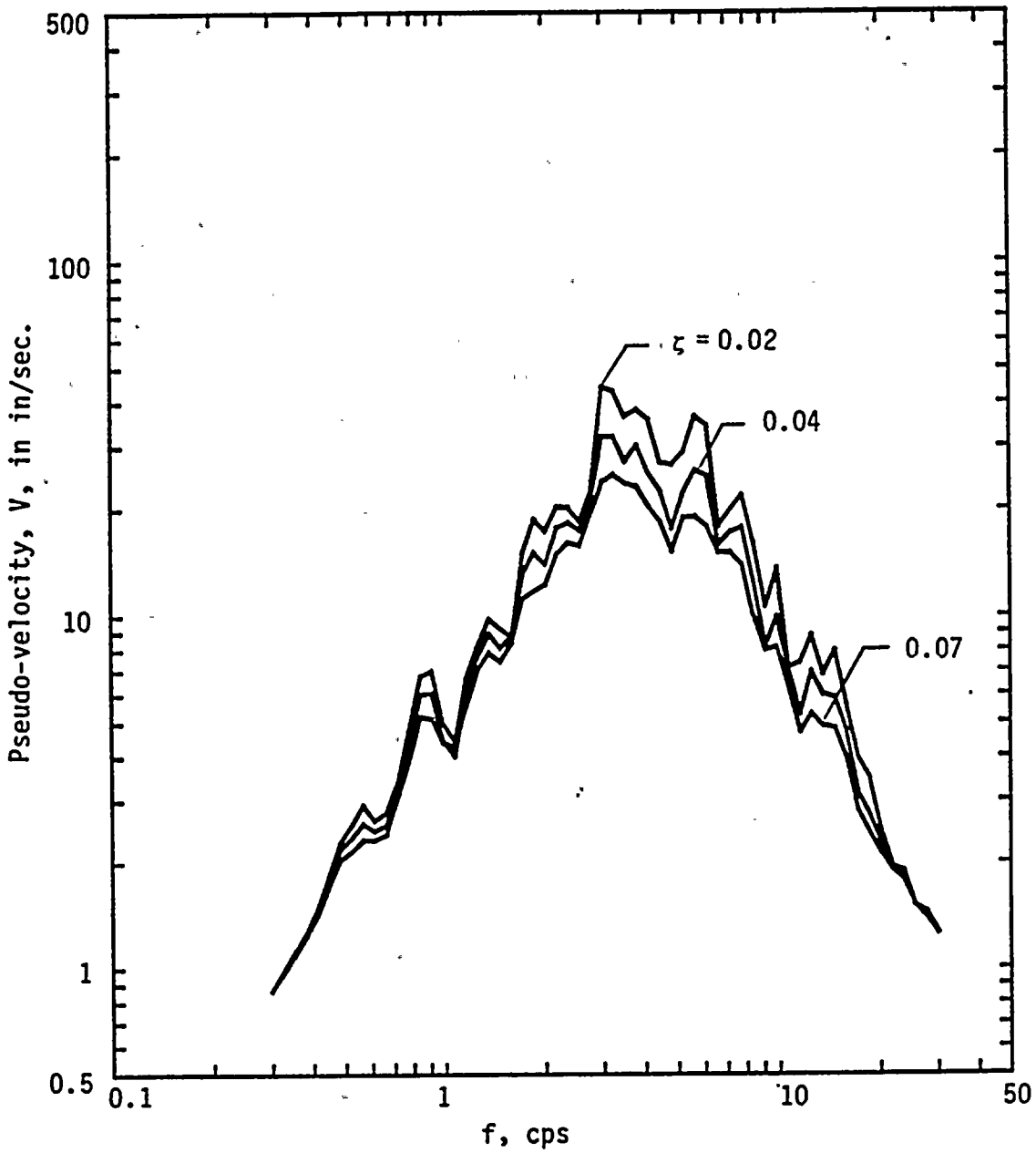

FIG. C.25 Pseudo-velocity Response Spectra for Systems Subjected to Numerically Generated Ground Motion Record No. 25

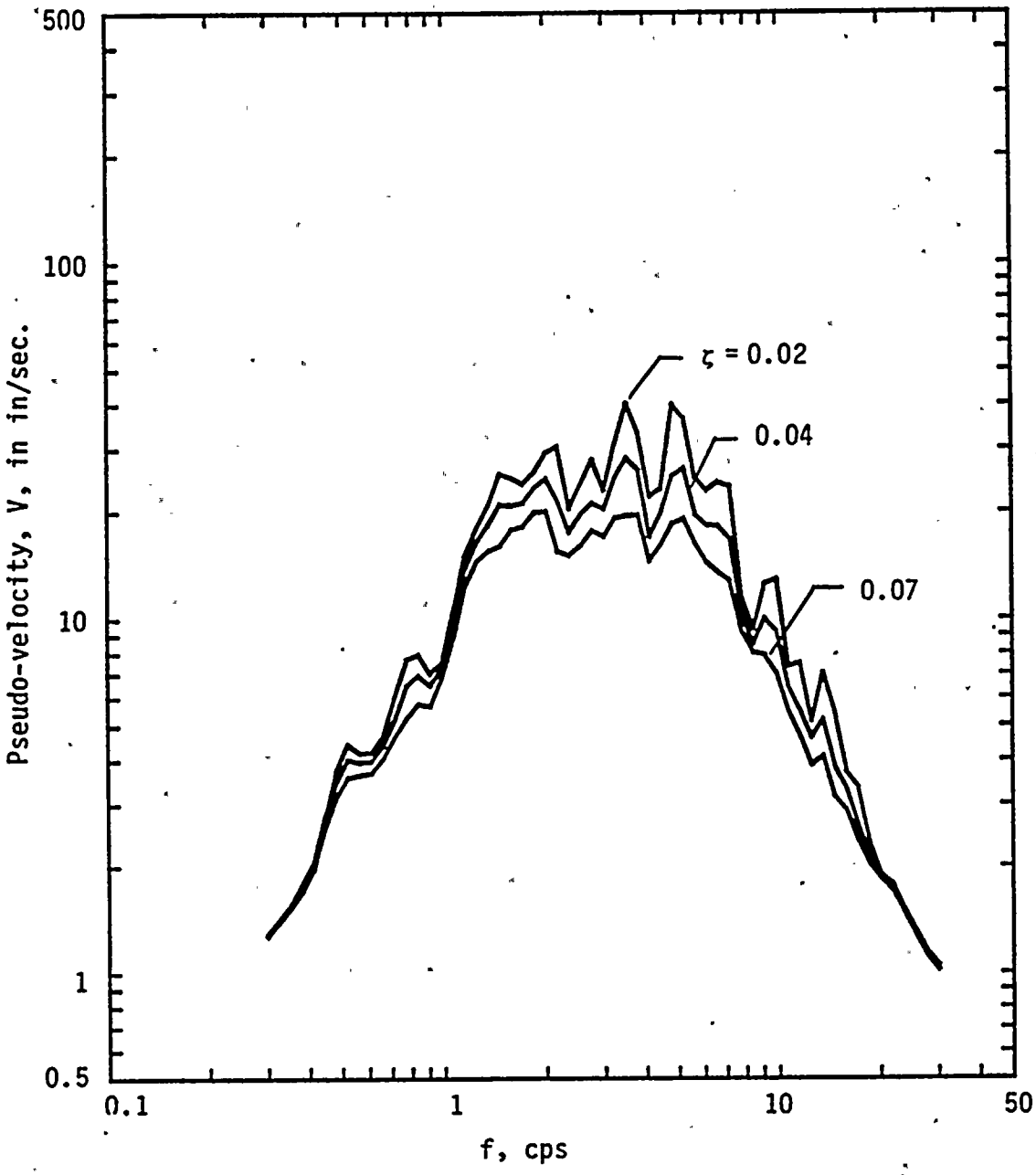

FIG. C.26 Pseudo-velocity Response Spectra for Systems Subjected to Numerically Generated Ground Motion Record No. 26

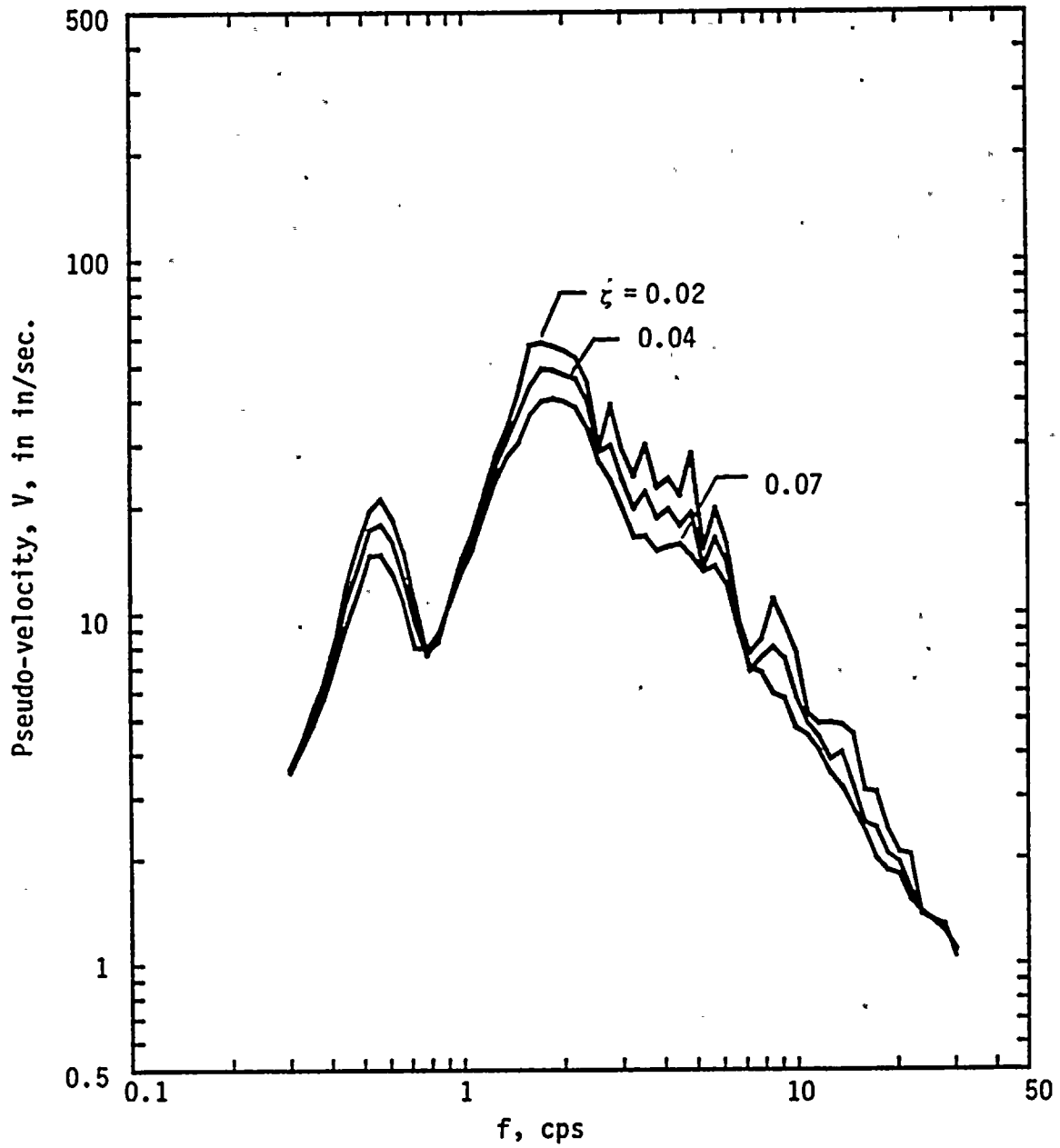

FIG. C.27 Pseudo-velocity Response Spectra for Systems Subjected to Numerically Generated Ground Motion Record No. 27

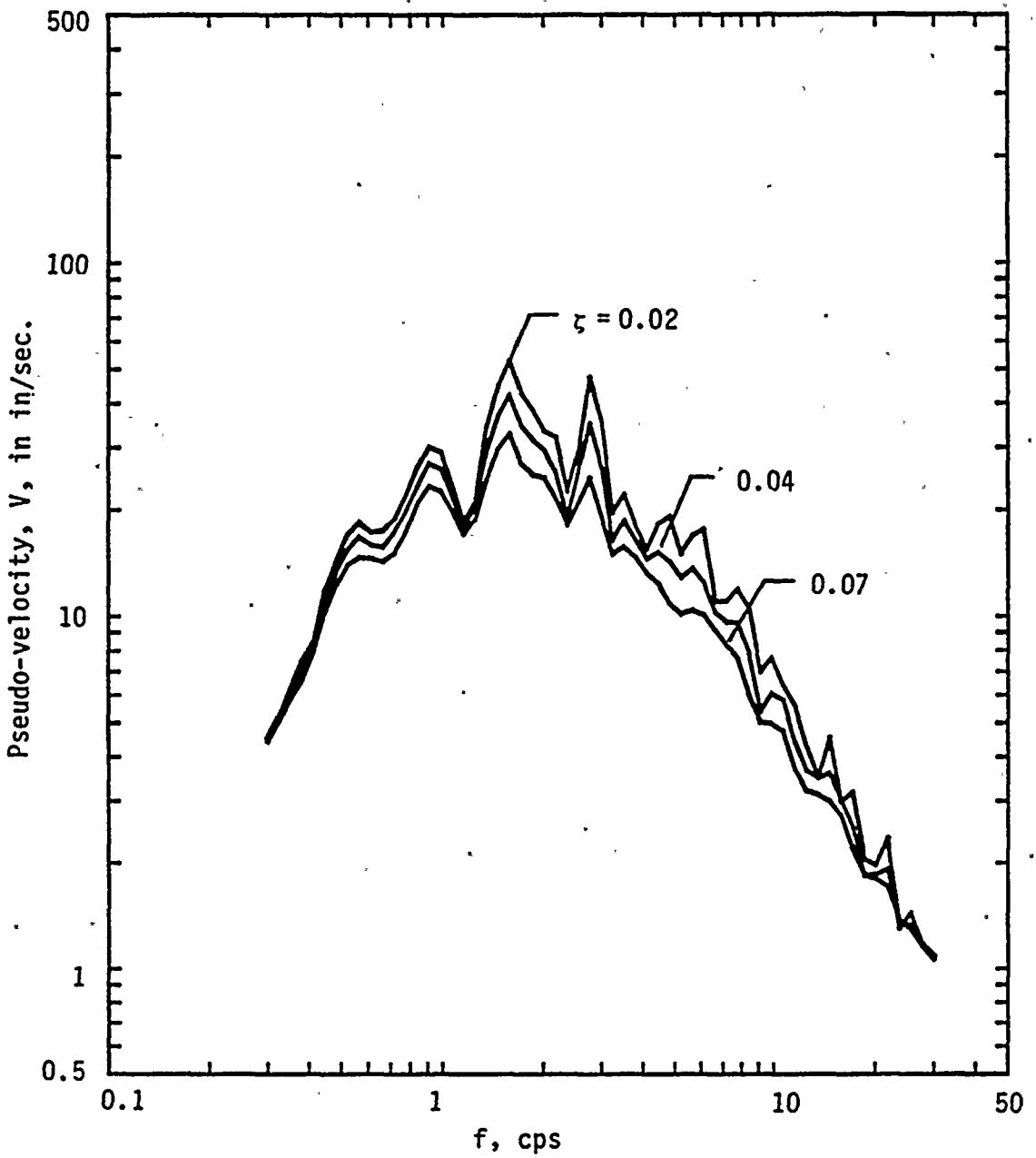

FIG. C.28 Pseudo-velocity Response Spectra for Systems Subjected to Numerically Generated Ground Motion Record No. 28

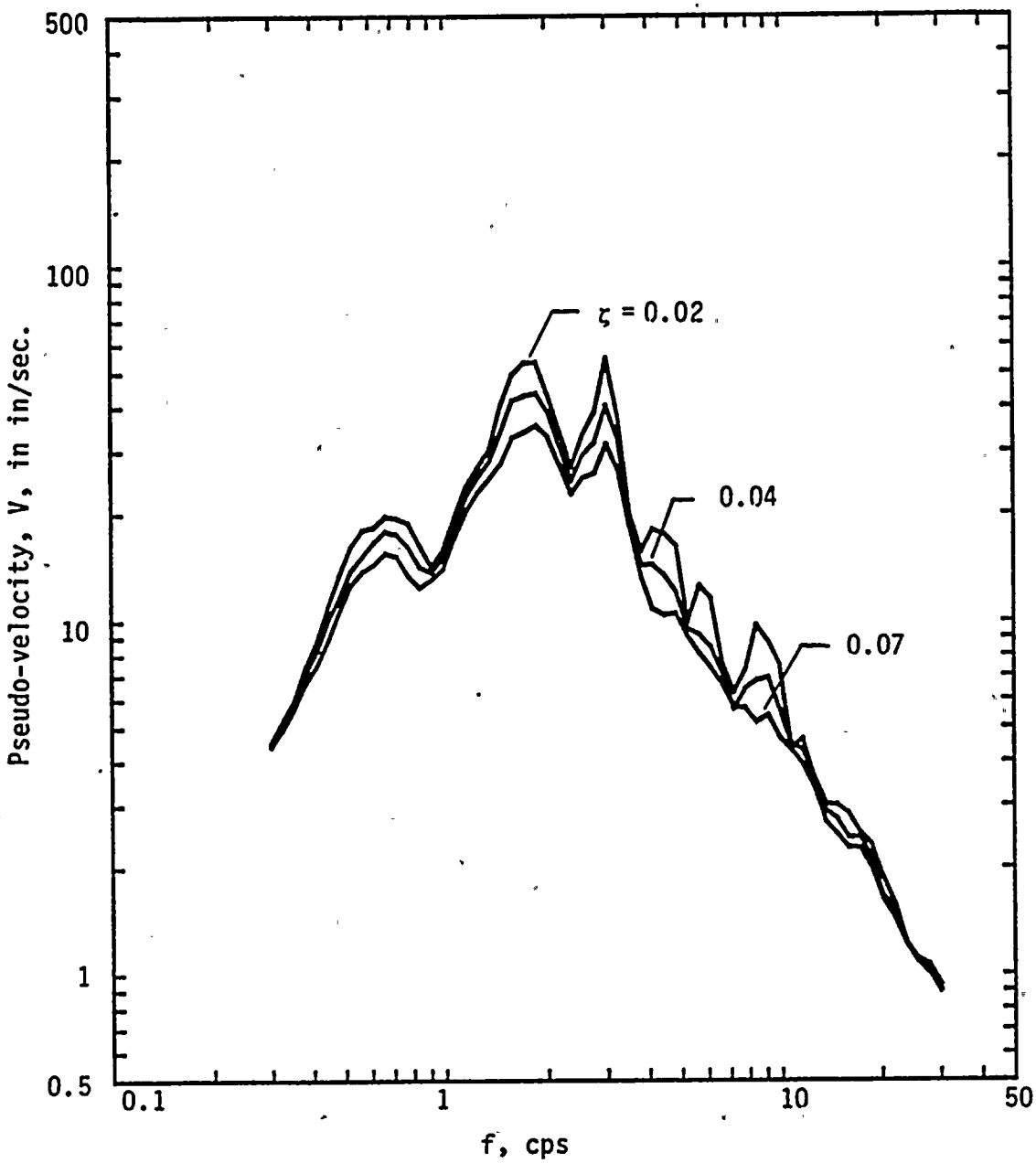

FIG. C.29 Pseudo-velocity Response Spectra for Systems Subjected to Numerically Generated Ground Motion Record No. 29

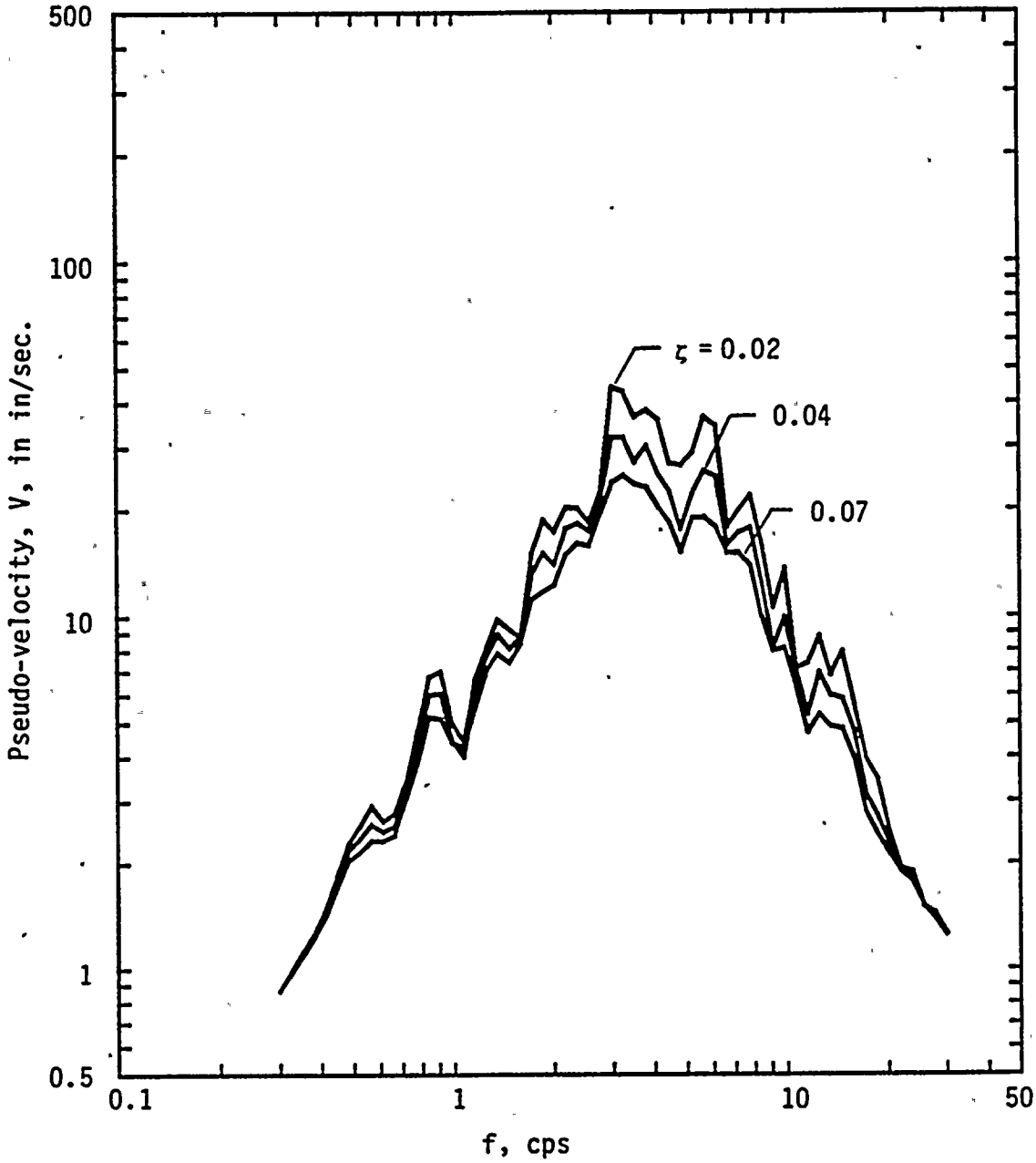

FIG. C.30 Pseudo-velocity Response Spectra for Systems Subjected to Numerically Generated Ground Motion Record No. 30

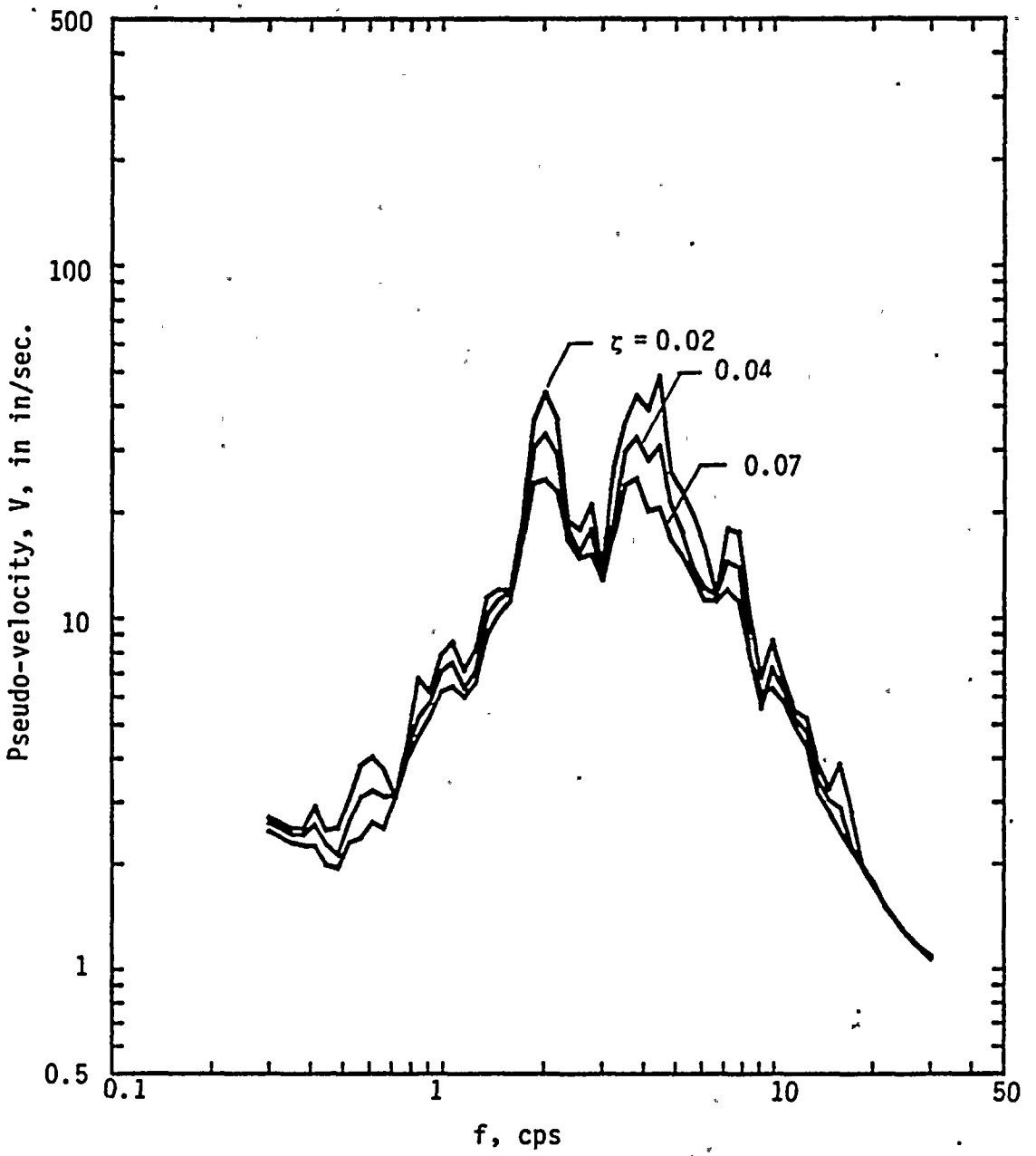

FIG. C.31 Pseudo-velocity Response Spectra for Systems Subjected to Numerically Generated Ground Motion Record No. 31

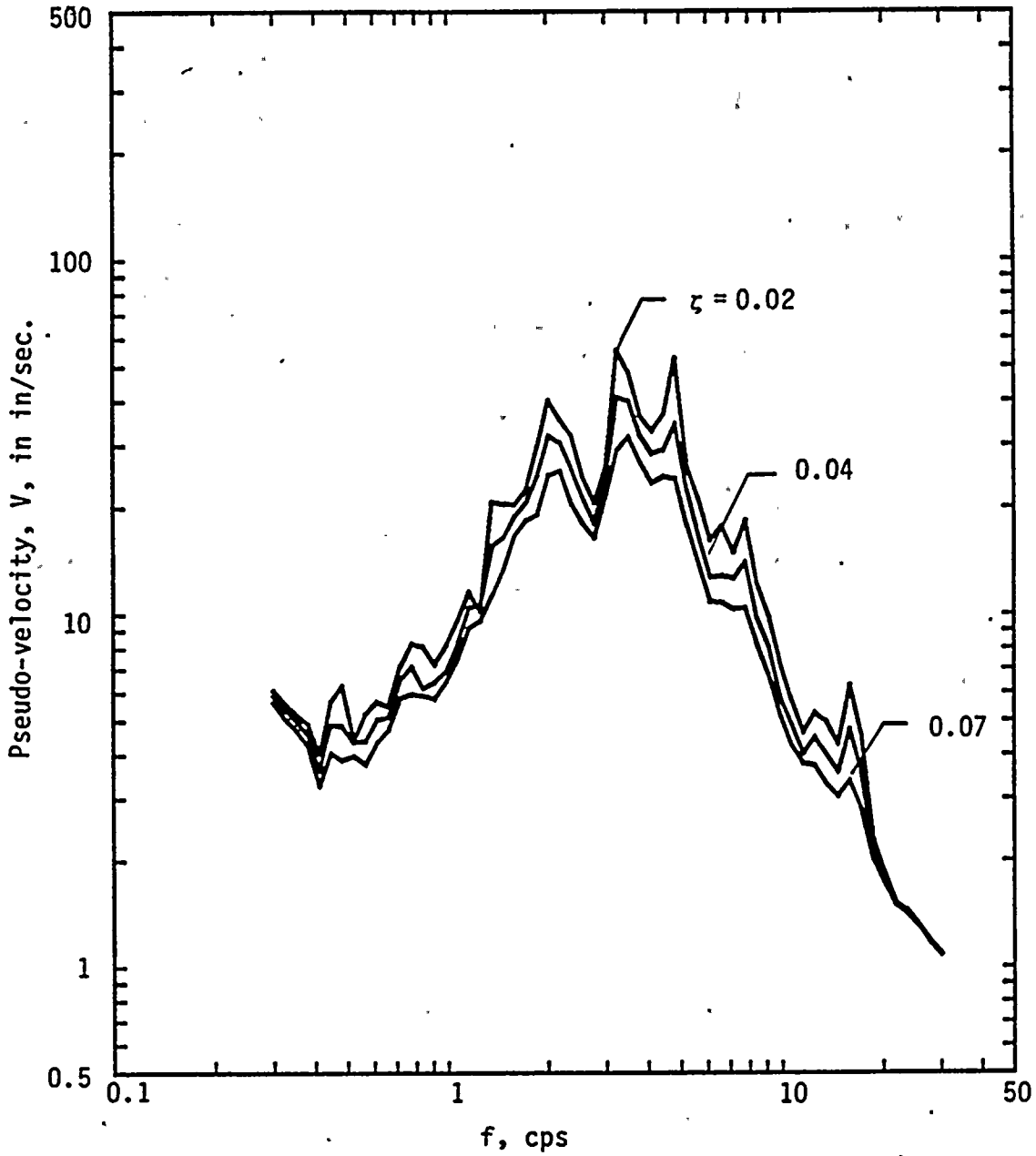

FIG. C.32 Pseudo-velocity Response Spectra for Systems Subjected to Numerically Generated Ground Motion Record No. 32

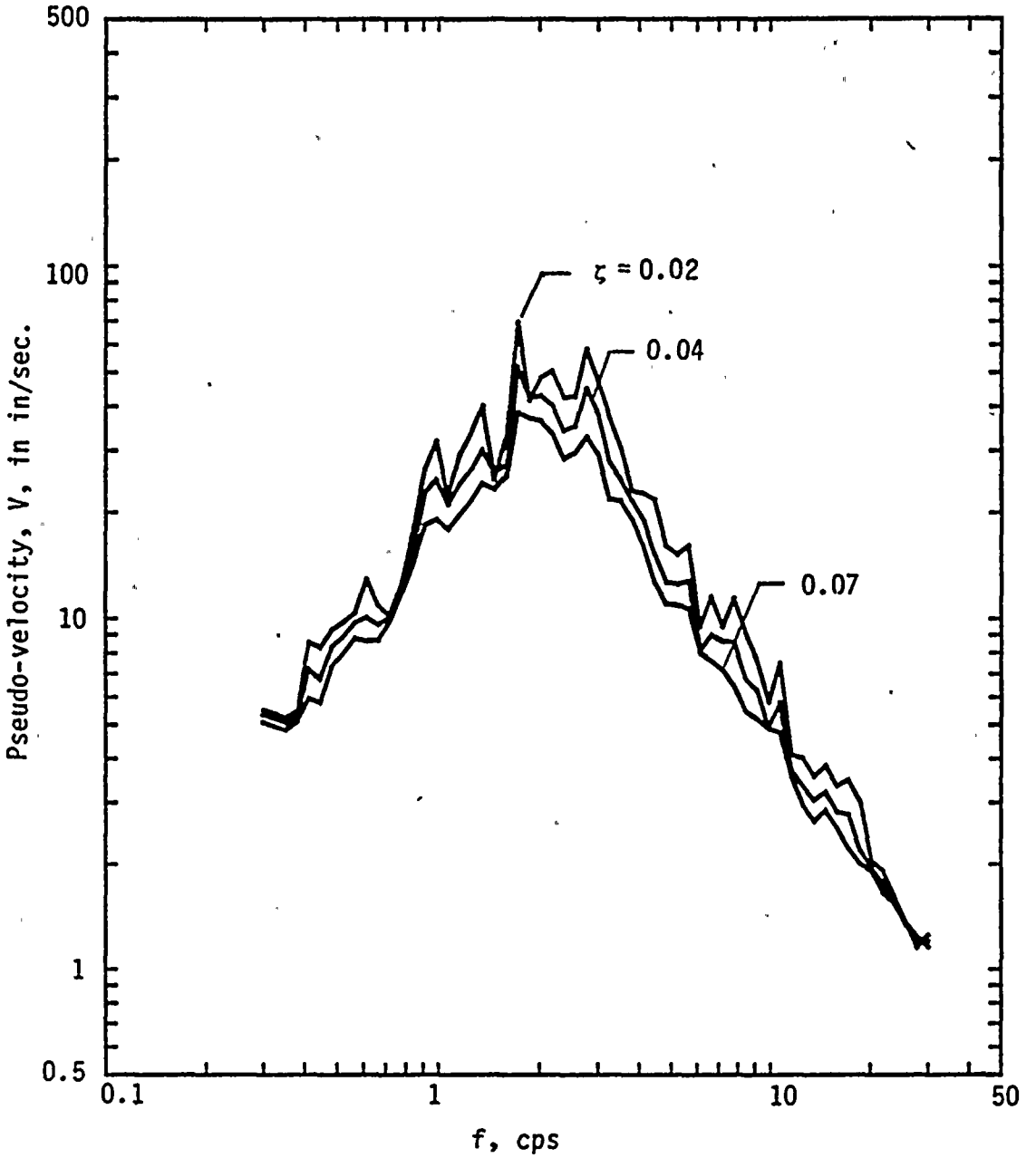

FIG. C.33 Pseudo-velocity Response Spectra for Systems Subjected to Numerically Generated Ground Motion Record No. 33

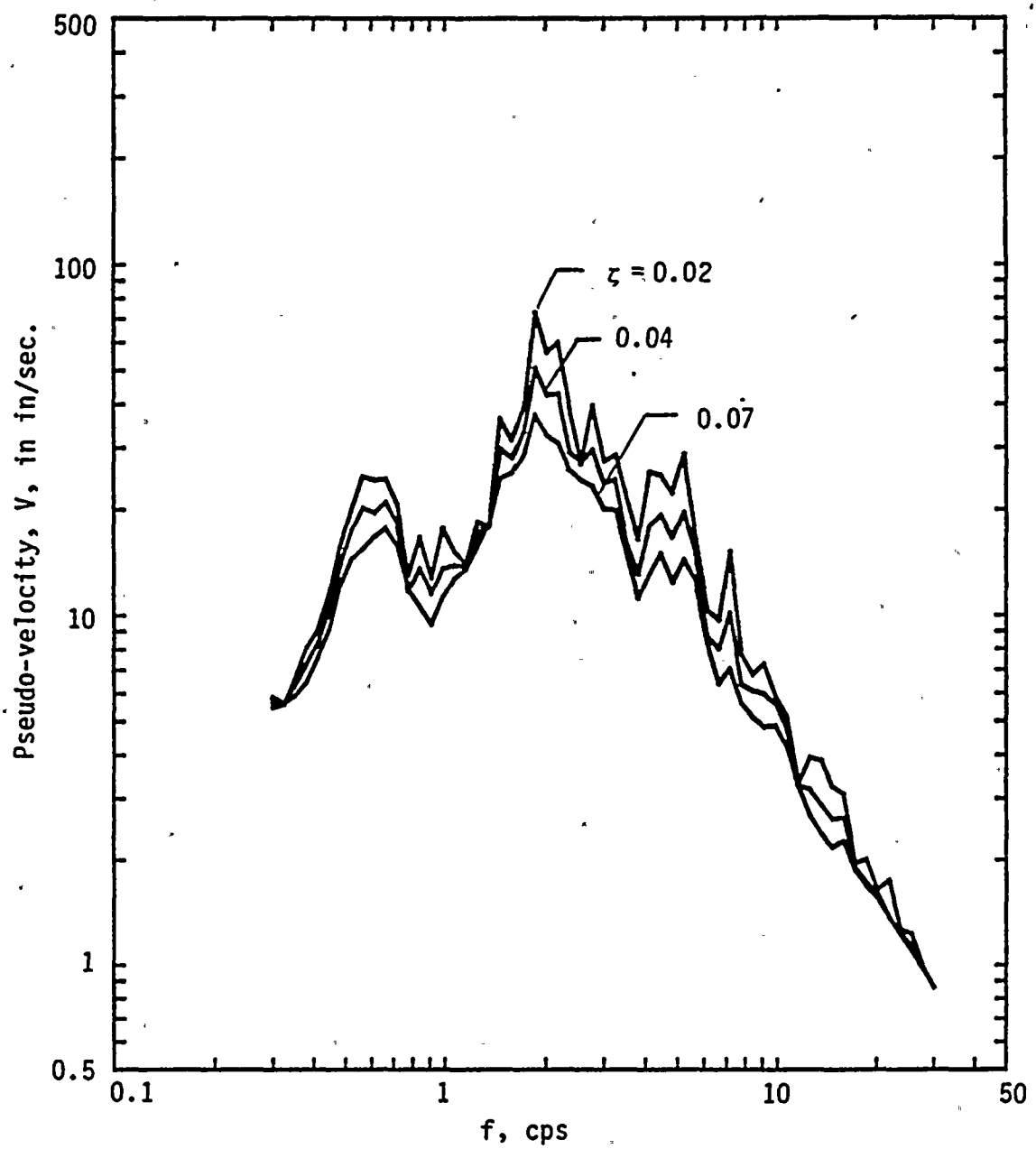

FIG. C.34 Pseudo-velocity Response Spectra for Systems Subjected to Numerically Generated Ground Motion Record No. 34

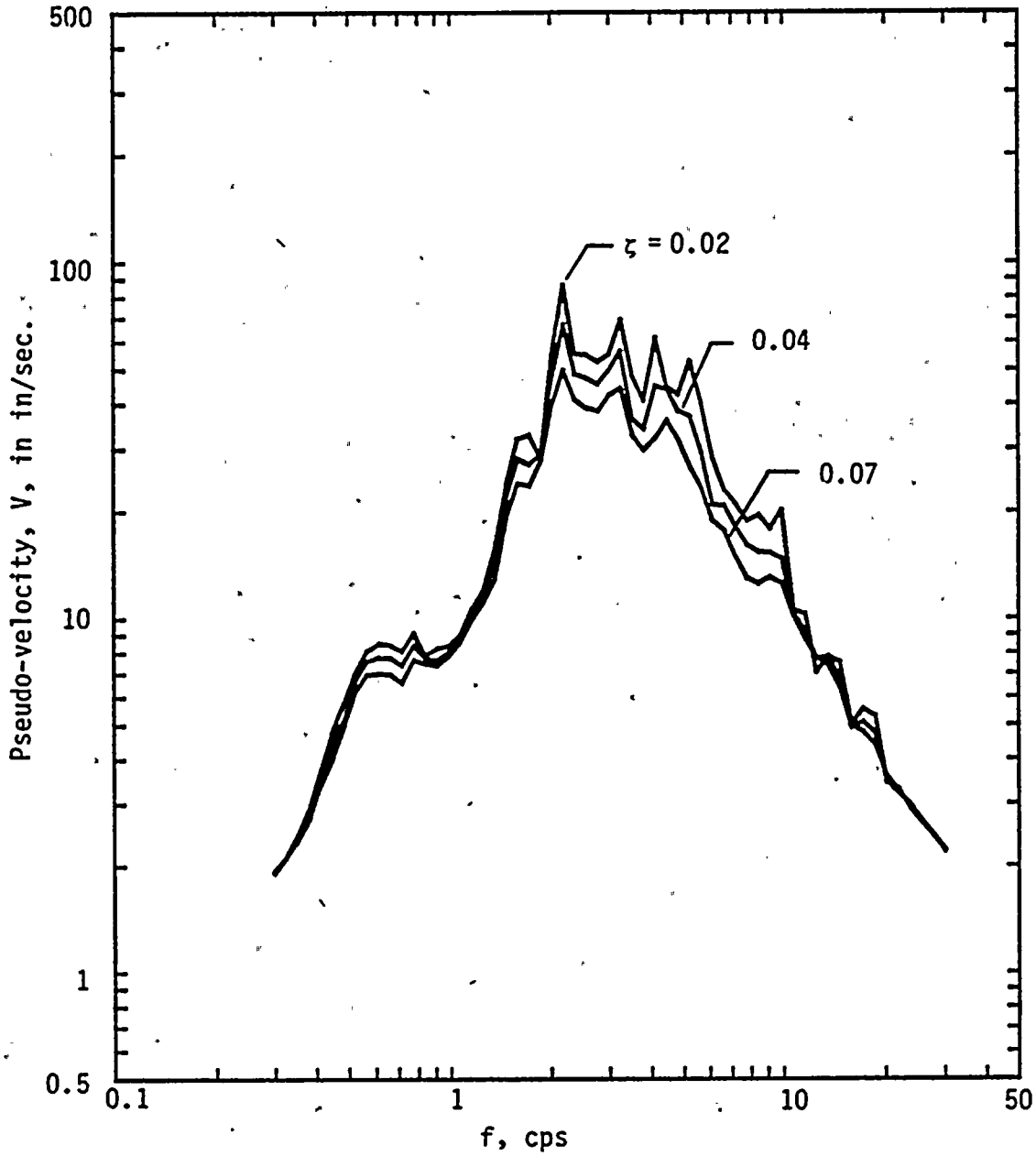

FIG. C.35 Pseudo-velocity Response Spectra for Systems Subjected to Numerically Generated Ground Motion Record No. 35

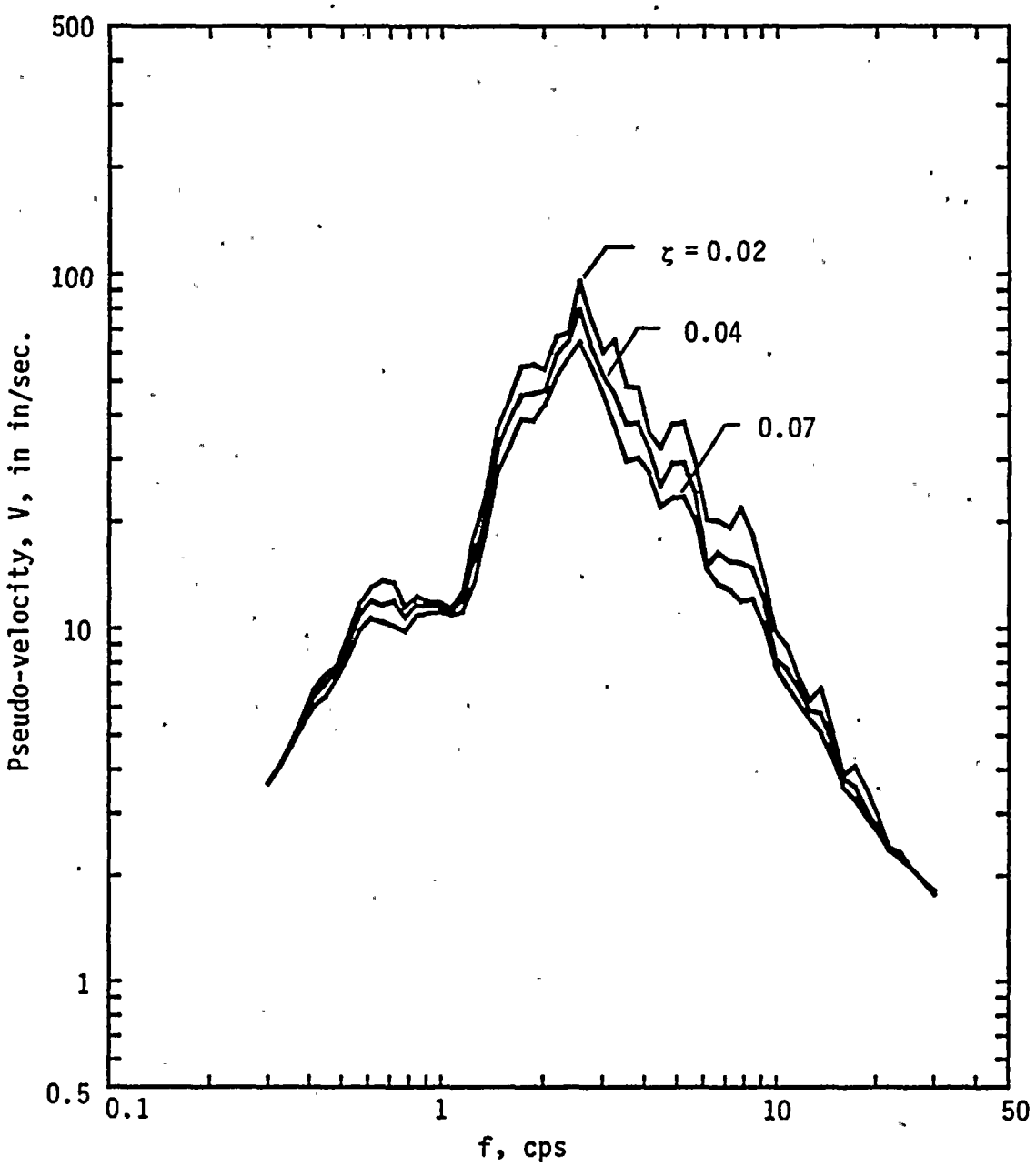

FIG. C.36 Pseudo-velocity Response Spectra for Systems Subjected to Numerically Generated Ground Motion Record No. 36

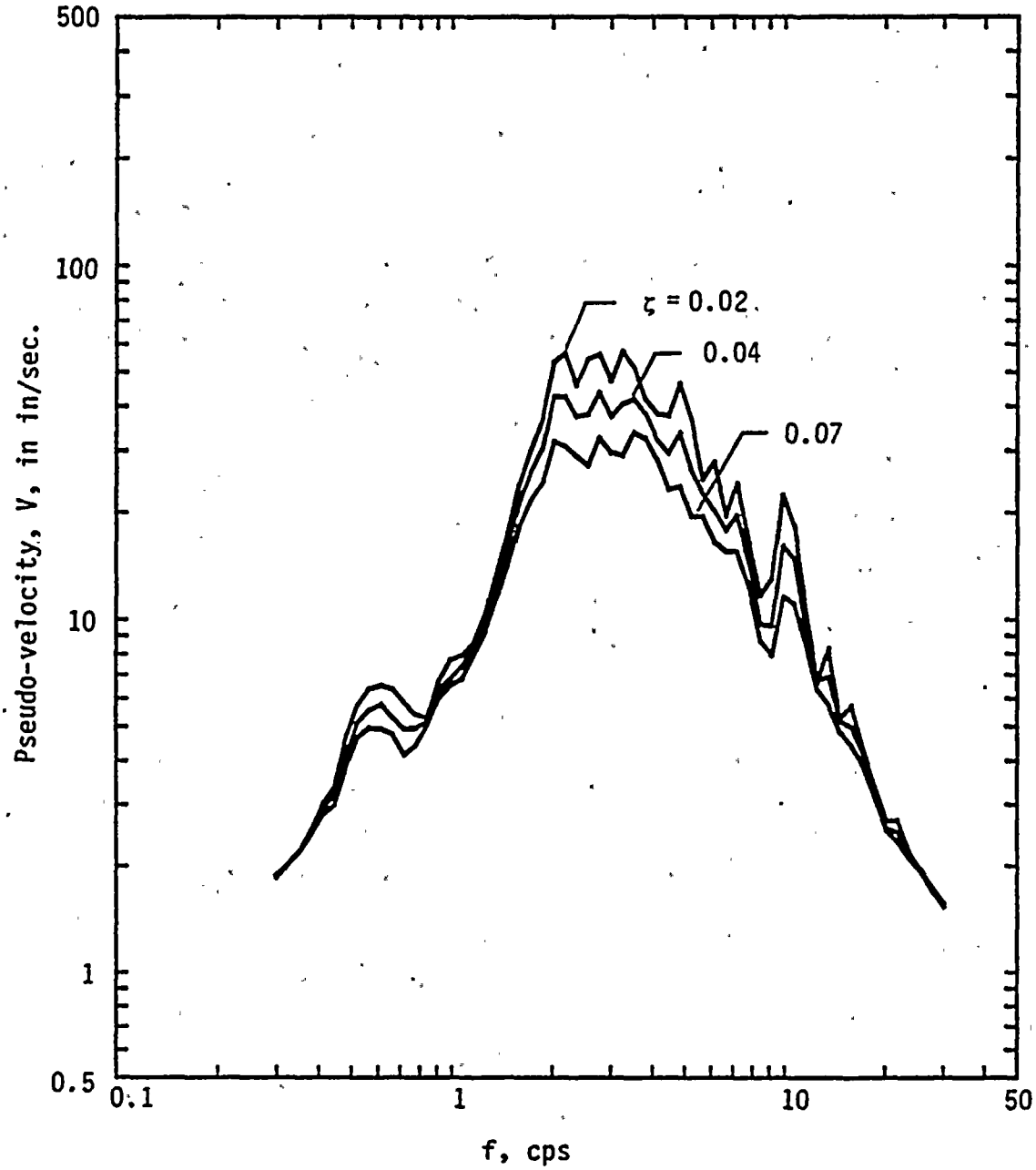

FIG. C.37 Pseudo-velocity Response Spectra for Systems Subjected to Numerically Generated Ground Motion Record No. 37

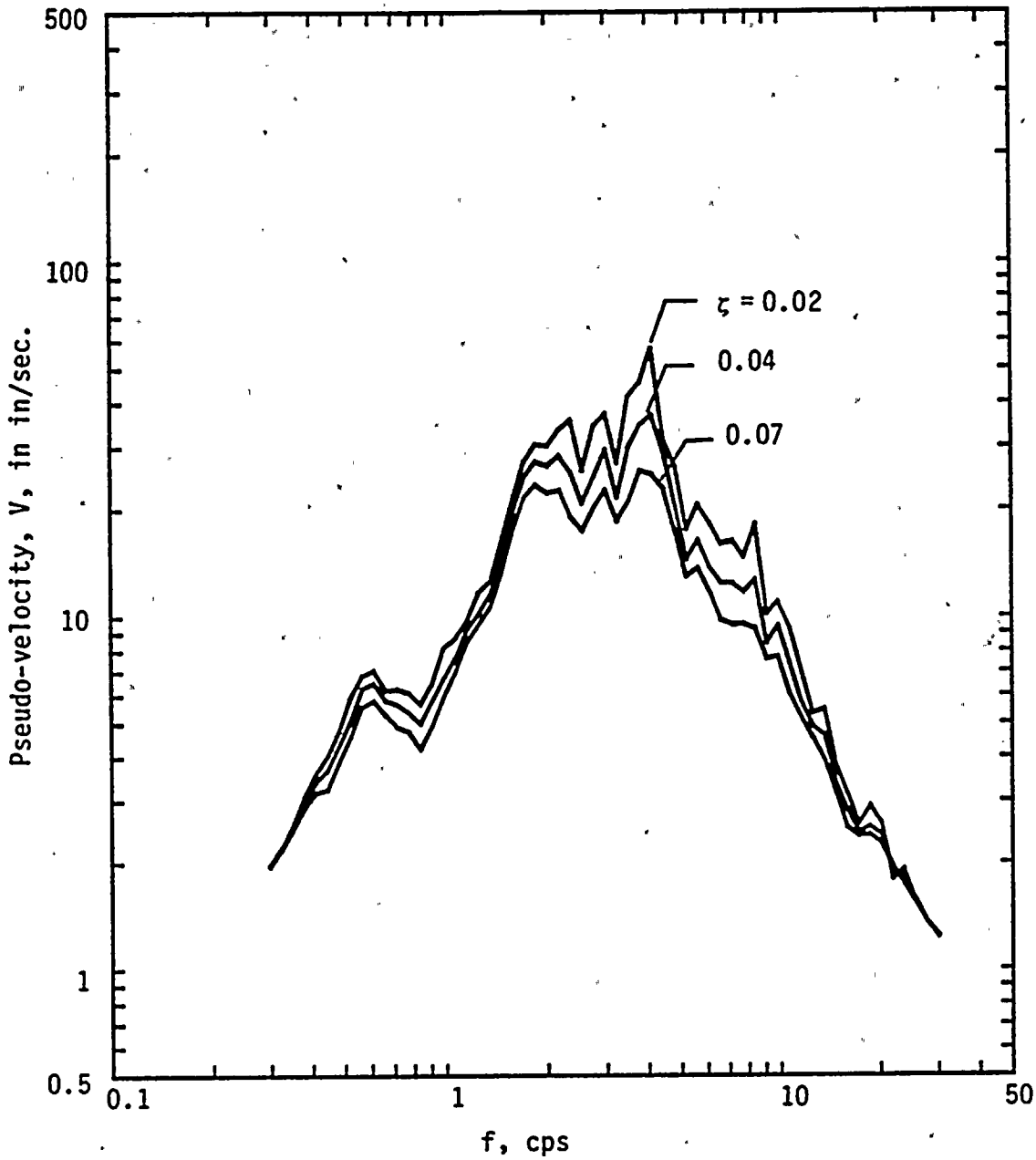

FIG. C.38 Pseudo-velocity Response Spectra for Systems Subjected to Numerically Generated Ground Motion Record No. 38

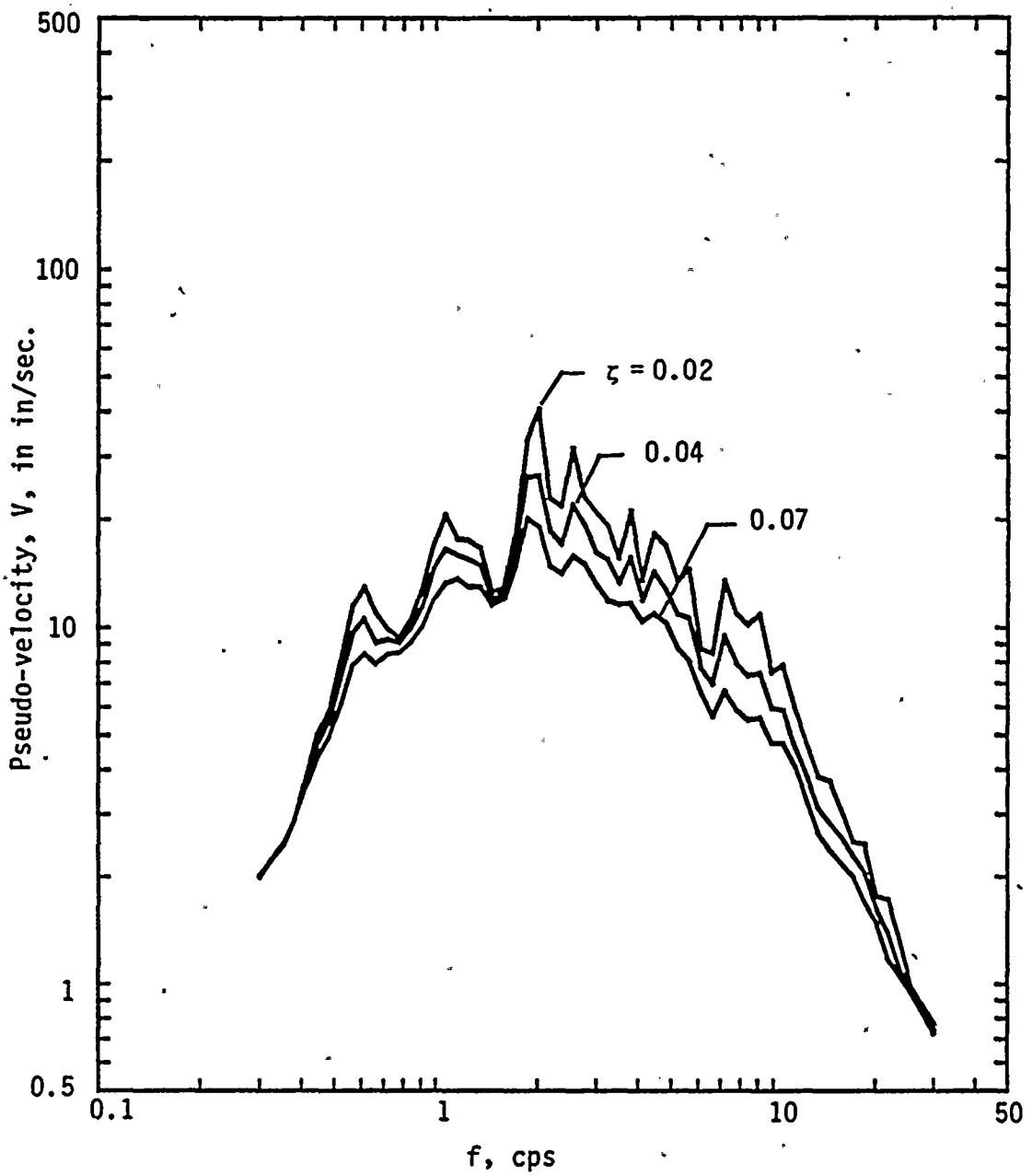

FIG. C.39 Pseudo-velocity Response Spectra for Systems Subjected to Numerically Generated Ground Motion Record No. 39

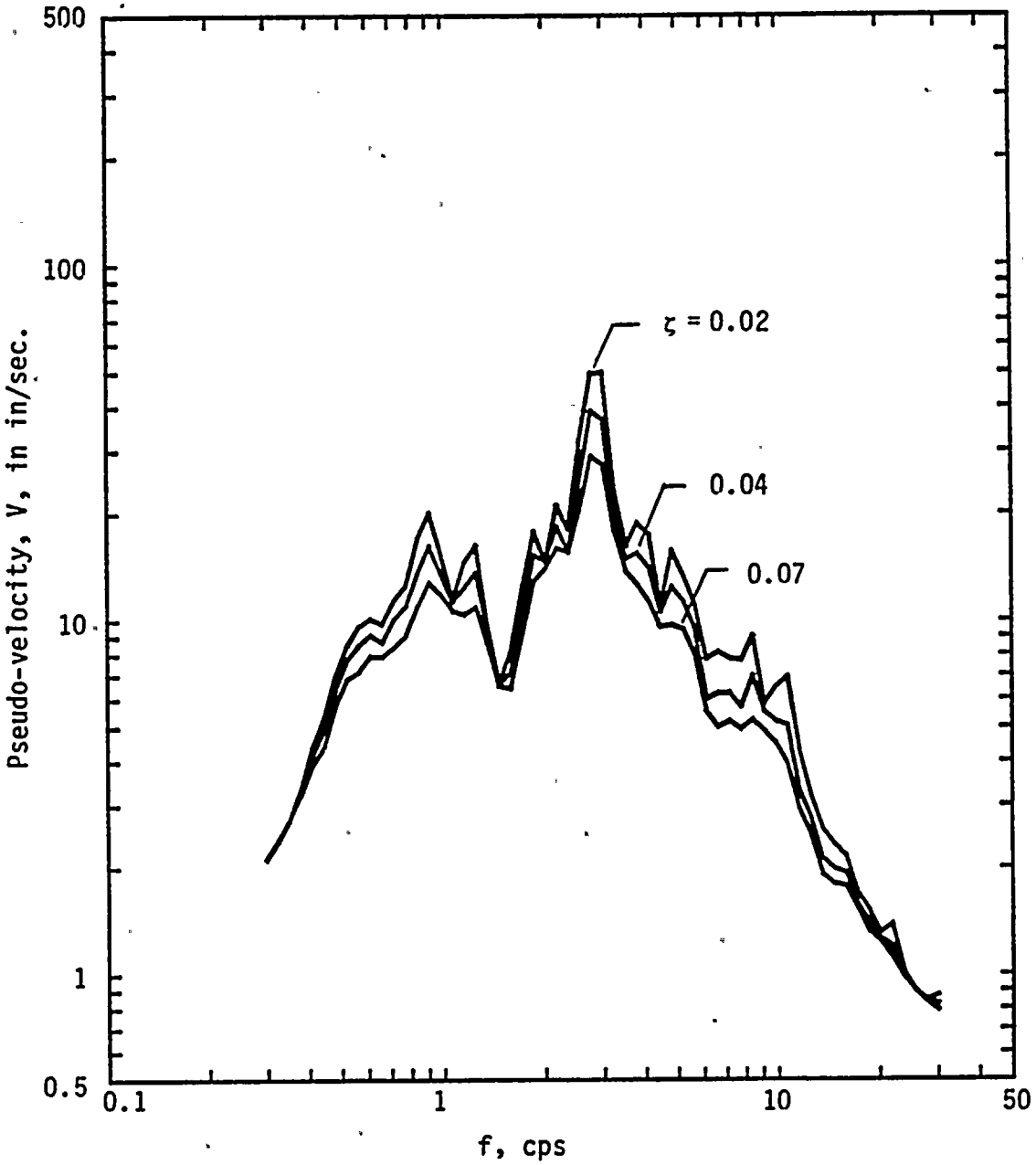

FIG. C.40 Pseudo-velocity Response Spectra for Systems Subjected to Numerically Generated Ground Motion Record No. 40

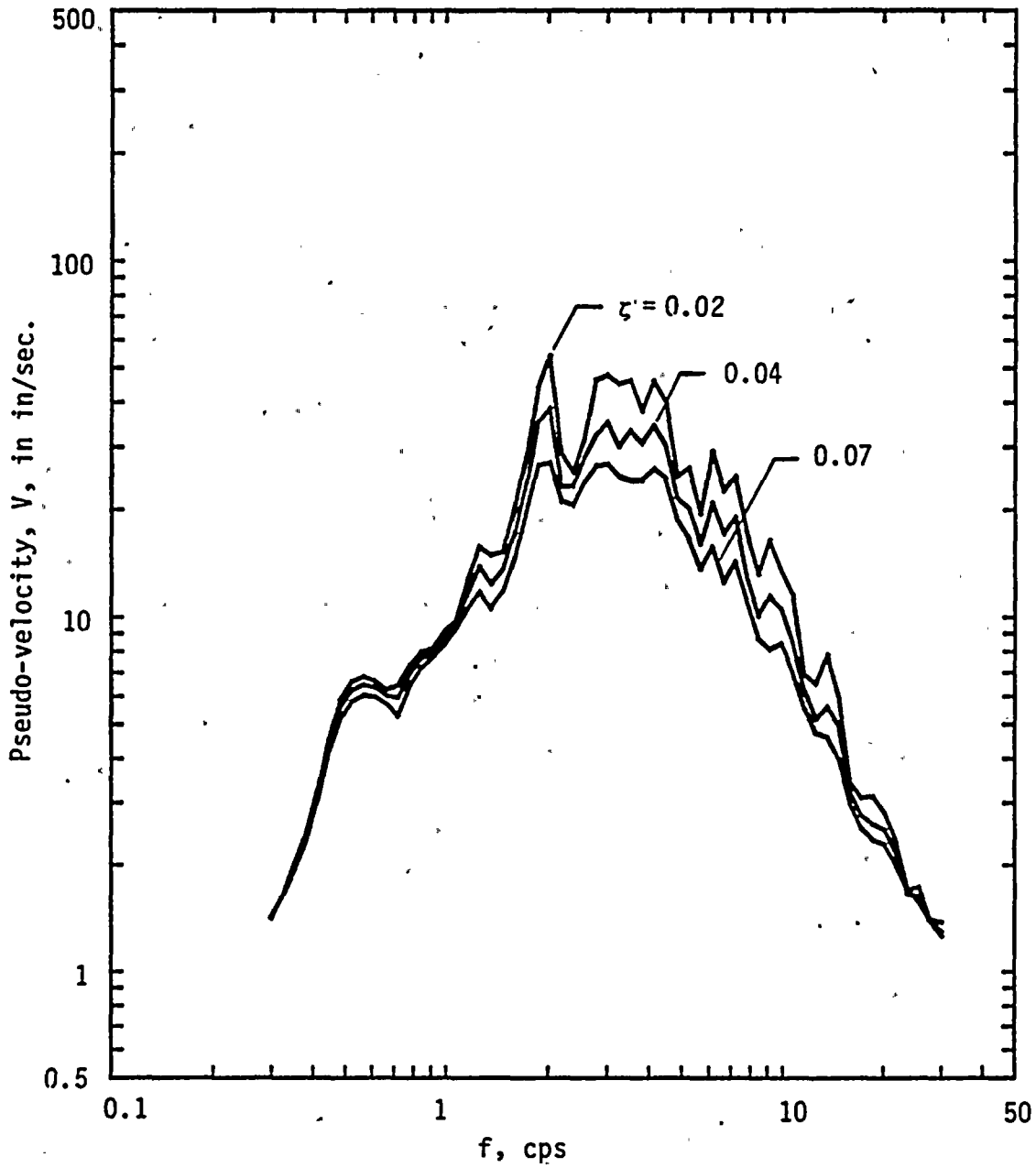

FIG. C.41 Pseudo-velocity Response Spectra for Systems Subjected to Numerically Generated Ground Motion Record No. 41

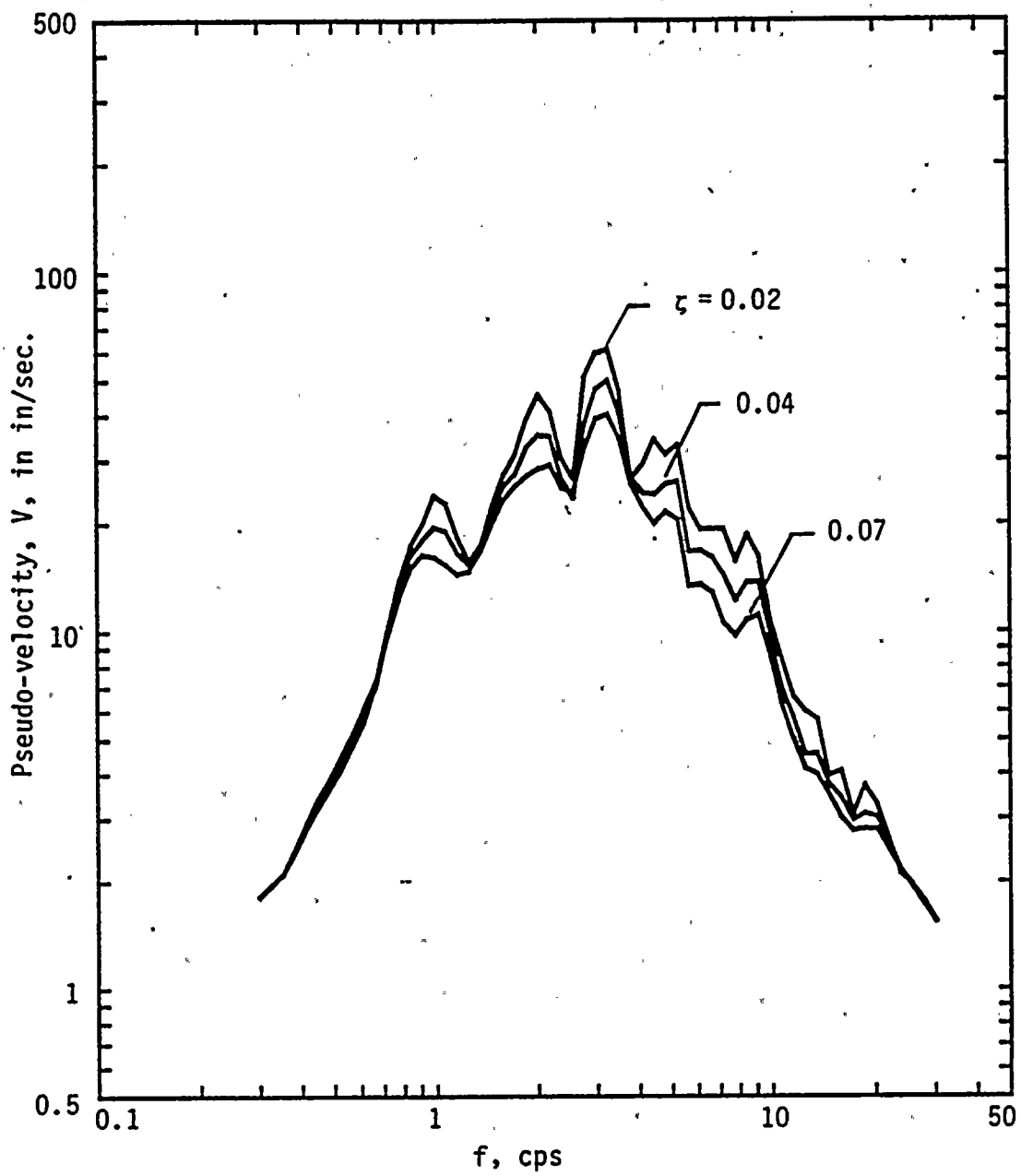

FIG. C.42 Pseudo-velocity Response Spectra for Systems Subjected to Numerically Generated Ground Motion Record No. 42

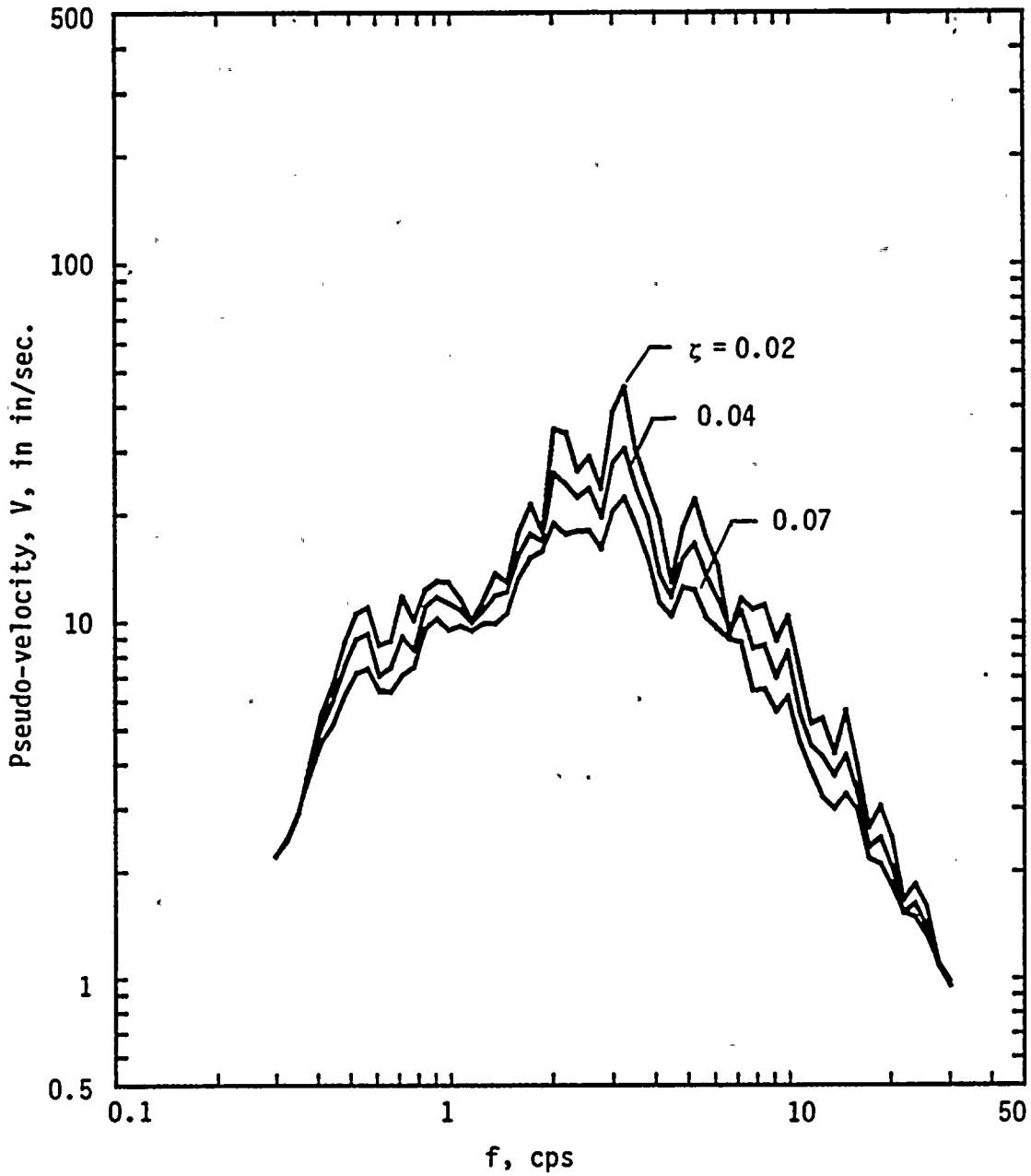

FIG. C.43 Pseudo-velocity Response Spectra for Systems Subjected to Numerically Generated Ground Motion Record No. 43

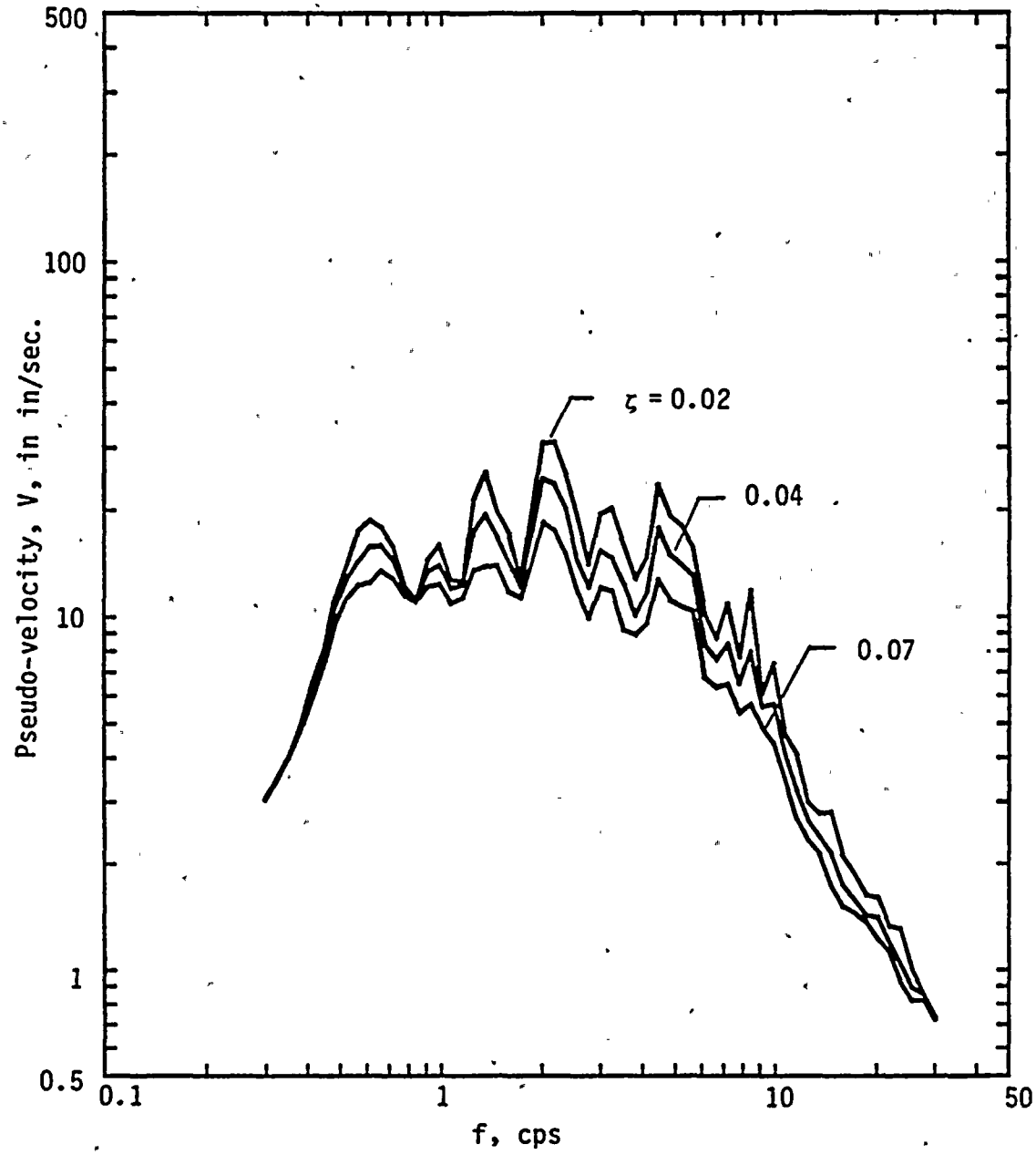

FIG. C.44 Pseudo-velocity Response Spectra for Systems Subjected to Numerically Generated Ground Motion Record No. 44

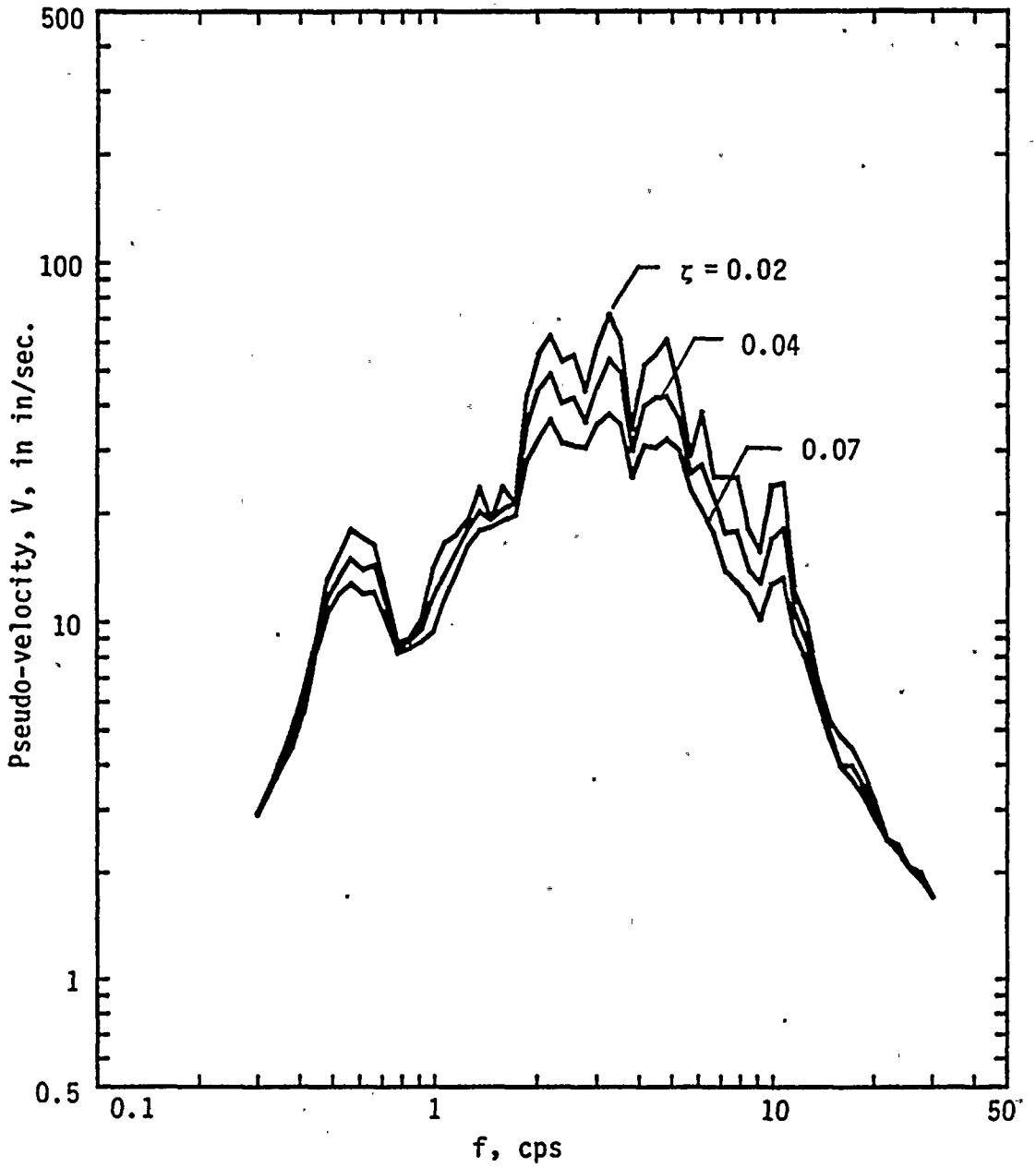

FIG. C.45 Pseudo-velocity Response Spectra for Systems Subjected to Numerically Generated Ground Motion Record No. 45

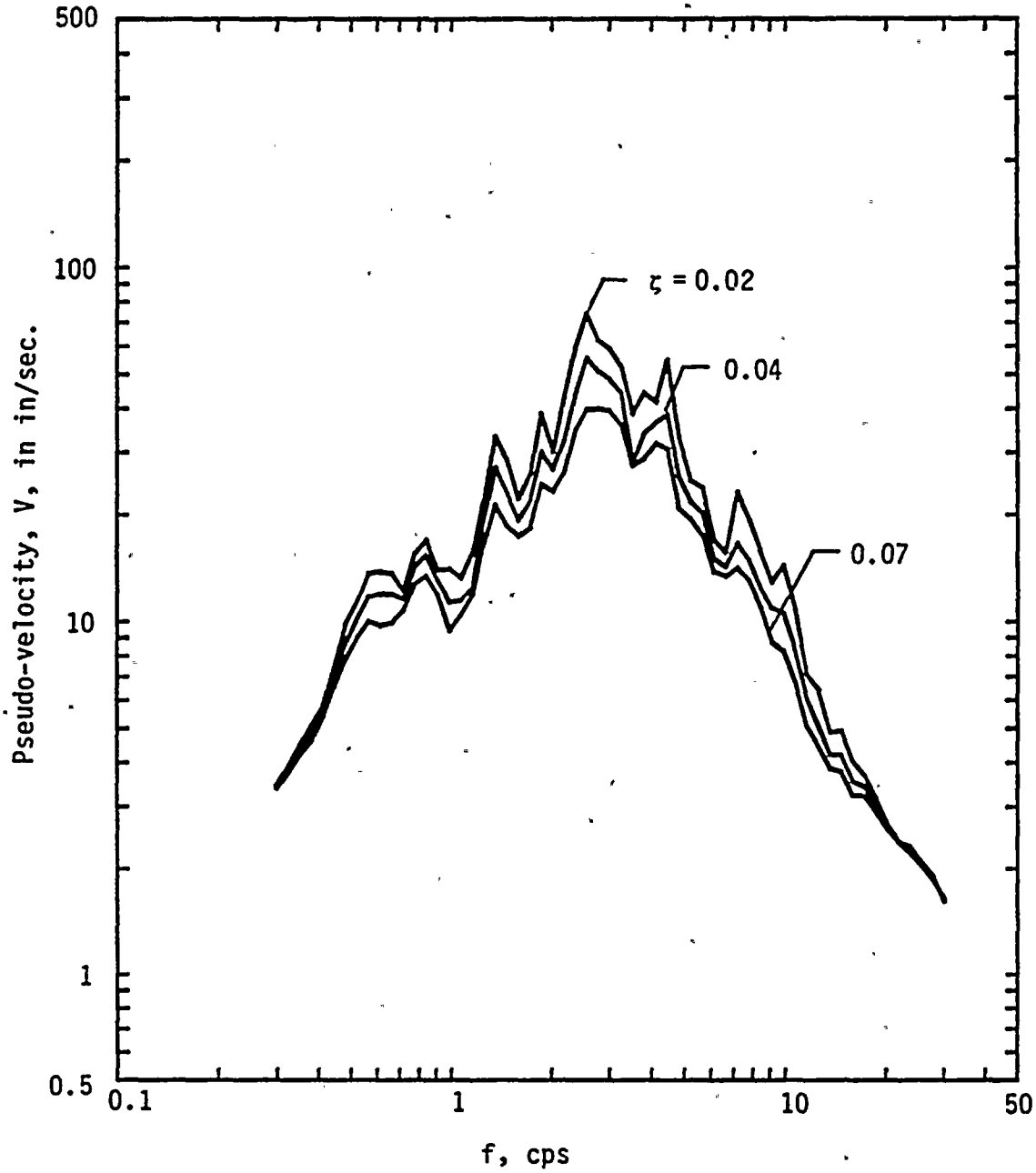

FIG. C.46 Pseudo-velocity Response Spectra for Systems Subjected to Numerically Generated Ground Motion Record No. 46

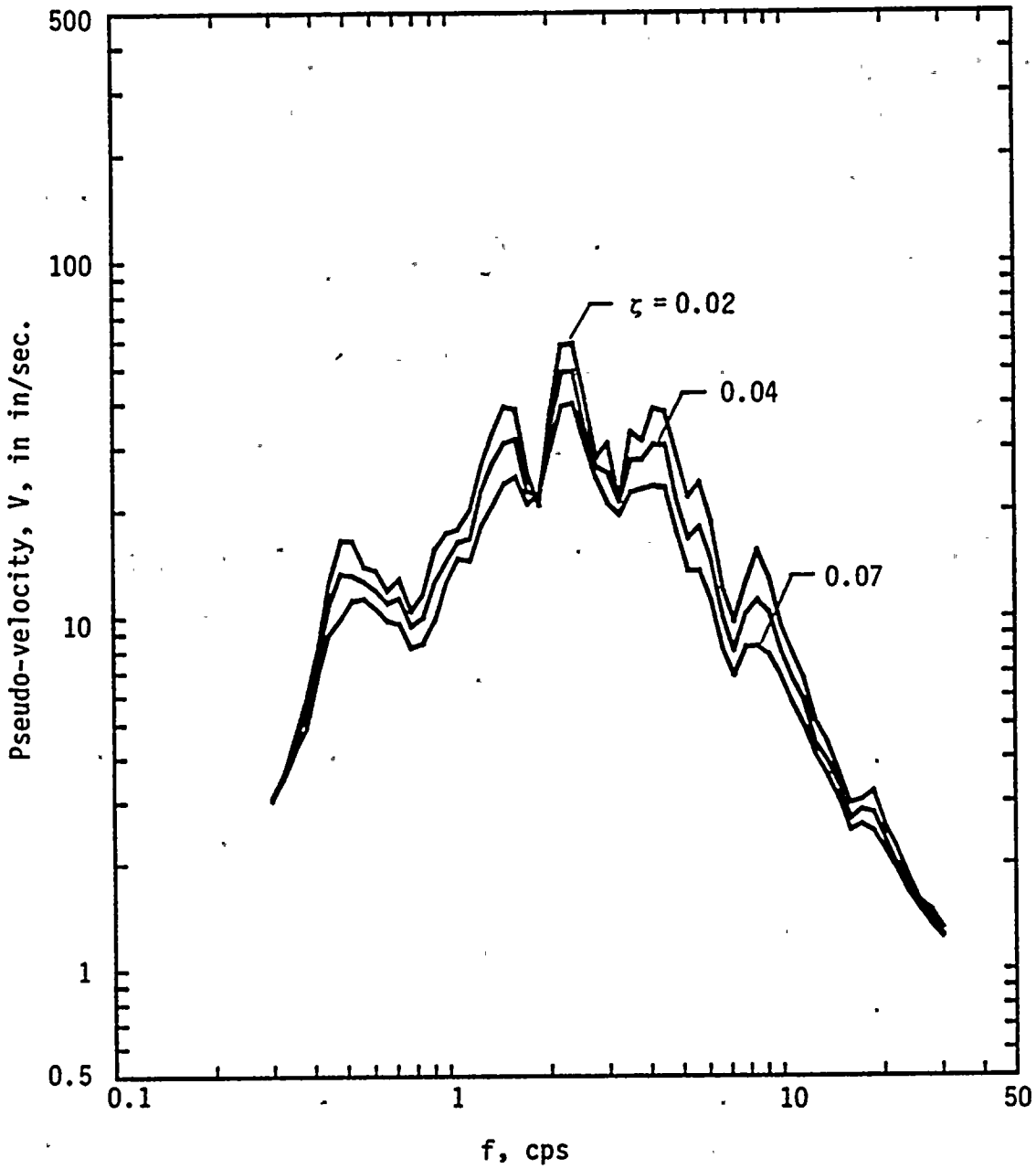

FIG. C.47 Pseudo-velocity Response Spectra for Systems Subjected to Numerically Generated Ground Motion Record No. 47

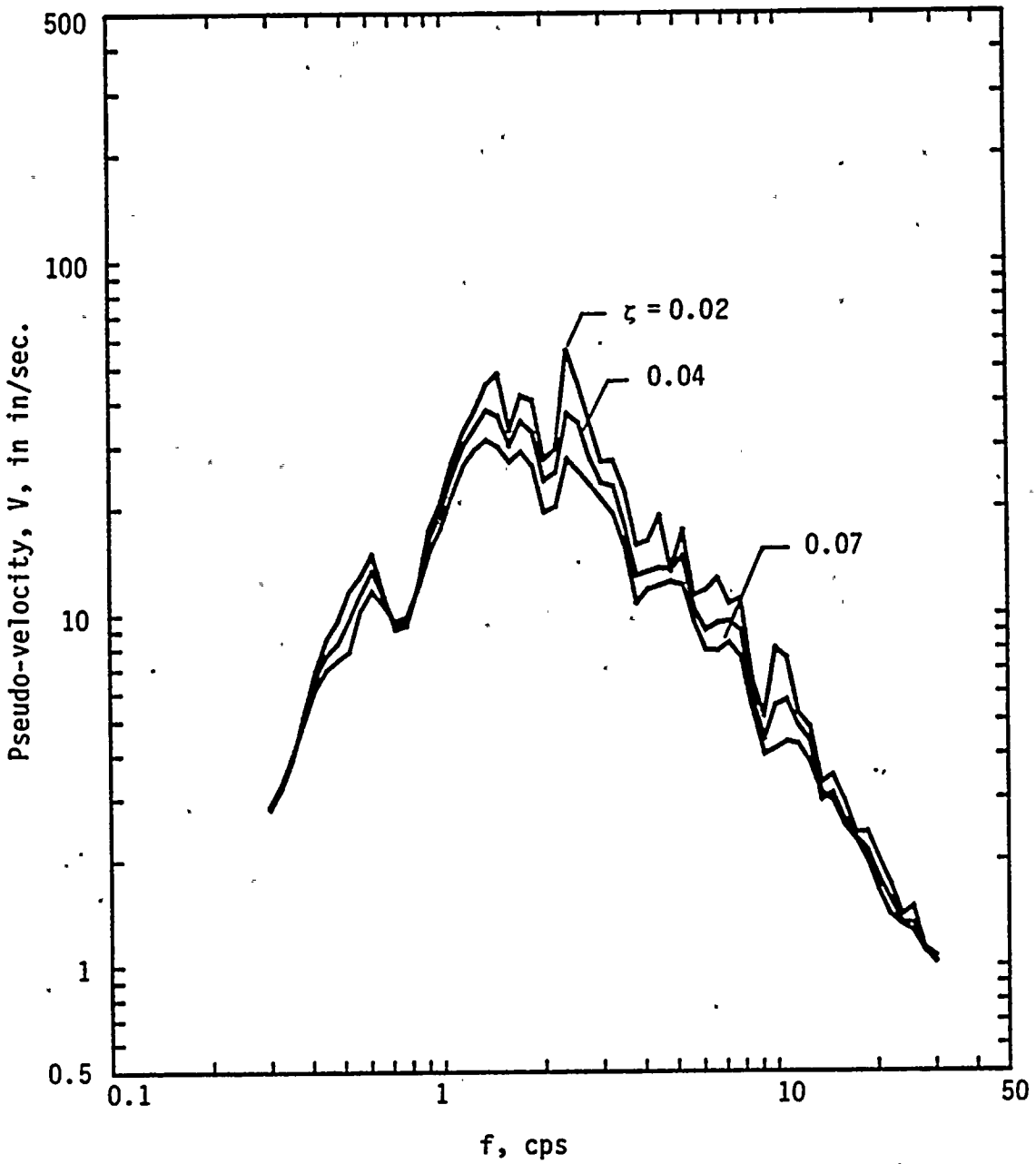

FIG. C.48 Pseudo-velocity Response Spectra for Systems Subjected to Numerically Generated Ground Motion Record No. 48

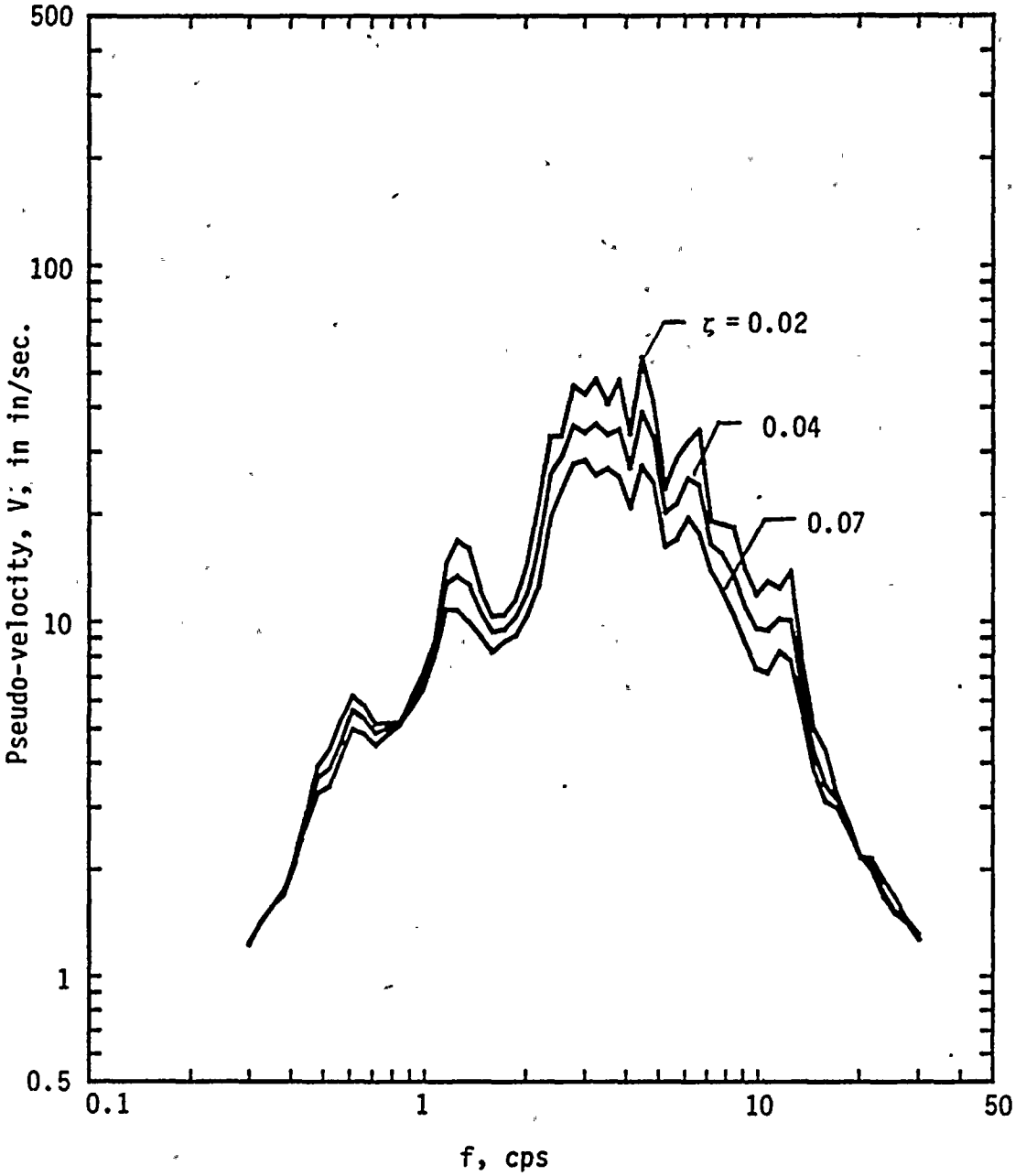

FIG. C.49 Pseudo-velocity Response Spectra for Systems Subjected to Numerically Generated Ground Motion Record No. 49

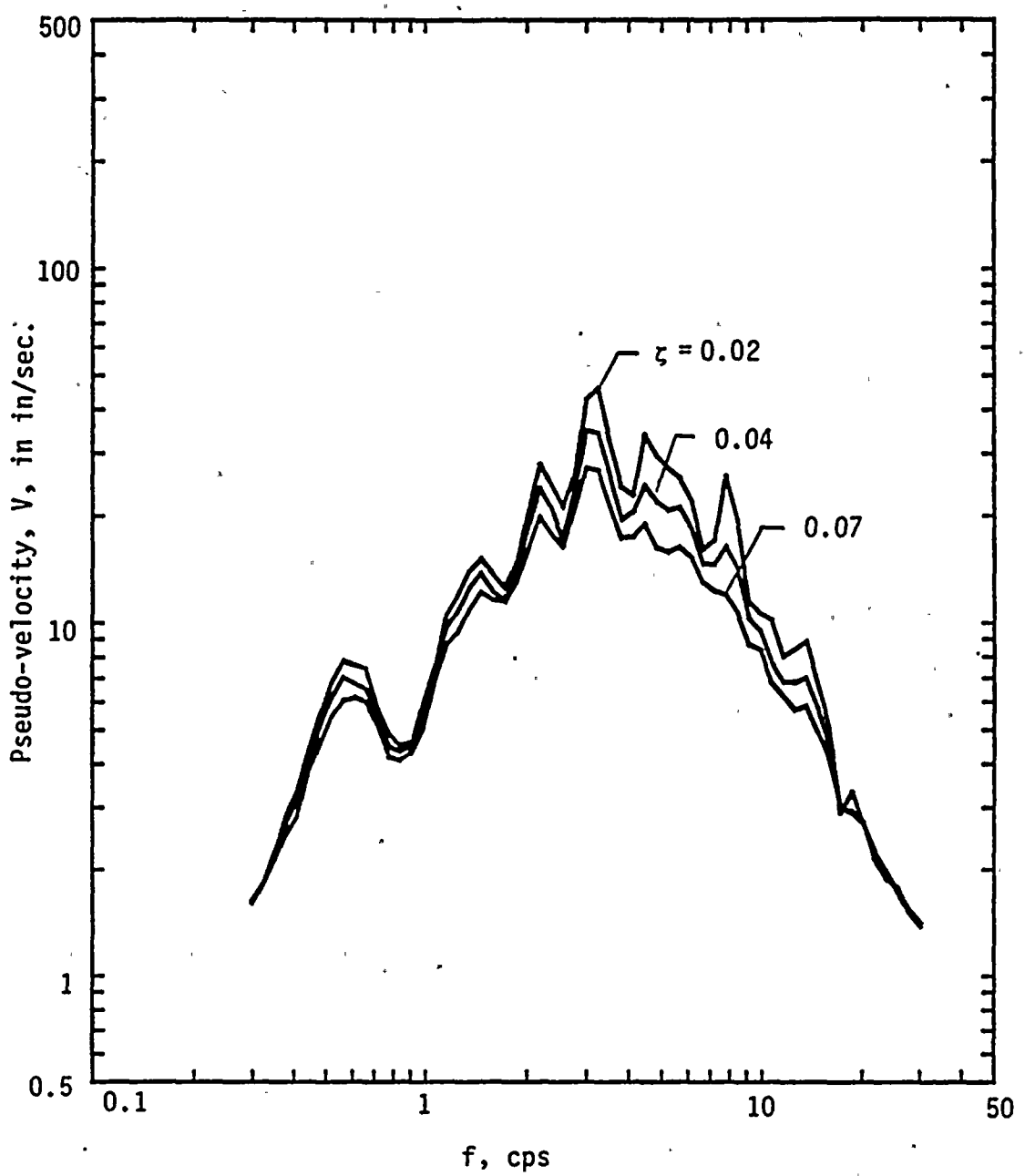

FIG. C.50 Pseudo-velocity Response Spectra for Systems Subjected to Numerically Generated Ground Motion Record No. 50

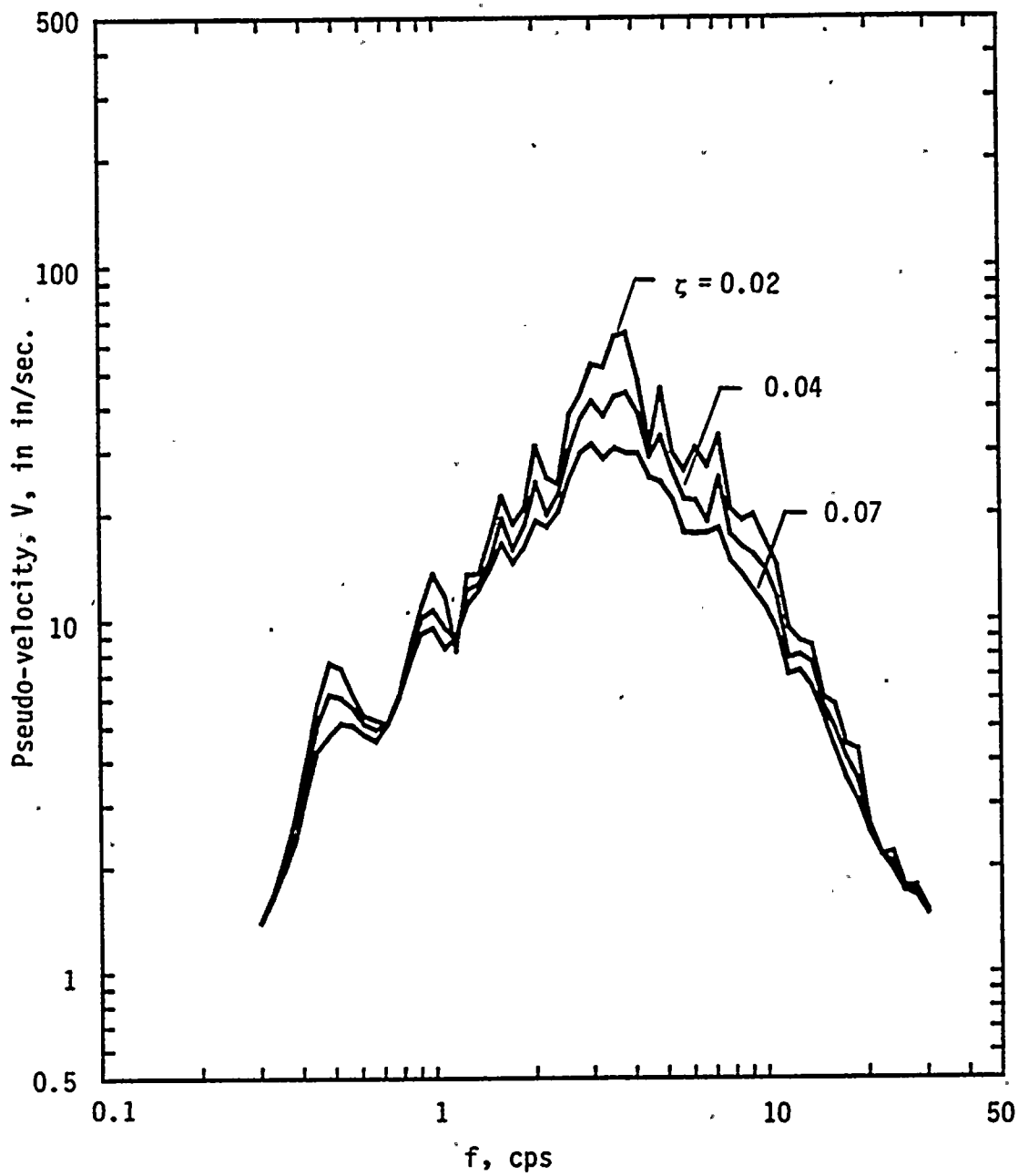

FIG. C.51 Pseudo-velocity Response Spectra for Systems Subjected to Numerically Generated Ground Motion Record No. 51

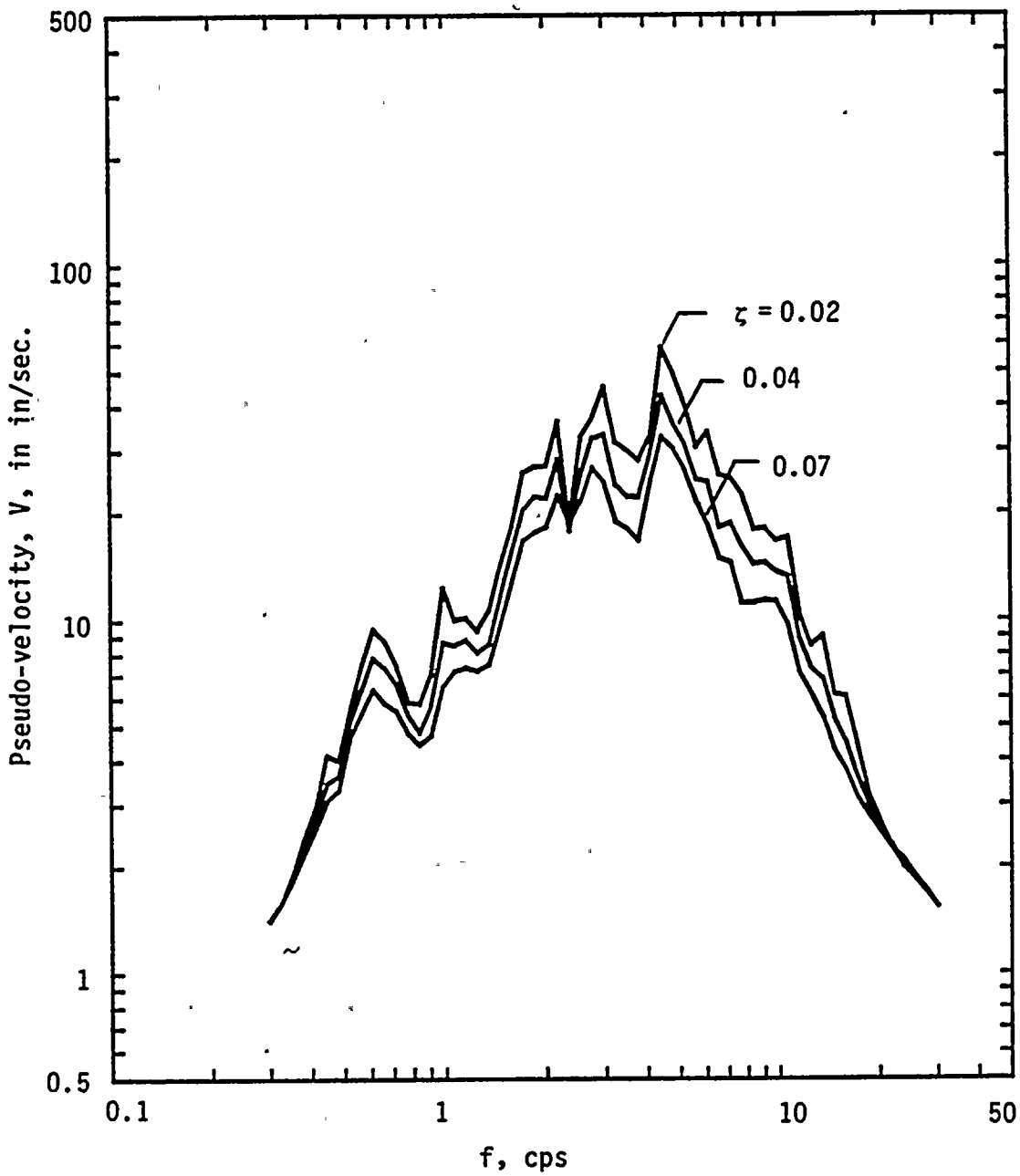

FIG. C.52 Pseudo-velocity Response Spectra for Systems Subjected to Numerically Generated Ground Motion Record No. 52